Universidad Carlos III de Madrid
www.uc3m.es

TESIS DOCTORAL

Análisis Experimental y Numérico del Proceso de Taladrado de Materiales Compuestos de Fibra de Carbono

Autor:

Norberto Feito Sánchez

Directores:

Dra. Mª Henar Miguelez Garrido
Dr. Jorge López Puente

Tutor:

Dra. Mª Henar Miguelez Garrido

DEPARTAMENTO DE INGENIERÍA MECÁNICA

Leganés, Julio del 2016

Universidad Carlos III de Madrid
www.uc3m.es

TESIS DOCTORAL

Análisis Experimental y Numérico del Proceso de Taladrado de Materiales Compuestos de Fibra de Carbono

Autor: *Norberto Feito Sánchez*

Directores: Mª Henar Miguelez Garrido

Jorge López Puente

Firma del Tribunal Calificador:

Firma

Presidente: Eugenio Giner Maravilla

Vocal: Antonino Morassi

Secretario: José Antonio Loya Lorenzo

Calificación:

Leganés, 11 de Julio del 2016

A mis padres, a mi hermano,

y en especial a mis abuelos.

Agradecimientos

Después de cuatro años intensos, en los que he aprendido muchísimo, he conocido gente increíble y viajé hasta el otro lado del mundo y más allá, hay muchas personas a las que quiero tener presente durante esta etapa final, que es a la vez el comienzo de otra.

Primeramente agradecer a mi directora, Mª Henar Miguelez, por confiar en mí y concederme la oportunidad de embarcarme en este mundo que es la investigación, el cual nunca pensé que me llegara a gustar tanto. Por permitirme crecer profesionalmente y guiarme con pasos firmes y seguros.

A Jorge López-Puente por su ayuda y su paciencia en el desarrollo de los modelos. Por enseñarme a comprender un poco más el mundo de los elementos finitos y su tiempo en las correcciones de artículos y conferencias.

Gracias a Pepe, a José Luis, a Antonio y José Díaz por los comienzos junto a ellos y su ayuda en la parte experimental de esta tesis. A Ana, a Belén y a Lourdes por su ayuda a entender un poco más la vida universitaria, su apoyo durante estos años y las buenas charlas durante las comidas.

Gracias a mis compañeros de departamento, a los que aún permanecen y los que ya no están, Miguel, Jesús, Fernando, Héctor, Carlos, Laura, Marcos y Víctor con los que he compartido momentos de risas, de estudios, de despacho y de cafetería entre tantos otros. Especialmente a Xavier y Patricia, que están ahí desde el principio. Gracias por los ánimos, los buenos consejos y las buenas conversaciones.

Thank you so much to Prof. Abbas Milani for giving me the chance to have the most incredible experience in my life and learn so much with you. I am very proud of our paper together.

Thanks to the research group of the Composites Laboratory of UBC Okanagan, especially to Bryn Crawford for all his kind help and warming welcome into the lab and the talks during lunch. I miss you so much friend.

Prof. Pedro Camanho thanks for your hospitality and for accept me as visitor research in the Universidade de Porto. I am very grateful for your dedication and for increase mi knowledge on the field of finite elements.

To my incredible Canadian friends! I have lived lot of adventures and unforgettable moments with all of you. Meesh, you are an example of self-improvement. I miss you so much friend. Weronika and Steve, the best roommates someone could have! Thank you for your patience with my english and for the long talks Weronika. Gracias a mis amigas Celine y Berta por las charlas de Skype y hacerme pasar los mejores días en Calgary. Faisal Islam, for your friendship. I hope to see you soon in India! Gracias a Juan y Karol por su amistad y su ayuda. To Antonio and Will for those trips together through Albert and BC. Spain is waiting for all of you guys!

Thanks to my Porto Friends. Rubicel por todas las aventuras, los viajes y el tiempo juntos. Nos vemos muy pronto. David and Ema, thanks for your friendship since the first moment. My friend Loris, the best Italian guy I have ever met! Thank you for your kindness, good talks and laughs. Finally thanks to my friend Fuji for the good times, for the invitations to lunch and for the laughs.

Quiero agradecer a todos mis amigos por su continuo apoyo y su confianza en mí en estos años. Sobran las palabras con todos ellos, pues ya son muchos años de amistad que se ha ido fortaleciendo con el paso del tiempo, pero no quiero dejar de mencionarlos aquí dándoles el hueco que les corresponde: Marina, Irina, Rocío, Montse, Alicia, Marisol, Pedro, Fabián, Jonatan, Susana, Verónica, Javier, Carlos, Artur, Manques, Lupi, Rosa, Carlos Sanz, Isabel y Emilia. A todos gracias de corazón. Sois los mejores, únicos e irremplazables.

Y por último, a mi familia, mis padres, mi hermano y mis abuelos, porque han estado, están y estarán en todo momento y sé que esto les hace muy felices.

Índice General

Resumen

El taladrado es un proceso fundamental previo al ensamblaje de componentes estructurales de material compuesto en diversas industrias como la aeroespacial. Los defectos inducidos durante el proceso de arranque de material pueden llevar al rechazo del componente con el consiguiente coste económico. Debido a la falta de homogeneidad y anisotropía de los laminados FRP (Fiber Reinforced Polymers), el proceso de perforación suele llevar asociados fenómenos de daño en el material (como la delaminación, el astillamiento del borde, la formación de grietas o el daño térmico) y el desgaste excesivo de la herramienta debido a la abrasividad de las fibras. Entre los daños mencionados, la delaminación ha sido identificada como el fenómeno más perjudicial, ya que conlleva una pérdida significativa de la resistencia y de la rigidez del laminado y, por consiguiente, afecta a su capacidad de carga. La identificación y prevención de éste fenómeno es, por lo tanto, particularmente importante para los componentes de material compuesto sometidos a cargas de compresión, cizalladura, cargas cíclicas o condiciones ambientales adversas durante períodos prolongados de tiempo. El daño en el material también depende de la geometría de la herramienta, del estado de desgaste de la broca y de los parámetros de corte. Por otro lado, es difícil encontrar en la bibliografía modelos numéricos 3D de taladrado que simulen el arranque de viruta incluyendo los movimientos de corte y avance de la broca. Sin embargo, el desarrollo de estos modelos puede ser un método efectivo para realizar estudios de optimización de la geometría de la herramienta y de los parámetros de corte, con el objetivo de mejorar la calidad de los agujeros y reducir el desgaste de la broca. Al mismo tiempo se consigue una reducción de recursos y tiempo en ensayos experimentales. Con el objetivo general de generar nuevo conocimiento sobre el campo del taladrado en materiales compuestos de fibra de carbono, se presenta esta tesis, con dos partes bien definidas. La primera parte, centrada en la experimentación, analiza la influencia de la geometría de la broca y del nivel de desgaste, considerando también la influencia de las variables de entrada (velocidad de avance, velocidad de corte y ángulo de punta) en las fuerzas de corte y el daño por delaminación. Estos ensayos también se utilizaron para la validación de los modelos numéricos desarrollados en la segunda parte, que consiste en la implementación de modelos numéricos 3D de taladrado basados en el método de los elementos finitos. Estos modelos validados son capaces de predecir el daño y la fuerza de avance para unos determinados parámetros de corte (velocidad de avance y velocidad de corte). Como complemento a ambos estudios, se han utilizado herramientas estadísticas para desarrollar modelos mecanísticos y ecuaciones predictivas útiles para evaluar las tendencias en el daño y apoyar a los modelos numéricos. Los conocimientos derivados de la presente tesis pueden servir de ayuda en la definición del fin de vida de la herramienta y constituyen una herramienta aplicable al diseño de nuevas geometrías de broca para este tipo de operaciones.

Abstract

Drilling of composite materials, is an essential pre-assembly process, for structural components in the aircraft industry. Induced damage, during the material removal processes, can result in the rejection of components and an increase in production cost. Due to the inherent inhomogeneity and anisotropy of Fiber Reinforced Polymers (FRP) laminates, and to the abrasive properties of the fibers, the drilling process is currently rife with damage phenomenon such as: spalling, delamination, chipping, fiber pull-out, crack formation, or thermal damage. Delamination has been identified as the most detrimental damage phenomenon for structural components as it results in a significant loss of strength and stiffness of the laminate, and consequently its load carrying capacity. Therefore, identification and prevention of this phenomenon becomes particularly important for composite components subject to adverse environmental conditions and compressive, shear, and cyclic loads over extended periods of time. Drilling induced damage depends also on several factors such as, drill bit geometry, cutting parameters, and tool wear. Furthermore, it is difficult to find literature on 3D models of drilling which are suitable for simulating chip removal, including both feed and rotation movements of the drill bit. Developing and using these tools leads to optimization studies about tool geometry and cutting parameters, which ultimately, reduces the number of tests and experimental time required. This thesis has been carried out with the main goal of generating new knowledge in the field of carbon fiber composite drilling and has two main parts. The first part, experimental, analyzes the influence of the drill bit geometry and the wear level considering also the input variables (feed rate, cutting speed, and point angle of the drill bit) in the cutting forces and in delamination damage. The second part, numerical, develops the 3D numerical models of drilling using finite element methodology. Using these models, predictions can be made in regards to the amount of damage caused by different feed forces and different cutting parameters (feed rate and cutting speed). Statistical tools have been used to support this study and to develop predictive and mechanistic models to estimate the damage incurred during the drilling process, evaluate trends, and support the numerical models. The knowledge derived from this thesis can be used to define the cutting life of a tool and will also be very useful in the design of new tool geometries to increase the efficiencies of composite material drilling.

Presentación

1. Introducción

Los materiales compuestos ofrecen una alta relación resistencia-peso y rigidez-peso, buena tolerancia al daño y excelente resistencia a la fatiga y a la corrosión. Estas propiedades los hacen altamente atractivos frente a los materiales convencionales para muchas aplicaciones estructurales. Además hay que añadir que, una de sus mayores ventajas es que se pueden fabricar muy próximos a la forma final deseada a un precio y calidad competitivos.

Con el creciente uso de los materiales compuestos en industrias como la aeroespacial, la naval o la automotriz entre otras, la optimización de los parámetros del proceso de mecanizado de los polímeros reforzados con fibras es cada vez más importante. Debido a la anisotropía y a la heterogeneidad inherente de este tipo de materiales, los daños debidos al mecanizado convencional en estos compuestos poliméricos son variados: delaminación, astillamiento del borde, formación de grietas, degradación térmica, etc.

Actualmente, las uniones más comunes entre componentes estructurales (entre los que se encuentran los materiales compuestos poliméricos) son las atornilladas o remachadas. La eficiencia de estas uniones depende de la calidad del agujero mecanizado. Sin embargo, las características de no homogeneidad, la anisotropía y la alta abrasividad de las fibras de estos materiales, implican una alta dificultad de mecanizado provocando un elevado desgaste de la herramienta y generando un daño sub-superficial que reduce drásticamente la vida en servicio del componente.

Las simulaciones numéricas de los procesos de taladrado mediante elementos finitos se presentan como una herramienta importante para comprender y optimizar los procesos de mecanizado. Los modelos permiten tener control sobre diferentes variables, como los parámetros de corte, y al mismo tiempo predecir el comportamiento bajo nuevas condiciones de diseño.

Las investigaciones llevadas a cabo hasta el momento de comenzar esta tesis en el ámbito numérico del taladrado se centraban, por un lado en modelos de corte ortogonal (tanto en 2D como en 3D), y por otro lado en simulaciones numéricas 3D simplificadas que tratan la broca como un punzón. En ambos casos la representación del proceso no es realista, al no tener en cuenta la compleja geometría de la broca y el movimiento de corte que conlleva el arranque de material.

Con el objetivo de avanzar en el conocimiento de los procesos de taladrado de materiales compuestos, y más concretamente en aquellos referentes a los reforzados con fibra de carbono, surge el planteamiento de la presente tesis. Por un lado, se pretende avanzar en el ámbito experimental con el objetivo de mejorar el proceso de taladrado desde el punto de vista de la competitividad del proceso y ausencia de daño crítico en el material. Por otro lado, se busca desarrollar herramientas de predicción válidas capaces de proporcionar información acerca de las relaciones entre los parámetros de corte, la geometría de la broca, los niveles de desgaste y los mecanismos de daño en el material. Los conocimientos generados permitirán en trabajos futuros, entre otras cosas, mejorar la definición del criterio de fin de vida de la herramienta y ayudar al diseño de nuevas geometrías de broca.

2. Objetivos

Para conseguir el objetivo general, se ha de abordar una serie de objetivos parciales relacionados con la experimentación y la simulación numérica definidos a continuación:

Experimentación: El primer paso se centra, por un lado, en ampliar la información existente en la literatura acerca del comportamiento en taladrado de los materiales compuestos LFRP o Polímeros Reforzados con Fibras Largas en español, (especialmente en lo concerniente al desgaste de herramientas) y por otro, en obtener la información necesaria para poder validar posteriormente los modelos que se desarrollen. Asimismo el estudio del material mecanizado debe aportar datos acerca del daño causado en el material en cada experimento. Se definen por tanto, los siguientes puntos:

- Selección de un rango de parámetros de corte (avance y velocidad de corte) en base a la literatura y al conocimiento industrial para materiales poliméricos reforzados con fibra de carbono.
- Realización de ensayos con herramientas convencionales, no convencionales y con geometrías de broca con desgaste controlado.
- Aplicación de técnicas de análisis de daño en el composite mediante microscopía y análisis de fuerzas de mecanizado obtenidas mediante dinamómetro rotativo.
- Realización de análisis estadísticos para estudiar la influencia de los diferentes parámetros de entrada en las variables de salida.

Simulación numérica: La segunda parte consiste en el desarrollo de modelos 3D que permitan reproducir el taladrado de material compuesto de fibra de carbono (tanto en cinta como en tejido), bajo distintas geometrías de herramienta, incluyendo el nivel de desgaste. Se deben considerar, por tanto, los movimientos de corte y avance de la broca de modo que se puedan relacionar los parámetros de entrada (parámetros de corte, geometría de broca) con los esfuerzos de mecanizado (par y fuerza de avance) y el daño inducido entre laminas (delaminación). Para conseguir estos objetivos deben cubrirse a su vez los siguientes puntos:

- Implementación de modelos de daño tanto para matriz como para fibra, incluyendo la degradación de las propiedades del material compuesto con el daño.
- Modelización del fenómeno de delaminación mediante láminas cohesivas.
- Desarrollo de estrategias de modelización que disminuyan el coste computacional en 3D (simplificación de modelos, estrategias de mallado).
- Desarrollo y optimización de modelos mecanísticos apoyados por las simulaciones numéricas.

3. Metodología

La metodología que se ha llevado a cabo para conseguir los objetivos anteriormente mencionados, consiste principalmente en una metodología mixta que combina estudios experimen-

tales y de modelización numérica. Los ensayos experimentales, aparte de tener valor en sí mismos aportando información novedosa en este campo, permiten la validación de los modelos. Estos modelos numéricos, por otro lado, amplían el conocimiento sobre las variables que intervienen en el proceso, como los modelos de daño del material, y que proporcionan asimismo información acerca de magnitudes de muy difícil medida. Se incluye una tercera metodología transversal basada en estudios estadísticos tanto en la parte experimental como numérica que incluye el desarrollo de modelos y ecuaciones de predicción de rápida ejecución.

Durante el trabajo experimental es preciso seleccionar cuidadosamente las herramientas y analizar su geometría para poder reproducirla mediante programas CAD (Computer-Aided Design según terminología inglesa). También se ensayan herramientas desgastadas artificialmente de modo que se tenga control sobre la variación geométrica de la broca. Las probetas taladradas se examinan para comprobar el nivel de daño mediante técnicas de microscopía. Respecto a los materiales a mecanizar se han seleccionado dos tipos de materiales reforzados con fibra de carbono de los que se dispone información sobre su caracterización, lo que facilita su posterior implementación en los modelos.

El trabajo numérico implica el desarrollo de modelos 3D complejos que incluyan los movimientos de rotación y avance de la herramienta. Es importante reproducir adecuadamente las propiedades mecánicas y resistentes del material modelizado, así como la geometría de la herramienta utilizada en los ensayos, lo que supone un proceso complejo. El fallo intra-laminar se implementa según la formulación de Hou o Hashin (dependiendo de la disposición de las fibras en el laminado) mediante una subrutina tipo VUMAT en ABAQUS/explicit, mientras que el daño inter-laminar se realiza mediante elementos cohesivos.

4. Aportaciones Originales

Las contribuciones originales llevadas a cabo en esta Tesis Doctoral se presentan a continuación:

- Comparación de nuevos diseños de geometrías de broca no convencionales en dos arquitecturas de material CFRP (Carbon Fiber Reinforced Polymers según terminología inglesa) distintas: apilado de capas unidireccionales o tejidas. Se presenta un análisis en profundidad que incluye las fuerzas de corte, el daño por delaminación, la calidad superficial y el desgaste de la herramienta con el número de taladros.

- Estudio de la influencia de los parámetros de corte en diferentes geometrías de broca con desgaste controlado, producido durante el taladrado de materiales compuestos de fibra de carbono. El estudio de la influencia de los parámetros de corte sobre brocas desgastadas es novedoso en la literatura.

- Desarrollo de modelos capaces de predecir la delaminación y la fuerza de avance mediante el uso de herramientas estadísticas como el análisis ANOVA (ANalysis Of VAriance según terminología inglesa), regresión múltiple o superficies de respuesta. La estrategia de optimización multi-objetivo aplicada a los parámetros de corte es una metodología utilizada por primera vez en la operación de taladrado con geometrías de broca desgastadas de materiales CFRPs.

- Desarrollo de modelos 3D que reproducen los movimientos de rotación y de avance de la broca así como la geometría de la misma para materiales compuestos de láminas tejidas. Entre las geometrías implementadas, las brocas desgastadas no tienen precedentes en la literatura. Los modelos han sido capaces de estimar daño por delaminación y fuerza de avance.

5. Estructura del Documento

La Tesis Doctoral ha dado lugar a la publicación de cinco artículos y un capítulo de libro. El presente documento se estructura en tres partes:

La primera parte, únicamente experimental, abarca cuatro capítulos que incluyen el estado del arte referente al campo del taladrado de materiales LFRPs y tres estudios publicados en revistas:

- **Capítulo 1:** Introduce el campo del taladrado de los materiales poliméricos reforzados con fibra y los problemas que derivan de este proceso.
- **Capítulo 2:** Presenta un estudio de geometrías de brocas no convencionales analizando la influencia de las fuerzas y los parámetros de corte en el daño del material.
- **Capítulo 3:** Realiza un análisis de la geometría de la broca y la influencia del desgaste en el daño del material. Aparte de la delaminación, otro tipo de defectos inducidos durante la operación de taladrado son analizados.
- **Capítulo 4:** Desarrolla un modelo mecanístico para geometrías nuevas y desgastadas basado en los ensayos experimentales, capaz de optimizar las variables del proceso de taladrado.

La segunda parte, relacionada con la modelización por elementos finitos del proceso de taladrado, abarca tres capítulos entre los que se encuentran el estado del arte y dos artículos publicados:

- **Capítulo 5:** Revisa la bibliografía referente a la modelización por elementos finitos de los procesos de mecanizado de este tipo de materiales, especialmente de la operación de taladrado.
- **Capítulo 6:** Presenta los resultados de un trabajo comparativo entre modelos 3D simples y complejos de taladrado en material compuesto de fibra de carbono unidireccional. Los resultados analizan las influencias de la secuencia de apilamiento y el uso de placa de apoyo entre otras variables.
- **Capítulo 7:** Desarrolla un nuevo modelo 3D completo para material compuesto tejido de fibra de carbono, y se válida para herramienta helicoidal, desgastada y con geometría escalonada.

En la tercera y última parte se recogen las principales conclusiones y las posibles líneas de trabajos futuros de investigación.

Parte I

Análisis Experimental del Taladrado en Materiales Compuestos de Fibra de Carbono

Capítulo 1

Estado del Arte del Taladrado de Materiales Compuestos

En este primer capítulo se recogen los principales avances que se han realizado en el análisis experimental del taladrado de materiales compuestos hasta la fecha. Se tratan las operaciones de taladrado (convencional, abrasivo, taladrado asistido por vibración y taladrado de alta velocidad), la influencia de la geometría de broca y de sus materiales en la calidad del agujero, los fenómenos de daño debidos al proceso de taladrado y los fenómenos de desgaste de la broca.

1.1 Características y Aplicaciones de los Laminados

Durante las décadas pasadas, la creciente demanda de estructuras cada vez más ligeras y resistentes por parte de numerosos sectores industriales, han estimulado un fuerte desarrollo en el campo de los materiales compuestos laminados de matriz polimérica reforzada con fibra. Este tipo de materiales engloba tres grandes grupos: laminados reforzados con fibra de carbono o CFRP (Carbon Fiber Reinforced Polymer) [1], laminados reforzados con fibra de vidrio o GFRP (Glass Fiber Reinforced Polymer) [2] y laminados de fibra de metal o FMLs (Fiber Metal Laminates) [3]. Debido a las considerables ventajas que presentan, la tendencia en la industria es utilizar estos materiales para reemplazar a los metálicos en una amplia gama de estructuras, incluyendo aeroespaciales, aeronáuticas o de defensa (Figura 1.1). E estos campos, los principales requerimientos son altas relaciones resistencia/peso y rigidez/peso [1].

Los métodos de unión de los componentes de materiales compuestos, requieren la realización de taladrados previos [4]. La eficiencia del perno de unión y la durabilidad dependen críticamente de la calidad de los agujeros mecanizados. Es por ello que existen varios procesos de taladrado comúnmente usados para la producción de juntas remachadas y atornilladas durante las operaciones de montaje de los diferentes componentes. Para asegurar una alta resistencia de la unión y una buena precisión en remaches y uniones atornilladas, los agujeros taladrados deben tener una calidad elevada. Sin embargo, algunas características especiales de los compuestos laminados tales como la no homogeneidad, la anisotropía y el carácter abrasivo y duro de las fibras de refuerzo, hacen que estos materiales sean difíciles de mecanizar [5,6]. Como consecuencia, el daño debido al mecanizado puede reducir la resistencia a la fatiga degradando el comportamiento del componente en servicio [7].

Entre los problemas causados por el taladrado la delaminación es considerado el más importante. El rechazo de las piezas de material compuesto debido a este tipo de daño llegó a ser hasta del 60% en la industria aeronáutica [8,9]. Debido a que el taladrado es a menudo una operación de mecanizado final previa al montaje de los componentes, cualquier daño que resulte en el rechazo del componente implica una pérdida costosa para la empresa. Para aumentar la eficiencia de esta operación es esencial entender el comportamiento de la misma mediante el análisis experimental y el desarrollo de modelos de predicción.

Figura 1.1: Materiales usados en el Airbus A350.

1.2 Laminados Compuestos CFRP y GFRP

Los laminados compuestos CFRP (Carbon Fiber Reinforced Polymer) y GFRP (Glass Fiber Reinforced Polymer) son con diferencia, los materiales poliméricos reforzados con fibra más comúnmente usados en la industria debido a sus excelentes propiedades mecánicas. Están formados por la combinación de un polímero que funciona como matriz y un refuerzo de fibras (de carbono o de vidrio principalmente).

Las fibras son ligeras, rígidas y resistentes y proporcionan la mayor parte de la rigidez y resistencia al material. Se utilizan a menudo como refuerzos continuos en una dirección (lámina unidireccional) o en dos direcciones (capas tejidas). La lámina de material compuesto se forma por el conjunto de un gran número de fibras en una placa delgada, denominada capa de preimpregnado, cuyo espesor es de aproximadamente 0,15 mm [10].

La matriz de polímero mantiene unidas las fibras entre sí transfiriendo la carga al refuerzo de fibras, y al mismo tiempo las protege contra los ataques del medio ambiente. Los polímeros termoplásticos y termoestables son las matrices más utilizadas [10], siendo estos últimos los que combinan mejores propiedades mecánicas, resistencia al medio ambiente, temperatura de trabajo y facilidad de proceso.

Una lámina preimpregnada con fibras unidireccionales (Figura 1.2A) tiene la máxima rigidez y resistencia en la dirección de las fibras y las propiedades mínimas en la dirección perpendicular a las mismas generando un material anisótropo. Sin embargo, una capa de preimpregnado de tejido (Figura 1.2B) tiene la máxima rigidez y resistencia en ambas direcciones del plano. Un laminado de material compuesto polimérico reforzado con fibra se consigue generalmente mediante la unión de varias láminas de preimpregnado con diferentes orientaciones de las fibras (cruzadas) para la fabricación de laminados compuestos cuasi-isótropos [11,12]. La Figura 1.2C muestra una secuencia de apilamiento típica de un material compuesto laminado FRP. Algunos laminados compuestos UD y tejido FRP utilizados en diferentes estudios de taladrado se enumeran en la Tabla 1.1.

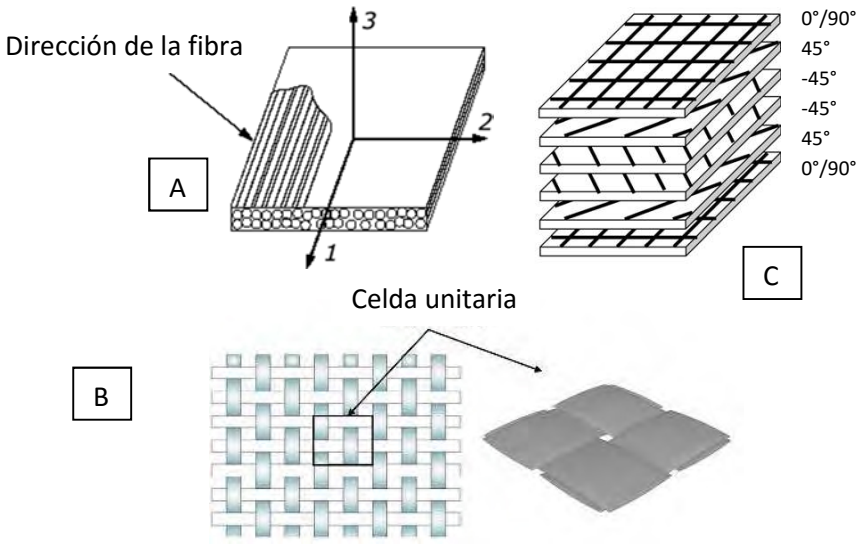

Figura 1.2: Lámina unidireccional, lamina bidireccional y secuencia de apilado para un material multidireccional.

Tabla 1.1: Compuestos laminados para taladrado estudiados en la literatura.

Material	Lámina	Referencias
CFRP	Unidirec-cional	Park *et al*. [11]; Bhatnagar *et al*. [12]; Lin *et al*. [13]; Chen [14]; Piquet *et al*. [15]; Murphy *et al*. [16]; Zhang *et al*. [17]; Wang *et al*. [18]; Zitoune *et al*. [19]; Sardinas *et al*. [20]; Durao *et al*. [21–23]; Rao *et al*. [24]; Zitoune *et al*. [25];Lee *et al*. [26]; Rawat *et al*. [27,28]; Shyha *et al*. [29]; Jahromi *et al*. [30]; Iliescu *et al*. [31]; Kalla *et al*. [32]; Rahme *et al*. [33]
	Tejido	Davim *et al*. [34-37]; Tsao *et al*. [38–44]; Hocheng *et al*. [45]; Gaitonde *et al*. [46]; Karnik *et al*. [47]; Faraz *et al*. [48]; Shyha *et al*. [49,29]; Liu *et al*. [50]; Lazar *et al*. [51]
GFRP	Unidirec-cional	Mathew *et al*. [523]; Ramkumar *et al*. [53,54]; Capello [55]; El-Sonbaty *et al*. [56]; Singh *et al*. [57,58]; Rao *et al*. [59]; Mkaddem *et al*. [60]; Lasri *et al*. [61]; Kilickap [62]
	Tejido	Khashaba *et al*. [63–65]; Velayudham *et al*. [66,67]; Arul *et al.* [68–70]; Abrao *et al*. [71]; Rubio *et al*. [72]; Isik *et al*. [73].

1.3 Operaciones de Taladrado

Aunque se han desarrollado en los últimos tiempos operaciones de mecanizado no convencionales para la realización de agujeros en materiales compuestos, como el mecanizado por láser [92-97], el mecanizado por chorro de agua [98-100], y el mecanizado por descarga eléctrica [101], el taladrado sigue siendo el proceso más utilizado. Este proceso cubre principalmente el taladrado convencional (Conventional drilling o CD), el taladrado abrasivo (Grinding drilling o GD), el taladrado asistido por vibración (Vibration-assisted twist drilling o VATD), y el taladrado a alta velocidad (High speed drilling o HSD). La Tabla 1.2 resume las características de las anteriores operaciones de taladrado en composite encontrados en la literatura.

1.3.1 TALADRADO CONVENCIONAL

Se puede comprobar en la Tabla 1.2 que entre los diferentes tipos de operaciones mencionadas, el taladrado convencional es la operación que más atención ha recibido sistemáticamente por parte de diferentes investigadores. Los estudios se centran, por un lado en el estudio del material y por otro en el estudio de las herramientas.

En el primer caso, las investigaciones centradas en el material, llevan a cabo un gran número de experimentos para estudiar la influencia de las variables de entrada (como la velocidad de giro y la velocidad de alimentación) en las variables de salida (como la delaminación y la fuerza de avance) [14,29,37,42,56,58,62,64,68,71,74-76,79,80,85,86,102]. Al mismo tiempo, se estudia también como reducir la delaminación inducida durante el taladrado [9,38,55,78,81-84].

En el segundo caso, la mayoría los trabajos centrados en la herramienta, analizan la influencia de la geometría o del material de la broca en la fuerza de avance y la calidad del agujero [2,15,23,34,35,39,40,44,45,49,51,67,71,73,77,81]. Un menor número de artículos analiza la influencia del desgaste de las mismas tanto en las fuerzas como en el daño generado [16,31,41, 65,66,77,87,88].

Tabla 1.2: Operaciones de taladrado típicas en compuestos laminados en la literatura.

Operación	Características	Referencias
Taladrado convencional (CD)	▪ Velocidad de corte < 100 m/min (en general la velocidad de giro, < 8000 rpm). ▪ Además de brocas helicoidales estándar, también se utilizaron otras brocas especiales, tales como brocas escalonadas, brocas de fresa, brocas punta central y broca de filos rectos.	Stone *et al*. [9]; Chen [14]; Piquet *et al*. [15]; Murphy *et al*. [16]; Sardinas *et al*. [20]; Durao *et al*. [23]; Iliescu *et al*. [31]; Davim *et al*. [34-37]; Hocheng *et al*. [45]; Lazar *et al*. [51] Capello [55]; El-Sonbaty *et al*. [56]; Singh *et al*. [57]; Kilickap [62]; Khashaba [63–65]; Velayudham *et al*. [66,67]; Arul *et al*. [68]; Abrao *et al*. [71]; Lee *et al*. [74]; Ramulu *et al*. [75]; Kim *et al*. [76]; Brinksmeier *et al*. [77]; Kim [78]; Zitoune *et al*. [19,79]; Shyha *et al*. [29,49, 80]; Enemuoh *et al*. [81]; Tsao *et al*. [41,43,82,83]; Jung *et al*. [84]; Mohan *et al*. [85,86]; Fernandes *et al*. [87,88];
Taladrado abrasivo (GD)	▪ Brocas de núcleo con partículas de PCD adheridas a la herramienta.	Park *et al*. [11]; Jain *et al*. [89]; Hocheng *et al*. [45,90]; Tsao *et al*. [39,40,42]
Taladrado asistido por vibración (VATD)	▪ La frecuencia utilizada en todos los estudios fue menor de 600 Hz. ▪ Las amplitudes de vibración fueron menores a 20 µm. ▪ La vibración longitudinal se aplicó a la broca helicoidal en la dirección de sus ejes.	Wang *et al*. [18]; Ramkumar *et al*. [53,54]; Arul *et al*. [68]; Zhang *et al*. [17,91]
Taladrado de alta velocidad (HSD)	▪ Velocidad de corte > 200 m/min.	Lin & Chen [13]; Gaitonde *et al*. [46];
	▪ Todos usan brocas helicoidales de carburo cementado.	Rawat *et al*. [27,28]; Iliescu *et al*. [31]; Karnik *et al*. [47]; Liu *et al*. [50]; Rubio *et al*. [72]

1.3.2 TALADRADO ABRASIVO

Con el fin de mejorar el rendimiento del taladrado sin delaminación, el taladrado abrasivo fue introducido por primera vez en materiales compuestos por Park *et al*. [11]. Consiste en el uso de una broca fabricada en material de alta resistencia con forma cilíndrica hueca (Core drill o broca de núcleo) y buena resistencia al desgaste. Adheridas al metal se encuentran las partículas PCD (Poly-Crystalline Diamonds) como se muestra en la Figura 1.3. El mecanismo de eliminación de material es únicamente mediante la abrasión generada entre las partículas PCD y el material. No existe contribución del filo de corte debido a que la broca es cilíndrica y hueca. Esto conlleva una disminución de la fuerza de empuje en comparación con el taladrado convencional de brocas helicoidales [42,89], proporcionando agujeros con muy poca delaminación [39,40]. Hocheng y Tsao establecieron un modelo de fuerza crítica de avance sin delaminación para este tipo de operación [45].

Figura 1.3: Brocas abrasivas o de núcleo.

1.3.3 TALADRADO ASISTIDO POR VIBRACIÓN

El taladrado asistido por vibración (Vibration-Assisted Twist Drilling o VATD) ha sido foco de gran interés en los últimos años. Este proceso basado en el sistema de taladrado convencional, consiste en incluir un movimiento vibratorio controlado a una baja (<1.000 Hz) o alta (> 1.000 Hz) frecuencia de baja amplitud de vibración en dirección paralela al eje de la broca (Figura 1.4), con suficiente amplitud como para provocar la interrupción en el corte. Esto hace que el VATD sea un proceso de corte intermitente y no de corte continuo, facilitando la rotura de la viruta y su posterior evacuación. El resultado del taladrado mejora en términos de temperatura alcanzada y de precisión del agujero. La fuerza de avance se ve reducida en un 20-30%, en comparación con el taladrado convencional [18,53,54,68], lo que conlleva una disminución del daño por delaminación. Como consecuencia, se demostró que la eficiencia del taladrado [19] y la vida útil de la herramienta pueden mejorarse con respecto al taladrado convencional de materiales compuestos cuando se emplea la metodología VATD [53,54,68].

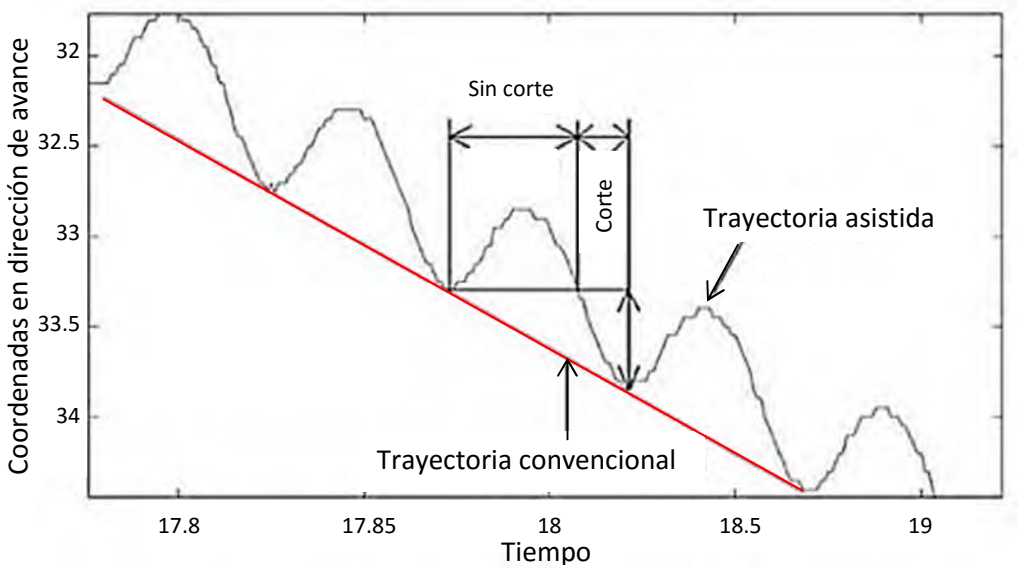

Figura 1.4: Comparación entre trayectoria de la herramienta en un proceso de taladrado convencional y asistido.

1.3.4 TALADRADO A ALTA VELOCIDAD

El taladrado de alta velocidad (Velocidad de corte > 9000 rpm) se ha convertido en una tecnología generalizada debido a que conduce a una mayor productividad. Al igual que el taladrado asistido por vibración, este proceso es una de los más prometedores para reducir la delaminación. A diferencia del taladrado convencional, esta operación tiene que ser llevada a cabo en un equipo de taladrado de alta velocidad, los cuales son generalmente muy caros. Debido a esto, son pocas las investigaciones desarrolladas en este campo [13,27,28,46,47,49,72]. Todas obtuvieron como resultado una menor delaminación debido a la reducción de las fuerzas de avance. También se presentaron los efectos de las variables del proceso (como la velocidad de corte, la velocidad de avance, y el ángulo de punta de la broca helicoidal) en la delaminación [27,46,47, 72]. Los resultados revelaron por un lado, una tendencia decreciente en el daño con el aumento de la velocidad de corte y por otro lado, que la combinación de una velocidad de avance baja y un ángulo de punta pequeño es esencial para minimizar la delaminación.

1.4 Geometrías de Brocas y Materiales

Actualmente existen muchas geometrías de brocas diferentes como se observa en la Tabla 1.3. De acuerdo con la geometría, las brocas utilizadas en la literatura se pueden dividir en seis categorías: broca helicoidal, broca escalonada, broca con punta central, broca tipo fresa, broca de filos rectos, y broca de núcleo. Unas cuantas geometrías típicas se muestran en la Figura 1.5. Los materiales que se utilizan suelen ser diferentes, tales como el acero de alta velocidad (HSS), el carburo cementado sin recubrimiento (grados ISO K10, K20, etc.), el carburo cementado con recubrimiento y el diamante policristalino (PCD). Diferentes brocas y materiales se han utilizado en diversos estudios para tener una mejor comprensión del taladrado de laminados compuestos. La Tabla 1.3 muestra que las brocas helicoidales fabricadas en HSS o con carburos sin recubrimiento son las más ensayadas. La aplicación de otro tipo de brocas, como la broca escalonada o de filos rectos, es también muy común para intentar mejorar el proceso de corte.

Figura 1.5: (A) Broca de punta central, (B) broca-daga, (C) broca de filos rectos, (D) broca tipo fresa y (E) broca escalonada.

Tabla 1.3: Geometrías y materiales de broca utilizadas en la literatura para el taladrado de materiales compuestos.

Geometría	Material	Referencias
Broca Helicoidal	Acero rápido	Chen [14]; Zhang *et al*. [17]; Wang *et al*. [28]; Davim *et al*. [35]; Tsao *et al*. [39–41]; Ramkumar *et al*. [53,54]; Capello [55]; El-Sonbaty *et al*. [56]; Singh *et al*. [57,58]; Kilickap [62]; Khashaba [63]; Abrao *et al*. [71]; Ramulu *et al*. [75]; Kim *et al*. [76]; Hocheng *et al*. [90]
	Carburo cementado sin recubrimiento	Davim *et al*. [2,34]; Park *et al*. [11]; Lin and Chen [13]; Chen [14]; Wang *et al*. [18]; Sardinas *et al*. [20]; Durao *et al*. [23]; Zitoune *et al*. [25]; Rawat *et al*. [27,28]; Iliescu *et al*. [31]; Gaitonde *et al*. [46]; Karnik *et al*. [47]; Faraz *et al*. [48]; Shyha *et al*. [49,80,104]; Lazar *et al*. [51]; Singh *et al*. [57]; Khashaba *et al*. [64,65]; Velayudham *et al*. [66,67]; Abrao *et al*. [71]; Rubio *et al*. [72]; Isik *et al*. [73]; Ramulu *et al*. [75]; Kim *et al*. [76]; Brinksmeier *et al*. [77]; Zitoune *et al*. [79]; Park *et al*. [104]
	Carburo cementado con recubrimiento	Iliescu *et al*. [31]; Shyha *et al*. [49,80,103]; Liu *et al*. [50]; Mohan *et al*. [85]
	Diamante policristalino (PCD)	Park *et al*. [104]
Broca escalonada	Acero rápido	Tsao *et al*. [39,40]; Tsao [43]; Hocheng *et al*. [90,45]
	Carburo cementado	Brinksmeier *et al*. [77]; Shyha *et al*. [29,49]; Durao *et al*. [23]
Broca de punta central	Acero rápido	Tsao *et al*. [39,40]; Hocheng *et al*. [90,45]
	Carburo cementado	Davim *et al*. [2,102]; Abrao *et al*. [71]; Rubio *et al*. [72]; Durao *et al*. [23]
Broca tipo fresa	Acero rápido	Tsao *et al*. [39,40]; Hocheng *et al*. [90,45]
	Carburo cementado	Faraz *et al*. [48]; Abrao *et al*. [71]
Broca de filos rectos	Carburo cementado	Piquet *et al*. [15]; Murphy *et al*. [16]; Faraz *et al*. [48]; Lazar *et al*. [51]; Fernandes *et al*. [87]
Broca de núcleo	Diamante policristalino (PCD)	Park *et al*. [11]; Tsao *et al*. [30,40,42]; Jain *et al*. [89]; Hocheng *et al*. [90,45]

La influencia de la geometría de la broca en la calidad de los taladros (como la reducción de la delaminación) ha sido estudiada por varios autores [13,25,39,45,71,72,90]. El material de la broca también desempeña un papel importante en muchos aspectos del taladrado, como la prolongación de la vida útil [14,31] o la reducción de la delaminación [71,76]. Las ventajas y beneficios del uso de brocas con diferentes geometrías y materiales en el taladrado de laminados compuestos se describen en detalle en las siguientes secciones.

1.5 Delaminación Inducida por Taladrado.

La delaminación es un fenómeno de fallo inter-laminar inducido por la operación de taladrado. Es el daño más importante cuando se taladra compuestos laminados debido a que no sólo afecta a la tolerancia de ensamblado y su capacidad portante, sino que también potencia el deterioro de la estructura en servicio a largo plazo bajo cargas de fatiga [7,46,89,105]. La Figura 1.6 muestra varias imágenes SEM del daño por delaminación.

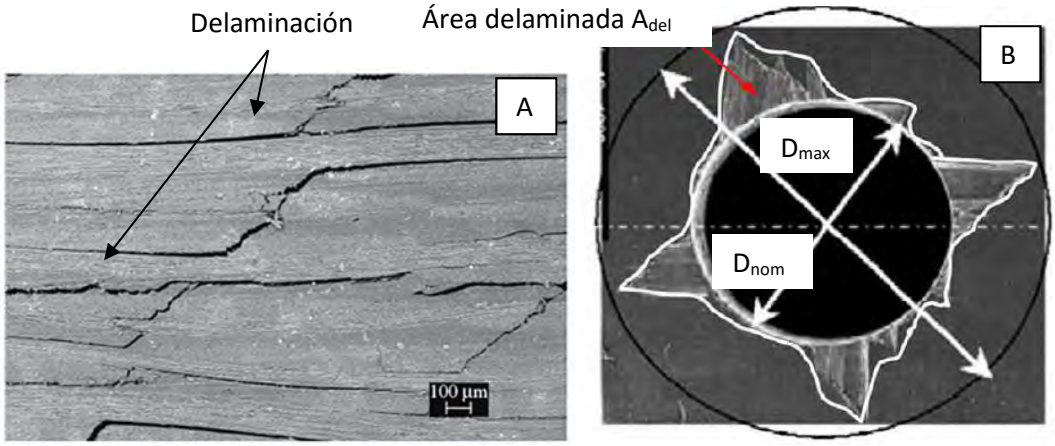

Figura 1.6: (A) Imagen SEM de delaminación de material FRP [106] y (B) Imagen de la superficie de material CFRP [27].

1.5.1 MECANISMOS DE DELAMINACIÓN INDUCIDA DURANTE EL TALADRADO

Las observaciones experimentales muestran que la delaminación inducida por el taladrado se produce en la periferia tanto a la entrada como a la salida de los agujeros taladrados. El ''Peel-up '' y el ''Push-out '' son dos mecanismos de delaminación distinguibles asociados a esta operación y referidos en la literatura [9,23,34,37,41,55,63,78,89-45,105,108,109].

La delaminación Peel-up se produce en el lado de entrada de la broca, alrededor del taladro como muestra la Figura 1.7B. Cuando los filos de corte de la broca hacen contacto con el material compuesto, aparece una fuerza de pelado a través de la pendiente de los canales de la broca que tira del material hacia arriba. Es entonces cuando se produce la separación de las capas entre sí y se genera el daño alrededor de la zona antes mencionada.

La delaminación Push-out se produce en la cara de salida, también en la periferia del agujero, como se observa en la Figura 1.8A. Cuando la broca se acerca al lado de la salida del agujero, las capas sin cortar debajo de la punta de la broca se hacen más susceptibles a la deformación debido a la disminución del grosor. La delaminación Push-out aparece si la fuerza de empuje aplicada a las capas sin cortar excede la resistencia de unión entre láminas. En la práctica, se ha encontrado que la delaminación asociada con el Push-out es más severa que la asociada con el Peel-up [29,63-65]. Por esta razón, la mayoría de los estudios anteriores prestan más atención a este segundo fenómeno que al primero.

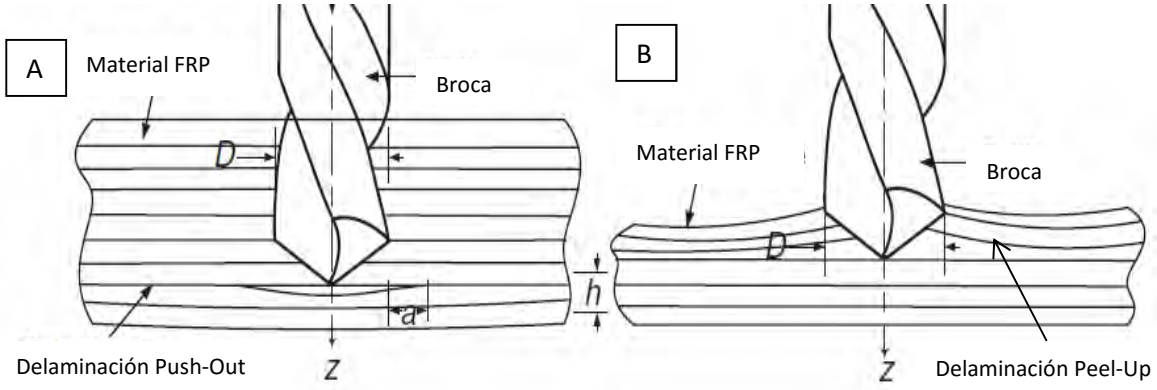

Figura 1.7: Mecanismos de delaminación en los materiales laminados FRP: (A) Peel-up y (B) Push-out.

1.5.2 MEDIDA DE LA DELAMINACIÓN

Existen varios parámetros para cuantificar el nivel de daño por delaminación alrededor del agujero taladrado. El primero es el factor de delaminación unidimensional (F_d). Observando la Figura 1.6B, se define como la relación entre el diámetro máximo (D_{max}) de la zona delaminada (círculo negro) y el diámetro nominal (D_{nom}) del orificio perforado (círculo blanco sólido). La ecuación 1.1 recoge esta expresión.

$$F_d = \frac{D_{\max}}{D_{nom}} \tag{1.1}$$

El criterio basado en F_d puede presentar, sin embargo, una incoherencia inherente; se puede obtener el mismo valor de delaminación en dos casos en los que la extensión diametral de la zona dañada sea la misma, pero con anchuras significativas distintas. En este caso, el factor no representará la zona real afectada en la periferia agujero [48]. Para representar el nivel de daño por delaminación en estas condiciones, puede ser más razonable utilizar el factor de delaminación bidimensional (F_a) descrito en la ecuación 1.2, donde A_{del} es el área delaminada (marcada por la línea blanca en la Figura 1.6B) y A_{nom} es el área nominal del taladro (círculo blanco sólido) [48].

$$F_a = \left(\frac{A_{del} - A_{nom}}{A_{nom}} \right)\% \tag{1.2}$$

Davim *et al.* [37] propusieron un tercer factor denominado factor de delaminación ajustado (F_{da}) basado en el análisis de imagen digital. La expresión viene definida mediante la ecuación 1.3, donde A_{max} es el área relacionada con el diámetro máximo de la zona de delaminación (D_{max}); los parámetros α y β se utilizan como pesos en las dos partes de la ecuación; la primera parte de esta ecuación representa la contribución del tamaño de la fisura, mientras que la segunda parte representa la contribución del área dañada. Pese a los beneficios que puede presentar esté último método, F_d se utiliza con más frecuencia que F_a y F_{da} debido a su uso más práctico.

$$F_{da} = \alpha \frac{D_{\max}}{D_{nom}} + \beta \frac{A_{\max}}{A_{nom}} \tag{1.3}$$

Por último, existen diferentes exámenes no destructivos comúnmente utilizados para observar el daño inducido por delaminación en el taladrado de compuestos laminados. Entre éstas metodologías se encuentran la microscopia óptica [2,28,34,35,46,47,66,76,102], el estereoscopio [48], ultrasonidos C-scan [39,41,44,45,67,45], técnica de fotografía digital [63-65], láser de técnica Moiré basado en sombra de imagen [108], y la tomografía de rayos X computarizada (CT) [14,22,23,40].

1.5.3 EFECTOS DE LAS VARIABLES DE ENTRADA EN LA DELAMINACIÓN

La Figura 1.8 recoge un resumen de los efectos de las variables de entrada (el avance, la velocidad de corte y el ángulo de punta de la broca) en la delaminación. En esta figura se observa que los resultados de diferentes investigaciones coinciden en la idea de que la delaminación aumenta con la velocidad de avance a cualquier velocidad de corte independientemente de la geometría de brocas. Este fenómeno se atribuye al aumento de la fuerza de empuje con el avance.

La relación entre la velocidad de corte y la delaminación, sin embargo, mostró un comportamiento distinto. Los investigadores observaron dos relaciones diferentes en función de las condiciones de corte, como muestra la Figura 1.8B. Davim *et al*. [2,34,35], Sardinas *et al*. [20], y Kilickap [62] indicaron que la delaminación aumentaba con la velocidad de corte durante el taladrado convencional. Sin embargo, Khashaba *et al*. [63,64] observó justo el efecto contrario durante el taladrado convencional en material tejido CFRP; Gaitonde *et al*. [46] también manifestó que el daño inducido disminuía con la velocidad de corte durante el taladrado de alta velocidad en laminados delgados de capas tejidas de CFRP. Pese a esta discordancia en los resultados, se concluyó que el efecto de la velocidad de avance en la delaminación es mucho mayor que el de la velocidad de corte. Los resultados experimentales obtenidos por la mayoría de los investigadores mostraron que la delaminación se producía incluso para avances pequeños. Por lo tanto, para prevenir la delaminación alrededor de los agujeros y mejorar, al mismo tiempo, la eficiencia del taladrado, se recomienda el uso de máquinas CNC de modo que se tenga un buen control sobre la variación del avance durante el proceso de taladrado.

Algunos investigadores analizaron el efecto del ángulo de punta de la broca helicoidal en la delaminación como se observa en la Figura 1.8C. Gaitonde *et al*. [46,47] observó que la tendencia de la delaminación es creciente con el ángulo de punta de la broca helicoidal (material de la herramienta: carburo cementado K20), tanto en el caso de taladrado convencional como en el de alta velocidad para compuestos laminados de capas tejidas CFRP. Sin embargo, Kilickap [62] mostró una tendencia opuesta durante el taladrado convencional de laminados con capas UD de GFRP (material de la herramienta: acero de alta velocidad).

Como se puede observar, existe en general una falta de consenso acerca de la influencia de determinados parámetros en la delaminación del material. Este hecho hace necesario que se continúe avanzando en el conocimiento del tema mediante nuevas investigaciones.

1. Davim *et al*. [2,35-36]
2. Rsardinas *et al*. [22]
3. Kilickap [63]
4. Khashaba *et al*. [64-65]
5. Gaitonde *et al*. [47-48]
6. Rubio *et al*. [73]
7. Rawat *et al*. [28]
8. Tsao *et al*. [41]
9. Arul *et al*. [70]

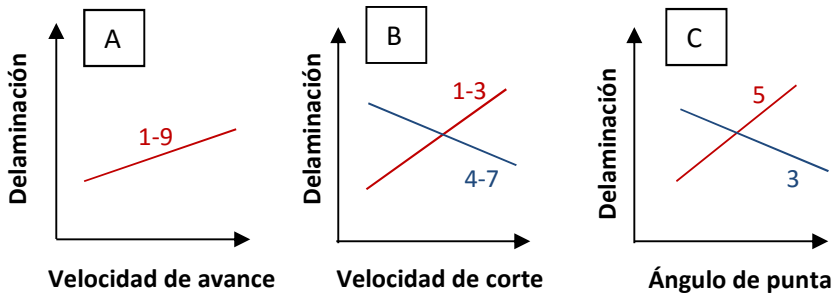

Figura 1.8: Efectos de las variables de entrada en la delaminación cuando se taladra materiales compuestos laminados.

A parte de los estudios centrados en el taladrado convencional, dos métodos de taladrado avanzado como son el taladrado asistido por vibración (VATD) y el taladrado de alta velocidad (HSD) se estudiaron con el objetivo de disminuir la delaminación. Utilizando brocas de acero rápido, Arul *et al*. [69] llevó a cabo una serie de experimentos, tanto en taladrado convencional como asistido por vibración, en material compuesto tejido GFRP con la intención de comparar la delaminación en ambas operaciones. Los resultados mostraron que el daño por delaminación en el caso del VATD fue menor que el inducido en el taladrado convencional debido a la disminución de la fuerza de avance. Gaitonde *et al*. [46,47], Rubio *et al*, [72] y Rawat & Attia [27] presentaron en sus investigaciones los efectos que los parámetros del proceso tienen en el taladrado convencional y de alta velocidad. Concluyeron que el HSD es una metodología prometedora debido a que el daño obtenido es menor que en el taladrado convencional.

Algunos modelos empíricos que describen la correlación entre el factor de delaminación inducida y las variables de entrada, obtenidos mediante la utilización de análisis de correlación lineal, se resumen en la Tabla 1.4. Los modelos proporcionan una buena estimación del factor de daño en condiciones de taladrado similares con brocas y materiales parecidos.

Tabla 1.4: Modelos empíricos de delaminación obtenidos utilizando análisis de regresión lineal.

Referencias	**Modelo empírico**	**Condiciones de taladrado**
Davim *et al*. [34]	**a.** $F_d = 0.966 + 1.085\cdot10^{-3}V_c + 0.134f$ **b.** $F_d = 1.006 + 1.980\cdot10^{-4}V_c + 0.021f$	Tejido CFRP (e = 3 mm) *Vc*: 30–50 m/min *f*: 0.05–0.20 mm/rev **a.** Broca helicoidal (Carburo) **b.** Broca de punta central (Carburo) Diámetro = 5 mm
Tsao *et al*. [39]	**a.** $F_d = 1.961 - 10.955f - 1.81\cdot10^{-4}S - 1.77\cdot 10^{-2}d$ **b.** $F_d = 1.539 - 2.274f - 7.81\cdot10^{-6}S - 1.7\cdot10^{-2}d$ **c.** $F_d = 1.508 - 3.385f + 8.681\cdot10^{-6}S - 1.49\cdot 10^{-2}d$	Tejido CFRP (e = 3 mm) *n*: 800 – 1200 rpm *f*: 0.01 – 0.03 mm/rev **a.** Broca helicoidal (HSS) **b.** Broca de punta central(HSS) **c.** Broca tipo fresa (HSS) Diámetro = 6, 8, 10mm
Sardinas *et al*. [20]	$F_d = 1.93f^{0.1429}\cdot V_c^{0.1022}$	UD CFRP *Vc*: 30–50 m/min *f*: 0.05–0.2 mm/rev Broca helicoidal (Carburo) Diámetro = 5 mm
Gaitonde *et al*. [46]	$F_d = -0.810444 - 1.889\cdot10^{-3}V_c - 0.109957f + 0.03454\,\theta + 1.1\cdot10^{-5}V_cf - 9\cdot10^{-6}V_c\theta + 1.67\cdot10^{-3}f\,\theta + 3\cdot10^{-6}V_c^2 + 5.53\cdot10^{-3}f^2 - 1.15\cdot10^{-4}\theta^2$	Tejido CFRP (T = 2.5 mm) *Vc*: 60–600 m/min *f*: 1–6 m/min Broca helicoidal (Carburo) Diámetro = 5 mm Ángulo de punta (θ): 85–130°
Khashaba *et al*. [65]	$F_d = 1.482 + 1.44\cdot10^{-3}V_c + 3.143f + 0.0193W$	Tejido GFRP (T = 8.3 mm) *Vc*: 6.5–50.5 m/min *f*: 0.056–0.45 mm/rev Broca helicoidal (Carburo) Diámetro = 8 mm Pre-desgaste de la herramienta (W): 0–$34\cdot10^{-4}$ g

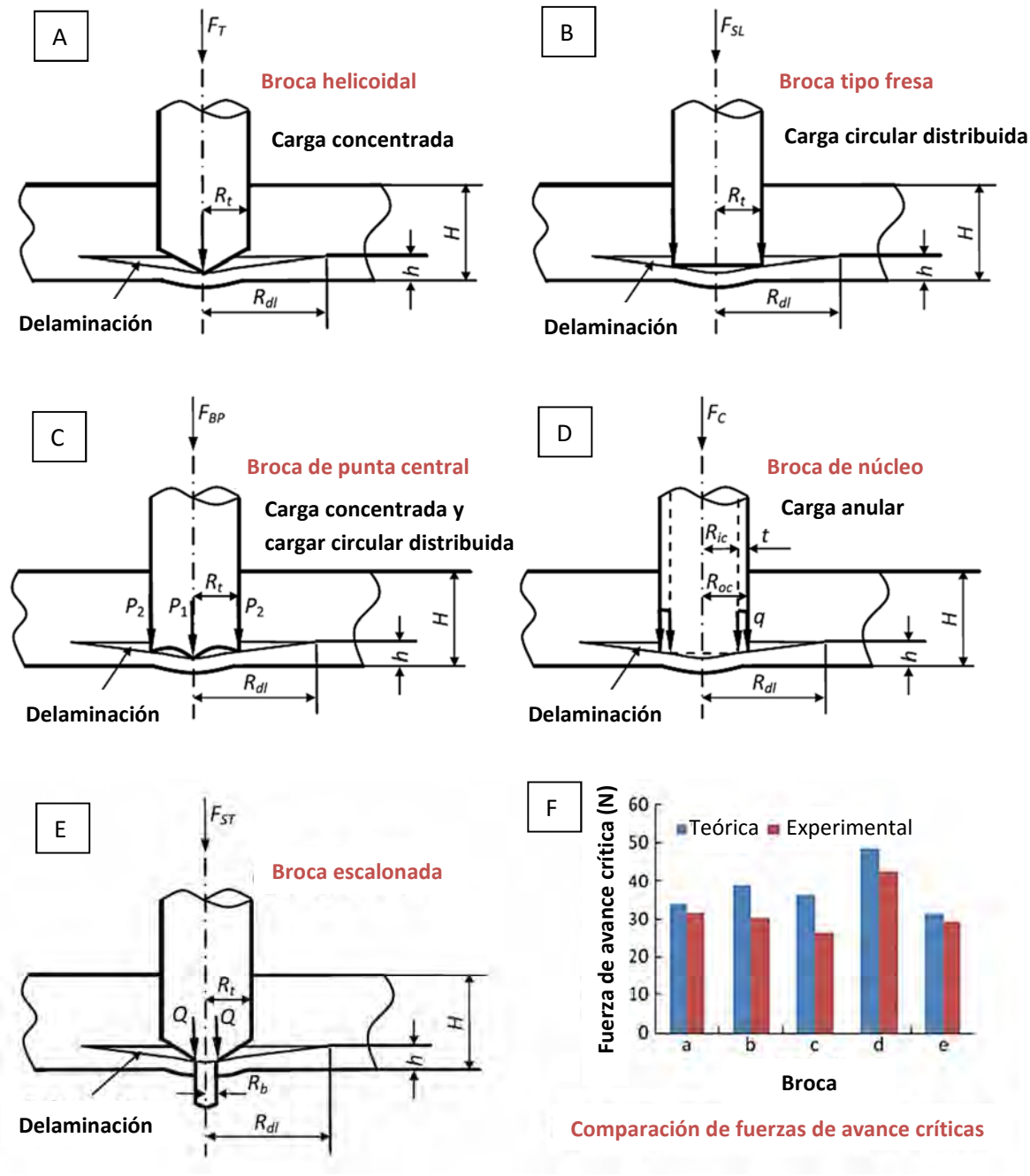

Figura 1.9: Esquemas de análisis de la delaminación para diferentes geometrías de broca ([45,90, 111]).

1.6 Fuerza de Avance

1.6.1 RELACIÓN ENTRE LA FUERZA DE AVANCE Y LA DELAMINACIÓN

La fuerza de avance durante el taladrado es uno de los factores claves que describe la maquinabilidad de los compuestos laminados LFRPs debido al hecho de que afecta directamente a la calidad de los agujeros taladrados [64]. El tamaño de la zona delaminada se ha relacionado con la fuerza de avance obtenida durante el taladrado. Los investigadores coinciden en la idea de que existe una fuerza crítica por debajo de la cual no aparece delaminación [111]. El primer

modelo analítico que determinó la fuerza crítica de avance fue desarrollado por Hocheng y Dharan [105]. Emplearon el método de mecánica de fractura elástica lineal (LEFM por sus siglas en inglés) para obtener el modelo de fuerza crítica de avance para una broca helicoidal relacionándolo con la delaminación de salida, la cual se usa como guía para prevenir la delaminación. En este modelo, la fuerza crítica de avance para el inicio de la delaminación (F_{CT}), simplificada como una carga puntual aplicada en el centro del agujero, depende de las propiedades de la pieza de trabajo (aproximado como cuasi-isótropo) y de las láminas sin cortar por debajo de la broca. Hocheng y Tsao también desarrollaron una serie de modelos analíticos comprensivos de fuerza de avance para diferentes geometrías de broca (Figura 1.9) que se compararon con el modelo convencional de broca helicoidal [90,45,111]. Todos estos modelos se recogen en la Tabla 1.5. La comparación entre los resultados predichos y experimentales de la fuerza de avance crítica se muestra en la Figura 1.9F, la cual revela que los modelos teóricos de la Tabla 1.5 estiman razonablemente bien.

La fuerza de empuje en el modelo desarrollado por Hocheng y Dharan [105] para la broca helicoidal se consideró como una carga concentrada aplicada en el centro de la broca. Sin embargo, en la realidad la fuerza se extiende sobre el borde de unión de los filos de corte en la primera fase de apertura de la grieta en modo I. Upadhyay y Lyon [109] modificaron el modelo mencionado anteriormente asumiendo la fuerza de empuje como una carga distribuida uniformemente sobre el diámetro de la broca en lugar de una carga concentrada, descrita por la siguiente ecuación:

$$F_{CT}^{*} = \frac{1}{\sqrt{1 - R_t^2 / 2R_{dl}^2}} F_{CT} \tag{1.4}$$

Tabla 1.5: Modelos empíricos de delaminación obtenidos utilizando análisis de regresión lineal para la Fig.1.9.

Geometría	Modelo de fuerza crítica	Observaciones
Broca helicoidal	$F_{CT} = \pi\left[\frac{8G_{IC}Eh^3}{3(1-\nu^2)}\right]^{1/2}$	E= Modulo elástico ν= Modulo de Poissom G_{IC}=Indice de energía crítica de deformación (modo I) R_t= Radio de la broca R_{dl}= Radio de delaminación $S=R_t/R_{dl}$ α=Ratio entre la carga concentrada (P1) y la carga circular periférica (P2) t=Espesor de la pared de la broca de nucleo R_{oc}= Radio exterior de la broca de nucleo $\gamma=R_{oc}/R_{dl}$ $\beta=t/R_{oc}$ R_b= Radio del escalón $\xi=R_b/R_t$
Broca tipo fresa	$F_{CSL} = \frac{1}{\sqrt{1-2S^2+S^4}} F_{CT}$	
Broca de punta central	$F_{CBP} = \frac{1+\alpha}{\sqrt{1+\alpha^2(1-2S^2+S^4)}} F_{CT}$	
Broca de nucleo	$F_{CC} = \frac{\beta(2-\beta)}{\sqrt{\left[1-(1-\beta)^4\right]-(1/2)\gamma^2\left[1-(1-\beta)^6\right]}} F_{CT}$	
Broca escalonada	$F_{CST} = \frac{\sqrt{2}}{1-\nu}\left\{\frac{\left[(1-\nu)+2(1+\nu)\xi^2\right]^2}{(1+\nu)\left[2(1-\nu)(1+2\nu^2)-12(12-4\nu+3\nu^2+3\nu^3)\xi^2-8(1+3\nu)\xi^2\ln\xi\right]}\right\}^{1/2} F_{CT}$	

Algunos autores también observaron una correlación positiva aproximadamente lineal entre la delaminación y la fuerza de avance para geometrías diferentes a la broca convencional helicoidal [39,45,48,64]. Este resultado confirma que la clave para evitar el daño durante el taladrado, para valores de fuerza mayores que la crítica, radica en la reducción de la fuerza de empuje a través de la optimización de las variables de entrada.

1.6.2 EFECTOS DE LAS VARIABLES DE ENTRADA EN LA FUERZA DE AVANCE

La fuerza de avance durante el taladrado de laminados compuestos depende de las variables de entrada, como son la velocidad de corte o velocidad de giro, la velocidad de avance, la geometría de la broca, el número de taladros (desgaste de la herramienta), y la operación de taladrado. La tendencia de los efectos de estas variables (en valor pico o media de fuerza de avance) se resumen en la Figura 1.10.

Se aprecia en las Figuras 1.10A y 1.10B que la mayoría de los investigadores encontraron que el efecto de la velocidad de corte en la fuerza de avance es insignificante, disminuyendo la fuerza ligeramente con el aumento de velocidad de corte. Contrario a esto, el efecto de la velocidad de alimentación en éste parámetro es notable, aumentando la fuerza con la velocidad de alimentación.

Pese a que se ha mencionado que la velocidad de corte no tiene una influencia importante en la fuerza de avance, Khashaba *et al*. [65] encontró que este parámetro se vuelve relevante cuando se incrementa el desgaste de la herramienta. La Figura 1.11 ilustra el efecto del pre-desgaste de la broca en la fuerza de empuje a diferentes velocidades de corte (velocidad de avance constante f = 0,22 mm/rev). Se observa que, en efecto, la influencia de la velocidad de corte en la fuerza cuando se utilizan brocas nuevas en material GFRP es despreciable. Sin embargo, cuando se usan brocas pre-desgastadas, la fuerza de empuje aumenta notablemente al junto con la velocidad de corte.

1. Chen 1997 [14]
2. El-Sonbaty *et al*. 2004 [56]
3. Khashaba 2004 [63]
4. Sardinas *et al*. 2006 [20]
5. Velayudham *et al*. 2005 [66]
6. Singh *et al*. 2008 [58]
7. Abrao *et al*. 2008 [71]
8. Liu *et al*. 2010 [50]
9. Khashaba *et al*. 2010 [64]
10. Zhang *et al*. 2001 [91]
11. Arul *et al*. 2006 [69]
12. Fernandes *et al*. 2006 [87]
13. Durao *et al*. 2010 [23]
14. Khasaba *et al*. 2010 [65]
15. Murphy *et al*. 2002 [16]
16. Faraz *et al*. 2009 [48]
17. Rawat *et al*. 2009 [27]

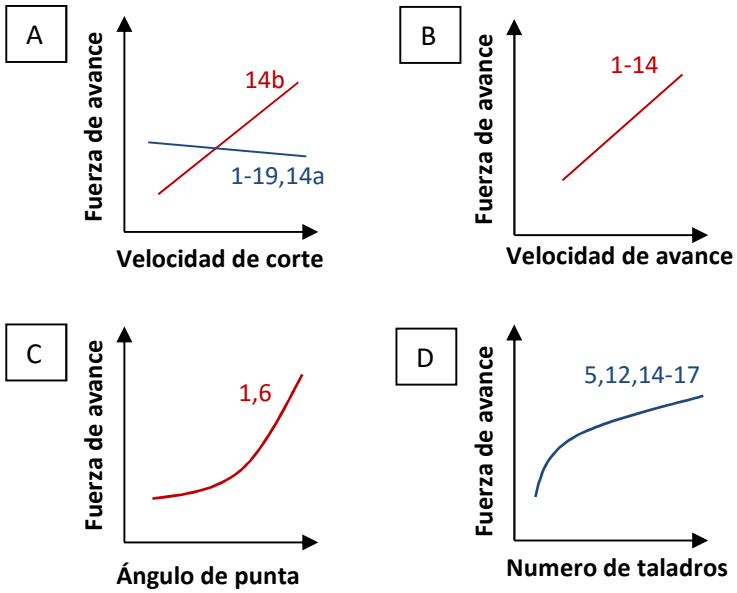

Figura 1.10: Esquemas de análisis de delaminación para diferentes brocas ([90,45,111]).

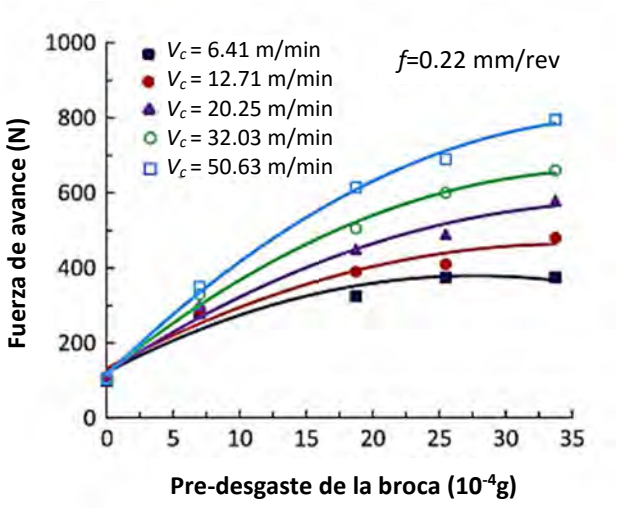

Figura 1.11: Efecto del pre-desgaste de la broca en la fuerza a diferentes velocidades de corte durante el taladrado de material GFRP [65].

La fuerza de avance no se ve solamente afectada por estas dos velocidades. La geometría de la broca también afecta significativamente a este parámetro. Por un lado, la Figura 1.10C pone de relieve que el ángulo de punta de la broca helicoidal tiene un claro efecto sobre la fuerza, incrementándose notablemente al aumentar el ángulo [14,58], por lo que un ángulo de punta pequeño es una buena opción para disminuir la fuerza de empuje. Por otro lado, Durao *et al*. [23] y Abrao *et al*. [71] se centraron en analizar el efecto de distintas geometrías de broca en la fuerza de avance durante el taladrado de materiales compuestos GFRP y CFRP respectivamente. Los valores de fuerza más bajos se obtuvieron al taladrar laminados utilizando brocas de punta central y escalonada frente a brocas helicoidales y brocas tipo fresa.

La influencia del número de taladrados en la fuerza de avance se resume en la Figura 1.10D. Se observa que, debido principalmente al desgate de la herramienta, cuanto mayor es el número de agujeros, mayor es la fuerza de avance [16,27,48,65,66,87]. Sin embargo, la velocidad de desgaste no es constante, siendo más alta en la primera etapa de la vida de la broca que en la etapa posterior. Este hecho se comentará más adelante.

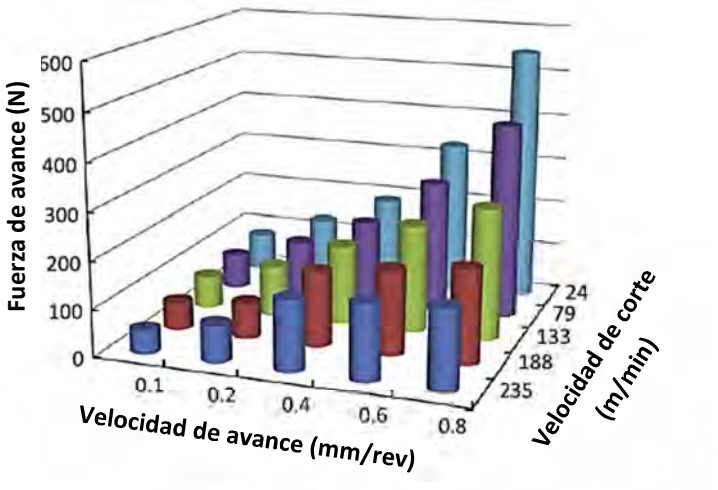

Figura 1.12: Efecto de la velocidad de corte y de la velocidad de avance en la fuerza durante el taladrado convencional y de alta velocidad para material CFRP [26].

En diversas investigaciones se encontró que la fuerza de avance, durante el taladrado asistido con vibración a baja frecuencia de laminados compuestos, es un 20-30% menor que la obtenida en el taladrado convencional en las mismas condiciones de corte [18,53,54,69,91]. La Figura 1.12 ilustra dicho efecto durante el taladrado de materiales CFRP bajo diferentes velocidades de alimentación utilizando brocas helicoidales de carburo cementado [27]. Se muestra como en el taladrado de alta velocidad (velocidad de corte> 80 m/min) la fuerza de avance es menor que en el taladrado convencional, especialmente a alta velocidad de alimentación (≥ 0.6 mm/rev). Sin embargo, el efecto de variar la velocidad de avance no es significativo cuando se trabaja a alta velocidad mientras que si lo es en el caso del taladrado convencional. Por lo tanto, es recomendable el uso de una alta velocidad de avance cuando se taladrada a alta velocidad para conseguir una reducción en la fuerza de empuje.

Varios modelos empíricos que relacionan la fuerza de avance y las variables de entrada obtenidos mediante análisis de regresión lineal se resumen en la Tabla 1.6.

Tabla 1.6: Modelos empíricos de la fuerza de avance cuando se taladra compuestos laminados.

Modelo empírico de fuerza de avance	**Condiciones de taladrado**	**Referencia**
$F_{T1} = (0.003S + 1.0467)\cdot[76.56(f\cdot d)^{0.39} + 1.047d^2]$ $F_{T2} = (0.0036S + 1.2128)\cdot[76.56(f\cdot d)^{0.39} + 1.047d^2]$ $F_{T3} = (0.0035S + 1.5159)\cdot[76.56(f\cdot d)^{0.39} + 1.047d^2]$	CFRP (T_1=2, T_2=2.2, T_3=5.2 mm); *S*: 750 – 1500 rpm; *f*: 0.03 – 0.12 mm/rev; Broca de filos rectos (Carburo); Diámetro (d) = 4.9 mm	Fernandes *et al*. [87,88]
$F_T = -23.03 + 54W_t + 0.181G - 224f + 9.575\cdot10^{-2}S$	Tejido CFRP (T = 3.6 mm); *S*: 800–1200 rpm; *f*: 0.0375–0.0625 mm/rev; Broca de núcleo (abrasivo de diamante); Tamaños de abrasivo (*G*): 100–400µm; Diámetro (*d*) = 10 mm; Espesor del núcleo (W_t): 0.8–1.2 mm;	Tsao *et al*. [42]
$F_T = 1.4365\theta + 402.8315f - 98.0319$	UD GFRP (T = 3 mm); *S*: 375–1500 rpm; *f*: 0.075–0.3 mm/rev; Broca helicoidal (HSS); Diámetro (d) = 6mm; Ángulo de punta (θ): 90–118°	Singh *et al*. [58]
$F_T = 115.82 - 0.912\gamma - 224.25\xi + 1.975\gamma\xi + 352.778f - 1.028\cdot10^{-3}S$	Tejido CFRP (T = 6 mm); *S*: 800–1200 rpm *f*: 0.01–0.03 mm/rev; Broca escalonada (HSS); Diámetro (d) = 10 mm; Longitud del primer escalón: 7 mm; Ratio entre diámetros (ξ): 0.2–0.6; Angulo del escalón (γ): 80–120°;	Tsao [43]
$F_T = -161 + 3.71V_C + 977.781f + 12.793w$	Ángulo de punta (θ): 118° Tejido GFRP (T = 8.3 mm); V_c: 6.5–50.5 m/min; *f*: 0.056–0.45 mm/rev; Broca helicoidal (Carburo); Diametro (d) = 8mm; Pre-desgaste (w): 0–$34\cdot10^{-4}$ g	Khashaba *et al*. [65]

1.7 Desgaste de la Herramienta

El desgaste de la herramienta puede ser el causante de algunos defectos como la delaminación, el astillamiento del borde o la formación de grietas [28,41,65]. Si estos daños son excesivos, pueden tener un impacto económico significativo, especialmente cuando el número de agujeros taladrados es alto. Por lo tanto, para lograr la calidad deseada en los taladros y prolongar la vida útil de la herramienta, es necesario entender cómo actúan los mecanismos de desgaste y cómo las variables de entrada afectan al desgaste de la broca. En comparación con el mecanizado de metales, las investigaciones sobre los fenómenos de desgaste en el taladrado de materiales compuestos son muy reducidas.

1.7.1 MECANISMOS DE DESGASTE DE LA HERRAMIENTA

El desgaste de la herramienta durante el taladrado de laminados LFRPs se produce de diferente manera, dependiendo de las combinaciones entre la herramienta/pieza de trabajo y los parámetros de taladrado. Diferentes materiales para herramienta, como el acero de alta velocidad (HSS) [71], el carburo cementado [28], y el carburos recubierto de diamante [31] han sido ensayados para entender los mecanismos de desgaste de la herramienta y poder extender la vida de la misma. Estos mecanismos se caracterizan por la carga fluctuante que actúa sobre el filo de corte (influenciada por la anisotropía de las fibras duras) y la interacción termo-mecánica entre la broca y el compuesto laminado debida a la muy baja conductividad térmica en comparación con los materiales metálicos. Las fibras duras y abrasivas causan un desgaste excesivo de la herramienta y generan calor por fricción, mientras que la matriz blanda y pegajosa genera un crecimiento de filo [14]. Se definen, por lo tanto, el desgaste abrasivo, el astillamiento, y la adhesión como los mecanismos de desgaste de la herramienta asociados al taladrado de materiales laminados FRPs.

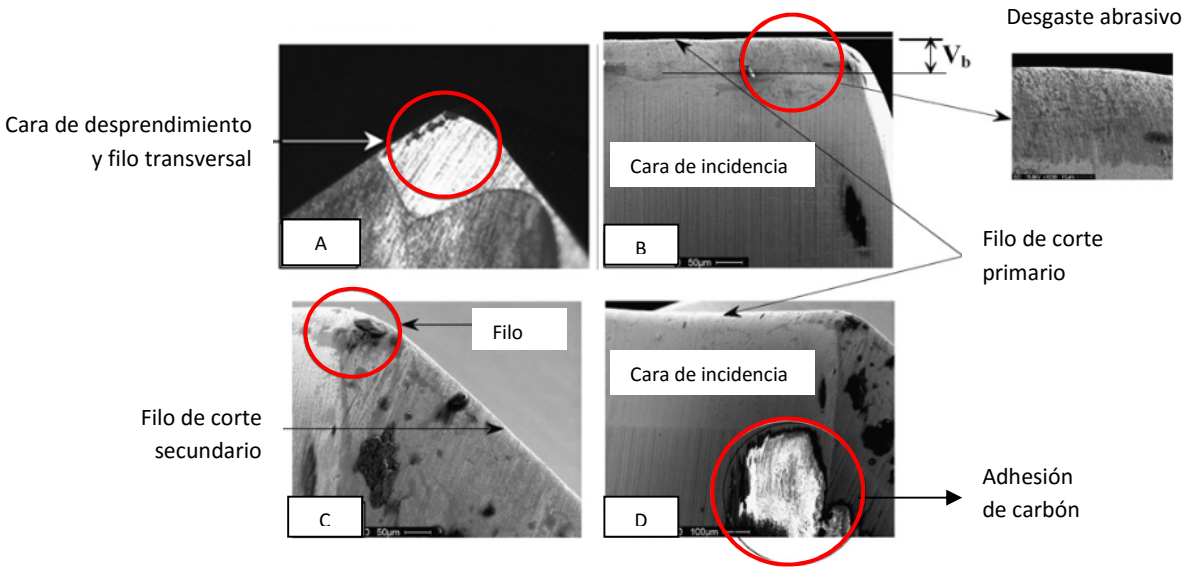

Figura 1.13: Imágenes SEM del desgaste observado durante el taladrado de material CFRP con una broca de carburo cementado (WC) una velocidad de corte de 15,000 rpm y velocidad de avance de 0.1 mm/rev: (A) astillamiento del filo transversal, (B) desgaste abrasivo en la cara de incidencia (próximo al eje de corte primario), (C) redondeo de filo y (D) adhesión de carbono en la cara de incidencia [28].

El mecanismo de desgaste abrasivo es un desgaste mecánico causado por la acción de erosión que las fibras duras causan en la broca. Varios trabajos de investigación identificaron este fenómeno como el desgaste dominante en la herramienta tanto en el taladrado convencional, como en el caso de alta velocidad. Se genera debido a la naturaleza altamente abrasiva de las fibras ya sean de carbono o de vidrio [14,28,31,66]. La Figura 1.13B muestra un ejemplo de este desgaste en la cara de desprendimiento de una broca helicoidal de carburo cementado sin recubrimiento, utilizada en el taladrado de alta velocidad de un material CFRP [28].

Es importante aclarar que, el desgaste de la herramienta no es siempre uniforme. Rawat y Attia [28] analizaron la evolución del desgaste durante el taladrado a alta velocidad de un laminado CFRP con brocas de carburo cementado. Las regiones de desgaste se dividieron en tres en función del desgaste de flanco V_b como se muestra en la Figura 1.14:

- En la región inicial (**zona primaria**), el desgaste de la herramienta fue causado por astillamiento y la formación de micro-grietas. Se observó en el filo transversal, en la cara de desprendimiento y en el filo secundario como muestra la fotografía de la Figura 5.13A. Durante el inicio de la operación, el astillamiento aparece debido a que el filo de la broca nueva (muy agudo), sufre las fuerzas de corte sobre un área de contacto relativamente pequeña, y no es capaz de soportar el alto estado tensional. Este fenómeno también fue observado por Lin y Chen [13] y Shyha *et al*. [29].

- En la región constante (**zona secundaria**), tras el desgaste inicial o redondeo del filo (Figura 5.13C), el área de contacto entre pieza y herramienta aumenta y las tensiones de contacto disminuyen. El desgaste abrasivo fue observado en la cara de incidencia, pero crece de forma más suave.

- En la región de desgaste grave (**zona terciaria**), el desgaste crece de nuevo más rápidamente. La adhesión de carbono se dio en la cara de incidencia debido a la alta temperatura del taladrado, (Figura 1.13D [28]). Un intenso desgaste por adherencia se observó también en la broca de carburo cementado en el taladrado de GFRP bajo condiciones de corte convencionales [66]. A pesar de ello, el desgaste adhesivo no fue tan dominante como el desgaste abrasivo.

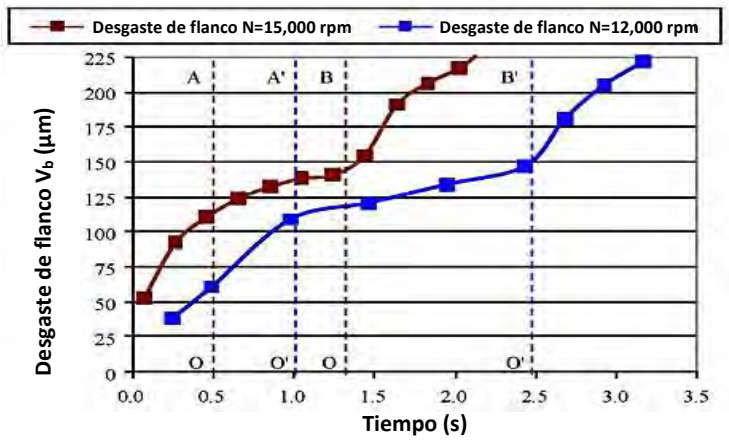

Figura 1.14: Progresión del desgaste de una broca de carburo para una velocidad de avance de 100 µm/rev. Las líneas OA y O´A´ indican el final de la región de desgaste primario y las líneas OB y O´B´ indican el final de región de desgaste secundario [28].

Aunque existen diferentes modos de desgaste de las herramientas de taladrado de compuestos laminados LFRPs, el desgaste del flanco es el más importante en la mayoría de condiciones de taladrado [14,28,29,31,48,66,75,76]. Por ejemplo, Iliescu *et al*. [31] encontró que apenas existía desgaste en la cara de desprendimiento. Sin embargo, si se encontró desgaste en la cara de incidencia cuando se utilizaron brocas helicoidales de carburo cementado con recubrimiento de diamante en compuestos laminados CFRP y condiciones de taladrado convencionales (Figura 1.15). En la cara de incidencia, el revestimiento de diamante desapareció en pequeños fragmentos, dejando el carburo sin protección. Por lo tanto, el desgaste del flanco es utilizado frecuentemente para describir el nivel de desgaste de las brocas.

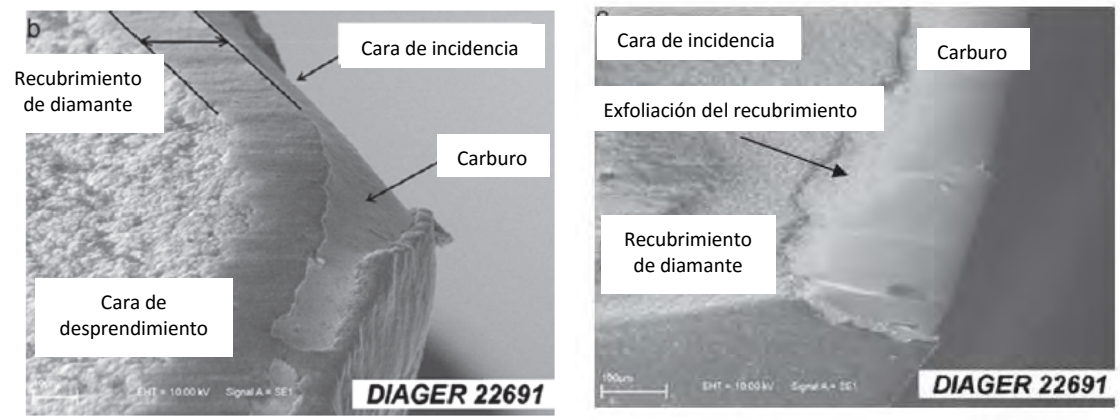

Figura 1.15: Exfoliación del recubrimiento de diamante de brocas de carburo con recubrimiento tras taladrar 309 agujeros en un compuesto laminado CFRP [31].

1.7.2 EFECTOS DE LAS VARIABLES DE ENTRADA EN EL DESGASTE DE LA HERRAMIENTA

El desgaste de flanco de la broca es sensible a los cambios en la velocidad de corte (velocidad de husillo) y a la velocidad de avance, como se muestra en la Figura 1.16. Se puede observar en dicha figura que, en general, el desgaste aumenta y la vida de la herramienta disminuye cuando se aumenta tanto la velocidad de corte como la velocidad de alimentación. Sin embargo, Ramkumar *et al*. [53] observó que durante la operación de taladrado asistido por vibración a baja frecuencia de un material compuesto GFRP, la selección de un avance optimo produce un desgaste mínimo en la herramienta.

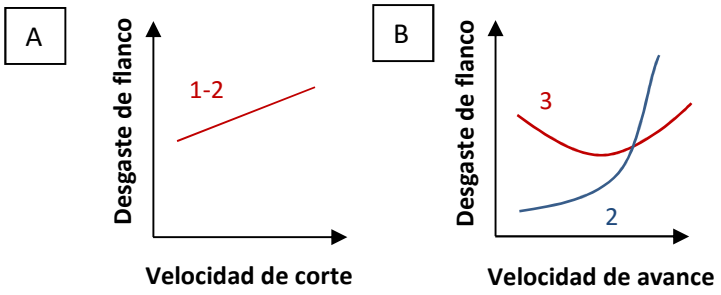

1. Rawat *et al*. 2009 [28]
2. Velayudham *et al*. 2005 [66]
3. Ramkumar *et al*. 2004 [53]

Figura 1.16: Efecto de los parámetros de corte en el desgaste durante el taladrado de compuestos laminados.

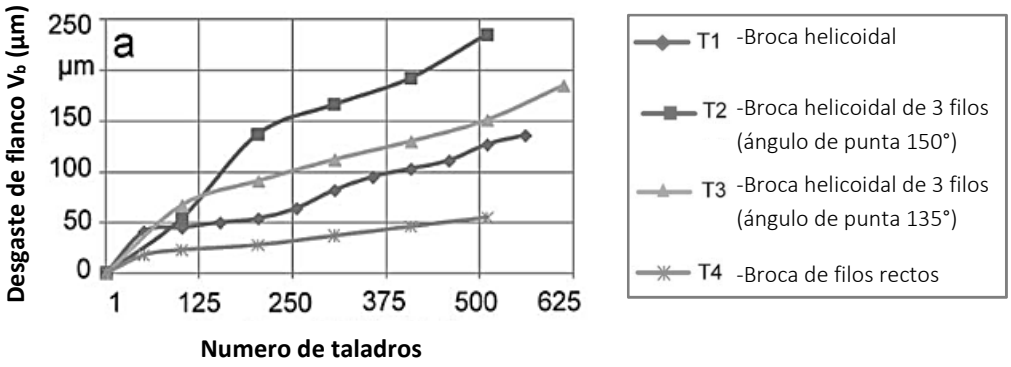

Figura 1.17: Progreso del desgaste de flanco para diferentes brocas. El material es CFRP tejido y las condiciones de corte son Vc=50 m/min *f*=0.1 mm/rev: [48].

El desgaste de la herramienta también depende de la geometría y del material de la broca. Las brocas de carburo cementado recubiertas presentaron una mejor resistencia que las brocas de metal duro sin recubrimiento durante el taladrado convencional de CFRP [16,49]. Faraz *et al*. [48] estudió también los efectos del desgaste en brocas con diferente geometría y materiales durante el taladrado convencional de compuestos laminados CFRP (Figura 1.17). El mayor desgaste de flanco se observó para la herramienta T2 debido al material K40, el cual es relativamente más susceptible al ataque abrasivo de las fibras de carbono. La broca de filos rectos presentó el desgaste del flanco más bajo. La resistencia al desgaste de esta geometría fabricada en carburo cementado también fue observada por Ramkumar *et al*. [54], quienes obtuvieron buenos resultados durante el taladrado asistido por vibración de compuestos laminados GFRP.

1.8 Reducción de la Delaminación en el Taladrado de Compuestos Laminados

Como se explicó anteriormente, las investigaciones experimentales indican que, para evitar la delaminación inducida por taladrado, la fuerza de avance aplicada a la pieza de trabajo no debe exceder la fuerza de avance crítica obtenida por los modelos teóricos. En general, esta fuerza crítica es función de los parámetros de corte, las propiedades del material de trabajo, los parámetros de la broca, y el espesor de las capas sin cortar bajo la broca. Sin embargo, la fuerza de avance depende también de ciertas características de la operación de taladrado en sí misma, como por ejemplo, el uso de placas de soporte bajo la pieza [45,55,82]. Por lo tanto, la mayoría de las investigaciones centradas en disminuir la delaminación, buscan, o bien aumentar la fuerza de avance crítica, o bien disminuir la fuerza durante el taladrado.

1.8.1 USO DE PLACAS DE APOYO

Un método efectivo para reducir el daño por delaminación, es mediante una placa de soporte colocada bajo el laminado del material compuesto para evitar la delaminación push-out. Esta metodología es muy habitual en la industria. Los resultados obtenidos por Capella [55] cuando se taladra con y sin placa de soporte utilizando una broca helicoidal demostraron la efectividad del método. El principal efecto es evitar la inflexión, proporcionando un refuerzo mecánico. Por lo tanto, una reducción significativa en la delaminación se puede lograr mediante la limi-

tación de la dinámica de la pieza. Tsao y Hocheng [82] presentan el efecto de la placa de soporte en la delaminación para geometrías de broca tipo fresa y broca de núcleo. Observaron que la delaminación con la placa de apoyo era menos probable que ocurriera debido al aumento de la fuerza de avance crítica.

1.8.2 USO DE BROCAS ESPECIALES

El uso de brocas helicoidales sin placa de soporte proporciona una relativa elevada fuerza de avance y una baja fuerza de avance crítica. Debido a esto, es difícil obtener un agujero libre de delaminación durante el taladrado convencional utilizando esta geometría [9,89]. Otra de las opciones que se presenta para minimizar la delaminación en el taladrado es el desarrollo de geometrías especiales, muchas de las cuales se han mencionado durante el capítulo. La ventaja de las brocas especiales en comparación con la broca helicoidal se basa, no solo variar el nivel de la fuerza crítica, sino también en su mayor umbral de velocidades de alimentación sin provocar delaminación, [45].

1.8.3 USO DE AGUJEROS PRE-TALADRADOS

El tercer y último método propuesto es la realización de un agujero piloto pre-taladrado. Un análisis tanto teórico como experimental fue realizado por Tsao y Hocheng utilizando brocas helicoidales [38] y de núcleo [83], respectivamente. Los resultados experimentales pusieron de relieve que el filo transversal de la broca helicoidal y la eliminación de la viruta en el caso de las brocas núcleo son las principales contribuciones a la fuerza de avance. Won y Dharan [112] también observaron que la fuerza de avance debida al filo transversal es un 40% de la fuerza total cuando la velocidad de avance es baja y del 60% cuando es alta. El agujero pre-taladrado elimina la fuerza causada por el filo transversal [38] o por la eliminación de la viruta [83]. El diámetro del agujero guía se fija igual a la longitud del filo transversal en la broca helicoidal o al diámetro interior en el caso de la broca de núcleo. Esta técnica puede proporcionar un enfoque útil para el taladrado de compuestos laminados a mayores velocidades de avance.

1.9 Referencias

[1] Soutis C. Fibre reinforced composite in aircraft construction. Progr Aerosp Sci 2005;41:143–51.
[2] Davim JP, Reis P, Antonio CC. Experimental study of drilling glass fiber reinforced plastics (GFRP) manufactured by hand lay-up. Compos Sci Technol 2004;64:289–97.
[3] Sinmazçelik T, Avcu E, Bora MÖ, Çoban O. A review: fibre metal laminates, background, bonding types and applied test methods. Mater Des 2011;32:3671–85.
[4] Hufenbach W, Dobrzan´ ski LA, Gude M, Konieczny J, Czulak A. Optimisation of rivet joints of CFRP composite material and aluminium alloy. J Achieve Mater Manuf Eng 2007;20:119–22.
[5] Teti R. Machining of composite materials. CIRP Annals – Manuf Technol 2002;51:611–34.
[6] Abrao AM, Faria PE, Campos Rubio JC, Reis P, Davim JP. Drilling of fiber reinforced plastics: a review. J Mater Process Technol 2007;186:1–7.
[7] Mishra R, Malik J, Singh I, Davim JP. Neural network approach for estimate the residual tensile strength after drilling in uni-directional glass fiber reinforced plastic laminates. Mater Des 2010;31:2790–5.
[8] Wong TL, Wu SM, Croy GM. An analysis of delamination in drilling composite materials. In: 14th National SAMPE technology conference. Atlanta, GA, USA; 1982. p. 471–383.

[9] Stone R, Krishnamurthy K. A neural network thrust force controller to minimize delamination during drilling of graphite-epoxy laminates. Int J Mach Tools Manuf 1996;36:985–1003
[10] Gay D, Hoa SV, Tsai SW. Composite materials design and applications. New York: CRC Press; 2003.
[11] Park KY, Choi JH, Lee DG. Delamination-free and high efficiency drilling of carbon fiber reinforced plastics. J Compos Mater 1995;29:1988–2002.
[12] Bhatnagar N, Ramakrishnan N, Naik NK, Komanduri R. On the machining of fiber reinforced plastic (FRP) composite laminates. Int J Mach Tools Manuf 1995;35:701–16.
[13] Lin SC, Chen IK. Drilling carbon fiber-reinforced composite material at high speed. Wear 1996;194:156–62.
[14] Chen WC. Some experimental investigation in the drilling of carbon fiber reinforced plastic (CFRP) composite laminates. Int J Mach Tools Manuf 1997;37:1097–108.
[15] Piquet R, Ferret B, Lachaud F, Swider P. Experimental analysis of drilling damage in thin carbon/epoxy plate using special drills. Composites: Part A 2000;31:1107–15.
[16] Murphy C, Byrne G, Gilchrist MD. The performance of coated tungsten carbide drills when machining carbon fibre-reinforced epoxy composite materials. In: Proceedings of the institution of mechanical engineers. Part B: journal of engineering manufacture, vol. 216; 2002. p. 143–52.
[17] Zhang LB, Wang LJ, Wang X. Study on vibration drilling of fiber reinforced plastics with hybrid variation parameters method. Composites: Part A 2003;34:237–44.
[18] Wang X, Wang LJ, Tao JP. Investigation on thrust in vibration drilling of drilling of fiber-reinforced plastics. J Mater Process Technol 2004;148:239–44.
[19] Zitoune R, Collombet F, Lachaud F, Piquet R, Pasquet P. Experiment calculation comparison of the cutting conditions representative of the long fiber composite drilling phase. Compos Sci Technol 2005;65:455–66.
[20] Sardinas RQ, Reis P, Davim JP. Multi-objective optimization of cutting parameters for drilling laminate composite materials by using genetic algorithms. Compos Sci Technol 2006;66:3083–8.
[21] Durao LMP, de Moura MFSF, Marques AT. Numerical simulation of the drilling process on carbon/epoxy composite laminates. Composites: Part A 2006;37:1325–33.
[22] Durao LMP, de Moura MFSF, Marques AT. Numerical prediction of delamination onset in carbon/epoxy composites drilling. Eng Fract Mech 2008;75:2767–78.
[23] Durao LMP, Goncalves DJS, Trvares JMRS, de Albuquerque VHC, Vieira AA, Marques AT. Drilling tool geometry evaluation for reinforced composite laminates. Compos Struct 2010;92:1545–50.
[24] Gopala Rao GV, Mahajan P, Bhatnagar N. Micro-mechanical modeling of machining of FRP composites – cutting force analysis. Compos Sci Technol 2007;67:579–93.
[25] Zitoune R, Collombet F. Numerical prediction of the thrust force responsible of delamination during the drilling of the long-fibre composite structures. Composites: Part A 2007;38:858–66.
[26] Lee SC, Jeong ST, Park JN, Kim SJ, Chao GJ. Study on drilling characteristic and mechanical properties of CFRP composites. Acta Mechanica Solida Sinica 2008;21:364–8.
[27] Rawat S, Attia H. Characterization of the dry high speed drilling process of woven composites using machinability maps approach. CIRP Annals – Manuf Technol 2009;58:105–8.
[28] Rawat S, Attia H. Wear mechanisms and tool life management of WC-Co drill during dry high speed drilling of woven carbon fibre composites. Wear 2009;267:1022–30.
[29] Shyha IS, Soo SL, Aspinwall D, Bradley S. Effect of laminate configuration and feed rate on cutting performance when drilling holes in carbon fibre reinforced plastic composites. J Mater Process Technol 2010;210:1023–34.
[30] Jahromi SS, Bahr B. An analytical method for predicting cutting forces in orthogonal machining of unidirectional composites. Compos Sci Technol 2010;70:2290–7.
[31] Iliescu D, Gehin D, Gutierrez ME, Girot F. Modeling and tool wear in drilling of CFRP. Int J Mach Tools Manuf 2010;50:204–13.
[32] Kalla D, Sheikh-Ahmad J, Twomey J. Prediction of cutting forces in helical end milling fiber reinforced polymers. Int J Mach Tools Manuf 2010;50:882–91.
[33] Rahme P, landon Y, Lachaud F, Piquet R, Lagarrigue P. Analytical models of composite material drilling. Int J Adv Manuf Technol 2011;52:609–17.
[34] Davim JP, Reis P. Drilling carbon fiber reinforced plastics manufactured by autoclave – experimental and statistical study. Mater Des 2003;24:315–24.
[35] Davim JP, Reis Pedro. Study of delamination in drilling carbon fiber reinforced plastic (CFRP) using design experiments. Compos Struct 2003;59:481–7.

[36] Davim JP, Reis P. Damage and dimensional precision on milling carbon fiber reinforced plastics using design experiments. J Mater Process Technol 2005;160:160–7.
[37] Davim JP, Rubio JC, Abrao AM. A novel approach based on digital image analysis to evaluate the delamination factor after drilling composite laminates. Compos Sci Technol 2007;67:1939–45.
[38] Tsao CC, Hocheng H. The effect of chisel length and associated pilot hole on delamination when drilling composite materials. Int J Mach Tools Manuf 2003;43:1087–92.
[39] Tsao vCC, Hocheng H. Taguchi analysis of delamination associated with various drill bits in drilling of composite material. Int J Mach Tools Manuf 2004;44:1085–90.
[40] Tsao CC, Hocheng H. Computerized tomography and C-Scan for measuring delamination in the drilling of composite materials using various drills. Int J Mach Tools Manuf 2005;45:1282–7.
[41] Tsao CC, Hocheng H. Effect of tool wear on delamination in drilling composite materials. Int J Mech Sci 2007;49:983–8.
[42] Tsao CC, Hocheng H. Parametric study on thrust force of core drill. J Mater Process Technol 2007;192–193:37–40.
[43] Tsao CC. Prediction of thrust force of step drill in drilling composite materials by Taguchi method and radial basis function network. Int J Adv Manuf Technol 2008;36:11–8.
[44] Tsao CC. Experimental study of drilling composite materials with step-core drill. Mater Des 2008;29:1740–4.
[45] Hocheng H, Tsao CC. Effects of special drill bits on drilling-induced delamination of composite materials. Int J Mach Tools Manuf 2006;46:1403–16.
[46] Gaitonde VN, Karnik SR, Campos Rubio J, Esteves Correia A, Abrao AM, Paulo Davim J. Analysis of parametric influence on delamination in high-speed drilling of carbon fiber reinforced plastic composites. J Mater Process Technol 2008;203:431–8.
[47] Karnik SR, Gaitonde VN, Campos Rubio J, Esteves Correia A, Abrao AM, Davim JP. Delamination analysis in high speed drilling of carbon fiber reinforced plastics (CFRP) using artificial neural network model. Mater Des 2008;29:1768–76.
[48] Faraz A, Biermann D, Weinert K. Cutting edge rounding: an innovative tool wear criterion in drilling CFRP composite laminates. Int J Mach Tools Manuf 2009;49:1185–96.
[49] Shyha IS, Aspinwall DK, Soo SL, Bradley S. Drill geometry and operating effects when cutting small diameter holes in CFRP. Int J Mach Tools Manuf 2009;49:1008–14.
[50] Liu D, Xu HH, Zhang CY, Yan HJ. Drilling force in high speed drilling carbon fibre reinforced plastics (CFRP) using half core drill. Adv Mater Res 2010;102–104:729–32.
[51] Lazar MB, Xirouchakis P. Experimental analysis of drilling fiber reinforced composites. Int J Mach Tools Manuf 2011;51:937–46.
[52] Mathew J, Ramakrishnan N, Naik NK. Investigations into the effect of geometry of a trepanning tool on thrust and torque during drilling of GFRP composites. J Mater Process Technol 1999;91:1–11.
[53] Ramkumar J, Aravindan S, Malhotra SK, Krishamurthy R. An enhancement of machining performance of GFRP by oscillatory assisted drilling. Int J Adv Manuf Technol 2004;23:240–4.
[54] Ramkumar J, Malhotra SK, Krishamurthy R. Effect of workpiece vibration on drilling of GFRP laminates. J Mater Process Technol 2004;152:329–32.
[55] Capello E. Workpiece damping and its effect on delamination damage in drilling thin composite laminates. J Mater Process Technol 2004;148:186–95.
[56] El-Sonbaty I, Khashaba UA, Machaly T. Factors affecting the machinability of GFR/epoxy composites. Compos Struct 2004;63:329–38.
[57] Singh I, Bhatnagar N. Drilling-induced damage in uni-directional glass fiber reinforced plastic (UD-GFRP) composite laminates. Int J Adv Manuf Technol 2006;27:877–82.
[58] Singh I, Bhatnagar N, Viswanath P. Drilling of uni-directional glass fiber reinforced plastics: experimental and finite element study. Mater Des 2008;29:546–53.
[59] Gopala Rao GV, Mahajan P, Bhatnagar N. Machining of UD-GFRP composites chip formation mechanism. Compos Sci Technol 2007;67:2271–81.
[60] Mkaddem A, Demirci I, EI Mansori M. A micro-macro combined approach using FEM for modeling of machining of FRP composites: cutting force analysis. Compos Sci Technol 2008;68:3123–7.
[61] Lasri L, Nouari M, EI Mansori M. Modeling of chip separation in machining unidirectional FRP composites by stiffness degradation concept. Compos Sci Technol 2009;69:684–92.
[62] Kilickap E. Optimization of cutting parameters on delamination based on Taguchi method during drilling of GFRP composite. Expert Syst Appli 2010;37:6116–22.
[63] Khashaba UA. Delamination in drilling GFR-thermoset composites. Compos Struct 2004;63:313–27.

[64] Khashaba UA, EI-Sobaty IA, Selmy AI, Megahed AA. Machinability analysis in drilling woven GFR/epoxy composites: part I – effect of machining parameters. Composites: Part A 2010;41:391–400.
[65] Khashaba UA, EI-Sobaty IA, Selmy AI, Megahed AA. Machinability analysis in drilling woven GFR/epoxy composites: part II – effect of drill wear. Composites: Part A 2010;41:1130–7.
[66] Velayudham A, Krishnamurthy R, Soundarapandian T. Evaluation of drilling characteristics of high volume fraction fibre glass reinforced polymeric composite. Int J Mach Tools Manuf 2005;45:399–406.
[67] Velayudham A, Krishnamurthy R. Effect of point geometry and influence on thrust and delamination in drilling of polymeric composites. J Mater Process Technol 2007;185:204–9.
[68] Arul S, Vijayaraghavan L, Malhotra SK, Krishnamurthy R. Influence of tool material on dynamics of drilling of GFRP composites. Int J Adv Manuf Technol 2006;29:655–62.
[69] Arul S, Vijayaraghavan L, Malhotra SK, Krishnamurthy R. The effect of vibratory drilling on hole quality in polymeric composites. Int J Mach Tools Manuf 2006;46:252–9.
[70] Arul S, Vijayaraghavan L, Malhotra SK. Online monitoring of acoustic emission for quality control in drilling of polymeric composites. J Mater Process Technol 2007;185:184–90.
[71] Abrao AM, Campos Rubio J, Faria PE, Davim JP. The Effect of cutting tool geometry on thrust force and delamination when drilling glass fibre reinforced plastic composite. Mater Des 2008;29:508–13.
[72] Rubio JC, Abrao AM, Faria PE, Correia AE, Davim JP. Effects of high speed in the drilling of glass fibre reinforced plastic: evaluation of delamination factor. Int J Mach Tools Manuf 2008;48:715–20.
[73] Isik B, Ekici E. Experimental investigations of damage analysis in drilling of woven glass fiber-reinforced plastic composites. Int J Adv Manuf Technol 2010;49:861–9.
[74] Lee SC, Jeong ST, Park JN, Kim SJ, Chao GJ. Study on drilling characteristic and mechanical properties of CFRP composites. Acta Mechanica Solida Sinica 2008;21:364–8.
[75] Ramulu M, Branson T, Kim D. A study on the drilling of composite and titanium stacks. Compos Struct 2001;54:67–77.
[76] Kim D, Ramulu MR. Drilling process optimization for graphite/bismaleimidetitanium alloy stacks. Compos Struct 2004;63:101–14.
[77] Brinksmeier E, Janssen R. Drilling of multi-layer composite materials consisting of carbon fiber reinforced plastics (CFRP), titanium and aluminum alloys. CIRP Annals – Manuf Technol 2002;51:87–90.
[78] Kim GW, Lee KY. Critical thrust at propagation of delamination zone due to drilling of FRP/metallic strips. Compos Struct 2005;69:137–41.
[79] Zitoune R, Krishnaraj V, Collombet F. Study of drilling of composite material and aluminium stack. Compos Struct 2010;92:1246–55.
[80] Shyha IS, Soo SL, Aspinwall DK, Bradley S, Dawson S, Pretorius CJ. Drilling of titanium/CFRP/aluminium stacks. Key Eng Mater 2010;447-448:624–33.
[81] Enemuoh EU, El-Gizawy AS, Okafor AC. An approach for development of damage-free drilling of carbon fiber reinforced thermosets. Int J Mach Tools Manuf 2001;41:1795–814.
[82] Tsao CC, Hocheng H. Effects of exit back-up on delamination in drilling composite materials using a saw drill and a core drill. Int J Mach Tools Manuf 2005;45:1261–70.
[83] Tsao CC. The effect of pilot hole on delamination when core drill drilling composite materials. Int J Mach Tools Manuf 2006;46:1653–61.
[84] Jung JP, Kim GW, Lee KY. Critical thrust force at delamination propagation during drilling of angle-ply laminates. Compos Struct 2005;68:391–7.
[85] Mohan NS, Ramachandra A, Kulkarni SM. Influence of process parameters on cutting force and torque during drilling of glass-fiber polyester reinforced composites. Compos Struct 2005;71:407–13.
[86] Mohan NS, Kulkarni SM, Ramachandra A. Delamination analysis in drilling process of glass fiber reinforced plastic (GFRP) composite materials. J Mater Process Technol 2007;186:265–71.
[87] Fernandes M, Cook C. Drilling of carbon composites using a one shot drill bit. Part I. Fiver stage representation of drilling and factors affecting maximum force and torque. Int J Mach Tools Manuf 2006;46:70–5.
[88] Fernandes M, Cook C. Drilling of carbon composites using a one shot drill bit. Part II. Empirical modeling of maximum thrust force. Int J Mach Tools Manuf 2006;46:76–9.
[89] Jain S, Yang DCH. Delamination-free drilling of composite laminates. ASME J Eng Indust 1994;116:475–81.
[90] Hocheng H, Tsao CC. Comprehensive analysis of delamination in drilling of composite materials with various drill bits. J Mater Process Technol 2003;140:335–9.

[91] Zhang LB, Wang LJ, Liu XY, Zhao HW, Wang X, Luo HY. Mechanical model for predicting thrust and torque in vibration drilling fibre-reinforced composite materials. Int J Mach Tools Manuf 2001;41:641–57.
[92] Lau WS, Lee WB, Pang SQ. Pulsed Nd:YAG laser cutting of carbon fibre composite materials. CIRP Annals – Manuf Technol 1990;39:179–82.
[93] Lau WS, Yue TM, Lee TC, Lee WB. Un-conventional machining of composite materials. J Mater Process Technol 1995;48:199–205.
[94] Mathew J, Goswami GL, Ramakrishnan N, Naik NK. Parametric studies on pulsed Nd:YAG laser cutting of carbon fibre reinforced plastic composites. J Mater Process Technol 1999;89–90:198–203.
[95] Genna AA, Mathew P. Analysis and prediction and laser cutting parameters of fibre reinforced plastics (FRP) composite materials. Int J Mach Tools Manuf 2002;42:105–13.
[96] Voisey KT, Fouquet S, Roy D, Clyne TW. Fibre swelling during laser drilling of carbon fibre composites. Optics Lasers Eng 2006;44:1185–97.
[97] Herzog D, Jaeschke P, Meier O, Haferkamp H. Investigations on the thermal effect caused by laser cutting with respect to static strength of CFRP. Int J Mach Tools Manuf 2008;48:1464–73
[98] Lemma E, Chen L, Siores E, Wang J. Study cutting fiber-reinforced composites by using abrasive water-jet with cutting head oscillation. Compos Struct 2002;57:297–303.
[99] Shanmugam DK, Nguyen T, Wang J. A study of delamination on graphite/epoxy composites in abrasive water jet machining. Composites: Part A 2008;39:923–9.
[100] Azmir MA, Ahsan AK. A study of abrasive water jet machining process on glass/epoxy composite laminate. J Mater Process Technol 2009;209:6168–73.
[101] Lau WS, Wang M, Lee WB. Electrical discharge machining of carbon fibre composite materials. Int J Mach Tools Manuf 1990;30:297–308.
[102] Davim JP, Reis P, Antonio CC. Drilling fiber reinforced plastics (FRPs) manufactured by hand lay-up-influence of matrix (Viapal VUP 9731 and ATLAC 382-05). J Mater Process Technol 2004;155–156:1828–33.
[103] Shyha IS, Soo SL, Aspinwall DK, Bradley S, Perry R, Harden P, et al. Hole quality assessment following drilling of metallic-composite stacks. Int J Mach Tools Manuf 2011;51:569–78.
[104] Park H, Beal A, Kim D, Kwon P, Lantrip J. Tool wear in drilling of composite/ titanium stacks using carbide and polycrystalline diamond tools. Wear 2011;271:2826–35.
[105] Hocheng H, Dharan CKH. Delamination during drilling in composite laminates. ASME J Eng Indust 1990;112:236–9.
[106] Paival JMF, Mayer S, Cerqueira M. Evaluation of mechanical properties of four different carbon/epoxy composites used in aeronautical field. Mat Res 2005; 8(1)
[107] Seif MA, Khashaba UA, Rojas-Oviedo R. Measuring delamination in carbon/ epoxy composites using a shadow moiré laser based imaging technique. Compos Struct 2007;79:113–8
[108] Abrate S, Walton DA. Machining of composite material. Part I: traditional methods. Compos Manuf 1992;3:75–83.
[109] Upadhyay PC, Lyons JS. On the evaluation of critical thrust for delamination free drilling of composite laminates. J Reinf Plast Compos 1999;18:1287–303.
[110] Gururaja S, Ramulu M. Modified Exit-ply Delamination Model for Drilling FRPs. J Compos Mater 2009;43(5);483-500.
[111] Hocheng H, Tsao CC. The path Towards delamination-free drilling of composite materials. J Mater Process Technol 2005;167:251-64
[112] Won MS, Dharan CKH. Chisel edge and pilot hole effects in drilling composite laminates. J Manuf Sci Eng 2002;124(2):242–7.

Capítulo 2

Experimental Analysis of Special Tool Geometries When Drilling Woven and Multidirectional CFRPs

La geometría de la herramienta es un parámetro que influye fuertemente en la calidad del agujero taladrado. En este capítulo, se realiza una comparación entre tres brocas con diseños no ensayados anteriormente en la literatura: Broca de punta central, broca escalonada y broca de filos rectos. Se comparan en términos de fuerzas de avance y delaminación para dos configuraciones distintas de laminados CFRP: tejido y multidireccional. La broca de filos rectos mostró los mejores resultados en cuanto a la productividad y la delaminación. Se encontraron también grandes diferencias en cuanto a la calidad del agujero entre ambos materiales: el material unidireccional presentó peores resultados que el tejido bajo las mismas condiciones de corte. Finalmente se realizó un análisis de varianza con el fin de analizar la influencia de cada parámetro en el daño, resultado la velocidad de avance el factor más influyente.

Este estudio se encuentra publicado bajo la siguiente referencia: **N. Feito**, A. Diaz-Álvarez, J.L. Cantero, M. Rodríguez-Millán, M. H. Miguélez. “Experimental analysis of special tool geometries when drilling woven and multidirectional CFRPs”, Journal of Reinforced Plastics and Composites (2016) Vol. 35, p. 33-55.

Experimental Analysis of Special Tool Geometries When Drilling Woven and Multidirectional CFRPs

Abstract

Drilling is one of the most frequent machining operations for carbon fiber-reinforced polymer composites, carried out prior to assembly between structural components using mechanical joining. Delamination is the main damage mechanism involved during carbon fiber-reinforced polymer composite drilling causing an elevated percentage of workpiece rejection. Tool geometry strongly influences drilling performance. In this paper, an original work dealing with the comparison between three recently developed configurations (Brad center, Step drill and Reamer drills) in terms of drilling forces and delamination both for woven and tape carbon fiber-reinforced polymers is presented. Reamer drill showed the best results concerning productivity and delamination. Strong differences were found when hole quality obtained in tape and woven composite was compared: multidirectional composite presented poorer hole quality than woven composite under the same cutting conditions. The analysis of variance was developed in order to analyze the influence of each parameter showing the importance of feed rate on surface damage.

Keywords: CFRPs, delamination, tool geometry, drilling.

2.1 Introduction

Long fiber-reinforced polymer composites are widely used in industry to manufacture lightweight structures due to their properties, mainly high strength-to-weight ratio, high fracture toughness and corrosion resistance [1]. In particular, carbon fiber-reinforced polymers (CFRPs) are commonly used in aircraft and aerospace industries due to their excellent mechanical properties and strength-to-weight ratio [2].

Although CFRPs are usually made close to the final shape of the component, some machining operations are usually required to achieve assembly and dimensional final specifications. Milling is usually carried out, and the importance of this operation has motivated the development of specific tools for composite machining [3,4]. Drilling is commonly needed prior to mechanical joining of high responsibility components those are exposed to thermo-mechanical loading during service life [5]. Surface integrity should be ensured avoiding component damage that could result in decreased service life performance. Delamination is one of the most important damage mechanisms when machining CFRPs [6]. The analysis of drilling is an active field of research because of the high value of this operation in industry: drilling is performed in a high value component, thus the rejection of the component involves elevated cost [7,8].

Although some modeling approaches has been done to the prediction of hole quality (see for instance a recent work of the authors [9]), most analysis are based on experiments due to the difficulty of modeling drilling. Drilling is a complex process, the hole quality mainly depends on the proper

selection of drilling parameters, the geometry of the drill and also the adequate statement of tool life in order to avoid excessive drill wear [10].

Tool manufacturers have made an effort in the development of new geometries trying to minimize machining induced damage on the component. Delamination is one of the most important defects induced during drilling due to the nature of the process with feed direction orthogonal to the laminate plane [11–13].

A brief state of the art giving the main contributions analyzing the performance of conventional drills and special geometries are provided below. The geometries, cutting conditions and material characteristics implemented in the tests revised in the literature are included in Table 2.1 in order to improve clarity and make easy for the reader to identify the drill geometry.

The influence of tool geometry when drilling multidirectional tape CFRPs was analyzed in Durao *et al*. [14] The authors carried out a study comparing five different drill geometries (twist with 120° and 85° point angles, Brad type, Dagger type and a customized Step drill) when drilling cross-ply material. Results showed that Twist and special Step drills did not show considerable changes in delamination when feed rate was increased. However, the same parameter had considerable impact in the case of Brad and Dagger drills. The 120° twist drill was recommended to work with high feed rates indicating the possibility of using special Step drill as a good alternative.

Marques *et al*. [15] compared a special Step drill with small section in the first step (1.25 mm), with the aim of creating a pilot hole, with a dagger drill, a brad drill and a conventional twist drill. It was proved that selective geometries combined with conservative cutting speed, low feed rate and a pilot hole cancel the chisel edge effect, reducing the risk of delamination.

Shyha *et al*. [16] analyzed the influence of the point angle and helix angle in cemented carbide drills for machining small holes without back support. Two drills with TiN coated and uncoated surface conditions were selected: stepped drill and conventional drill bit. With a criterion of maximum admissible flank wear equal to 100 mm, the selection of uncoated step drill and high feed rate increased tool life. The reduction of the feed force was attributed to the lower interaction between chisel edge / workpiece material when using the stepped drill geometry. Also high feed rate reduces the contact time between the cutting tool and workpiece material thus reducing abrasive action.

Piquet *et al*. [17] compared reamer drill bit with three cuttings edges with conventional twist drill. It was recommended to drill a previous hole in order to neutralize the chisel edge effect in the case of twist drill. However, applying a variable feed rate to the reamer drill bit case in relation to its geometry, the defects were reduced significantly without need of pre-drilled hole.

Xu *et al*. [18] analyzed the effect of PCD coating for both standard twist drill and special-geometry dagger drill when drilling high-strength T800S/250F carbon/ epoxy composite. The tensile strength and tensile modulus of T800S fiber increase, respectively, 67% and 28% when compared to conventional T300 fiber, resulting in much poorer machinability during the drilling process. The drills showed severe coating peeling and edge chipping due to the use if the high-strength special fibers. Delamination damage was reduced for the PCD dagger

drill when compared to twist drill due to the multi-edge involved in drilling which behave like reamer-finishing action on the machined hole wall surface.

A recent research focusing on drilling multidirectional CFRP laminates with double point angle PCD drills was carried out by Karpat *et al*. [19] In this study, a mechanistic model was proposed in order to analyze the effect of drill geometry (chisel edge length, primary and secondary edge lengths and angles) and cutting parameters. Thrust force and torque were also estimated according to orientation-ply laminate.

On the other hand, woven CFRP composites present some advantages when compared with tape laminates and they are increasingly used in different industrial sectors. The woven configuration architecture of the layer results in enhanced mechanical properties. Davim and Reis [20] carried out one of the earliest studies focused on drilling woven composite. Two drills, helical and Brad & Spur drills, were selected to analyze the correlation between cutting parameters and delamination. A strong influence of feed rate on entry delamination was shown for both geometries. Brad & Spur drill produced less delamination than Straight drill.

In a similar study developed by Grillo *et al*. [21] Spur drill, helicoidal drill with a 140° point angle and four flutes drill were compared. Spur geometry presented improved behavior when compared with the 140° point angle helical drill and the four flute drill. Negligible delamination extension in both sides of the hole was found for this drill working with spindle speed equal to 6750 rpm and feed rate equal to 2025 mm/min. For higher feed rate, delamination was caused mainly at the entrance of the hole.

Hocheng and Tsao [22] carried out experiments on woven CFRPs with large thickness using several special drill bits: twist drill, saw drill, candle stick drill, core drill and Step drill. Delamination at the hole exit was reduced using a drill with a small chisel edge; thus, saw and core drills showed the best results.

The special drill design known as step-core drills were studied by Tsao [23]. This type of drills presents a conventional inner geometry with an outer part producing grinding of the hole wall. In this study, the external part presented the nominal diameter and the internal part was, respectively, twist drill, saw drill and candlestick drill. It was concluded that the diameter ratio (relation between core external diameter and the inner part diameter) and the feed rate were the most influencing parameters on the thrust force. This force increased with the feed rate and when the ratio decreased. It was also proved that the combination of high diameter ratio, low feed rate and high spindle speed minimizes delamination. Tsao and Chiu [24] compared, in other study, step and non-step Core drills thereby introducing a relative motion between the inner and outer parts of the drill. Experimental results showed that the cutting velocity ratio, feed rate and inner drill type were the most important variables to control the thrust force in these cases. Combining high negative relative motion and low feed rate was recommended in order to reduce delamination damage.

Lazar and Xirouchakis [25] developed experimental tests on woven carbon and glass fiber composites using three different drill geometries: tapered drill, 8 facet drill and 2 facet twist drills. The hole diameter varied slightly with each geometry but was always around and smaller than 6 mm. The machinability was comparable for both ma-

terials, despite the better mechanical properties of CFRP. The highest loads were found at the tool tip in the vicinity of the chisel edge for all cases. It is also found that the maximum load per ply varied mainly with the axial feed rate and tool geometry, while the spindle speed had negligible influence.

Tungsten carbide (WC) stepped drill was used by Shyha *et al*. [26] to machine small diameter hole in woven CFRP composite. Most drills tested at the highest feed rate level (0.4 mm/rev) experienced catastrophic failure. The reduction of strength of the drill was due to the small diameter of the pilot segment of the tool. Maximum feed rate equal to 0.2 mm/rev for the stepped drill configuration was recommended in order to avoid drill failure.

Murphy *et al*. [27] studied tungsten carbide (WC) drills coated with titanium nitride (TiN) and diamond-like carbon (DLC) in drilling woven CFRP composite. Torque and thrust force increased with the evolution of cutting time as a consequence of flank wear enhancement. The wear increased significantly during the early stage of the tool life (approximately up to seven holes), later the subsequent wear rate was reduced. This phenomenon is due to the transition between primary and secondary wear zones, a typical pattern also found when drilling metallic materials (see Sandvik handbook [28]). Wear progression influenced the thrust force and the torque in a similar way: these variables showed higher increase in the primary wear zone than in the second wear zone. Tool wear progression resulted in fiber damage in terms of pull-out and spalling. Drilling-induced damage was found to be similar for all types of coating used; moreover, the use of coating showed negligible benefit in this case.

Ramirez *et al*. [29] and Mondelin *et al*. [30] identified abrasion as the main wear mechanism when drilling woven CFRP. The influence of wear in torque and thrust force was proven and in consequence, in the hole quality.

The effect of worn tools in thrust forces and delamination was analyzed in a previous work of the authors [31] Two different uncoated worn geometries (flank wear and honed cutting edge) and three different drill point angles were tested on woven CFRPs. Negligible influence of the point angle on thrust force was found when drilling with fresh drills. However, drill point angle influenced thrust force when it was combined with the effect of wear progression. This fact is important for drill geometry selection since the evolution of wear could lead to inacceptable levels of thrust force. Wear progression had a different effect on delamination at the entry and exit hole. While entry delamination diminished with wear progression, exit delamination was enhanced. The most favorable results concerning delamination were obtained with the lowest value of the drill point angle: delamination factor at entry and exit hole increased with the drill point angle. This result is important for the workpiece inspection after drilling, establishing critical zones. In addition, during the drill selection, the favorable effect of low drill point should be accounted for. Finally, analysis of variance (ANOVA) study highlighted that in the cases analyzed, wear and point angle were the most influential parameters on thrust force and delamination.

Cutting edge rounding (CER) was introduced by Faraz *et al*. [32] as a significant tool wear mechanism in drilling woven CFRP composite. It was proved that null magnitude of CER is never realizable independent of the drills bit geometry and the flank

wear. Correlations between the CER and the drilling loads and delamination on CFRP were observed. This phenomenon was also studied for coated and uncoated drill tips by Wanga *et al*. [33]. Ultra-hard diamond coating tools reduced this type of wear significantly. However, AlTiN-coated drill did not show significant differences with uncoated drill due to its oxidation during machining.

Table 2.1: Summary of contributions of different authors to comparing different geometries.

Drill bit geometry	CFRP Material	References	Cutting conditions
Twist drill [25] 	Tape	Durao *et al*. [14]	Thickness: 4 mm; Diameter: 6 mm; Feed rate: 0.02, 0.06, 0.12 mm/rev; Cutting speed: 53 m/min; Coated: Uncoated.
		Shyha *et al*. [16]	Thickness: 3 mm; Diameter: 1.5 mm; Feed rate: 0.1, 0.2 mm/rev; Cutting speed: 15, 45 m/min; Coated: Uncoated and TiN coated and quasi-isotropic CFRP laminate.
		Xu *et al*. [18]	Thickness: 2.6 mm; Diameter: 4.9 mm; Feed rate: 0.002-0.018 mm/rev; Cutting speed: 2000-10000 rpm; Coated: PCD.
		Marques *et al*. [15]	Thickness: 4mm and stacking sequence $[0/-45/90/+45]_{4s}$.Diameter: 6 mm; Feed rate: 0.01, 0.025, 0.05 mm/rev; Cutting speed: 30–102 m/min; Coated: Uncoated and K20 carbide.
		Piquet *et al*. [17]	Thickness: 2.8 and 3.36mm and stacking sequence were firstly a plate composed of ten plies $[90/+45/0/-45/0]_S$, and secondly a plate consisting of 12 plies $[90/+45/0/0/-45/0]_S$. Diameter: 4.8 mm; Feed rate: 0.05, 0.125 and 0.2 mm/rev; Cutting speed: 3100 rpm; Coated: Uncoated.
	Woven	Davim *et al*. [20]	Thickness: 3 mm; Diameter: 5 mm; Feed rate: 0.05-0.2 mm/rev; Cutting speed: 30-50 m/min; Coated: Uncoated
		Grillo *et al*. [21]	Thickness: 3 mm; Diameter: 5 mm; Feed rate: 112.5-2025 mm/min; Cutting speed: 2250-6750 rpm; Coated: Uncoated
		Hocheng *et al*. [22]	Thickness: 6 mm; Diameter: 10 mm; Feed rate: 0.003-0.0133 mm/rev; Cutting speed: 900, 1000 rpm; Coated: Uncoated
		Lazar *et al*. [25]	Thickness: 10 mm; Diameter: 5.6 mm; Feed rate: 0.02-0.2 mm/rev; Cutting speed: 500- 5000 rpm; Coated: Uncoated
Brad drill [1] 	Tape	Durao *et al*. [14]	Thickness: 4mm; Diameter: 6 mm; Feed rate: 0.02, 0.06, 0.12 mm/rev; Cutting speed: 53 m/min; Coated: Uncoated.
		Marques *et al*. [15]	Thickness: 4mm ans stacking sequence $[0/-45/90/+45]_{4s}$; Diameter: 6 mm; Feed rate: 0.01, 0.025, 0.05 mm/rev; Cutting speed: 30-102 m/min; Coated: Uncoated and K20 carbide.

Drill bit geometry	CFRP Material	References	Cutting conditions
Brad & Spur drill [37] 	Woven	Davim *et al*. [20]	Thickness: 3 mm and 13 layers of composite; Diameter: 5 mm; Feed rate: 0.05-0.2 mm/rev; Cutting speed: 30-50 m/min; Coated: Uncoated.
		Grillo *et al*. [21]	Thickness: 3mm and 13 layers of composite; Diameter: 5 mm; Feed rate: 112.5-2025 mm/min; Cutting speed: 2250-6750 rpm; Coated: Uncoated
Dagger drill [38] 	Tape	Durao *et al*. [14];	Thickness: 4mm; Diameter: 6 mm; Feed rate: 0.02, 0.06, 0.12 mm/rev; Cutting speed: 53 m/min; Coated: Uncoated
		Xu *et al*. [18]	Thickness: 2.6mm and high-strength CFRP composite consists of 7 layers with stacking sequence [45/90/135/0/135/90/45]; Diameter: 4.9 mm; Feed rate: 0.002–0.018 mm/rev; Cutting speed: 2000–10,000 rpm; Coated: PCD.
		Marques *et al*. [15]	Thickness: 4mm and stacking sequence $[0/-45/90/+45]_{4s}$; Diameter: 6 mm; Feed rate: 0.01, 0.025, 0.05 mm/rev; Cutting speed: 30–102 m/min; Coated: Uncoated.
Step drill [1] 	Tape	Durao *et al*. [14]	Thickness: 4mm; Diameter: 6 mm; Feed rate: 0.02, 0.06, 0.12 mm/rev; Cutting speed: 53 m/min; Coated: Uncoated.
		Marques *et al*. [15]	Thickness: 4mm and stacking sequence $[0/-45/90/+45]_{4s}$; Diameter: 6 mm; Feed rate: 0.01, 0.025, 0.05 mm/rev; Cutting speed: 30-102 m/min; Coated: Uncoated
		Shyha *et al*. [16]	Thickness: 3 mm; Diameter: 1.5 mm; Feed rate: 0.1, 0.2 mm/rev; Cutting speed: 15, 45 m/min; Coated: Uncoated and TiN coated and quasi-isotropic CFRP laminate.
		Shyha *et al*. [26]	Thickness: 3 mm; Diameter: 1.5 mm; Feed rate: 0.2, 0.4 mm/rev; Cutting speed: 45 m/min; Coated: Uncoated.
	Woven	Hocheng *et al*. [22]	Thickness: 6 mm; Diameter: 10 mm; Feed rate: 0.003-0.0133 mm/rev; Cutting speed: 900, 1000 rpm; Coated: Uncoated.
		Shyha *et al*. [26]	Thickness: 3 mm; Diameter: 1.5 mm; Feed rate: 0.2, 0.4 mm/rev; Cutting speed: 45 m/min; Coated: Uncoated.
Double point angle drill [25] 	Tape	Karpat *et al*. [19]	Thickness: 10 mm; Diameter: 6.4 mm; Feed rate: 0.02-0.15 mm/rev; Cutting speed: 5000 rpm; Coated: PCD.
	Woven	Lazar *et al*. [25]	Thickness: 10 mm; Diameter: 5.36 mm; Feed rate: 0.02-0.2 mm/rev; Cutting speed: 500- 5000 rpm; Coated: Uncoated.
Four flute drill [21] 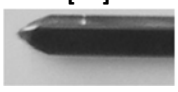	Woven	Grillo *et al*. [21];	Thickness: 3mm and 13 layers of composite; Diameter: 5 mm; Feed rate: 112.5-2025 mm/min; Cutting speed: 2250-6750 rpm; Coated: Uncoated.

Drill bit geometry	CFRP Material	References	Cutting conditions
Saw drill [22] 	Woven	Hocheng *et al*. [22]	Thickness: 6 mm; Diameter: 10 mm; Feed rate: 0.003-0.0133 mm/rev; Cutting speed: 900, 1000 rpm; Coated: Uncoated.
Candle stick drill [22] 	Woven	Hocheng *et al*. [22]	Thickness: 6 mm; Diameter: 10 mm; Feed rate: 0.003-0.0133 mm/rev; Cutting speed: 900, 1000 rpm; Coated: Uncoated.
Core drill [22] 	Woven	Hocheng *et al*. [22]	Thickness: 6 mm; Diameter: 10 mm; Feed rate: 0.003-0.0133 mm/rev; Cutting speed: 900, 1000 rpm; Coated: Uncoated.
Compound Core drill [24] 	Woven	Tsao *et al*. [24]	Thickness: 4 mm and 16 layers of composite; Diameter: 10 mm; Feed rate: 10, 15, 20 mm/min; Cutting speed: 1088, 1224 and 1360 rpm for outer drills and 1000 and 1214 rpm for inner drills; Coated: Uncoated.
Step Core drill [23] 	Woven	Tsao *et al*. [24]	Thickness: 4 mm and 16 layers of composite; Diameter: 10 mm; Feed rate: 10, 15, 20 mm/min; Cutting speed: 1088, 1224 and 1360 rpm for outer drills and 1000 and 1214 rpm for inner drills; Coated: Uncoated.
		Tsao [23]	Thickness: 4 mm and 16 layers of composite; Diameter: 10 mm; Feed rate: 8, 12, 16 mm/min; Cutting speed: 800, 1000, 1200 rpm; Coated: Uncoated.
Tapered drill reamer [25] 	Tape	Murphy *et al*. [27]	Thickness: 4-4.5 mm and 30 plies with a stacking sequence of {weave/90/+45/-45/0/0/-45/+45/-45/+45/+45/-45/90/0/90}s; Diameter: 6.35 mm; Feed rate: 0.0485mm/rev; Cutting speed: 60 m/min; Coated: TiN coating and DLC.
		Piquet *et al*. [17]	Thickness: 2.8 and 3.36mm and stacking sequence were firstly a plate composed of ten plies $[90/+45/0/-45/0]_S$, and secondly a plate consisting of 12 plies $[90/+45/0/0/-45/0]_S$; Diameter: 4.8 mm; Feed rate: 0.05, 0.125 and 0.2 mm/rev; Cutting speed: 3100 rpm; Coated: Uncoated.
	Woven	Lazar *et al*. [25]	Thickness: 10 mm; Diameter: 5.55 mm; Feed rate: 0.02-0.2 mm/rev; Cutting speed: 500- 5000 rpm; Coated: Uncoated.

The comparison between woven and tape composite seems to be interesting since few papers include information on both materials configuration. Shya *et al*. [26] analyzed the behavior of both composite types when drilled with a stepped drill and two feed rates. Results showed a better delamination resistance of the woven composite.

Not only mechanical damage is important when drilling CFRP composites. Also the temperature at the workpiece could affect surface quality of the component and its measurement during process is difficult. Some attempts have been done in the estimation of thermal effects when machining CFRPs [34,35]

In this paper, an experimental approach to the analysis of the performance of three different drill geometries, in terms of thrust force, torque and delamination, is presented. The selected geometries were Brad drill (without SPUR zone), special step drill bit with small section change (from 4mm to 6mm step diameter) and a new design of Reamer drill bit. The tools were tested in both multidirectional tape and woven CFRP composite. The influence of cutting parameters (cutting speed and feed rate) has been compared for the three geometries. Finally, the ANOVA analysis allowed understanding the influence of the cutting parameters in cutting forces and delamination damage and the contribution of each one for both materials analyzed.

2.2 Experimental Setup

In this section, the experimental equipment, including materials, tools and measurement systems used in the drilling tests and in the further hole quality analysis are briefly described.

Table 2.2: Mechanical properties of the CFRP [39,40].

Property	Woven	Tape
E_1 (GPa)	68	173
E_2 (GPa)	68	7.36
E_3 (GPa)	10	7.36
υ_{12}	0.22	0.33
G_{12} (GPa)	5	3.89
X_t (MPa)	795	2998
X_c (MPa)	860	1414
Y_t (MPa)	795	37
X_c (MPa)	860	169
S_t (MPa)	98	120

2.2.1 MATERIALS

Two CFRP materials were tested in this study. The first material is bidirectional (woven) based on AS-4 carbon fiber and 8552-epoxy matrix. The total thickness was 2.2mm and it was composed of 10 plies with the same orientation (direction 1 at 0°). The second material is a laminate composed by 24 unidirectional plies. It was manufactured from carbon IM7 fiber and MTM-45-1 epoxy resin and presented a quasi-isotropic lay-up with stacking sequence $[45/-45/0/90]_{3S}$. The final thickness of each plate was approximately 3 mm.

The mechanical properties for both materials are shown in Table 2.2. E_i is elastic modulus in the direction i; ν_{ij} Poisson coefficient; G_{ij} elastic modulus in shear directions; X_t, Y_t and S_t maximum tensile stress in longitudinal and shear directions, respectively; X_c and Y_c maximum compressive stress in longitudinal directions.

2.2.2 DRILL GEOMETRIES AND CUTTING PARAMETERS

Three different types of drill bits with nominal diameter equal to 6 mm were tested with both materials (see Figure 2.1): a Brad center drill, a new step drill with a

length of step equal 6.6 cm and a section changing from 4mm to 6mm (the stepped geometries in the literature usually present a section change higher than 2 mm) and a Reamer drill with four cutting edges (a new geometry, not previously tested in the literature).

Helix Angle		
30°	20°	0°
Clearance Angle		
9°	9°	9°

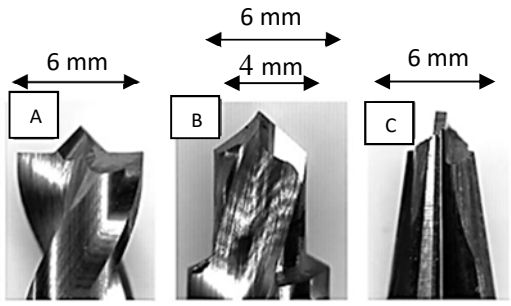

Figure 2.1: Geometries for Brad center drill (A), Step drill (B) and Reamer drill (C).

All drills, manufactured by Guhring, Inc.[36] were based on a CW substrate without coating and tested in fresh conditions in order to avoid the effect of wear evolution.

The tests were carried out in dry conditions to avoid the composite contamination with the cutting fluid. No pre-drilled hole was made for any case. The experimental tests were performed with cutting parameters in the range recommended by the tool manufacturer (see Table 2.3).

2.2.3 MACHINE TOOL

A machining center B500 KONDIA, equipped with a Kistler 6123C rotating dynamometer was used for drilling tests and in process monitoring of the thrust force (F_y) and the torque (M_z) (Figure 2.2A).

The composite was confined during drilling into a specially designed box connected to the vacuum in order to collect the chip avoiding the dispersion of the fibers into the environment or the contact with the machine and its operator.

Drilling tests were performed using a supporting back plate (previously drilled with a hole with a diameter close to the nominal diameter). This procedure, commonly used in industry, is expected to diminish delamination damage.

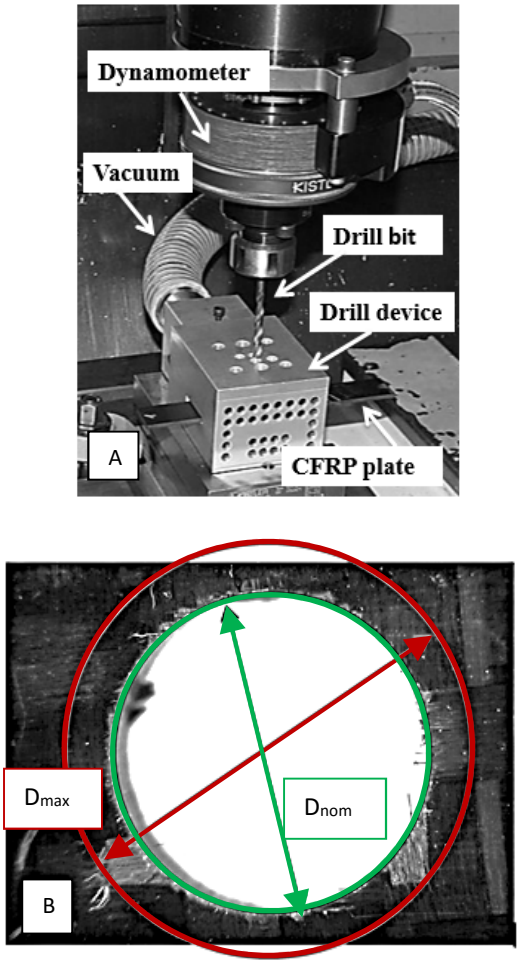

Figure 2.2. (A) Experimental set-up and (B) measurement of diameters for calculation of delamination factor.

Table 2.3. Cutting parameters used in drilling tests: *f* feed rate and *V* cutting speed.

Parameter	Range		
***f* [mm/rev]**	0.05	0.1	0.15
***V* [m/min]**	25	50	100

2.2.4 DELAMINATION MEASUREMENT

Delamination damage was quantified in terms of the delamination factor (F_d), defined as the ratio between the maximum diameter of delaminated area and the nominal diameter of the hole (see Figure 2.2B). Despite this factor does not account for the damaged area, it is the most used approach in the literature due to its simplicity. The hole quality was evaluated using an optical microscope (Optika SZR) in order to obtain the diameter of delaminated area. This measurement technique just considers the surface layers delamination where the damage area is externally exposed since the most critical damage modes are entry delamination (peel-up) and exit delamination (push out). Peel-up delamination is found around the hole entrance periphery as a consequence of the peeling force through the slope of the drill flutes, resulting in separation of the upper plies. On the other hand, push-out occurs due to the maximum thrust force reached when the tool tip breaks through the bottom face of the laminate, where the maximum delamination is usually originated. Thus, internal layers delamination was not accounted.

2.3 Results and Discussion

Experimental results were evaluated in terms of cutting forces measured during drilling and delamination damage. The entrance and exit hole are critical zones usually exhibiting the largest delaminated area. When the cutting edges of drill bit make contact with the material, a peeling force through results in separating the upper plies from the laminate. This effect is remarkable when acute edges are used (corresponding to new unused tools). When edge wear progresses, this force is decreased since the geometry becomes to round. Wear progression elevates the thrust force but decreases the peel force thus leading to reduced peel-up and enhanced push-out delamination [31].

On the other hand, thrust force and torque depend on the drill geometry: both shape and magnitude are affected by the drill geometry [14,17]. An example is given in the Figure 2.3, showing evolution of thrust force and torque with drill bit progress recorded during drilling tests of woven material (feed rate 0.1 mm/rev and cutting speed 100 m/min). Similar curves shape was obtained for the tape composite.

The graph corresponding to Brad drill clearly shows the point corresponding to the maximum thrust force and torque, both reached when the brad tip has penetrated completely across the laminate. The point angle of the drill (180°) leads to a rapid increase of the forces and the maximum is reached very fast.

When step drill is considered, two peaks indicate the maximum level of thrust and torque corresponding to both steps of the drill. The first one is due to the effect of the point of the drill bit (F_1 and T_1) and the second one is due to the action of the second step (F_2 and T_2).

Finally, the evolution obtained with the Reamer drill shows a first peak in the thrust force (corresponding to the entrance of conical part of the drill) followed by a plateau, and this zone corresponds with the maximum value of the torque (appearing when the cylindrical part of the drill is cutting). The absolute level of thrust force presents the lowest values for the step drill. The reamer and brad drill showed similar values

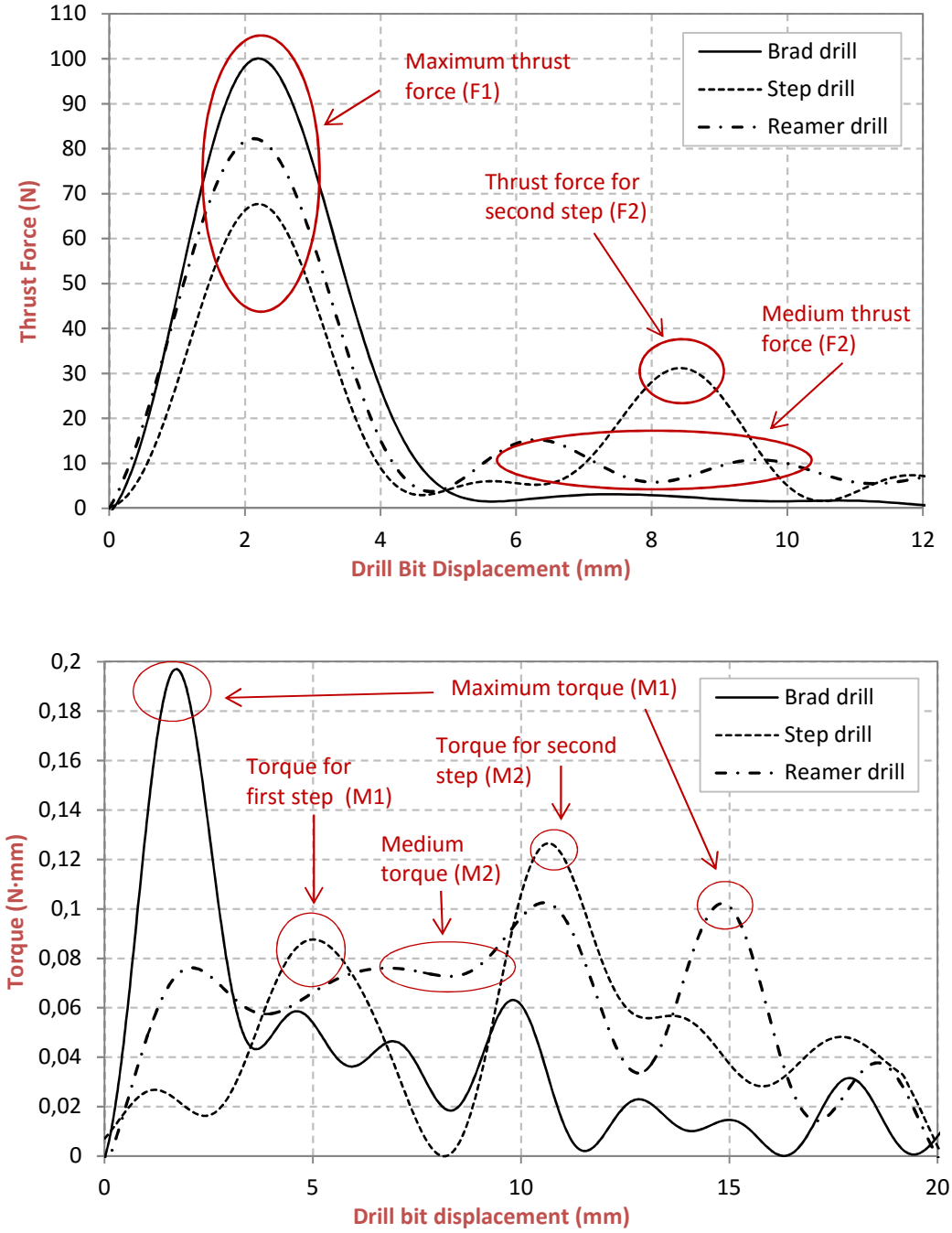

Figure 2.3: Evolution of thrust force and torque for the different geometries analyzed in case of woven material. Cutting conditions: f=0.1 mm/rev and V=100 m/min.

of maximum thrust force, slightly higher for brad drill.

2.3.1 WOVEN COMPOSITE

Thrust force and torque

Figure 2.4 shows the level of the significant values of thrust force and torque defined in the previous section under the different cutting conditions tested for each drill geometry.

In all cases, the maximum level of thrust force increased (F_1) with feed rate; however, for step drill and Reamer drill, the effective medium force (denoted F_2 in Figures 2.4C and 2.4E) showed negligible influ-

ence of cutting conditions. This fact was also verified in previous works [25,26]. On the other hand, Brad drill led to increased thrust force with feed rate (up to 92%).

Spindle speed had an opposite effect and in general thrust force decreased with cutting speed (up to 45%). The brad drill bit registered the maximum thrust forces while the lowest values were found for Reamer drill.

Torque analysis increased with feed rate for all cases (Figures 2.4B, D, F). Varia-

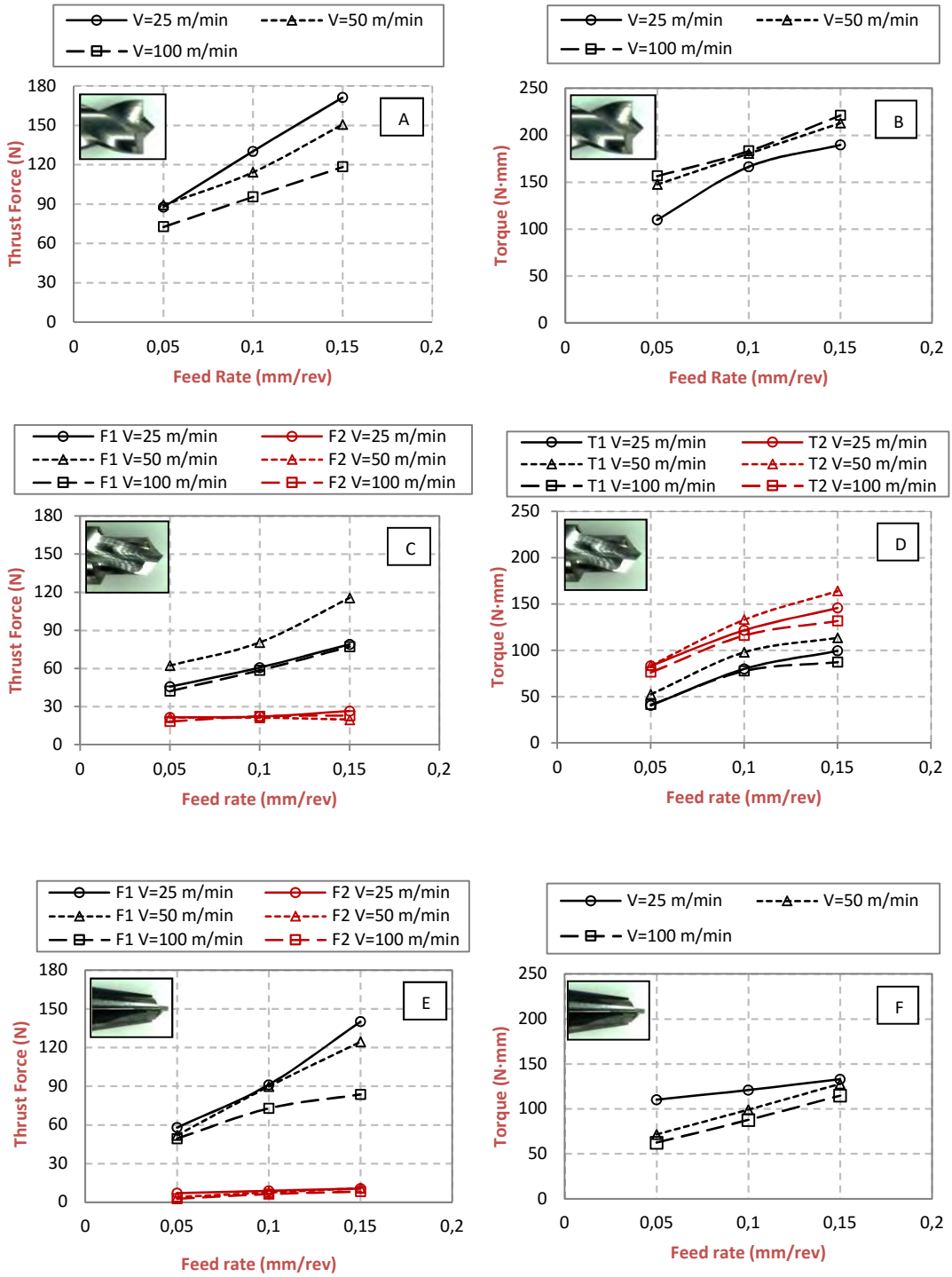

Figure 2.4: Variation of thrust force versus feed rate for Brad drill (A), Step drill (C) and Reamer drill (E) and torque versus feed rate for Brad drill (B), Step drill (D) and Reamer drill (F) for woven material.

tions up to 63%, 96% and 84% were observed for Brad drill, step drill and reamer drill, respectively. However, cutting speed presented different effect in function of the geometry; Brad drill had a positive growing while Reamer has a negative trending. Also minimum torque was found for Reamer drill whereas the highest values were observed for Brad drill.

Delamination

Figure 2.5 shows delamination factor calculated both at entry and exit hole for woven material. Maximum entry delamination increased up to 10% for the case of Brad drill and 18% for the Reamer drill when feed rate increases. Step drill did not present significant variation. Concerning the influence of cutting speed, peel-up extension increased for Brad and step drill (8% and 4%). The opposite trend was observed for Reamer drill: entrance delamination decreased with the spindle speed up to 15%.

Exit delamination increased up to 17.5% for Brad drill and 10% for step drill with feed rate, while reamer drill showed negligible variation with feed rate. Exit delamination increased with cutting speed for Brad drill and step drill (up to 10 % and 6%, respectively) while it was decreased up to 3% for Reamer drill. Comparing the effect of drill geometry, the lowest entry delamination was obtained with the step drill (F_d=1.04) and the highest with Brad drill (F_d=1.45). The most beneficial configuration seems to be the step drill, probably due to the multistep drill.

In the case of exit delamination, the lowest extension of this defect was ob-

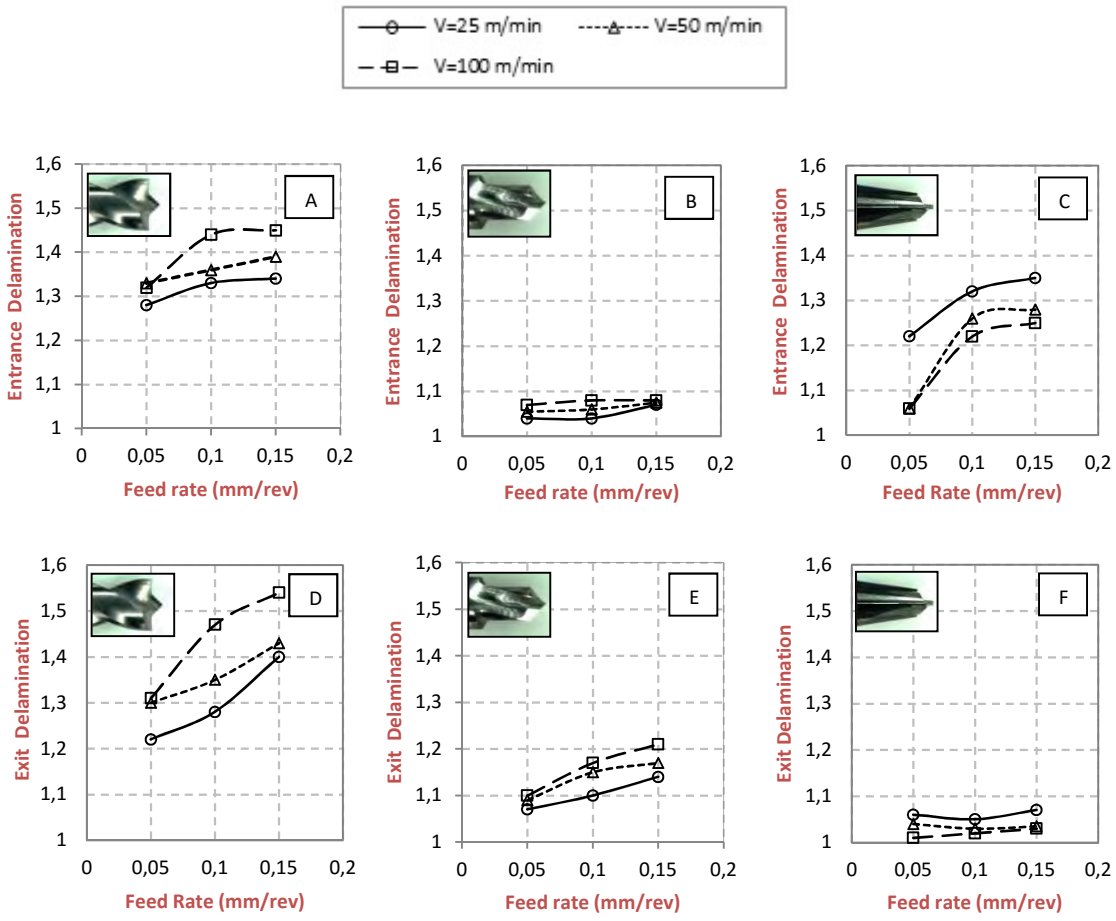

Figure 2.5: Delamination factor versus feed rate for Brad drill (A, D), Step drill (B, E) and Reamer drill (C, F) for woven material.

served for Reamer drill (F_d=1.01) and the highest for Brad drill (F_d=1.54). Exit delamination is related to thrust force and hole configuration. In the case of brad drill, exhibiting the highest value of trust force, it is also observed the highest value of delamination factor at the hole exit. Although reamer and step drill presented similar level of trust force, it is observed smaller extension of delamination for reamer drill. This effect could be related to the multistep configuration of the step drill, the final hole is machined on a previous hole made with the tip of the drill. The ability to resist de-

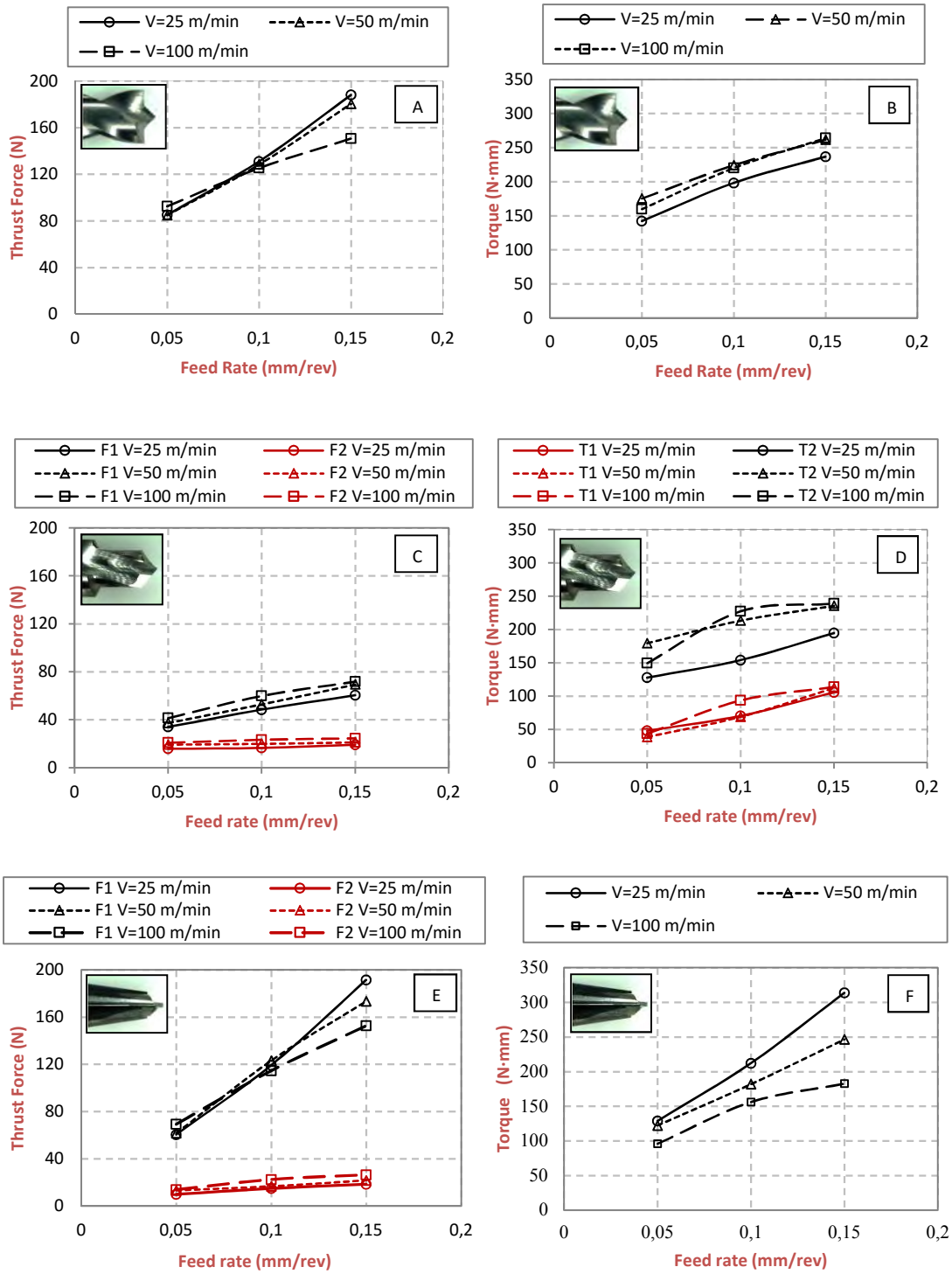

Figure 2.6: Variation of thrust force versus feed rate for Brad drill (A), Step drill (C) and Reamer drill (E) and torque versus feed rate for Brad drill (B), Step drill (D) and Reamer drill (F) for tape material.

lamination at the interface is lower than in the case of reamer drill, machining the intact plate of composite.

2.3.2 MULTIDIRECTIONAL COMPOSITE

Thrust force and torque

The evolution of cutting forces with cutting time for the tape composite showed similar trends than those obtained for the woven material. Thrust force increased with feed rate for all geometries analyzed (see Figure 2.6). The increment of effective force (F_2 in the case of step and Reamer drills) was around 112% for Brad drill, 18% for step drill and a 90% for Reamer drill. Cutting speed variation did not induce significant changes in the thrust force at low feed rates. However, when spindle speed increased the influence was enhanced, especially in the case of Brad drill: thrust force reduction around 20% was observed.

The maximum level of thrust force presented the lowest values for the step drill. The reamer and brad drill showed similar values of maximum thrust force. This behavior is in agreement with previous work in the literature [14].

Torque increased with feed rate up to 66% for Brad drill, a 60% for step drill and a 144% for Reamer drill. Enhanced cutting speed led to increased torque in the case of Brad drill (24%) and step drill (48%) while for Reamer drill involved torque decrease (72%).

Delamination

Delamination factor measured for the three geometries is presented in Fig. 7. In

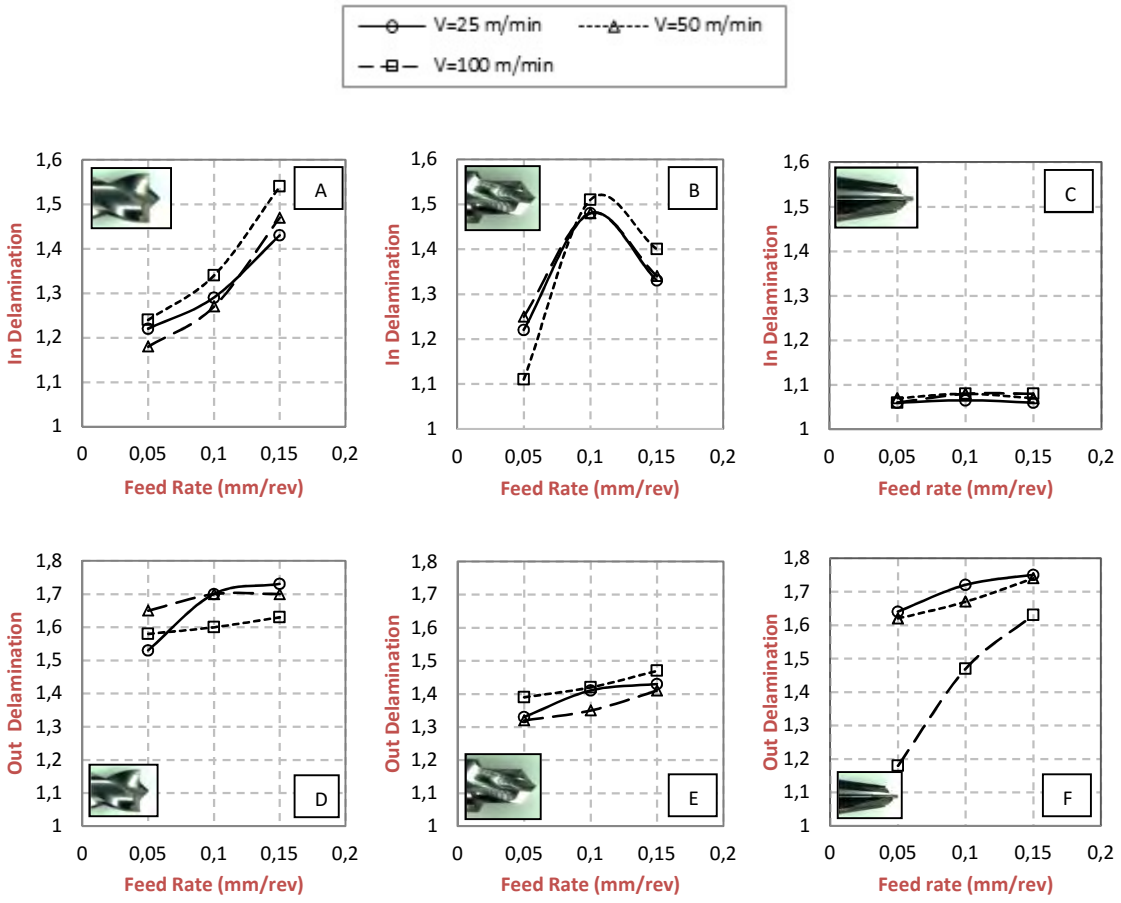

Figure 2.7: Delamination factor versus feed rate for Brad drill (A, D), Step drill (B, E) and Reamer drill (C, F) for tape material.

general the increase of feed rate lead to enhanced delamination. Peel up delamination factor was increased up to 24% for Brad drill. Step drill showed a maximum in delamination for the intermediate value of the cutting speed (50 m/min) and for the highest value of velocity the delamination factor decreases again. Entry delamination increased with cutting speed up to 8% for Brad drill and 5% for step drill. Reamer drill did not show influence of cutting speed in the case of entry delamination.

Exit delamination increased with feed rate up to 11%, 6% and 38% for Brad drill, step drill and Reamer drill, respectively. Variations with cutting speed were small for the brad and step drill (lower than 8%) while delamination factor increased up to 37% for Reamer drill.

The maximum entry delamination extension was found for Brad drill (F_d=1.54) while the minimum was obtained with Reamer drill (F_d=1.08). Concerning exit delamination, Brad drill showed the worst results (F_d=1.73) and step drill the best (F_d=1.32). This is mainly due to the low thrust force of the step drill in the last ply for this kind of materials. However, when drilling with low feed rate reamer drill improved the step drill results (F_d=1.18) in agreement with results provided in the literature [14].

2.3.4 COMPARISON BETWEEN WOVEN AND MULTIDIRECTIONAL COMPOSITES

Thrust force and delamination.

Trust force obtained when drilling woven and multidirectional composite are not directly comparable because the thickness of the laminates are not the same (the woven composite was 2.2 mm thick and the multidirectional composite was 3 mm thick). In order to compare both materials, the forces have been normalized with the thickness of the material. The general trend was that thrust forces were higher for woven material than for tape material (see Figure 2.8A showing an example). This behavior is related to the enhanced mechanical properties of the woven composite involving superior breakage energy.

On the other hand, delamination extension found for unidirectional material is in most cases higher than that observed for woven material. Woven structure gives a clear advantage when drilling induced delamination should be minimized: although higher forces are required to perforate the material, at the same time separation between plies is more difficult. An example of this behavior is provided in Figure 2.8B where thrust force and exit delamination have been presented for Brad drill comparing both types of composites.

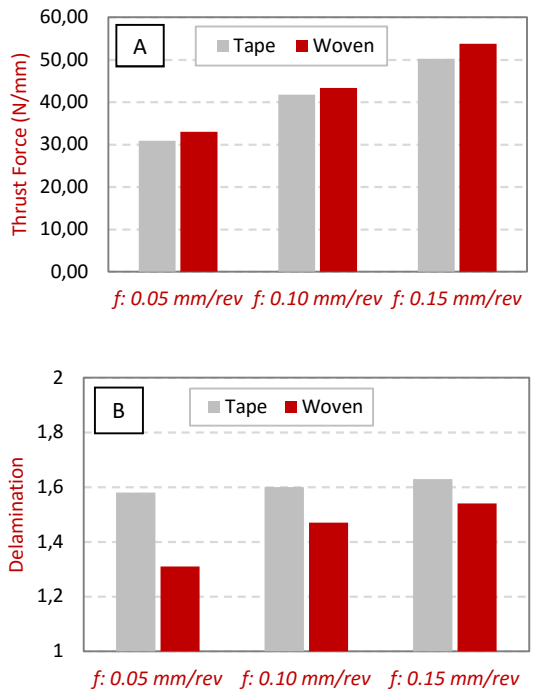

Figure 2.7: Variation of thrust force (A) and exit delamination (B) for Brad drill. Cutting speed: 100 m/min.

ANOVA analysis

An ANOVA analysis using the software StatGraphics software has been developed for each geometry and material in order to study the influence and contribution of the input variables (feed rate, cutting speed) on the output variables (thrust force, torque and delamination factor at the entrance and the exit hole).

In Table 2.4, the ANOVA results for Brad drill can be observed. All the outputs for woven material are significant (F-ratio>6.94, P-value<0.05). In general, feed rate presents more contribution (between 60% and 80%) than cutting speed but the analysis puts in relief that this parameter should be taken into account due to the influence in the results (between 22% and 37%). For the tape material, the contribution of the cutting speed decreases appreciably in comparison with woven and for thrust force and peel-up is not significant (F-ratio<6.94, P-value>0.05). Table 2.5 shows the results for step drill bit. Different contributions from the cutting parameters are highlighted in the ANOVA analysis for both materials. For the woven composite, the force at the first step F_1 presents significance with the cutting parameters, with a main contribution of the feed rate around 64% (F-ratio >6.94, P-value <0.05). In contrast, the force at the second step F_2 has no significant influence on the thrust force (F-ratio <6.94, P-value >0.05). This result is coherent with the values showed on the previous Figure 2.4C where the force is almost constant for the second step of the drill (F_2) and also with the ANOVA results obtained by Shya *et al*. [16]. The rest of the outputs depend on both cutting parameters. The contribution of the cutting speed is lower for the torque (same contribution for step 1 and 2) and for the push-out delamination, but not for peel-up (almost 50% each one) this result is in concordance with the mechanism involved in drilling [1]. On the other hand, tape material shows influence of cutting parameters in both thrust force and torque, while the feed rate shows significant contribution in both delamination damages.

The last drill bit analyzed is Reamer drill which results are showed in Table 2.6. As it is observed for the step drill, only feed rate is significant for the maximum thrust force (F_1) and no cutting parameter is significant for medium thrust force (F_2) (F-ratio<6.94, P-value >0.05) in the case of woven material. This fact involves that values are very similar for all cutting parameters on the range selected for F_2 as can be observed in the Figure 2.4E. For delamination damage in this case, opposite to the two tools analyzed before, only cutting speed is significant and have an important contribution (between 58% and 88%).

The case for tape material is similar to previous drills. Both parameters are influent on the outputs (F-ratio>6.94, P-value<0.05) except for peel-up, where only cutting speed is significant. It is relevant that cutting speed has also high contribution in pushout (50%) in contrast to the other two drill bits for which the influence of the cutting speed in delamination is between 23% and 30%.

Other surface defects

Finally, comparing other superficial defects observed after drilling both materials are commented in this section. Tape material is more vulnerable to damage: surface quality is always inferior for the tape composite than for the woven laminate for any of the selected geometries (Figure 2.9). Fraying defect is found for all cases: Reamer and step drills present this defect especially at the exit and Brad drill at the entrance.

Table 2.4: Comparison of ANOVA analysis for thrust force, torque, peel-up and push-out between woven and tape materials for Brad drill bit.

	Woven							Tape						
	Factor	**Sum of Squares**	**Df**	**Mean Square**	**F-Ratio**	**P-Value**	**Contribution**	**Factor**	**Sum of Squares**	**Df**	**Mean Square**	**F-Ratio**	**P-Value**	**Contribution**
Thrust Force	V (m/min)	1.81E+03	2	9.06E+02	9.57	0.0299	22.5%	V (m/min)	2.21E+02	2	1.11E+02	0.73	0.5376	1.9%
	f(mm/rev)	6.06E+03	2	3.03E+03	32.04	0.0035	75.2%	*f*(mm/rev)	1.10E+04	2	5.48E+03	36.04	0.0028	95.4%
	Error:	3.78E+02	4	9.46E+01	-	-	2.3%	Error:	6.09E+02	4	1.52E+02	-	-	2.6%
	Total:	8.25E+03	8	4.03E+03	-	-	-	Total:	1.18E+04	8	5.75E+03	-	-	-
Torque	V (m/min)	1.69E+03	2	8.44E+02	13.45	0.0168	18.4%	V (m/min)	1.33E+03	2	6.63E+02	32.08	0.0034	8.8%
	f(mm/rev)	7.37E+03	2	3.68E+03	58.73	0.0011	80.3%	*f*(mm/rev)	1.37E+04	2	6.83E+03	330.35	0.0000	90.9%
	Error:	2.51E+02	4	6.27E+01	-	-	1.4%	Error:	8.27E+01	4	2.07E+01	-	-	0.3%
	Total:	9.31E+03	8	4.59E+03	-	-	-	Total:	1.51E+04	8	7.51E+03	-	-	-
Peel-Up	V (m/min)	2.43E-02	2	1.21E-02	15.61	0.0129	29.5%	V (m/min)	8.09E-03	2	4.04E-03	6.28	0.0584	6.7%
	f(mm/rev)	5.66E-02	2	2.83E-02	36.4	0.0027	68.7%	*f*(mm/rev)	1.11E-01	2	5.55E-02	86.14	0.0005	92.2%
	Error:	3.11E-03	4	7.78E-04	-	-	1.9%	Error:	2.58E-03	4	6.44E-04	-	-	1.1%
	Total:	8.40E-02	8	4.12E-02	-	-	-	Total:	1.22E-01	8	6.02E-02	-	-	-
Push-Out	V (m/min)	2.96E-02	2	1.48E-02	12.87	0.0181	36.8%	V (m/min)	3.89E-03	2	1.94E-03	25	0.0055	23.1%
	f(mm/rev)	4.86E-02	2	2.43E-02	21.13	0.0075	60.4%	*f*(mm/rev)	1.28E-02	2	6.41E-03	82.43	0.0006	76.0%
	Error:	4.60E-03	4	1.15E-03	-	-	2.9%	Error:	3.11E-04	4	7.78E-05	-	-	0.9%
	Total:	8.28E-02	8	4.03E-02	-	-	-	Total:	1.70E-02	8	8.43E-03	-	-	-

Df: Degrees of freedom; F Ratio: F-test value(F(α=5%)=6.94); P-Value: P-test value (Significant at the 5% level).

Table 2.5: Comparison of ANOVA analysis for thrust force, torque, peel-up and push-out between woven and tape materials for Step drill bit.

	Woven						Tape					
	Factor	**Sum of Squares**	**Df**	**Mean Square**	**F-Ratio**	**P-Value**	**Contribution**	**Factor**	**Sum of Squares**	**Df**	**Mean Square**	**F-Ratio**	**P-Value**	**Contribution**
Thrust Force 1	V (m/min)	1.32E+03	2	6.62E+02	18.37	0.0096	34.14%	V (m/min)	1.55E+02	2	7.75E+01	23.68	0.0061	10.4%
	f(mm/rev)	2.49E+03	2	1.24E+03	34.47	0.003	64.05%	*f*(mm/rev)	1.32E+03	2	6.61E+02	201.89	0.0001	89.1%
	Error:	1.44E+02	4	3.60E+01	-	-	1.86%	Error:	1.31E+01	4	3.27E+00	-	-	0.4%
	Total:	3.95E+03	8	1.94E+03	-	-	-	Total:	1.49E+03	8	7.42E+02	-	-	-
Thrust Force 2	V (m/min)	1.06E+01	2	5.28E+00	1.16	0.4006	34.49%	V (m/min)	5.07E+01	2	2.54E+01	53.86	0.0013	78.0%
	f(mm/rev)	1.10E+01	2	5.49E+00	1.21	0.3889	35.89%	*f*(mm/rev)	1.33E+01	2	6.67E+00	14.17	0.0153	20.5%
	Error:	1.82E+01	4	4.55E+00	-	-	29.74%	Error:	1.88E+00	4	4.71E-01	-	-	1.4%
	Total:	3.97E+01	8	1.53E+01	-	-	-	Total:	6.60E+01	8	3.25E+01	-	-	-
Torque 1	V (m/min)	6.15E+02	2	3.08E+02	16.32	0.0119	11.07%	V (m/min)	1.95E+02	2	9.74E+01	1.45	0.3358	2.75%
	f(mm/rev)	4.91E+03	2	2.45E+03	130.11	0.0002	88.23%	*f*(mm/rev)	6.76E+03	2	3.38E+03	50.33	0.0015	95.42%
	Error:	7.54E+01	4	1.89E+01	-	-	0.68%	Error:	2.68E+02	4	6.71E+01	-	-	1.90%
	Total:	5.60E+03	8	2.78E+03	-	-	-	Total:	7.22E+03	8	3.54E+03	-	-	-
Torque 2	V (m/min)	7.55E+02	2	3.77E+02	19.59	0.0086	11.0%	V (m/min)	4.78E+03	2	2.39E+03	11.27	0.0227	36.9%
	f(mm/rev)	6.05E+03	2	3.02E+03	156.99	0.0002	88.4%	*f*(mm/rev)	7.74E+03	2	3.87E+03	18.25	0.0098	59.8%
	Error:	7.70E+01	4	1.93E+01	-	-	0.6%	Error:	8.48E+02	4	2.12E+02	-	-	3.3%
	Total:	6.88E+03	8	3.42E+03	-	-	-	Total:	1.34E+04	8	6.47E+03	-	-	-
Peel-Up	V (m/min)	1.13E-02	2	5.63E-03	8.45	0.0366	46.4%	V (m/min)	4.67E-04	2	2.33E-04	0.07	0.9359	0.3%
	f(mm/rev)	1.17E-02	2	5.83E-03	8.75	0.0346	48.1%	*f*(mm/rev)	1.32E-01	2	6.62E-02	19.11	0.009	94.7%
	Error:	2.67E-03	4	6.67E-04	-	-	5.5%	Error:	1.39E-02	4	3.47E-03	-	-	5.0%
	Total:	2.56E-02	8	1.21E-02	-	-	-	Total:	1.47E-01	8	6.99E-02	-	-	-
Push-Out	V (m/min)	4.87E-03	2	2.43E-03	14.6	0.0145	29.2%	V (m/min)	6.69E-03	2	3.34E-03	14.68	0.0144	34.7%
	f(mm/rev)	1.15E-02	2	5.73E-03	34.4	0.003	68.8%	*f*(mm/rev)	1.22E-02	2	6.08E-03	26.68	0.0049	63.0%
	Error:	6.67E-04	4	1.67E-04	-	-	2.0%	Error:	9.11E-04	4	2.28E-04	-	-	2.4%
	Total:	1.70E-02	8	8.33E-03	-	-	-	Total:	1.98E-02	8	9.65E-03	-	-	-

Df: Degrees of freedom; F Ratio: F-test value(F(α=5%)=6.94); P-Value: P-test value (Significant at the 5% level).

Table 2.6: Comparison of ANOVA analysis for thrust force, torque, peel-up and push-out between woven and tape materials for Reamer drill bit.

	Woven							Tape						
	Factor	**Sum of Squares**	**Df**	**Mean Square**	**F-Ratio**	**P-Value**	**Contribution**	**Factor**	**Sum of Squares**	**Df**	**Mean Square**	**F-Ratio**	**P-Value**	**Contribution**
Thrust Force 1	V (m/min)	1.23E+03	2	6.15E+02	3.46	0.1344	16.31%	V (m/min)	2.01E+02	2	1.00E+02	0.64	0.5743	1.10%
	f(mm/rev)	5.95E+03	2	2.97E+03	16.72	0.0114	78.90%	*f*(mm/rev)	1.77E+04	2	8.87E+03	56.51	0.0012	97.18%
	Error:	7.11E+02	4	1.78E+02	-	-	4.72%	Error:	6.28E+02	4	1.57E+02	-	-	1.72%
	Total:	7.89E+03	8	3.77E+03	-	-	-	Total:	1.86E+04	8	9.13E+03	-	-	-
Thrust Force 2	V (m/min)	1.06E+01	2	5.30E+00	2.56	0.1925	27.8%	V (m/min)	6.73E+01	2	3.37E+01	15.45	0.0131	30.7%
	f(mm/rev)	2.34E+01	2	1.17E+01	5.63	0.0686	61.3%	*f*(mm/rev)	1.47E+02	2	7.37E+01	33.83	0.0031	67.3%
	Error:	8.29E+00	4	2.07E+00	-	-	10.9%	Error:	8.71E+00	4	2.18E+00	-	-	2.0%
	Total:	4.23E+01	8	1.91E+01	-	-	-	Total:	2.23E+02	8	1.10E+02	-	-	-
Torque	V (m/min)	1.68E+03	2	8.41E+02	10.07	0.0274	35.6%	V (m/min)	9.46E+03	2	4.73E+03	7.61	0.0433	25.7%
	f(mm/rev)	2.88E+03	2	1.44E+03	17.25	0.0108	60.9%	*f*(mm/rev)	2.62E+04	2	1.31E+04	21.04	0.0075	71.0%
	Error:	3.34E+02	4	8.35E+01	-	-	3.5%	Error:	2.49E+03	4	6.22E+02	-	-	3.4%
	Total:	4.90E+03	8	2.37E+03	-	-	-	Total:	3.81E+04	8	1.84E+04	-	-	-
Peel-Up	V (m/min)	1.07E-03	2	5.33E-04	9.14	0.0322	58.2%	V (m/min)	2.89E-04	2	1.44E-04	13	0.0178	75.4%
	f(mm/rev)	6.50E-04	2	3.25E-04	5.57	0.0698	35.5%	*f*(mm/rev)	7.22E-05	2	3.61E-05	3.25	0.1451	18.8%
	Error:	2.33E-04	4	5.83E-05	-	-	6.4%	Error:	4.44E-05	4	1.11E-05	-	-	5.8%
	Total:	1.95E-03	8	9.17E-04	-	-	-	Total:	4.06E-04	8	1.92E-04	-	-	-
Push-Out	V (m/min)	2.45E-03	2	1.23E-03	21	0.0076	88.0%	V (m/min)	1.33E-01	2	6.65E-02	10.34	0.0263	50.0%
	f(mm/rev)	2.17E-04	2	1.08E-04	1.86	0.2689	7.8%	*f*(mm/rev)	1.21E-01	2	6.04E-02	9.39	0.0308	45.4%
	Error:	2.33E-04	4	5.83E-05	-	-	4.2%	Error:	2.57E-02	4	6.43E-03	-	-	4.8%
	Total:	2.90E-03	8	1.39E-03	-	-	-	Total:	2.80E-01	8	1.33E-01	-	-	-

Df: Degrees of freedom; F Ratio: F-test value(F(α=5%)=6.94); P-Value: P-test value (Significant at the 5% level).

On the other hand, fraying area found in woven material was very small (Figure 2.10). Only step geometry caused some chipping at the entrance and exit hole. In Figure 2.10, it can be observed also that surface quality for Reamer drill bit is the best in both sides of the hole.

Tool wear evolution

Analyzing the experimental results for exit delamination, the minimum damage working with the most productive cutting parameters (f=0.15 mm/rev and V=100 m/min) were given by the reamer drill in the case of woven material and the step drill in the case of tape material.

There is not a general criterion indicating that the end of tool life is reached. Adherence of resins and fibers to cutting edges, enhanced sound and vibration and even resin burning are phenomena indicating excessive wear of the drill. In this case, to observe the wear evolution and its influence in the delamination damage, a total of 60 holes were machined with both drills. Despite the elevated number of holes machined and the abrasion of carbon fibers,

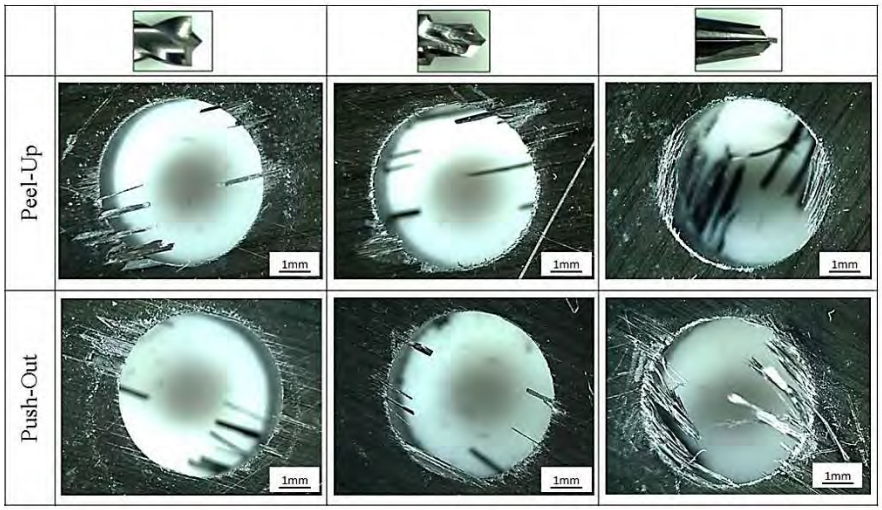

Figure 2.9: Delamination damage and other defects in multidirectional material for the three different drill geometries (V=100 m/min, f=0.1 mm/rev).

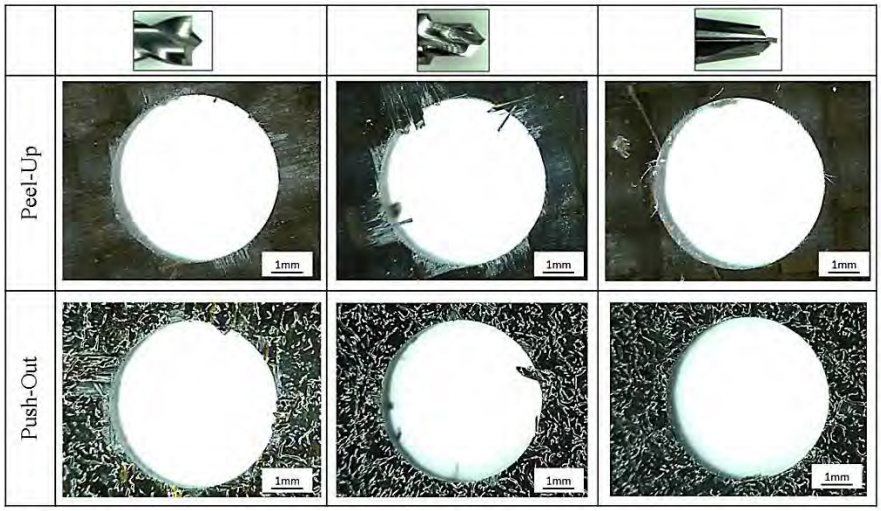

Figure 2.10: Delamination damage in woven material for the three different drill geometries (V=100 m/min, f=0.1 mm/rev).

the wear did not present a rapid evolution.

Figures 2.11 and 2.12 show the evolution of delamination factor versus the number of drilled holes for both cases analyzed. The increment of the damage extension is slower at the hole exit than at the entrance in the case of woven composite. Peel-up increases considerably after drilling 40 holes. Chipping and spalling defects can be also appreciated at the entry of the hole (Figure 2.9) decreasing the surface quality.

For the multidirectional composite, delamination increases for both entrance and exit delamination (Figure 2.10). The increment is approximately lineal and for low number of drill holes peel up is larger than push out. On the other hand, fraying can be observed in both sides of the hole, being lower at the entrance. The fraying at exit increases with the number of holes and the length of threads is longer.

It is worth noting that the drills seem to be almost intact for the number of holes machined; however, the quality of the hole became poor as the number of holes machined with the drill increased. The observation of the tool gives minor information about the end of tool criterion. The evolution of hole quality as wear progresses should be accounted in order to establish the end of tool life criterion leading to drill replacement.

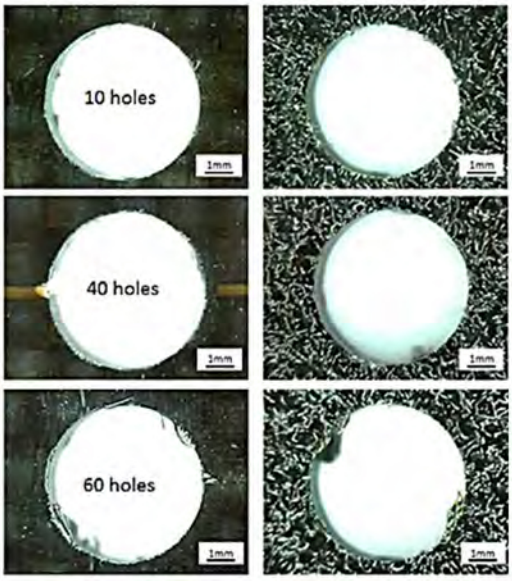

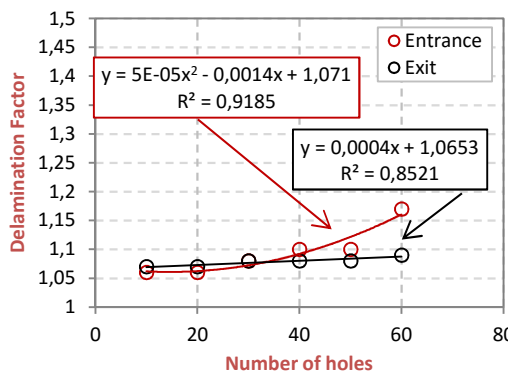

Figure 2.11: Entry and exit delamination for woven material vs. number of drill holes.

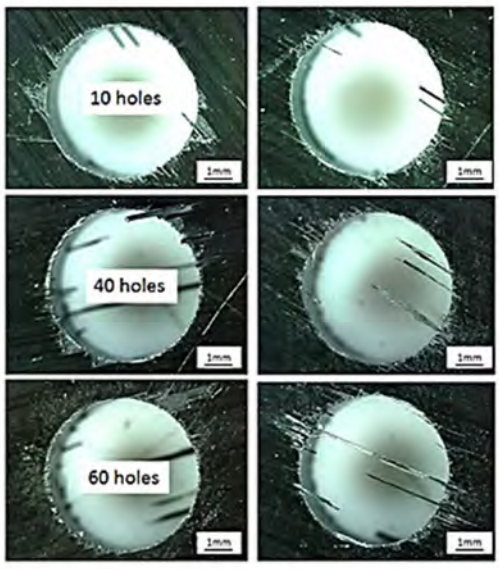

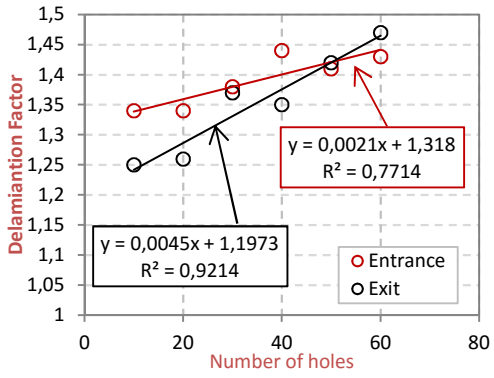

Figure 2.12. Entry and exit delamination for multidirectional material vs. number of drill holes.

2.4 Conclusions

In this paper, the influence of different drill geometries in drilling both tape and woven composite has been analyzed. The geometries selected are based in recent designs of the tool manufacturer especially in the case of Reamer drill bit.

Some conclusions concerning the behavior of different geometries tested in this study are summarized below.

- It was shown that Reamer drill is the most adequate geometry for drilling woven materials (between the geometries analyzed in the work) with low feed rate and high cutting speed. The torque and thrust force obtained are the lowest and delamination extension is small (between 1.01 and 1.08). For this tool the influence of cutting parameters in thrust force is low.
- Reamer drill could be also recommended for tape material, working with low feed rate and high cutting speed. In this case, the cutting speed is important due to the influence of this parameter in delamination is high. The range of delamination factor is in the range 1.06–1.18. However, in this case, the occurrence of other surface defects such as fraying is severe.
- Brad drill presented the highest thrust forces and consequently the worst surface quality.

Concerning the influence of the laminate configuration, it can be concluded that tape material is more susceptible to suffer delamination damage, experiencing stronger delamination although thrust forces were lower. Fraying defect was observed for all drill holes. The superficial quality showed for woven is always superior for all conditions analyzed.

This is an important conclusion of the work: woven composite not only exhibits enhanced mechanical properties, as it is well known, but also presents better surface quality when drilled.

Concerning the influence of cutting parameters, the ANOVA analysis showed that the most influential parameter on thrust force and torque is in general feed rate. However, cutting speed is not negligible in many cases and its influence depends on the drill geometry. For the special case of Reamer drill bit, the ANOVA showed that feed rate has no influence on delamination damage while cutting speed has an important contribution (between 50% and 88%).

Finally, it has been proved that wear has an important impact on the final quality of the hole. In the case of woven material, Reamer drill presented proper behavior when the drill bit is new leading to reduced delamination. As wear progresses, the entry damage increases quickly. However, in the case of tape composite, step drill shows similar growing trend for both entry and exit delamination. The establishment of the end of tool life criterion should be done accounting for the final quality of the hole, in terms of maximum number of holes machined with the drill.

2.5 Declaration of Conflicting Interests

The author(s) declared no potential conflicts of interest with respect to the research, authorship, and/or publication of this article.

2.6 Funding

The author(s) disclosed receipt of the following financial support for the research, authorship, and/or publication of this article: This work was supported by the Ministry of Economy and Competitiveness of Spain (DPI2011-25999) and the FPI subprogram (BES-2012-055162).

2.7 References

[1] Liu DF, Tang YJ, Cong WL. A review of mechanical drilling for composite laminates. Compos Struct 2012; 94: 1265–79.

[2] Davim JP. Machining composite materials. London: ISTE-Wiley, 2010.

[3] López De Lacalle N, Lamikiz A, Campa FJ, Valdivieso A, Etxeberria I. Design and test of a multitooth tool for CFRP milling. J Compos Mater 2009; 43:3275–90.

[4] Girot F, Iliescu D, Valdivieso AF, Gutiérrez-Orrantia ME, Lopez de Lacalle NL. Experimental study and modelling of tool wear during drilling and trimming of CFRP. Revue des Composites et des Materiaux Avances 2013; 23(3):357–85.

[5] Santiuste C, Barbero E, Miguélez MH. Computational analysis of temperature effect in composite bolted joints for aeronautical applications. J Reinf Plast Compos 2011; 30:3–11.

[6] Santiuste C, Olmedo A, Soldani X, Miguelez MH. Delamination prediction in orthogonal machining of carbon long fiber reinforced polymer composites. J Reinf Plast Compos 2012; 31:875–85.

[7] Krishnaraj V, Zitoune R, Davim JP. Drilling of polymer-matrix composites. Heidelberg: Springer, 2013.

[8] Davim JP. Drilling of composite materials. New York: NOVA Publishers, 2009.

[9] Feito N, López-Puente J, Santiuste C, Miguelez MH. Numerical prediction of delamination in CFRP drilling. Compos Struct 2014; 108:677–83.

[10] Abrao AM, Campos Rubio JC, Faria PE, Davim JP. The effect of cutting tool geometry on thrust force and delamination when drilling glass fibre reinforced plastic composite. Mater Des 2008; 29(2):508–13.

[11] Gaitonde VN, Karnik SR, Campos J, Correia AE, Abrão AM, Davim JP. Analysis of parametric influence on delamination in high-speed drilling of carbon fiber reinforced plastic composites. J Mater Process Technol 2008; 203(1):431–38.

[12] Campos J, Abrao AM, Faria PE, Correia AE, Davim JP. Effects of high speed in the drilling of glass fibre reinforced plastic: evolution of the delamination factor. Int J Mach Tools Manuf 2008; 48(6):715–20.

[13] Davim JP, Campos J, Abrao AM. A novel approach based on digital analysis to evaluate the delamination factor after drilling composite laminates. Compos Sci Technol 2007; 67:1939–45.

[14] Durao P, Gonçalves JS, Tavares RS, Albuquerque C, Vieira A, Marques T. Drilling tool geometry evaluation for reinforced composite laminates. Compos Struct 2010; 92(7):1545–50.

[15] Marques T, Durao M, Magalhaes A, Silva JF, Tavares RS. Delamination analysis of carbon fibre reinforced laminates: evaluation of a special step drill. Compos Sci Technol 2009; 69:2376–23.

[16] Shyha S, Aspinwall DK, Soo SL, Bradley S. Drill geometry and operating effects when cutting small diameter holes in CFRP. Int J Mach Tools Manuf 2009; 49:1008–14.

[17] Piquet R, Lachaud F, Ferret B, Swider P. Experimental analysis of drilling damage in thin carbon/epoxy plate using special drills. Compos Part A 2000; 31(10):1107–15.

[18] Xu J, An Q, Chen M. A comparative evaluation of polycrystalline diamond drills in drilling high-strength T800S/250F CFRP. Compos Struct 2014; 117:71–82.

[19] Karpat Y, Bahtiyar O, Deger B, Kaftanoğlu B. A mechanistic approach to investigate drilling of UD-CFRP laminates with PCD drills. CIRP Ann – Manuf Tech 2014; 63:81–4.

[20] Davim JP, Reis P. Drilling carbon fiber reinforced plastics manufactured by autoclave-

experimental and statistical study. Mater Des 2003; 24:315–24.

[21] Grilo TJ, Paulo RMF, Silva CRM, Davim JP. Experimental delamination analyses of CFRPs using different drill geometries. Compos Part B 2013; 45:1344–50.

[22] Hocheng H, Tsao CC. Effects of special drill bits on drilling-induced delamination of composite materials. Int J Mach Tools Manuf 2006; 46:1403–16.

[23] Tsao CC. Experimental study of drilling composite materials with step-core drill. Mat Des 2008; 29:1740–44.

[24] Tsao CC, Chiu YC. Evaluation of drilling parameters on thrust force in drilling carbon fiber reinforced plastic (CFRP) composite laminates using compound core-special drills. Int J Mach Tools Manuf 2011; 51:740–4.

[25] Lazar MB, Xirouchakis P. Experimental analysis of drilling fiber reinforced composites. Int J Mach Tools Manuf 2011; 51:937–46.

[26] Shyha S, Soo L, Aspinwall D, Bradley S. Effect of laminate configuration and feed rate on cutting performance when drilling holes in carbon fibre reinforced plastic composites. J Mater Process Technol 2010; 210:1023–34.

[27] Murphy C, Byrne G, Gilchrist MD. The performance of coated tungsten carbide drills when machining carbon fibre-reinforced epoxy composite materials. Proc Instn Mech Engrs, Part B: J Eng Manuf 2002; 216:143–52.

[28] Sandvik Coromant. Modern metal cutting: a practical handbook. 1st ed. North American, Sandviken, Sweden: Sandvik Coromant, 1994.

[29] Ramirez C, Poulachon G, Rossi F, M'Saoubib M. Tool wear monitoring and hole surface quality during CFRP drilling. In: Procedia CIRP (ed) 2nd conference on surface integrity (CSI), Nottingham, UK, 28 May–30 May 2014, pp. 163–168.

[30] Mondelin A, Furet B, Rech J. Characterisation of friction properties between a laminated carbon fibres reinforced polymer and a monocrystalline diamond under dry or lubricated conditions. Tribol Int 2010; 43:1665–73.

[31] Feito N, Díaz-Álvarez J, Díaz-Álvarez A, Cantero JL, Miguelez MH. Experimental analysis of the influence of drill point angle and wear on the drilling of woven CFRPs. Mater 2014; 7:4258–71.

[32] Faraz A, Biemann D, Weinert K. Cutting edge rounding: an innovative tool wear criterion in drilling CFRP composite laminates. Int J Mach Tools Manuf 2009; 49:1185–96.

[33] Wanga X, Kwona PY, Sturtevantb C, Kim D, Lantrip J. Tool wear of coated drills in drilling CFRP. J Manuf Processes 2013; 15:127–35.

[34] Díaz-Álvarez J, Olmedo A, Santiuste C, Miguelez MH. Theoretical estimation of thermal effects in drilling of woven carbon fiber composite. Mater 2014; 7:4442–54.

[35] Santiuste C, DÍaz-Álvarez J, Soldani X, Miguelez MH. Modelling thermal effects in machining of carbon fiber reinforced polymer composites. J Reinf Plast Compos 2014; 33:758–66.

[36] Guhring Inc. http://www.guhring.com/

[37] http://www.montanabrandtools.com/products/bradpoint-drill.

[38] http://superiortoolservice.com.nobullsoftware.com/Composite.aspx.

[39] Ridgard C. Complex structures for manned/unmanned aerial vehicles. Low temp composite processing mechanical property data. Air Force Research Laboratory. AFRL-RX-WP-TM-2008-4054; 2008.

[40] Varas D, Artero-Guerrero JA, Pernas-Sánchez J, López-Puente J. Analysis of high velocity impacts of steel cylinders on thin carbon/epoxy woven laminates. Compos Struct 2013; 95:623–9.

Capítulo 3

Experimental Analysis of the Influence of Drill Point Angle and Wear on the Drilling of Woven CFRPs

Este capítulo analiza la influencia del ángulo de punta y del desgaste de las brocas helicoidales en el daño generado durante el taladrado de materiales CFRPs tejidos. Ambos parámetros son factores importantes que influyen en la calidad del agujero y en las fuerzas de mecanizado. Se ensayaron tres ángulos de punta diferentes representativos de las brocas de uso común en la industria. Por otro lado, se consideraron dos geometrías desgatadas que reproducen los patrones de desgaste observados comúnmente cuando se taladra materiales compuestos: el desgaste de flanco y el achaflanado de la punta. Los resultados mostraron que la influencia cruzada del ángulo de punta y del desgaste es significativa en la fuerza de avance. La calidad superficial se evaluó en términos de delaminación y defectos superficiales mostrando el daño inter-laminar tendencias opuestas a la entrada y a la salida del agujero según el tipo de desgaste. Además, se comprobó que entre los parámetros de corte, la influencia del avance sigue siendo dominante en el daño superficial.

Este estudio se encuentra publicado bajo la siguiente referencia: **N. Feito**, J. Díaz-Álvarez, A. Díaz-Álvarez, J.L. Cantero, M. H. Miguélez. “Experimental analysis of the influence of drill point angle and wear on the drilling of woven CFRPs”, Materials (2014) Vol. 7, p. 4258-4271.

Experimental Analysis of the Influence of Drill Point Angle and Wear on the Drilling of Woven CFRPs

Abstract

This paper focuses on the effect of the drill geometry on the drilling of woven Carbon Fiber Reinforced Polymer composite (CFRPs). Although different geometrical effects can be considered in drilling CFRPs, the present work focuses on the influence of point angle and wear because they are the important factors influencing hole quality and machining forces. Surface quality was evaluated in terms of delamination and superficial defects. Three different point angles were tested representative of the geometries commonly used in the industry. Two wear modes were considered, being representative of the wear patterns commonly observed when drilling CFRPs: flank wear and honed cutting edge. It was found that the crossed influence of the point angle and wear were significant to the thrust force. Delamination at the hole entry and exit showed opposite trends with the change of geometry. Also, cutting parameters were checked showing the feed's dominant influence on surface damage.

Keywords: drilling, woven CFRPs, surface quality, wear.

3.1 Introduction

Carbon Fiber Reinforced Polymer (CFRP) composites combine fatigue and corrosion resistance, light weight and high specific stiffness and strength. These properties make CFRPs suitable for a wide range of structural applications [1]. Within this family of materials, woven graphite fiber epoxy composites have been extensively used in aerospace, automotive and civil applications. Woven CFRPs exhibit higher strength-to weight ratio and higher fracture toughness than unidirectional composites [2].

Although composite components are manufactured close to the final shape, they usually require machining operations in order to achieve dimensional tolerances and assembly specifications. In most cases the component is drilled previously to mechanical joining [3]. Drilling operations of woven carbon composite CFRPs should be designed to be productive processes ensuring the quality of the resultant component. This operation is performed in a high value component; the susceptibility of the composite to undergo machining-induced damage highlights the importance of controlling the process. The composite is exposed to the generation of damage during processing, mainly delamination. This phenomenon is related to machining parameters and drill geometry. Drilling operations of CFRPs involve strong tool wear due to the presence of hard fibers; wear progression leads to variations of the initial geometry of the drill [4].

Various authors have studied CFRPs drilling, mainly in the case of unidirectional composites. A brief summary of the contributions focusing on woven CFRP drilling is presented in the following paragraphs.

Karpat *et al*. [5] analyzed the drilling performance of the double point angle drill for woven CFRP laminates. Uncoated carbide drill and diamond coated carbide drills with different drill point angles were tested in drilling experiments of thick fabric woven CFRP laminates. The feed was more influential than cutting speed on damage generation. At elevated feed rates, the hole diameter tolerance was observed to be more critical than the hole exit delamination.

The influence of the drill point angle on the machining forces and the drill hole quality (in terms of delamination, fraying and burr formation) was analyzed in [6] for woven CFRPs. Increased point angles resulted in enhanced thrust force; however, the torque remains almost constant. The quality at the hole entrance was enhanced when increasing point angles while it was poorer at the exit. The increment of cutting speed lead to negligible differences in the hole quality but resulted in increased thrust forces and decreased drilling torques. This behavior was also observed when drilling cross-ply composite materials with twist drill bits [7]: point angle equal to 120° produced less delamination at hole entry than point angle equal to 85° even though the thrust force was higher in the former case.

The influence of different types of tool geometry when drilling unidirectional CFRP [0/90]13 was analyzed in [8]. “SPUR” drill bit (commonly used for wood materials) gave the best results causing small damage extension in the hole perimeter. On the other hand, a twist drill presented higher delamination located at the hole entrance. Similar tests were carried out on unidirectional CFRPs in [9] showing no advantage for step drill when compared with commercial drill bit, which reduced the surface damage.

On the other hand, wear evolution influences drill geometry. The initial design of the fresh tool is modified because of wear progression and, consequently, the effective cutting geometry is varied.

Mayuet *et al*. [10] carried out drilling tests of woven CFRP with conventional carbide drill geometry. It was demonstrated that the abrasion due to the presence of hard fibers was the dominant wear mechanism. The matrix adhesion had a much lower effect. The influence of wear in hole quality was demonstrated since delamination at the hole exit increased significantly as the number of machined holes increased.

Illiescu *et al*. [11] analyzed the influence of feed rate and tool wear in drilling of woven CFRPs with coated and uncoated drills. The feed rate and tool wear were the most significant factors affecting the thrust force. The torque was much less sensitive to wear than the thrust force. The contact length and the axil force applied at the cutting edge were the main factors involved in wear evolution, in both cases considered (coated and uncoated drills).

Shyha *et al*. [12] analyzed the drilling of small holes (1.5 mm); with two different geometries: conventional twisted and stepped. Delamination at the hole entrance was higher for the stepped drill than for the twisted drill. Increases in the feed rate also lead to delamination enhancement. However, the increment of point angle, from 118° to 140°, lead to decrease of delamination.

Rawat and Attia [13] analyzed the tool wear mechanisms of carbide tools in high speed drilling (10,000–15,000 rpm) of woven CFRPs. Fracture (chipping) at the beginning of drilling process and subsequent abrasion were the main wear mechanisms. Abrasive wear on the flank face of

the primary cutting edge was stronger than the wear at the rake face.

The influence of cutting edge rounding (CER) and its correlation with surface damage in drilling of woven CFRPs was analyzed in [14]. A correlation between delamination, machining forces and cutting edge rounding was found. Numerical analysis of the influence of CER in the elemental case of orthogonal cutting has been developed by the authors in [15]. The interest of analyzing drilling-induced delamination has motivated the recent development of complex models for drilling. These numerical models have shown good correlation between measured and predicted torque and thrust force as well as delamination extension [16,17].

Although drilling operations of woven composite have motivated the development of different studies, it is still a challenge to advance the comprehension of the effect of tool geometry and the level of wear. In fact the analysis of the crossed effect of the tool geometry and the geometrical changes due to wear progression has been poorly developed in the literature.

The objective of this paper is analyzing the effect of the drill point angle combined with the geometrical effect of drill wear evolution. Two different types of wear modes were studied: flank wear (commonly identified in the literature as the dominant wear mode) and cutting edge honing (resulting from the transition from new acute to used cutting edge). The effect of cutting parameters (cutting speed and feed rate) were also studied. Resultant thrust force and torque have been evaluated together with surface integrity, analyzed in terms of delamination at the entrance and exit of the hole.

3.2 Experimental Work

3.2.1 WORKPIECE MATERIAL

The material studied in this work is a woven CFRP composite, based on AS-4 carbon fiber and epoxy matrix (55.29% resin content) manufactured by Hexcel Composites (Madrid, Spain). The specimens were cut in plates of 120 mm × 29 mm and 2.2 mm thick, composed of 10 plies with the same fiber orientation. The characteristics and mechanical properties of the workpiece provided by the composite manufacturer are presented in the Table 3.1, where ρ is density; E_i elastic modulus in the direction i; υ_{ij} Poisson coefficient; G_{ij} elastic modulus in shear directions; X_t, Y_t and S_t maximum tensile stress in longitudinal and shear directions respectively; X_c and Y_c maximum compressive stress in longitudinal directions.

3.2.2 DRILLS

Uncoated helicoidal carbide drills recommended by the manufacturer GHU-RING for CFRPs drilling were used. Nominal diameter was equal to 6 mm with 30° helix angle. Three different values of the point angle 90°, 118° and 140° were used. Three different stages concerning wear evolution

Table 3.1: Characteristics and mechanical properties of the composite.

ρ	$E_1 = E_2$	E_3	υ_{12}	$\upsilon_{13} = \upsilon_{23}$
1570 Kg/m^3	68 GPa	10 GPa	0.22	0.49
G_{12}	$G_{23}=G_{13}$	$X_t = Y_t$	$X_c = Y_c$	S_t
5 GPa	4.5 GPa	795 MPa	860 MPa	98 MPa

were tested: fresh drill, flank wear equal to 0.3 mm and honed cutting edge with length equal to 0.05 mm (see Figure 3.1).

The worn geometries were artificially generated using grinding. The level of wear has been stated according to values corresponding to the end of tool life in the literature. Faraz *et al*. [14] reported a value of flank around 0.25 mm corresponding with advanced wear progression. On the other hand, honed edge is an approximation to chipping wear observed in drilling CFRP. As drilling starts chipping appears because acute cutting edges are not able to tolerate high stress. This phenomenon was reported by Rawat *et al*. [13] with an extension of honed edge zone similar to that considered in the present work.

3.2.3 MACHINING TESTS

The drilling tests were carried out on a machining center (B500 KONDIA, Kondia, Elgoibar, Spain). The machining center was equipped with a rotating dynamometer (Kistler 9123C, Winterthur, Switzerland) used for the measurement of the three force components F_x, F_y, F_z and the drive moment M_z on the rotating tool. The acquisition system coupled to the machine tool is shown in Figure 3.2.

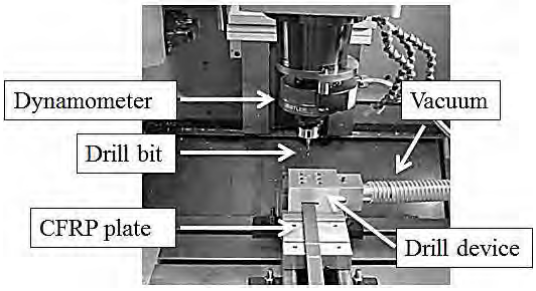

Figure 3.2: Experimental device for drilling tests.

Drilling induced damage was quantified in terms of the delamination factor (F_d) being the ratio between the maximum diameter of delaminated area and the nominal diameter of the hole (see Figure 3.3).

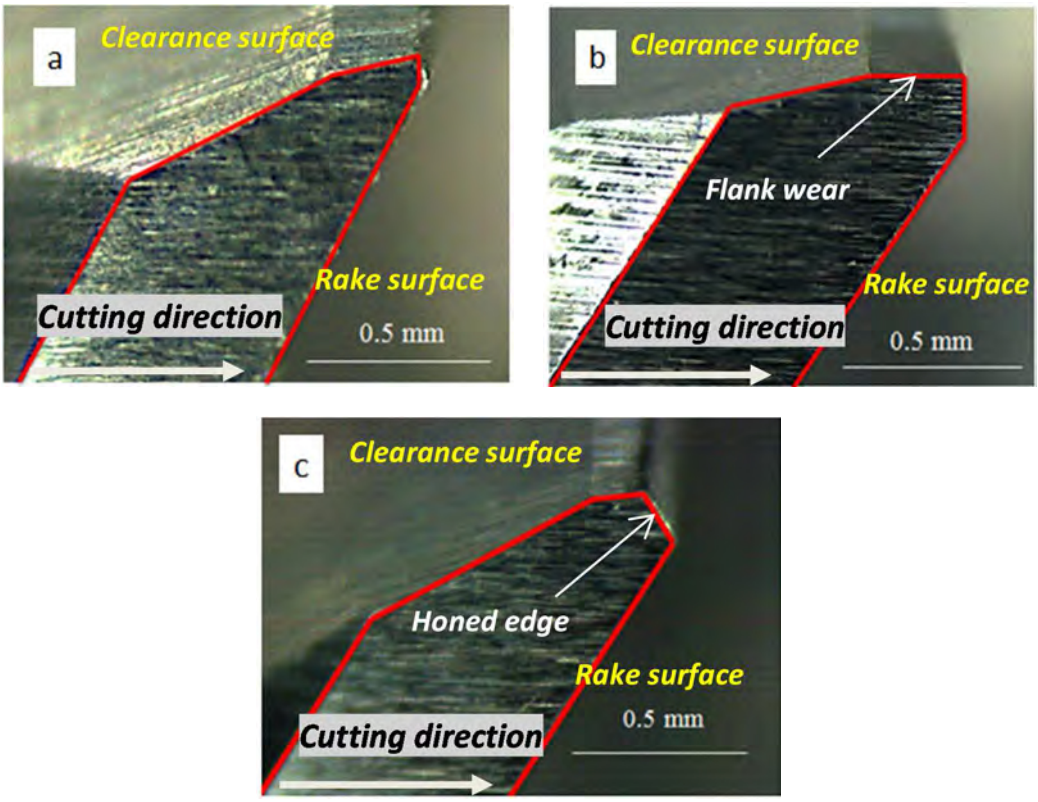

Figure 3.1: Edge geometry of the drills: (A) fresh tool; (B) flank wear; and (C) honed edge.

Other defects induced during machining were analyzed from observation of images of the machined hole obtained with a stereo microscope (Optika SZR, Ponteranica, Italy).

Concerning the cutting conditions, the drilling experiments were conducted without coolant and the cutting parameters summarized in Table 3.2. Machining operations in composites are commonly carried out in dry conditions because it is required to avoid the composite contamination with the cutting fluid. The machining parameters (cutting speed 25–100 m/min and feed 0.05–0.2 mm/rev) were selected following the recommendations of the drills manufacturer GUHRING for drilling CFRPs.

Table 3.2: Cutting parameters used in drilling tests: *f*, feed and *V*, cutting speed.

Parameter	Range		
f [mm/rev]	0.05	0.1	0.15
V [m/min]	25	50	100

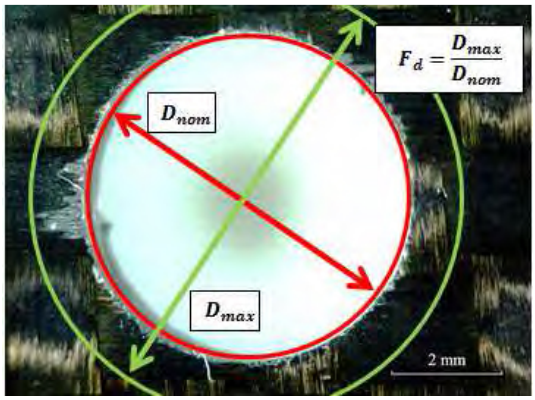

Figure 3.3: Example of delaminated specimen for calculation of delamination factor F_d.

Drilling tests were performed using a supporting back plate previously drilled with hole diameter equal to 6.2 mm. The use of back plate is commonly desired in industry when drilling plates of composite in order to diminish delamination. The influence of the position of the drilled hole related to the textile float was not considered in this paper. Although this parameter may influence the delamination, the drilling tests were carried out in random relative positions of the drill to the textile float. Observed delamination did not show significant differences for the tests carried out in the same cutting conditions despite the variations of the relative position drilled hole/float, indicating low influence of this parameter.

3.3 Results and Discussion

3.3.1 THRUST FORCE AND TORQUE

The evolution of thrust force and torque with cutting time was recorded using the dynamometer. The maximum level of thrust force obtained during drilling tests is presented in Figure 3.4. The maximum thrust force obtained with new and worn drills is presented for the different values of point angle and cutting speed considered. It is possible to observe the negligible influence of the point angle on thrust force when fresh drill is used since the projection of the resultant force in the axial direction is the same for all point angles. The increment of feed lead to thrust force enhancement (the maximum values of thrust force obtained with new tools ranged between 50 and 150 N for all cases tested).

Honed tools showed increasing thrust force (around 50%–65%) with the increment of point angle. The thrust force also increases with the point angle when the flank wear geometry is tested. Relative variations around 100% are observed when the angle ranged from 90° to 140°. This trend is observed for all values of cutting speed analyzed.

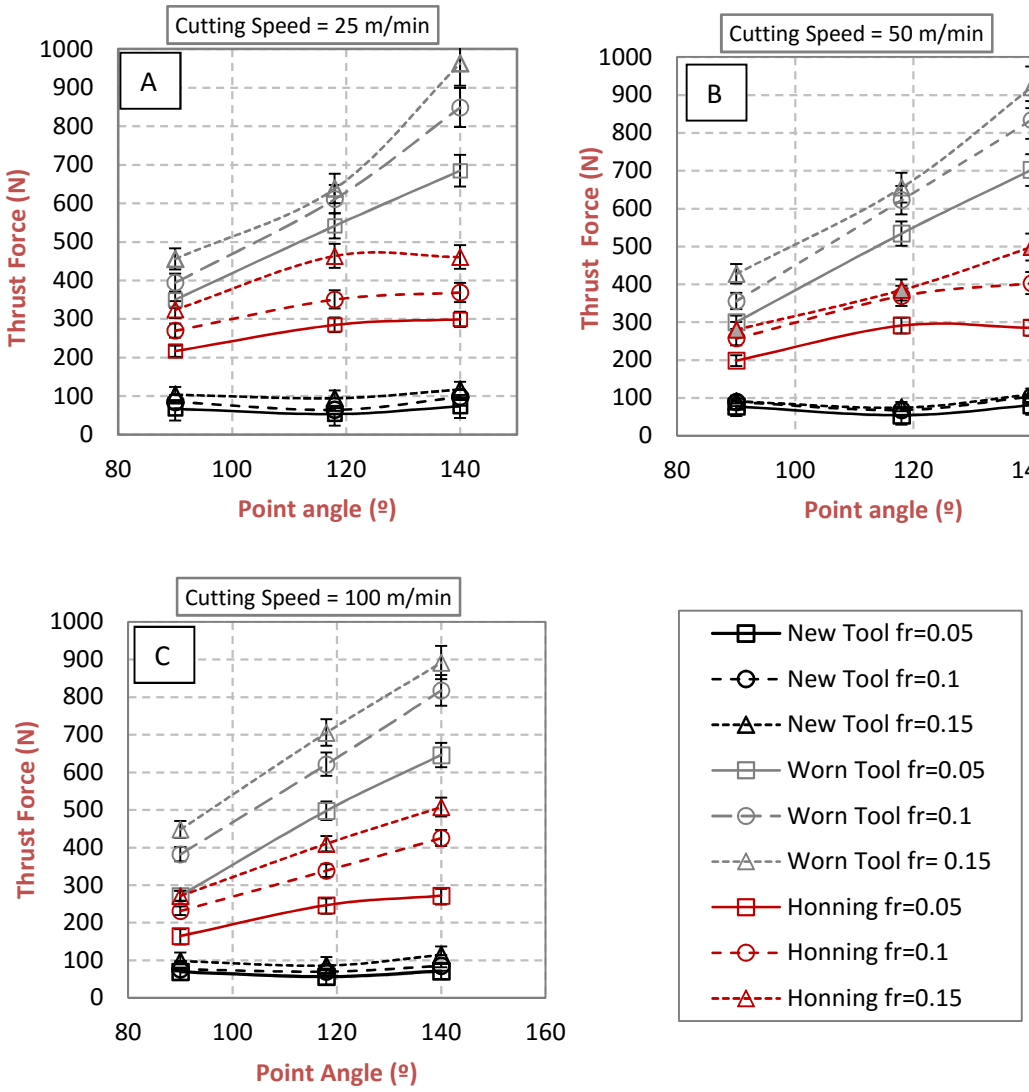

Figure 3.4: Thrust force for three point angles at different cutting speeds (measurement variations are indicated including error bars): (A) cutting speed 25 m/min; (B) cutting speed 50 m/min; and (C) cutting speed 100 m/min.

The enhancement of the feed also resulted in increased thrust force in all cases analyzed. The variation is small for the fresh geometry. However, the increment of thrust force with feed reached increments around 50% and 70% when drilling with flank and honing wear respectively.

The increased values of thrust force due to the use of worn tools are related to enhanced risk of delamination. This trend is observed in the range of cutting speed tested (25–100 m/min). The progression of wear in both cases analyzed (flank wear and honed edge), increases the effect of the feed and the point angle on the thrust force.

In the case of new tool, torque decreased when the point angle increased from 90° to 118° and increased slightly when the angle changed from 118° to 140°. However, for both worn tools, flank wear and honed edge, maximum values of the torque were observed for the point angle 118°. The influence of feed in torque was much higher than in the thrust force, for all cases. The increment of feed leads to torque enhancement in the range 53%–100%.

Table 3.3: ANOVA analysis developed for thrust force.

Factors	SS	DF	MS	F	F *	P *
A: Geometry	3.57 10^6	2	1.79 10^6	242.83	3.12	0.0000
B: Point Angle	525385	2	262692	35.71	3.12	0.0000
C: Cutting Speed	3023.19	2	1511.59	0.21	3.12	0.8147
D: Feed rate	192734	2	96367.1	13.1	3.12	0.0000
Residual	529651	72	7356.26	–	–	–
Total	4.82E+06	80	–	–	–	–

SS: Sum of squares; DF: Degrees of freedom; MS: Mean square; F: F-test value; P *: Probability; * Significant at the 5% level

Concerning the influence of cutting speed, slight decrease of thrust force and torque were observed when the velocity was increased. This trend has been also reported in other works in the literature for woven [12,14] and unidirectional composites [7].

ANOVA analysis presented in Table 3.3 showed that the main contributing factors for thrust force were tool geometry, point angle and feed rate. For all cases, p-value < 0.05 and Test F >> F_α = 5%. The cutting velocity factor did not present a statistical significance because p-value > 0.05 and Test F < F_α = 5%. This analysis corroborates the previous discussion concerning the prevalent influence of the worn geometry and the thrust force. On the other hand Davim *et al*. [18] showed the same effect with ANOVA analysis in previous research.

3.3.2 SURFACE QUALITY

The hole quality was evaluated in terms of hole diameter, delamination factor at the entrance and exit of the hole and other qualitative defects related to surface damage.

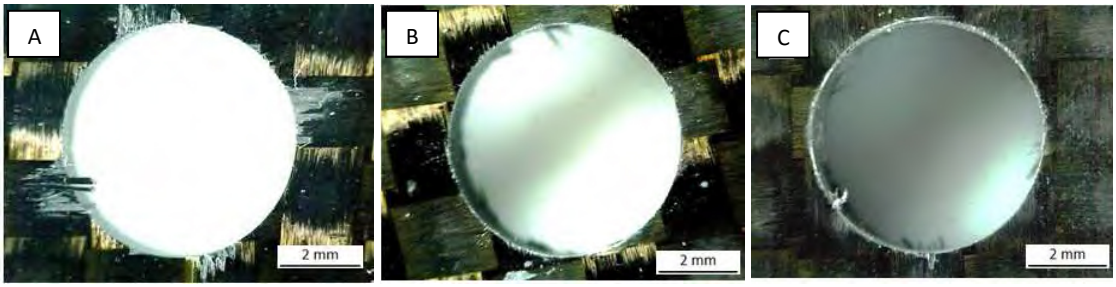

Figure 3.5: Peel up delamination at the hole entrance for new tool (A), flank wear tool (B) and honed edge tool (C) with point angle 118°, V = 50 m/min and f = 0.05 mm/rev.

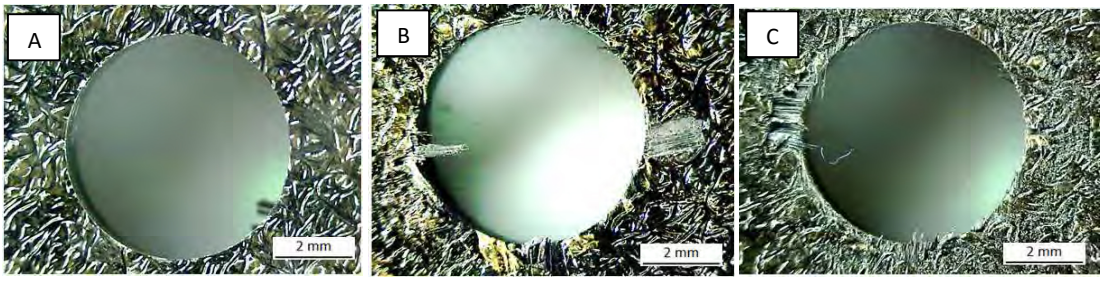

Figure 3.6: Push out delamination at the hole exit for new tool (A), flank wear tool (B) and honed edge tool (C) with point angle 118°, V = 50 m/min and f = 0.05 mm/rev.

The diameter was measured after each drilling test using a micrometer Mitotuyo model 368-101 (Kawasaki, Japan). The values of diameter measured showed a reasonable quality for a drilling operation with a nominal drill diameter equal to 6 mm.

The delamination factor F_d, was calculated as the ratio between maximum diameter of delaminated area and the nominal diameter of the drill (6 mm). The drilled holes were examined with an optical microscope in order to measure the delaminated area. Examples of delamination at the hole entrance (peel up) and at the exit (push out) are shown in Figures 3.5 and 3.6.

The maximum delamination factor obtained after drilling tests at the hole entry and exit is presented in Figures 3.7 and 3.8 respectively.

Delamination factor at the hole entry increased with point angle when drilling with a new tool. However, when a worn tool is used the influence of point angle is almost negligible. Concerning the influence of wear in the delamination factor at hole entry it is observed that the worn geometry produces less fraying of the fibers, and thus the extension of delamination is lower than in the case of fresh geometry. This behavior is consistent with the trends reported in [5] where similar effect was observed with angle point higher than 180°. The lowest delamination factor was obtained for drills exhibiting flank wear (in the range 1.14–1.18) while honed drills lead to slightly increased entrance delamination (around 1.3).

The delamination factor at the hole exit increased with wear, showing that the holes machined with flank wear the highest delaminated areas. This fact is related to the increment of the thrust force with wear progression.

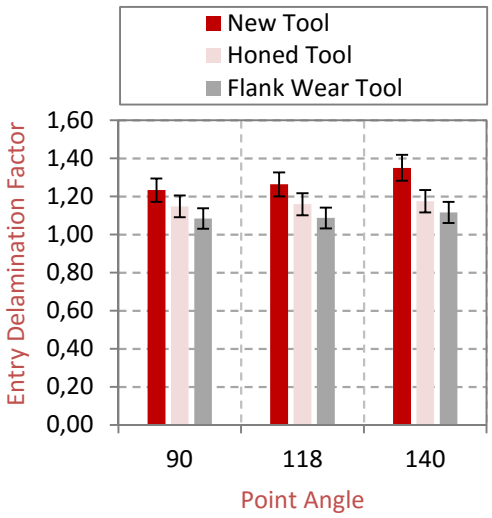

Figure 3.7: Maximum delamination at the hole entry (measurement variations are indicated including error bars).

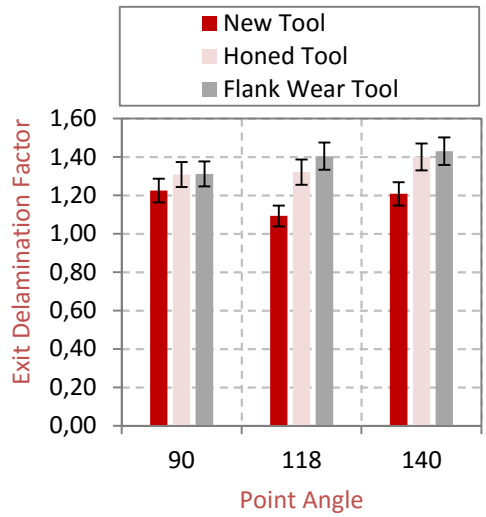

Figure 3.8: Maximum delamination at the hole exit (measurement variations are indicated including error bars).

The opposite effect of wear in the delamination factor considered at the hole exit and entrance can be explained as follows: when the cutting edges of drill bit make contact with the material, a peeling force through the slope of the drill results in separating the plies from each other. When the edge starts to wear, this force diminishes due to the decreasing sharpness. This fact

Table 3.4: ANOVA results for entry delamination factor.

Factors	SS	DF	MS	F	F *	P *
A: Geometry	0.485973	2	0.24299	60.58	3.12	0.0000
B: Point Angle	0.05018	2	0.02509	6.26	3.12	0.0031
C: Cutting Speed	0.020491	2	0.01025	2.55	3.12	0.0848
D: Feed rate	0.118565	2	0.05928	14.78	3.12	0.0000
Residual	0.28877	72	0.00401	–	–	–
Total	0.96398	80	–	–	–	–

SS: Sum of squares; DF: Degrees of freedom; MS: Mean square; F: F-test value; P *****: Probability; ***** Significant at the 5% level.

Table 3.5: ANOVA results for exit delamination factor.

Factors	SS	DF	MS	F	F *	P *
A: Geometry	0.722067	2	0.361033	36.05	3.12	0.0000
B: Point Angle	0.108919	2	0.054459	5.44	3.12	0.0063
C: Cutting Speed	0.008956	2	0.004478	0.45	3.12	0.6412
D: Feed rate	0.138689	2	0.069344	6.92	3.12	0.0018
Residual	0.721059	72	0.010015	–	–	–
Total	1.69969	80	–	–	–	–

SS: Sum of squares; DF: Degrees of freedom; MS: Mean square; F: F-test value; P *: Probability; * Significant at the 5% level.

elevates the thrust force but diminishes the peel force, leading to reduced peel up (related to hole entrance delamination) and elevated push out (corresponding to exit delamination) mechanisms.

Tables 3.4 and 3.5 show the results of the ANOVA analysis corresponding to the entry and exit delamination factor. Drill geometry is the main factor with statistical and physical significance on delamination factor (p-value < 0.05 and Test F >> F_α = 5%). Feed rate and point angle might have a low contribution to delamination but not a negligible one (Test F > F_α = 5%). Finally, for both cases cutting speed is not a significant factor (p-value > 0.05 and Test F < F_α = 5%). Shyha *et al*. [12] and Davim *et al*. [18] came to the same conclusion with a similar ANOVA analysis for CFRP woven composites.

It was possible to observe other defects related to the hole quality. Normally, fraying (Figure 3.9) was not observed at hole entrance for all geometries tested. Fraying was observed at the hole exit with both worn geometries. Flank wear produced less fraying than honed edge tool, and in some cases, it could be confused with chipping. It was observed that this defect increases when the point angle is higher, 118° and 140°. This defect showed a negligible dependence on feed.

Concerning chipping (Figure 3.10), all geometries showed this defect both at the hole entry and exit. For worn tools, this defect was observed more frequently than for new tools and was enhanced for high feed. Increasing cutting speed has the same effect but less marked.

Another frequent surface defect was spalling, also observed with all geometries analyzed, but in different ways. For the honing tool, this defect was observed in a

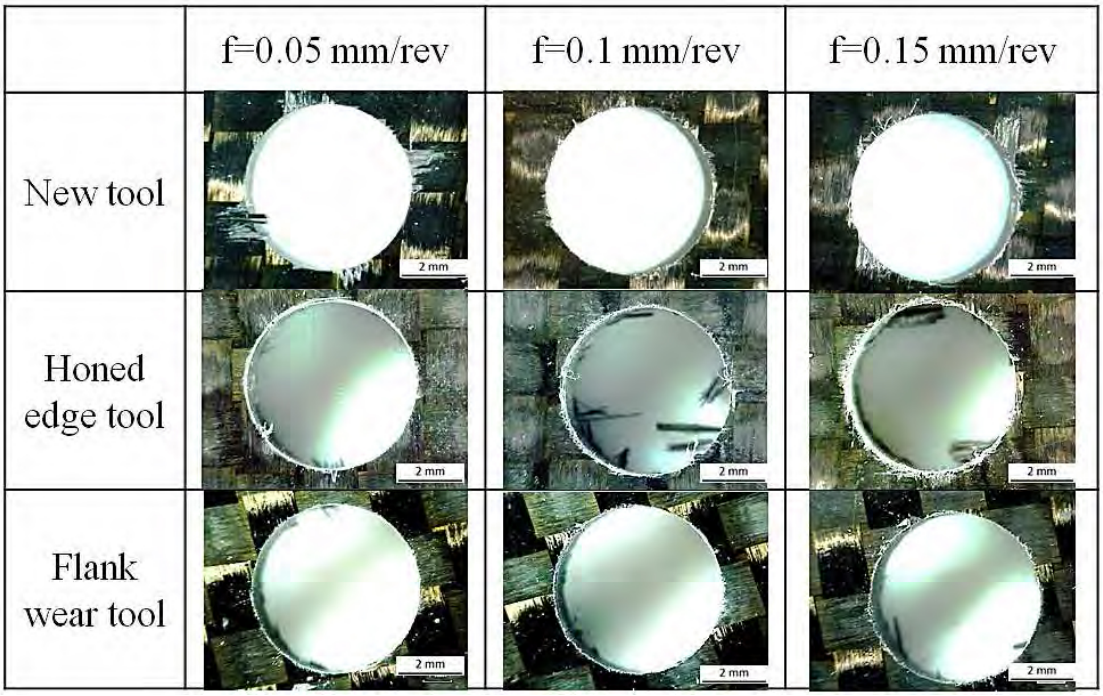

Figure 3.9: Hole entry quality variation with feed for different geometries with 180° point angle and V = 50 m/min.

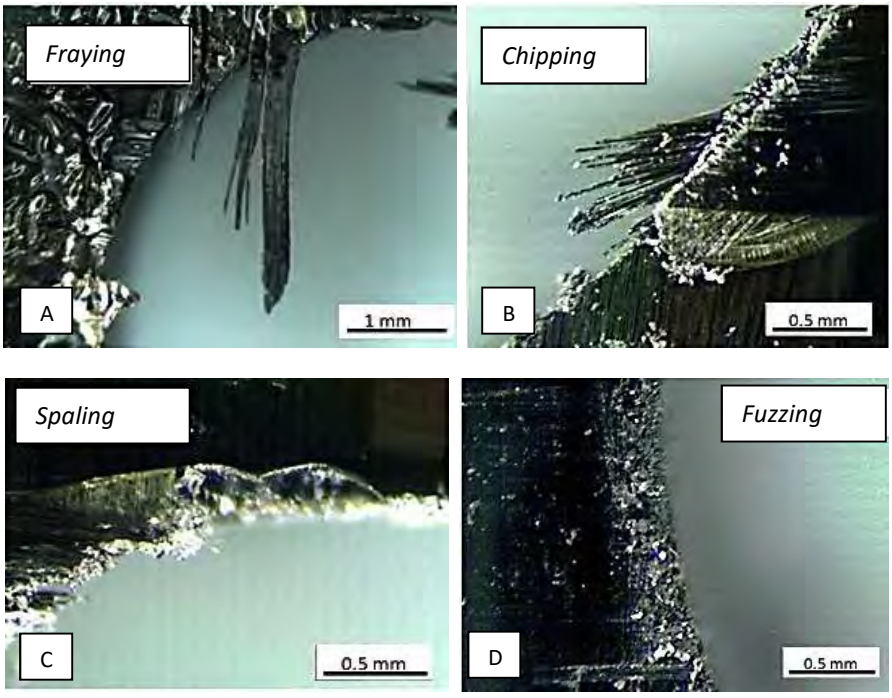

Figure 3.10: Different defects related with hole quality found after drilling. (A) fraying; (B) chipping; (C) spalling; and (D) fuzzing.

homogeneous area surrounding the hole entry, and located at some affected points at exit. Holes machined with flank wear and fresh tool showed this defect in concentrated zones at the hole entry and exit respectively, but it was more severe than that found with honing geometry. It was mainly observed with high feeds (0.15 mm/rev).

Finally, fuzzing (Figure 3.10) increased with point angle and feed and appeared mainly associated to machining with the

honed edge. It was normally found together with spalling.

3.4 Conclusions

In this paper the influence of drill point angle and worn geometry in drilling of woven CFRP composite has been analyzed. The main contribution of the paper is the analysis of the crossed effect of the drill point angle and the geometrical changes due to wear progression. Moreover, the worn geometry was artificially generated ensuring the level and type of wear imposed and avoiding coupled effects of different wear patterns combined in the tool.

The following conclusions can be drawn:

Drill point angle influenced thrust force when it was combined with the effect of wear progression. However, fresh tools showed negligible influence of the drill point angle on thrust force. This fact is important for drill geometry selection since the evolution of wear could lead to inacceptable levels of thrust force.

Wear progression had a different effect on delamination at the entry and exit hole. While entry delamination diminished with wear progression, exit delamination was enhanced. The most favorable results concerning delamination were obtained with the lowest value of the drill point angle: delamination factor at entry and exit hole increased with the drill point angle. This result is important for the workpiece inspection after drilling, establishing critical zones. In addition, during the drill selection, the favorable effect of low drill point should be accounted for.

ANOVA analysis showed that the most influential parameters on thrust force and delamination were tool geometry (wear and point angle) and feed, while cutting speed has negligible influence. This result is important in order to define productive processes with high removal rates ensuring quality requirements of the workpiece.

3.5 Acknowledgments

The authors acknowledge the financial support for the work to the Ministry of Economy and Competitiveness of Spain under the project DPI2011-25999.

3.6 Author Contributions

José Díaz-Álvarez, Antonio Díaz-Álvarez and José Luis Cantero developed drilling tests and data treatment. Norberto Feito and María Henar Miguélez analyzed delamination and studied the crossed influence of the parameters involved. All authors collaborated in preparing figures and tables and Norberto Feito and María Henar Miguélez wrote the paper.

3.7 Conflicts of Interest

The authors declare no conflict of interest.

3.8 References

[1] Huang, X. Fabrication and Properties of Carbon Fibers. Materials 2009; 2:2369–403.

[2] Teti, R. Machining of composites materials. Ann. CIRP 2002, 51, 611–634.

[3] Santiuste C, Barbero E, Miguélez M.H. Computational analysis of temperature effect in composite bolted joints for aeronautical applications. J Reinf Plast Compos 2011; 30:3–11.

[4] Liu D, Tang YJ, Cong WL. A review of mechanical drilling for composite laminates. Compos Struct 2012; 94:1265–79.

[5] Karpat Y, Deger B, Bahtiyar O. Drilling thick fabric woven CFRP laminates with double point angle drills. J Mater Process Technol 2012; 212:2117–27.

[6] Heisel U, Pfeifroth T. Influence of Point Angle on Drill Hole Quality and Machining Forces when Drilling CFRP. Proc CIRP 2012; 1:471–6.

[7] Durão P, Gonçalves JS, Tavares RS, de Albuquerque C, Aguiar A, Torres A. Drilling tool geometry evaluation for reinforced composite laminates. Compos Struct 2010; 92:1545–50.

[8] Grilo TJ, Paulo RMF, Silva CRM, Davim JP. Experimental delamination analyses of CFRPs using different drill geometries. Compos Part B 2013; 45:1344–50.

[9] Marques T, Durão M, Magalhães G, Silva JF, Tavares RS. Delamination analysis of carbon fibre reinforced laminates: Evaluation of a special step drill. Compos Sci Technol 2009; 69: 2376–82.

[10] Mayuet P, Gallo A, Portal A, Arroyo P, Alvarez M, Marcos M. Damaged Area based Study of the Break-IN and Break-OUT defects in the Dry Drilling of Carbon fiber Reinforced Plastics (CFRP). Proc Eng 2013; 63:743–51.

[11] Iliescu D, Gehin D, Gutierrez ME, Girot F. Modeling and tool wear in drilling of CFRP. Int J Mach Tools Manuf 2010; 50:204–13.

[12] Shyha IS, Aspinwall DK, Soo SL, Bradley S. Drill geometry and operating effects when cutting small diameter holes in CFRP. Int J Mach Tools Manuf 2009; 49:1008–14.

[13] Rawat S, Attia H. Wear mechanisms and tool life management of WC–Co drills during dry high speed drilling of woven carbon fibre composites. Wear 2009; 267:1022–30.

[14] Faraz A, Biermann D, Weinert K. Cutting edge rounding: An innovative tool wear criterion in drilling CFRP composite laminates. Int J Mach Tools Manuf 2009; 49:1185–96.

[15] Soldani X, Santiuste C, Muñoz-Sánchez A, Miguélez MH. Influence of tool geometry and numerical parameters when modeling orthogonal cutting of LFRP composites. Compos Part A 2011; 42:1205–16.

[16] Feito N, López-Puente J, Santiuste C, Miguélez MH. Numerical prediction of delamination in CFRP drilling. Compos Struct 2014; 108:677–83.

[17] Phadnis VA, Farrukh M, Anish R, Silberschmidt VV. Drilling in carbon/epoxy composites: Experimental investigations and finite element implementation. Compos. Part A Appl Sci Manuf 2013; 47:41–51.

[18] Davim JP, Reis P. Drilling carbon fiber reinforces plastic manufactures by autoclave experimental and statistical study. Mater Des 2003; 24:315–24.

Capítulo 4

Drilling Optimization of Woven CFRP Laminates under Different Tool Wear Conditions: A Multi-Objective Design of Experiments Approach

La geometría de la herramienta es un factor que se ve afectado por los múltiples ciclos de trabajo debido a la naturaleza altamente abrasiva de las fibras. En este capítulo, se presenta un estudio que mejora la comprensión sobre la influencia de los parámetros de corte en la calidad de los taladros en tejidos CFRP, teniendo en cuenta las diferentes condiciones de desgaste de las herramientas. Mediante análisis estadístico se cuantificó la significancia de cada parámetro del proceso (velocidad de corte, velocidad de avance y el ángulo de punta de la herramienta), así como sus interacciones, en la generación de daño por delaminación y en la fuerza de avance de diferentes tipos de herramientas desgastadas. Por último, se presenta una estrategia de optimización multi-objetivo para seleccionar los rangos óptimos de trabajo de los parámetros de diseño que pueden minimizar las variables de salida antes mencionadas.

Este estudio se encentra publicado bajo la siguiente referencia: N. Feito, A. S. Milani, A. Muñoz-Sánchez. “Drilling optimization of woven CFRP laminates under different tool wear conditions: a multi-objective design of experiments approach”, Structural and Multidisciplinary Optimization (2015) Vol. 53, p. 239-251.

Drilling Optimization of Woven CFRP Laminates Under Different Tool Wear Conditions: A Multi-Objective Design of Experiments Approach

Abstract

The cutting tool geometry is known to be an influential factor on damage induced during drilling of composite materials. Conversely, the geometry of the tool is affected under multiple drilling cycles due to highly abrasive nature of fibers. Building on earlier reports, the aim of this work is to create a better understanding of cutting parameters on the quality of drilled woven carbon fiber reinforced polymer (CFRP) laminates, given different tool wear conditions. Namely, a full factorial design of experiments has been conducted to quantify the significance of each process parameter (cutting velocity, feed rate and tool point angle), as well as their interactions, on the generation of entry- and exist- delaminations as well as the thrust force for different tool types. Finally, using a response surface methodology, a multi-objective optimization strategy has been presented to select optimum ranges of design parameters that can minimize the aforementioned output variables collectively. Such knowledge may be useful to explore further improvements toward defect-free drilling of woven CFRP composites.

4.1 Introduction

The application of Carbon Fiber Reinforced Polymer (CFRP) composites in modern industries is growing fast. Among different types of such materials, woven CFRPs have proven to be appealing material solutions in a broad range of applications, mainly due to their combined fatigue and corrosion resistance, light weight, high specific stiffness and strength properties, along with superior impact fracture toughness compared to unidirectional composites (Huang 2009; Santiuste *et al*. 2011; Teti 2002). Their conformability under different manufacturing methods is also agreeable.

In aircraft industries, CFRP composite parts are normally processed in near-net shapes. However, to achieve required dimensional tolerances, cured sub-components often need machining before assembly. Today, drilling is still among most common manufacturing processes used to join composites through mechanical joins like screws, rivets and bolts. (Santiuste *et al*. 2011). During drilling operation, however, composites are very prone to damage of different types, with delamination being the most major one as recognized by many other researchers (Teti 2002; Liu *et al*. 2012). This phenomenon is defined as inter-ply failure located on the entry and the exit of the drilled hole and is highly related to the choice of machining parameters as well as the drill geometry. On the other hand, the geometry of the drill bit is often worn over time due to the presence of hard fibers.

Earlier studies on the influence of cuttings parameters on delamination damage in drilling woven CFRP materials show that the cutting speed would be the least influential parameter (Heisel and Pfeifroth 2012). On the other hand, cutting speed has

shown some slight influence on the cutting force. Instead, it has been shown that the feed rate is much more influential on both damage generation (delamination) and thrust force during drilling of composites (Shyha *et al*. 2009; Davim and Reis 2003). As another cutting parameter, variation of the point angle of the drill bit has shown different results on the generation of delamination and cutting force. In general, it has been reported that increasing the point angle enhances the thrust force while the torque remains nearly constant (Heisel and Pfeifroth 2012). Increasing the point angle in conventional drills has also improved the quality of the hole in entry (less delamination), but it worsened the hole quality at the exit (Heisel and Pfeifroth 2012). The same effect has been observed at the entry of the hole in cross-ply composite materials with twist drill bits (Durão *et al*. 2010). In particular in the latter study, the thrust force was higher for 120° compared to 85° point angle bit, while delamination at the hole entry was lower for the former case (Durão *et al*. 2010). In another study it was observed that with a double-point angle drill bit, the hole diameter tolerance criterion is more critical at elevated feed rates than the exit delamination (Karpat *et al*. 2012).

Concerning worn drill bits, occasionally used in manufacturing of CFRPs, earlier studies have proven that the wear is mainly caused via tool abrasion by hard fibers (Mayuet *et al*. 2013). The abrasion of the tool geometry in conventional drill bits, as the number of machining cycles is increased, can increase the part delamination damage at the exit of the hole. For tests at high rotational speeds (10.000–15.000 rpm), the abrasive wear has been found to be more significant than chipping on the primary cutting edge (Rawat and Attia 2009). For both tools, coated and uncoated, it has been observed that the axial force is the main factor in increasing the tool wear at the cutting edge. Moreover, the contact length has a contribution in tool wear. In fact, relating to other cutting parameters, increasing the feed rate yields higher thrust forces and consequently a higher tool wear. Drill torque has been reported to be much less sensitive to wear compared to the thrust force (Iliescu *et al*. 2010).

Effect of specific features of the tool geometry, e.g., variation of cutting edge roundness due to abrasion, was studied in (Faraz *et al*. 2009) during drilling of woven CFRP materials. Both delamination and cutting forces presented a positive correlation with the cutting edge roundness. The influence of CER for orthogonal cutting has been studied previously by the third author and co-workers (Soldani *et al*. 2011). Other wear mechanisms reported for drilling CFRPs include the presence of chipping on the edge (Rawat and Attia 2009) and, to a more limited extend, the adhesion of the matrix to the cutting tool (Mayuet *et al*. 2013).

When compared to the above experimental works, numerical models on predicting delamination during composite drilling have been developed more recently (Soldani *et al*. 2011; Feito *et al*. 2014a; Phadnis *et al*. 2013). Some of these finite element based models are aimed not only at estimating delamination, but also the torque and feed force, and their correlations with the underlying mechanical properties of the forming material at different (macro/meso/micro) scales.

4.1.1 MOTIVATION OF THE PRESENT STUDY

Limited ‘statistical’ studies have been carried out in the literature to gain more

robust information regarding the individual and combined (interactive) effects of cutting parameters on different (multiple) drilling output variables, especially given the non-repeatable/random nature of such manufacturing process for composites. The recent studies on drilling optimization of FRP composites (e.g., (Sonkar *et al*. 2014; Abhishek *et al*. 2014)) did not verify if there is a statistical significance of process parameters (i.e., cause and effect/hypothesis testing) prior to applying a single or multi-objective optimization algorithm to minimize/maximize the process outputs via changes the input parameters. Pertinent to hypothesis testing, the study (Davim and Reis 2003) showed that with a significance level of 5%, the cutting speed has a less influence on the peel-up, when compared to the effect of feed rate. However on push-out, contribution percentages of both of these cutting parameters were nearly the same under different tool geometries. For small drills, the study (Shyha *et al*. 2009) used an ANOVA analysis (Montgomery 2009) (with α=5 %) using six input parameters. For the entry delamination, the drill type was found to be the only significant parameter, with no influence from cutting parameters. The point angle and feed rate were significant parameters on the thrust force, and the cutting speed and feed rate were influential on the resultant torque.

In the above statistical studies, however, interactions of cutting parameters were not taken into account. In addition, to the best of authors' knowledge, it has not been shown how an optimum set of woven CFRP cutting parameters can be selected in order to optimize *multiple* process outputs of interest (e.g., the entry and exist delaminations as well as the thrust force simultaneously) and under different *tool wear conditions*. Generally speaking, an optimum set of parameters for a given single design objective such as entry delamination may not be coincident with that of another criterion such as exist delamination. These gaps constituted the main motivation of the present work. In addition to a brand new tool, two different types of tool wear types were considered: the flank wear (commonly identified in the literature as the dominant wear mode) and the cutting edge honing (resulting from the transition of the tool from new to used).

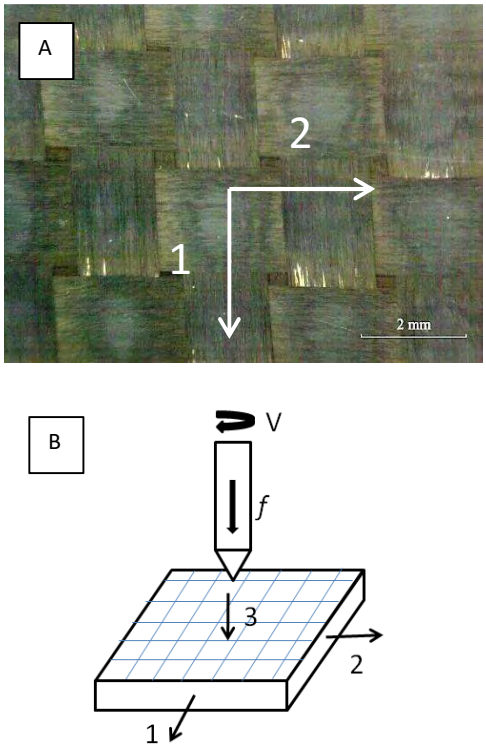

Figure 4.1: Top view of the woven material showing directions 1 and 2 (A) and schematic view of the cutting test configuration including main directions of woven material (B).

4.2 Experimental Procedure

4.2.1 WORKPIECE MATERIAL

Drilling tests were carried out on plates of 120 mm in length× 29 mm in width×2.2 mm in thickness. Each ply is composed of 10 plies of plain woven CFRP with

Table 4.1: Mechanical properties of the woven CFRP tested where ρ is the density; E_i elastic modulus in the in plane direction i; υ_{12} in plane Poisson's ratio; X_t, Y_t and St maximum tensile stress in the longitudinal and shear directions, respectively; X_c and Y_c maximum compressive stress in the longitudinal directions.

Nominal fiber volume	ρ	$E_1 = E_2$	E_3	υ_{12}	$X_t = Y_t$	$X_c = Y_c$	S_t
55.29 %	1570 Kg/m^3	68 GPa	10 GPa	0.31	793 MPa	860 MPa	98 MPa

AS-4 fibres and 8552-epoxy manufactured by Hexcel Corporation.

All the laminate plies have the same warp and weft fiber orientation (Figure 4.1). Mechanical properties provided by the manufacturer are also shown in Table 4.1.

4.2.2 DRILL TOOLS AND SET-UP

Uncoated helicoidal carbide drills recommended by manufacturer (GUHRING) for CFRP drilling were used. The tool nominal diameter was 6 mm with a 30° helix angle. Three different values of the point angle, 90°, 118° and 140°, were considered. In addition, three different conditions concerning tool wear were tested: a brand new drill, flank wear equal to 0.3 mm, and honed cutting edge with a length equal to 0.05 mm (see Figure 4.2). These wear values were established according to the earlier tests by Faraz *et al*. (Faraz *et al*. 2009) in the case of flank wear, and by Rawat *et al*. (Rawat and Attia 2009) in the case of honed edge wear. The honed edge is an approximation to chipping wear observed in drilling CFRPs. These worn geometries were artificially generated on the drill bits using grinding process.

The drilling tests were carried out on a B500 KONDIA machining unit without coolant, while a Kistler dynamometer (9123C) was used to measure the induced thrust force, F_y. The drilling velocity V, feed rate f and point angle α were applied for each wear level (Figure 4.3), resulting in a total of 81 tests. Upon drilling each sample, the damage intensity around the hole was identified as the ratio of the maximum damage diameter (D_{max}) to the nominal diameter (D_{nom}).

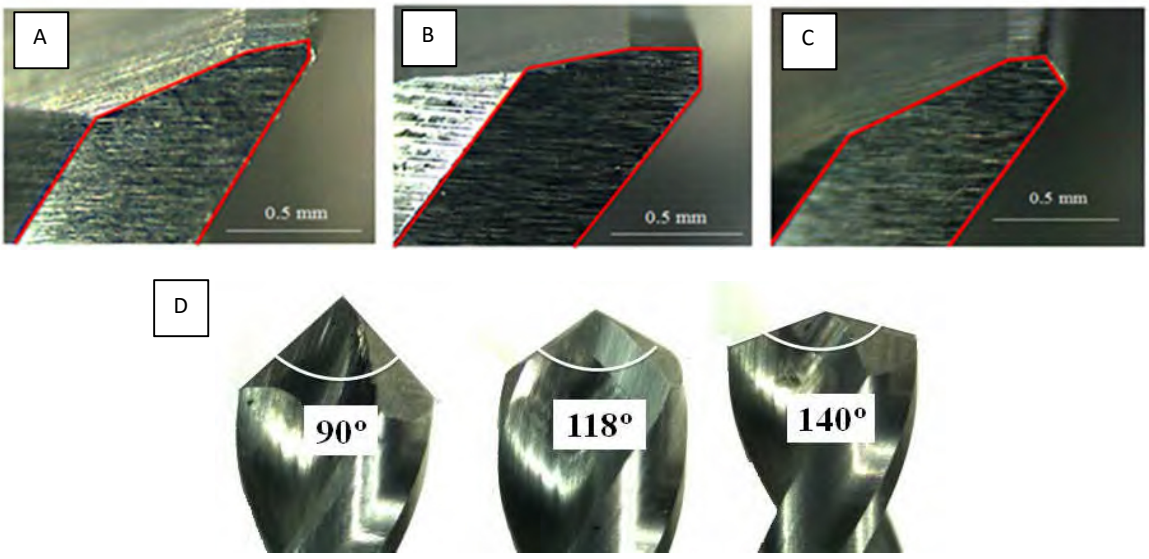

Figure 4.2: Edge geometries of drill bits tested; A new tool, B honed edge tool, and C flank worn tool. Under each tool type, three point angles (90°, 118°, and 140°) were chosen as shown in D for the new tool case.

α (°)	V (m/min)	*f* (mm/rev)	Set-Up
90	25	0.05	1
		0.1	2
		0.15	3
	50	0.05	4
		0.1	5
		0.15	6
	100	0.05	7
		0.1	8
		0.15	9
118	25	0.05	10
		0.1	11
		0.15	12
	50	0.05	13
		0.1	14
		0.15	15
	100	0.05	16
		0.1	17
		0.15	18
140	25	0.05	19
		0.1	20
		0.15	21
	50	0.05	22
		0.1	23
		0.15	24
	100	0.05	25
		0.1	26
		0.15	27

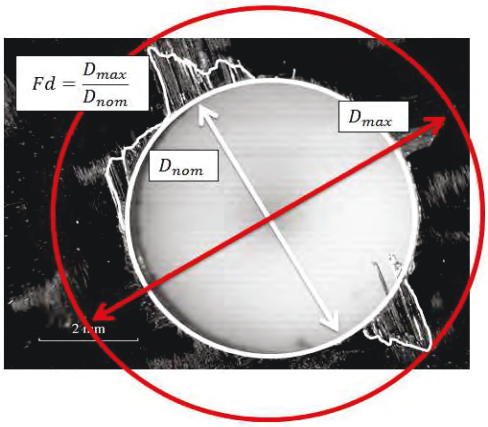

Figure 4.3: Schematic of delamination under each combination of process parameters. Note that the same full factorial design has been implemented for three wear levels (as a fourth factor)

4.2.3 ANALYSIS PROCEDURE

The statistical treatment of test data was made in three phases. The first phase was based on a full-factorial analysis of variance (ANOVA) (Montgomery 2009). The ANOVA analysis was specifically aimed to study the influence of the cutting parameters on quality of drilled parts under different tool geometries (wear levels). Interactions between drilling parameters were also considered to analyze whether they have any statistical relevance to the CFRP drilling process. In the second phase, based on the data from the factorial design, a response surface methodology (RSM) was implemented to establish input–output relations for the process variables and subsequently to locate the optimum drilling set-up given each response variable and tool wear level. For this RSM stage, the form of the relationships between each output response (thrust force, in- delamination and out- delamination) and the independent/process variables (point angle, feed rate and cutting speed) was unknown. Thus, the first step was to select a suitable approximation model between dependent and independent variables via testing p-value of different multiple regression models (Montgomery 2009). Due to anticipated nonlinear trends for all the study parameters, a general second order approximation was needed (equation 4.1), where β_0, β_i, β_{ii} and β_{ij} are model constants and xi and x_j are the cutting parameters (here k=3):

$$y = \beta_0 + \sum_{i=1}^{k} \beta_i x_i + \sum_{i=1}^{k} \beta_{ii} x_i^2 +$$

$$\sum_{i=1}^{k-1} \sum_{j=2}^{k} (\beta_1)_{ij} x_i x_j + \sum_{i=1}^{k-1} \sum_{j=2}^{k} (\beta_2)_{ij} x_i x_j^2 +$$

$$\sum_{i=1}^{k-1} \sum_{j=2}^{k} (\beta_3)_{ij} x_i^2 x_j + \sum_{i=1}^{k-1} \sum_{j=2}^{k} (\beta_4)_{ij} x_i^2 x_j^2 \quad (4.1)$$

Finally, once equations are fitted for each of the three tool wear levels, in the third phase, a 'multi-objective' optimization model was employed to identify a set of cutting parameters that can minimize the

thrust force, in-delamination, and out-delamination responses, at the same time. More specifically, for each tool wear level, the multi-objective regression model (equation 4.2) was defined by summing the three individual response equations fitted from phase 2. In the multi-objective model, which is also normalized and weighted, F_t (θ,V,f) is the prediction equation for the thrust force, F_{max} is the maximum thrust force reached during tests for a given tool wear condition, $F_{d\text{-}in}$ (θ,V,f) is the prediction equation for in delamination, $F_{d\text{-}out}$ (θ,V,f) is the predict equation for out-delamination, and ω_1, ω_2 and ω_3 are the weighting factors.

$$y = \omega_1 \times \frac{F_t(\theta,V,f)}{F_{\max}} + \omega_2 \times F_{d-in}(\theta,V,f) + \omega_3 \times F_{d-out}(\theta,V,f) \quad (4.2)$$

To find the multi-objective optimum point for each tool wear level, the weighting factors can be selected by an expert designer to reflect the relative importance of the three criteria (responses). Subsequently equation 4.2 can be minimized. For a non-expert designer, however, a sensitivity analysis of weights should be carried out before making a final decision (these practical notions are discussed in following sections).

Table 4.2: ANOVA results for the thrust force (highlighted rows indicate significant factors with a p-value<5%).

	Factor	Sum of squares	DF	Mean Square	F-Value	p-value	Contribution of SS_{Mean}	Significance
New Tool	**Point angle (A)**	2.99E+03	2	1.49E+03	1.41E+02	5.76E-07	37.23%	Very High
	Cutting speed (B)	5.28E+01	2	2.64E+01	2.50E+00	1.44E-01	0.66%	Insignificant
	Feed rate (C)	4.61E+03	2	2.31E+03	2.18E+02	1.06E-07	57.46%	Very High
	AB	1.36E+02	4	3.40E+01	3.21E+00	7.50E-02	0.85%	Insignificant
	AC	1.26E+02	4	3.15E+01	2.98E+00	8.82E-02	0.79%	Insignificant
	BC	4.42E+02	4	1.10E+02	1.04E+01	2.91E-03	2.75%	Very Low
	Residual	8.46E+01	8	1.06E+01	-	-	0.26%	-
	Total	8.44E+03	26	-	-	-	100%	-
Honed Edge Tool	**Point angle (A)**	1.00E+05	2	5.01E+04	1.29E+02	8.28E-07	47.41%	Very High
	Cutting Speed (B)	1.63E+03	2	8.15E+02	2.09E+00	1.86E-01	0.77%	Insignificant
	Feed rate (C)	1.01E+05	2	5.05E+04	1.30E+02	8.02E-07	47.80%	Very High
	AB	4.62E+03	4	1.15E+03	2.96E+00	8.93E-02	1.09%	Insignificant
	AC	8.29E+03	4	2.07E+03	5.32E+00	2.18E-02	1.96%	Very Low
	BC	2.49E+03	4	6.22E+02	1.60E+00	2.65E-01	0.59%	Insignificant
	Residual	3.11E+03	8	3.89E+02	-	-	0.37%	-
	Total	2.21E+05	26	-	-	-	100%	-
Flank Wear Tool	**Point angle (A)**	8.55E+05	2	4.27E+05	1.06E+03	1.98E-10	84.74%	Very High
	Cutting Speed (B)	2.38E+03	2	1.19E+03	2.96E+00	1.09E-01	0.24%	Insignificant
	Feed rate (C)	1.41E+05	2	7.05E+04	1.75E+02	2.49E-07	13.97%	Very High
	AB	3.90E+03	4	9.76E+02	2.42E+00	1.33E-01	0.19%	Insignificant
	AC	1.27E+04	4	3.16E+03	7.86E+00	7.09E-03	0.63%	Very Low
	BC	3.11E+03	4	7.78E+02	1.93E+00	1.98E-01	0.15%	Insignificant
	Residual	3.22E+03	8	4.03E+02	-	-	0.08%	-
	Total	1.02E+06	26	-	-	-	100%	-

4.3 Results and Discussion

The raw experimental data for thrust force, in- and out-delaminations under tested drilling configurations were previously published in the study (Feito *et al*. 2014b). This work is directly focused on statistical evaluation of main and interaction factor effects as well as the multi-objective optimization process under different tool wear levels.

4.3.1 THRUST FORCE

Table 4.2 shows the results obtained from the ANOVA analysis on the thrust force response. It is observed that only two of the three cutting parameters are related to the thrust force, namely the point angle and the feed rate, independently of the tool geometry (i.e., p-value<0.05 for all three wear levels). The relative percentage contributions of these factors, however, change when the wear level increases on the drill bit; for the new tool the feed rate has the main influence (57.46 %). On contrary, the point angle is the dominant factor controlling the thrust force in the case of the flank worn tool (84.74 %). Honed edge tool shows comparable contributions of the two factors. *These results suggest that as the tool bit is worn due to drilling cycles, under a given feed rate, a significant increase of thrust force may be experienced*.

Cutting speed did not show a statistically significant influence on the thrust force for any tool case (p-value>0.05). However, based on Table 4.2, for the case of new tool it has a slight influence in combination with other significant parameters (namely, the interaction factor BC). The influence of this interaction is relatively low for the case of new tool (2.75 %), which practically means it is not as important as the point angle factor. Similarly, for both worn tools, the interaction factor AC has marginally contributed to the variation of thrust force (less than 2 %).

4.3.2 ENTRY DELAMINATION

For the case of entry delamination or peel up, the ANOVA results are shown in Table 4.3. The feed rate indicates the maximum contribution for all tool types. It is interesting that for the worn tools, this factor contribution increases by ~25 % for the flank wear tool and ~65 % for the honed edge tool, compared to the new tool. *This suggests that as the drill bit is worn, the same feed rate can cause less entry delamination in the CFRP laminate (or in a different way, to avoid excessive delamination, the feed rate should be low for new tools)*; see also (Feito *et al*. 2014b). Regarding the rest of parameters, the new and flank wear tools have almost the same sensitivity to the point angle (29.02 vs. 21.91 %) followed by the cutting speed (15.42 vs. 17.62 %). Results for the honed edge tool, however, show a different behavior. The feed rate has a huge influence on the entry delamination (62.97 %) followed by the point angle (~15.81 %), while the cutting speed is no longer significant in this case. Finally, it can be observed that while the p-values for all interaction factors are greater than 0.05 (i.e., statistically insignificant), their contribution for factors such as AB under the honed edge tool is calculated as high as 11.19 %. This is partly because the random error (residual) for the entry delamination measurement has been relatively high (~3.5 %) when compared to the other responses.

4.3.3 EXIT DELAMINATION

The last output parameter individually analyzed is the exit delamination or push

Table 4.3: ANOVA results for in-delamination (highlighted rows indicate significant factors with a p-value<5%).

	Factor	Sum of squares	DF	Mean Square	F-Value	p-value	Contribution of SS_{Mean}	Significance
New Tool	Point angle (A)	6.50E-02	2	3.20E-02	9.52E+00	0.77%	29.02%	Very High
	Cutting speed (B)	3.30E-02	2	1.70E-02	4.89E+00	4.10%	15.42%	Very Low
	Feed rate (C)	8.40E-02	2	4.20E-02	1.24E+01	0.36%	38.08%	Very High
	AB	3.60E-02	4	8.88E-03	2.62E+00	11.50%	8.05%	Insignificant
	AC	5.51E-03	4	1.38E-03	4.10E-01	79.97%	1.25%	Insignificant
	BC	2.30E-02	4	5.63E-03	1.66E+00	25.07%	5.11%	Insignificant
	Residual	2.70E-02	8	3.39E-03	-	-	3.08%	-
	Total	2.70E-01	26	-	-	-	100%	-
Honed Edge Tool	Point angle (A)	1.24E-02	2	6.21E-03	4.47E+00	4.96%	15.81%	Very Low
	Cutting Speed (B)	1.02E-03	2	5.10E-04	3.67E-01	70.36%	1.30%	Insignificant
	Feed rate (C)	4.95E-02	2	2.47E-02	1.78E+01	0.11%	62.97%	Very High
	AB	1.76E-02	4	4.40E-03	3.17E+00	7.75%	11.19%	Very Low
	AC	4.06E-03	4	1.01E-03	7.30E-01	59.59%	2.58%	Insignificant
	BC	4.13E-03	4	1.03E-03	7.43E-01	58.88%	2.62%	Insignificant
	Residual	1.11E-02	8	1.39E-03	-	-	3.53%	-
	Total	9.98E-02	26	-	-	-	100%	-
Flank Wear Tool	Point angle (A)	7.14E-03	2	3.57E-03	8.13E+00	1.18%	21.91%	Very Low
	Cutting Speed (B)	5.74E-03	2	2.87E-03	6.53E+00	2.08%	17.62%	Very Low
	Feed rate (C)	1.56E-02	2	7.81E-03	1.78E+01	0.11%	47.94%	Very High
	AB	2.46E-03	4	6.14E-04	1.40E+00	31.79%	3.77%	Insignificant
	AC	1.02E-03	4	2.56E-04	5.82E-01	68.48%	1.57%	Insignificant
	BC	2.94E-03	4	7.34E-04	1.67E+00	24.87%	4.50%	Insignificant
	Residual	3.52E-03	8	4.39E-04	-	-	2.70%	-
	Total	3.84E-02	26	-	-	-	100%	-

out. Table 4.4 shows the corresponding ANOVA. All the three drilling parameters are significant for the exist-delamination using the new tool and flank worn tools. In both tool cases, the point angle is the most influential factor (~40 % contribution). As the tool is worn, the exit delamination generally increases. This high contribution of point angle on the exit delamination is opposite to the entry delamination based on results in previous section, where the feed rate had the highest contribution. *This suggests that for these tool bits, given that the interaction AC is trivial in both Tables 4.2 and 4.3, designers may use the feed rate effect to better control (lower) the extension of in-delamination, while using the point angle effect to better control (lower) the exist delamination*. It is also interesting that for the new tool and flank worn tool, the cutting speed is influential on the exist delamination, in contrast to previous sections.

For the case of honed edge tool, similar to the entry delamination case, the point angle and feed rate become significant, but not the cutting speed. However, for this tool the contribution of feed rate is higher than point angle, when compared to the new tool and flank worn tools. Generally, as reviewed in the introduction, lower feed rates

Table 4.4: ANOVA results for out-delamination (highlighted rows indicate significant factors with a p-value<5%).

	Factor	Sum of squares	DF	Mean Square	F-Value	p-value	Contribution of SS_{Mean}	Significance
New Tool	**Point angle (A)**	5.80E-02	2	2.90E-02	2.39E+01	4.00E-04	41.82%	Very High
	Cutting speed (B)	1.30E-02	2	6.27E-03	5.21E+00	3.56E-02	9.04%	Very Low
	Feed rate (C)	2.50E-02	2	1.20E-02	1.03E+01	6.10E-03	17.31%	Very High
	AB	6.20E-02	4	1.50E-02	1.28E+01	1.50E-03	21.63%	Very High
	AC	7.79E-03	4	1.95E-03	1.62E+00	2.60E-01	2.81%	Insignificant
	BC	1.60E-02	4	3.92E-03	3.26E+00	7.29E-02	5.65%	Insignificant
	Residual	9.63E-03	8	1.20E-03	-	-	1.74%	-
	Total	1.90E-01	26	-	-	-	100%	-
Honed Edge Tool	**Point angle (A)**	1.48E-01	2	7.40E-02	1.20E+01	3.95E-03	34.31%	Very High
	Cutting Speed (B)	1.68E-02	2	8.38E-03	1.35E+00	3.12E-01	3.88%	Insignificant
	Feed rate (C)	2.03E-01	2	1.01E-01	1.64E+01	1.49E-03	46.97%	Very High
	AB	9.06E-02	4	2.27E-02	3.66E+00	4.59E-02	10.50%	Low
	AC	4.07E-03	4	1.02E-03	1.64E-01	9.51E-01	0.47%	Insignificant
	BC	8.59E-03	4	2.15E-03	3.47E-01	8.39E-01	1.00%	Insignificant
	Residual	4.95E-02	8	6.19E-03	-	-	2.87%	-
	Total	5.20E-01	26	-	-	-	100%	-
Flank Wear Tool	**Point angle (A)**	1.18E-01	2	5.90E-02	2.42E+01	4.07E-04	43.52%	Very High
	Cutting Speed (B)	7.10E-02	2	3.55E-02	1.45E+01	2.17E-03	26.19%	Very High
	Feed rate (C)	4.30E-02	2	2.15E-02	8.80E+00	9.54E-03	15.85%	Very High
	AB	5.26E-02	4	1.32E-02	5.39E+00	2.10E-02	9.71%	Low
	AC	5.61E-03	4	1.40E-03	5.75E-01	6.89E-01	1.04%	Insignificant
	BC	1.03E-02	4	2.57E-03	1.05E+00	4.38E-01	1.90%	Insignificant
	Residual	1.95E-02	8	2.44E-03	-	-	1.80%	Insignificant
	Total	3.20E-01	26	-	-	-	100%	-

and higher point angles result in lower in-delamination. However, as will be shown in the next section, there are several conflicts in such trends under other criterion (e.g., minimization of exit-delamination), hence justifying the need for a 'multi-objective' optimization approach. Finally, it is evident from Table 4.4 that *the exit delamination is more sensitive to the tool geometry condition (wear) and is a more complex response to minimize* (e.g., notice the effect of AB interaction which is not negligible in this case under all tool types; the other two interactions (AC and BC), however, seem insignificant with a maximum influence of 5.7 %).

4.3.4 REGRESSIONS

The correlation between the cutting factors (cutting speed, feed rate and point angle) and the dependent variables (thrust force, peel-up delamination and push-out delamination) were obtained using multiple linear regression and test data from designed experiment as in Figures 4.3, 4.4 and 4.5. The fitted equations are presented in Table 4.5 where Ft represent the thrust force, $F_{d\text{-}in}$ the entry delamination, $F_{d\text{-}out}$ the

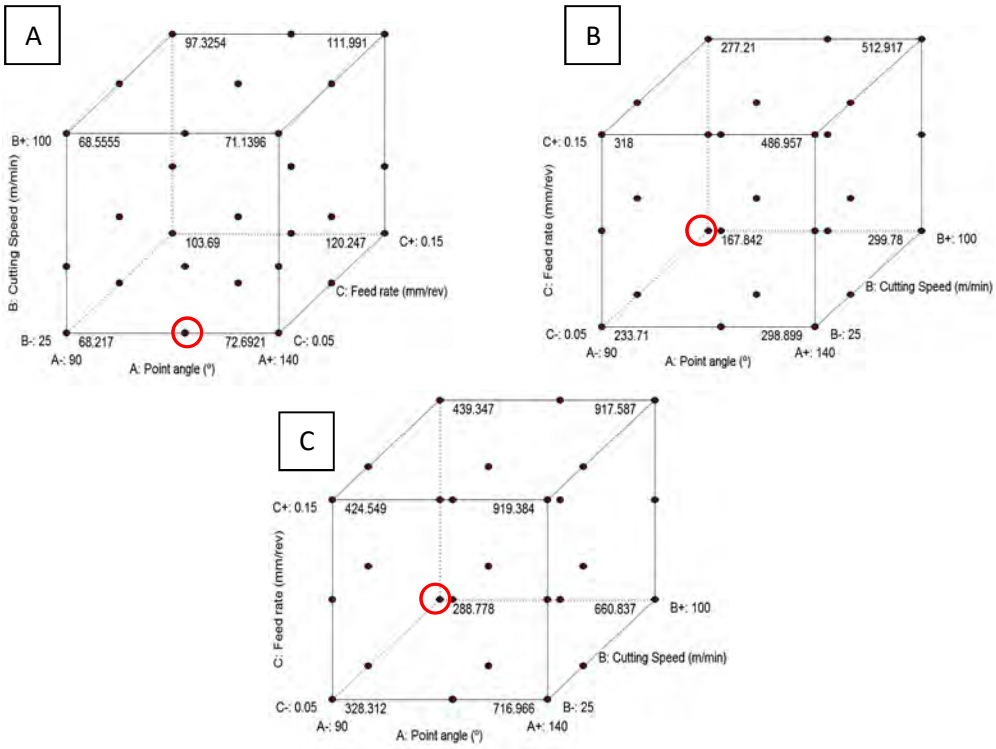

Figure 4.4: Variation of the thrust force for (A) the new tool, (B) honed edged tool, and (C) flank wear tool as a function of cutting variables.

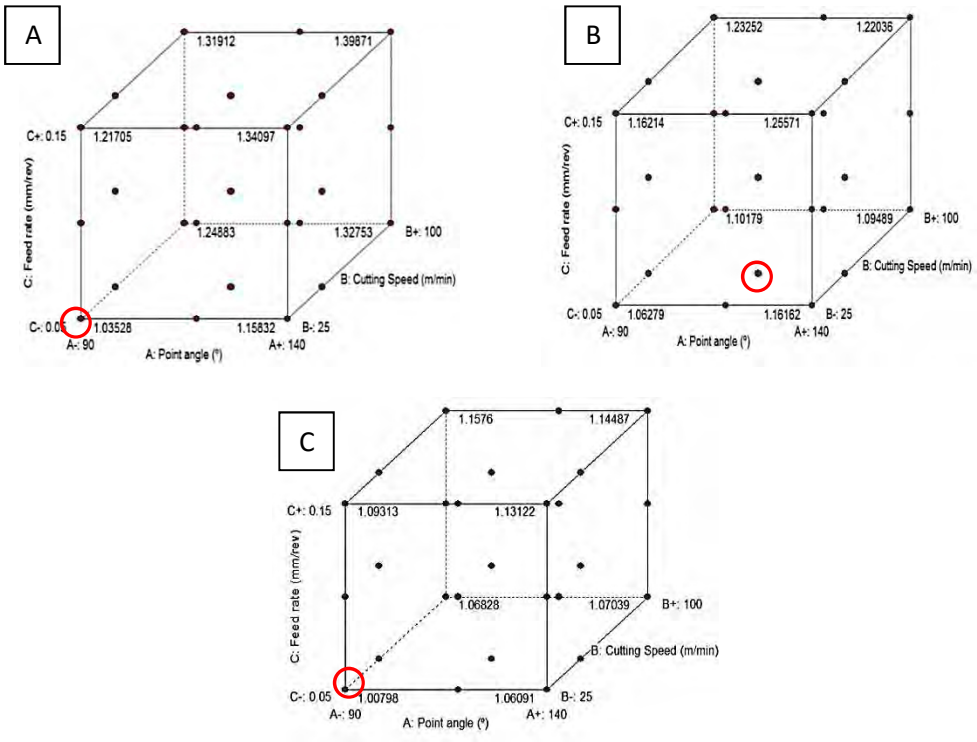

Figure 4.5: Variation of the entry delamination for (A) the new tool, (B) honed edged tool, and (C) flank wear tool as a function of cutting variables.

Table 4.5: Regression equations for thrust force, peel up, and push responses out for different tool geometries.

	Fitted equations	R^2
New Tool	F_t = 504.2035 - 8.9386ϑ - 0.03889V + 976.7025f + 0.0354ϑV - 4.8606ϑf - 23.5586Vf + 0.0381ϑ^2 - 0.0122V^2 + 505.3006f^2 - 0.0001$\vartheta^2 V$ + 0.045 $\vartheta^2 f$ - 1.6567e-5ϑV^2 - 15.3854 ϑf^2 + 0.1404$V^2 f$ + 25.5897Vf^2	0.96
	$F_{d\,in}$ = -5.7535 + 0.1125ϑ + 0.0598V + 95.6124f - 0.0008ϑV - 1.5999ϑf - 0.0905Vf - 0.0005ϑ^2 - 5.288e-5V^2 - 4442.823f^2 + 3.627e-6$\vartheta^2 V$ + 0.0072$\vartheta^2 f$ + 7.5553ϑf^2 + 0.3783Vf^2 - 0.0342$\vartheta^2 f^2$	0.87
	$F_{d\,out}$ = 1.5158 - 0.0109ϑ + 0.1163V - 27.4703f - 0.002ϑV + 0.7454ϑf - 0.5047Vf + 1.75e-5ϑ^2 - 0.0009V^2 + 185.86667f^2 + 1.076e-5$\vartheta^2 V$ - 0.0034$\vartheta^2 f$ + 1.6e-5ϑV^2 - 4.3705ϑf^2 + 0.0035$V^2 f$ + 2.2533Vf^2 - 8.53e-8$\vartheta^2 V^2$ + 0.0195$\vartheta^2 f^2$ - 0.0151$\vartheta^2 f^2$	0.95
Honed edge Tool	F_t = 233.8026 - 0.1789ϑ - 2.6474V - 1108.5187f + 0.0178ϑV + 20.7536ϑf + 3.3438Vf	0.96
	$F_{d\,in}$ = -2.76332 + 0.0623ϑ + 0.1877V - 20.2656f - 0.003ϑV + 0.4477ϑf - 0.2832Vf - 0.0003ϑ^2 - 0.0013V^2 + 157.2017f^2 + 1.2e-5$\vartheta^2 V$ - 0.0018$\vartheta^2 f$ + 2.1e-5ϑV^2 - 3.2388ϑf^2 + 0.00241$V^2 f$ + 1.6152Vf^2 - 9.07e-8$\vartheta^2 V^2$ + 0.0133$\vartheta^2 f^2$ - 0.0132$V^2 f^2$	0.89
	$F_{d\,out}$ = -4.9926 + 0.1169ϑ + 0.3191V - 75.5488f - 0.006θV + 1.338ϑf + 0.0681Vf - 0.0005ϑ^2 - 0.0021V^2 + 390.0332f^2 + 2.73e-5$\theta 2 V$ - 0.0057$\vartheta^2 f$ + 3.85e-5ϑV^2 - 6.8446ϑf^2 + 0.0001$V^2 f$ - 0.2157Vf^2 - 1.754e-7$\vartheta^2 V^2$ + 0.0291$\vartheta^2 f^2$ - 0.0011$V^2 f^2$	0.90
Flank wear Tool	Ft = -311.5443 + 6.8219ϑ - 0.4910V - 1129.9914f - 0.0044ϑV + 21.2362ϑf + 7.2443Vf	0.98
	$F_{d\,in}$ = 0.9156 - 0.0029ϑ + 0.0064V + 4.7056f + 3.1956e-5ϑV - 0.0435ϑf - 0.0713Vf + 1.294e-5ϑ^2 - 4.12e-5V^2 + 6.5013f^2 - 1.364e-7$\vartheta^2 V$ + 0.0003$\vartheta^2 f$ - 1.13e-7ϑV^2 - 0.1603ϑf^2 + 0.0004$V^2 f$ + 0.1286Vf^2	0.90
	$F_{d\,out}$ = -6.4478 + 0.1299ϑ + 0.39225V - 42.4574f - 0.0067ϑV + 0.8083ϑf - 0.213Vf - 0.0005ϑ^2 - 0.003V^2 + 240.2445f^2 + 2.82e-5$\vartheta^2 V$ - 0.003$\vartheta^2 f$ + 5.11e-5ϑV^2 - 4.3768ϑf^2 + 0.0023$V^2 f$ + 0.758Vf^2 - 2.15e-7$\vartheta^2 V^2$ + 0.0168$\vartheta^2 f^2$ - 0.009$V^2 f^2$	0.93

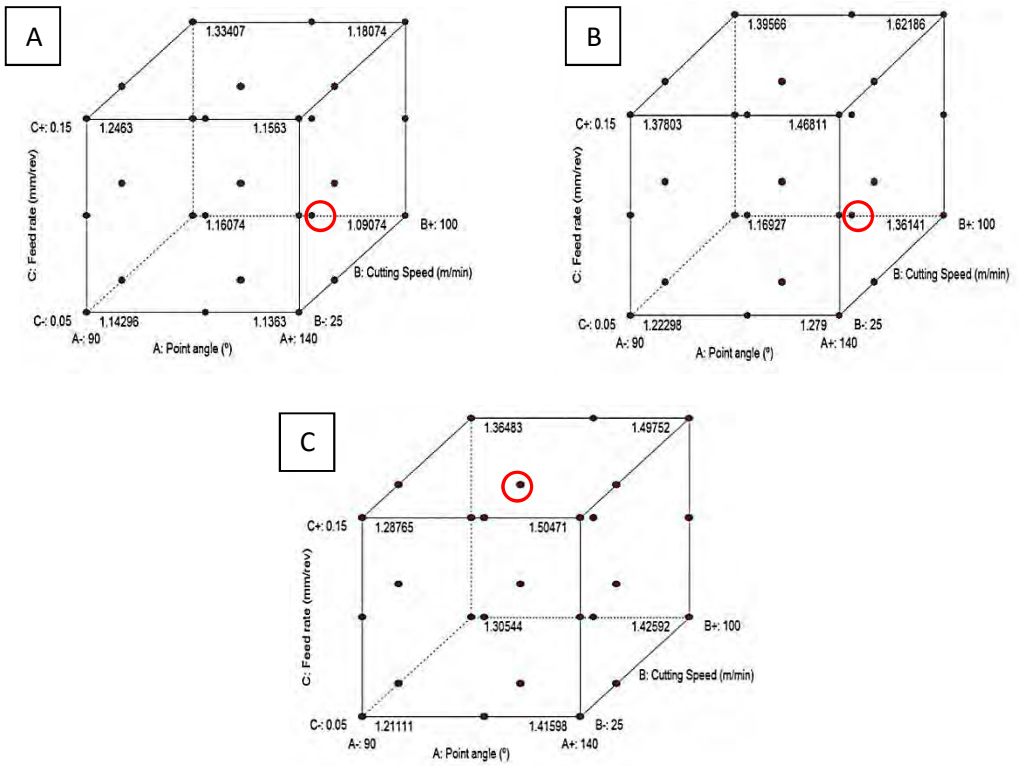

Figure 4.6: Variation of the exit delamination for (a) the new tool, (b) honed edged tool, and (c) flank wear tool as a function of cutting variables.

Table 4.6: Comparison between validation experiments and estimated values by regression equations.

Tool type	Point angle (º)	Cutting speed (m/min)	Feed rate (mm/rev)	Thrust Force		Entry Delamination		Exit Delamination	
				Experimental	Estimated	Experimental	Estimated	Experimental	Estimated
New Tool	118	75	0.1	119.10	117.62	1.22	1.28	1.14	1.12
	118	75	0.2	187.70	171.15	1.26	1.30	1.27	1.23
Honed Tool	118	75	0.1	290.86	320.79	1.06	1.09	1.29	1.31
	118	75	0.2	438.26	469.91	1.10	1.12	1.33	1.35
Flank Wear Tool	118	75	0.1	638.86	612.60	1.07	1.10	1.22	1.25
	118	75	0.2	804.28	801.52	1.12	1.11	1.22	1.20

exit delamination, θ the point angle, V the cutting speed and *f* the feed rate. The higher-order interactions have been included to improve the accuracy of the predictions. All the fits prese nted a statistically significant R^2 value.

Table 4.6 shows results of a set of validation experiments that were performed at new design points to assess the predictably of identified regression equations in Table 4.5. The maximum relative difference between the experimental value and the predicted value was 9.7 % for the thrust force, 4.9 % for entry delamination, and 3.3 %for the exit delamination, providing a good confidence level regarding the applicability of the prediction equations.

4.3.5 OPTIMIZATION PROCESS

Table 4.7 presents the optimum solution that minimizes each dependent variable separately (i.e., single objective optimization). In this table, 'A' columns refer to the best solutions obtained from a 'discrete' single-objective optimization, i.e., using only tested configurations with the select levels of point angle {90°, 118°, 140°}, cutting speed {25 m/min, 50 m/min, 100 m/min}and feed rate {0.05 mm/rev, 0.1 mm/rev, 0.15mm/rev}. These single-objective optimum points are also marked as circles in Figures 4.4, 4.5 and 4.6 (indicating that the optimum solution can change in the design space from one response to another and/or between different tool conditions). Columns 'B' in Table 4.7 refer to the

Table 4.7: Cutting parameters for the case of discrete (A columns) and continuous (B columns) optimizations of each response variable separately (note: optimum solutions may not be extrapolated to ranges outside those tested).

		Thrust Force		Peel-Up		Push-Out	
		A	B	A	B	A	B
New tool	Point angle (º)	118	114	90	90	118	107
	Cutting Speed (m/min)	25	25	25	25	100	69
	Feed Rate (mm/rev)	0.05	0.05	0.05	0.05	0.05	0.09
Honed Edge tool	Point angle (º)	90	90	118	116	118	106
	Cutting Speed (m/min)	100	100	50	73	100	98
	Feed Rate (mm/rev)	0.05	0.05	0.05	0.05	0.05	0.05
Flank Wear tool	Point angle (º)	90	90	90	92	118	113
	Cutting Speed (m/min)	100	100	25	25	50	65
	Feed Rate (mm/rev)	0.05	0.05	0.05	0.05	0.15	0.15

'continuous' optimization solutions via minimizing the fitted equations (RSM approach) in Table 4.5, based on the continuous ranges of independent variables: point angle [90–140°], cutting speed [25 m/min-100 m/min] and feed rate [0.05 mm/rev–0.15 mm/rev].

Table 4.7, it can be observed that for a given tool wear condition, the optimum set of cutting parameters changes notably from one response variable to another (e.g., for a new tool, the continuous optimum solution of point angle is 114° for thrust force, 90° for peel-up, and 107° for push out criteria). Such conflicts point to the fact that there is no unique solution that can minimize all the criteria perfectly, hence the need for a weighted multi-objective optimization to arrive at an overall optimum solution. Nevertheless, from Table 4.7 it can be said that, in general, low feed rates are desirable for most cases.

Table 4.8 presents the multi-objective optimization results under different weighting factor combinations according to equation 4.2. The weight associated to each response variable defines the relative importance of corresponding criterion to the designer. In the first attempt, the three design criteria (output variables) were assumed to have an equal importance ($\omega_1=\omega_2=\omega_3=1$). For the second scenario, only in- and out delaminations are assumed to have high weights ($\omega_1<\omega_2=\omega_3$). For the last case, only the exit delamination is considered to be highly important for the designer, on account of the fact that it is normally more severe than the entry delamination in practice ($\omega_1=\omega_2<\omega_3$). From results in Table 4.8, for all weighting cases, *a low feed rate is recommended for all tool wear conditions*. The latter recommendation can also be noticed from the general performance trends shown in Figure 4.7. Multi-objective optimum value of point angle changes between the tool conditions, but within a limited range of 90°–120° (i.e., low to medium point angles are recommended for overall optimization of CFRP drilling under different tool conditions). For more detailed design guidelines, *when the geometry of the drill bit deteriorates due to the wear process, subsequent drillings with smaller point angles (90°–100°) would be theoretically preferred, whereas for new tools (no wear) a medium range point angle (100°–120°) is optimum*. Optimum level of cutting speed is well varied depending on the given tool geometry. *If the wear is found on the drill bit on the honed edge, it would be recommended to continue the drilling with an*

Table 4.8: Multi-objective optimum set of cutting parameters for different tool wear conditions tested.

	ω_1	ω_2	ω_3	Point angle (º)	Cutting Speed (m/min)	Feed Rate (mm/rev)
New Tool	1	1	1	108	25	0.05
	0.2	1	1	101	25	0.05
	0.2	0.2	1	119	100	0.07
Honed Edge Tool	1	1	1	90	100	0.05
	0.2	1	1	109	87	0.05
	0.2	0.2	1	106	98	0.05
Flank Wear Tool	1	1	1	90	25	0.05
	0.2	1	1	90	25	0.05
	0.2	0.2	1	113	63	0.15

increased cutting speed (~100 m/min in the current study) as compared to the flank wear as well as the new tool conditions where generally a lower cutting speed is suitable to avoid the entry and exit delaminations. Recall that according to sensitivity results in Table 4.2, the thrust force is not affected as much by the cutting speed.

Finally, Table 4.9 shows an example of comparison between average exit delamination measured and the damage estimated using the optimum set of parameters for the case of $\omega_1=\omega_2<\omega_3$. In the optimized drilling set-up, the delamination has been reduced by 13.73–26.36 % depending on the tool condition.

Table 4.9: Comparison between average exit delamination observed during measurements and the estimated delamination under optimum drilling parameters in Table 4.7 for the case of ω1 = ω2=0.2, ω3=1

	Average experimental delamination (Figure 3)	Estimated delamination with optimized set-up	Relative difference (improvement)
New Tool	1.16	1.02	13.73%
Flank Wear Tool	1.39	1.10	26.36%
Honed Edge Tool	1.37	1.13	21.24%

4.4 Conclusions

Based on the factorial design and optimization study presented in this work on CFRP drilling, the following conclusions could be drawn:

Feed rate and point angle are the factors with highest influence on the thrust force. When the tool is new, the point angle is the most influent parameter. When the tool geometry changes due to wear, the feed rate becomes more important. Cutting speed is not a relevant factor on the thrust force.

Feed rate is the most important factor on the entry delamination for new tool

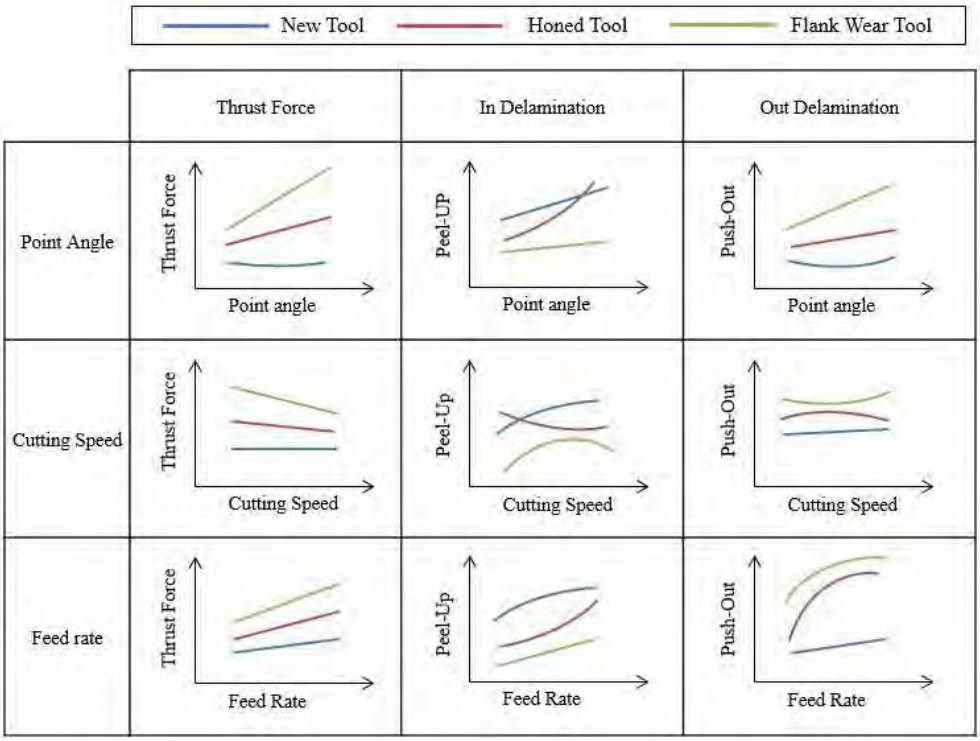

Figure 4.7: Overall variation of the CFRP drilling quality with the drill point angle, cutting speed and feed rate, under different wear conditions (trends have been plotted based on test data in [20]).

and flank worn tool. Opposite to this, point angle has a strong influence on the exist delamination. Cutting speed is significant for both delamination cases but its influence is generally low, when compared to other cutting parameters. Honed edge tool shows a notably different behavior that the other tool cases. Feed rate is the most influence for this kind of wear condition, either for in-delamination or out-delamination.

The single optimization of the three output responses showed that under different drilling set-ups a low feed rate (0.05 mm/rev) is most frequently preferred. Point angles in a range of 90° to 114° are recommended to cutting speed would keep the response values low, hence maintaining the drilling quality. Peel-up decreases with choosing medium point angles (90°–116°) and low cutting speeds (25 m/min). The opposite effect was found for push-out where higher point angles (107°–113°) and higher cutting speeds (69 m/min–98 m/min) would improve the results; this observation is also in alignment with the earlier reports (Heisel and Pfeifroth 2012; Feito *et al*. 2014b) and suggest that depending on the wear type and/or a particular design objective, the cutting parameters can be changed to maximize the process quality. However, this may be viewed as a complex paradigm for practical applications, leading to the following multi-objective/overall optimization results.

4.4.1 OVERALL RECOMMENDATION

From a multi-objective, practical optimization perspective, considering Figure 4.7 and that a manufacturer would normally prefer to choose one tool in the beginning and use it until its failure, a low feed rate would be recommended (~0.05 mm/rev) for CFRP drillings. A choice of low point angle in the range of 90°–108° is recommended to reduce delamination as the geometry will change due to wear phenomenon. Only the cutting speed would be the one parameter that should be modified from ~25 m/min to ~100 m/min when the wear increases on the drill bit, especially for the honed edge wear case. The drilling parameter interactions, overall, did not show a dominant statistical significance under different measured responses and hence the aforementioned individual factors may be employed independently to control the quality of drilled composite parts.

Future study may include the experimental valuation of optimization results under different tool wear conditions, along with evaluation of the effect of part thickness and/or use of other types of composite materials/fiber architectures. As well, further development and validation of advanced numerical models of composites drilling, e.g., (Faraz *et al*. 2009; Soldani *et al*. 2011; Feito *et al*. 2014), may be conducted using experimental data, along with an in-depth understanding of the macro/meso level mechanisms that correlate to cutting parameters and lead to damage during the process. Eventually using such models, new/customized drilling tools may be developed for composites. The effect of curing/post curing of polymeric composite samples can be another area of future study to evaluate to which extent it may affect the drilling quality for CFRPs.

4.5 Acknowledgments

The authors acknowledge the financial support for this work from the Ministry of Economy and Competitiveness of Spain under the project DPI2011-25999 and FPI subprogram with the reference BES-2012-055162, and the Natural Sciences and Engineering Research Council (NSERC) of Cana-

da. Constructive comments by the anonymous reviewers, as well as great discussions by Mr. B. Crawford and Mr. J. Torres from the Composites Research Network (CRN) are acknowledged.

4.6 References

[1] Abhishek K, Datta S, Mahapatra SS. Optimization of thrust, torque, entry, and exist delamination factor during drilling of CFRP composites. Int J Adv Manuf Technol 2014; 76(1):401–16.

[2] Davim JP, Reis P. Drilling carbon fiber plastics manufactures by autoclave – experimental and statistical study. Mater Des 2003; 24:315–24.

[3] Durão P, Gonçalves JS, Tavares RS, de Albuquerque C, Aguiar A, Torres A. Drilling tool geometry evaluation for reinforced composite laminates. Compos Struct 2010; 92:1545–50.

[4] Faraz A, Biermann D, Weinert K. Cutting edge rounding: an innovative tool wear criterion in drilling CFRP composite laminates. Int J Mach Tools Manuf 2009; 49:1185–96.

[5] Feito N, López-Puente J, Santiuste C, Miguélez MH. Numerical prediction of delamination in CFRP drilling. Compos Struct 2014; 108:677–83.

[6] Feito N, Díaz-Álvarez J, Díaz-Álvarez A, Cantero JL, Miguélez MH. Experimental analysis of the influence of drill point angle and wear on the drilling of woven CFRPs. Materials 2014; 7:4258–71.

[7] Heisel U, Pfeifroth T. Influence of point angle on drill hole quality and machining forces when drilling CFRP. Proc CIRP 2012; 1:471–6.

[8] Huang X. Fabrication and properties of carbon fibers. Materials 2009; 2: 2369–403.

[9] Iliescu D, Gehin D, Gutierrez ME, Girot F. Modeling and tool wear in drilling of CFRP. Int J Mach Tools Manuf 2010; 50:204–13.

[10] Karpat Y, Deger B, Bahtiyar O. Drilling thick fabric woven CFRP laminates with double point angle drills. J Mater Process Technol 2012; 212:2117–27.

[11] Liu D, Tang YJ, Cong. A review of mechanical drilling for composite laminates. Compos Struct 2012; 94:1265–79.

[12] Mayuet P, Gallo A, Portal A, Arroyo P, Alvarez M, Marcos M. Damaged area based study of the Break-IN and Break-OUT defects in the dry drilling of carbon fiber reinforced plastics (CFRP). Proc Eng 2013; 63:743–51.

[13] Montgomery DC. Design and Analysis of Experiments. John Wiley & Sons, Inc 7th ed, 2009 ISBN 978-0-470-12866-4

[14] Phadnis VA, Farrukh M, Anish R, Silberschmidt VV. Drilling in carbon/epoxy composites: experimental investigations and finite element implementation. Compos Part A 2013; 47:41–51.

[15] Rawat S, Attia H. Wear mechanisms and tool life management of WC–Co drills during dry high speed drilling of woven carbon fibre composites. Wear 2009; 267:1022–30.

[16] Santiuste C, Barbero E, Miguélez MH. Computational analysis of temperature effect in composite bolted joints for aeronautical applications. J Reinf Plast Compos 2011; 30:3–11.

[17] Shyha IS, Aspinwall DK, Soo SL, Bradley S. Drill geometry and operating effects when cutting small diameter holes in CFRP. Int J Mach Tools Manuf 2009; 49:1008–14.

[18] Soldani X, Santiuste C, Muñoz-Sánchez A, Miguélez MH. Influence of tool geometry and numerical parameters when modeling orthogonal cutting of LFRP composites. Compos Part A 2011; 42:1205–16.

[19] Sonkar V, Abhishek K, Datta S, Mahapatra SS. Multi-objective optimization in drilling of GFRP composites: a degree of similarity approach. Procedia Mater Sci 2014; 6:538–43.

[20] Teti R. Machining of composites materials. Ann CIRP 2002; 51:611–34.

Parte II:

Análisis Numérico del Taladrado en Materiales Compuestos de Fibra de Carbono

Capítulo 5

La Simulación Numérica de los Procesos de Mecanizado de LFRPs

Este capítulo presenta el estado del arte en lo referente al modelado del mecanizado de materiales poliméricos reforzados con fibras largas (LFRP). Los materiales LFRP se clasifican como difíciles de cortar debido a la presencia de fibras duras, siendo especialmente vulnerables al daño inducido por el mecanizado. Aunque el estudio de corte de composites es un enfoque relativamente nuevo, la modelización numérica del mecanizado puede ser una herramienta de ayuda interesante en el análisis del proceso de taladrado. Por eso se recoge en este capítulo un resumen de las principales aportaciones en el ámbito de la simulación del corte de materiales LFRP, dando al lector información sobre el desarrollo de modelos numéricos así como diversos aspectos mecánicos de diferentes procesos de corte.

5.1 Introducción

Los estudios experimentales del mecanizado de materiales de baja maquinabilidad, entre los que se incluyen los compuestos LFRPs, consumen mucho tiempo y son caros. Por otra parte, los riesgos para la salud asociados con la inhalación de la fibra y el contacto con la piel, reducen la posibilidad de llevar a cabo una amplia investigación experimental en mecanizado de este tipo de materiales. Además, la forma del material compuesto, generalmente de paredes delgadas, también complica la ejecución de las pruebas, que se realizan con frecuencia a velocidades de corte bajas obtenidas después de un proceso de posicionamiento complejo de la máquina-herramienta [1-4].

Los modelos numéricos se presentan como una solución a estos problemas. La metodología basada en los elementos finitos (FEM por sus siglas en inglés) ofrece la posibilidad de completar los estudios experimentales evitando, tanto los problemas técnicos, como el elevado coste experimental. Otra ventaja es la posibilidad de desacoplar los parámetros que influyen en el problema y que dependen a su vez de un gran número de variables. El interés en el modelado del mecanizado de materiales compuestos ha motivado una revisión reciente de los modelos presentes en la literatura en corte ortogonal [5].

En comparación con la gran cantidad de trabajos científicos que se ocupan del corte de metales, existe una cantidad limitada de literatura técnica centrada en el análisis por elementos finitos de los procesos de corte de materiales compuestos LFRP. La mayor parte de estos estudios ponen su atención en el proceso de corte ortogonal. Aunque esta peración no es un proceso industrial en sí mismo, es objeto de estudio debido a su simplicidad, incluso en el caso de materiales metálicos [6,7]. Algunos ejemplos relevantes de las estrategias de modelado y criterios de daño para el corte ortogonal de materiales compuestos se pueden encontrar en la literatura científica [8-12].

Dentro de los trabajos sobre el modelado del corte ortogonal en materiales LFRP, la gran mayoría se basa en modelos bidimensionales (2D) y asumen la hipótesis de tensión plana. Las fuerzas de corte y el daño intra-laminar se pueden predecir usando este enfoque sencillo. Sin embargo, esta técnica no es adecuada para predecir la delaminación, uno de los defectos más importantes inducidos durante el mecanizado y relacionada con las tensiones fuera del plano. El enfoque 2D sólo permite modelar las láminas unidireccionales, siendo su uso prácticamente inexistente en aplicaciones reales. Recientemente se han desarrollado algunos modelos en 3D de corte ortogonal con el fin de predecir el daño por delaminación y reproducir diferentes secuencias de apilamiento [13,14].

En cuanto a las operaciones de taladrado, los primeros modelos desarrollados en la literatura fueron modelos simplificados cuasi-estáticos tridimensionales. En estos modelos, la broca se asemeja a un punzón que ejerce una fuerza constante sobre el material para predecir la delaminación. Este enfoque ha sido utilizado, por ejemplo, por Durao *et al*. [15, 16] y Singh *et al*. [17] en estudios de taladrado de materiales poliméricos reforzados con fibra de vidrio. Los resultados mostraron la influencia del ángulo de punta o de la geometría de la broca en el daño inducido. Igualmente, se relacionó la delaminación con la fuerza de avance aplicada sobre el lamina-

do [18], que es uno de los factores más influyentes en la generación del fallo fuera del plano durante el taladrado [19].

Finalmente, la simulación del proceso 3D completo de taladrado en materiales compuestos incluye el arranque de viruta del material y los movimientos de rotación y penetración de la broca. También conlleva implementar geometrías de herramientas complejas para reproducir el proceso lo más fielmente posible. Hasta la fecha sólo se han llevado estudios con geometrías de herramienta sencillas [20,21] debido a la complejidad de modelar, por un lado, los movimientos mencionados, y por otro, implementar los criterios de daño y erosión de los elementos, y que conllevan un alto coste computacional.

5.2 Corte Ortogonal

En los siguientes apartados se comentan los principales aspectos de la implementación de modelos 2D y 3D de corte ortogonal, y el uso de los elementos cohesivos para estimar el daño por delaminación.

5.2.1 MODELADO 2D

El enfoque macro-mecánico, que considera el material compuesto como un material homogéneo anisótropo, es la metodología más comúnmente utilizada en la literatura. En general, la orientación unidireccional de la fibra es asumida en los enfoques de dos dimensiones. Uno de los primeros estudios de corte ortogonal de láminas unidireccionales basado en elementos finitos fue llevado a cabo por Arola y Ramulu [8]. El modelo fué capaz de predecir fuerzas de corte y el estado tensional del material para diferentes orientaciones de la fibra. Otro de los primeros trabajos en modelado FEM 2D fue desarrollado por Ramesh *et al*. [22] para estudiar la influencia de la orientación en cuatro materiales FRP diferentes. Se implementaron mecanismos de fallo basados en la rotura fibra-matriz concluyendo que la carga necesaria para inducir el fallo depende de la orientación de las fibras.

Modelos más avanzados y complejos fueron posteriormente presentados por Nayak y Bhatnagar [1,2] y Mahdi y Zhang [9,10]. Los primeros llevaron a cabo simulaciones en elementos finitos del mecanizado de GFRP con fibras unidireccionales, cuyos resultados apoyaron el estudio de Arola *et al*. [23]. Mahdi y Zhang utilizaron tanto en 2D como en 3D enfoques para simular el corte del compuesto. El análisis 2D reprodujo un material homogéneo equivalente que predice las fuerzas de corte de materiales FRP relacionándolas con la orientación de las fibras.

Todos los trabajos anteriormente mencionados indicaron que el grado de profundidad del daño y la fuerza de corte aumentan al incrementar la orientación de la fibra. Sin embargo la estimación de la fuerza de avance no fue satisfactoria, presentando una gran diferencia con los resultados experimentales.

En un estudio más reciente, Arola *et al*. [23] se centró en la influencia de la geometría de la herramienta para reducir las fuerzas de corte y el daño sub-superficial durante el mecanizado ortogonal de materiales unidireccionales FRP. La Figura 5.1 presenta un esquema del modelo. El

criterio de fractura viene gobernando por un criterio de tensión crítica en los nodos de unión de los elementos, mostrado en la ecuación 5.1.

$$f = \sqrt{\left(\frac{\sigma_n^{'}}{\sigma^f}\right)^2 + \left(\frac{\tau_1}{\tau_1^f}\right)^2 + \left(\frac{\tau_2}{\tau_2^f}\right)^2} \; ; \sigma_n^{'} = \max(\sigma_n, 0) \tag{5.1}$$

donde σ_n and τ_1 son las tensiones normal y a cortante en el plano, σ^f y τ_1^f son la resistencia normal y a cortante en el plano, y τ_2 y τ_2^f son la tensión a cortante y rigidez transversal respectivamente fuera del plano del material. Los nodos del vértice de la grieta se despegan cuando la ecuación 5.1 alcanza el valor 2 dentro de una tolerancia del 10% según la ecuación 5.2

$$1 - f_{tol} \leq f \leq 1 + f_{tol} \tag{5.2}$$

De nuevo, este estudio mostró una buena aproximación a las fuerzas de corte experimental, mientras que las fuerzas de avance no obtuvieron una buena predicción. El mismo problema fué observado en simulaciones numéricas de corte ortogonal de metal debido a la dificultad de reproducir la compleja interacción entre la herramienta y la pieza de trabajo (véase por ejemplo [24]).

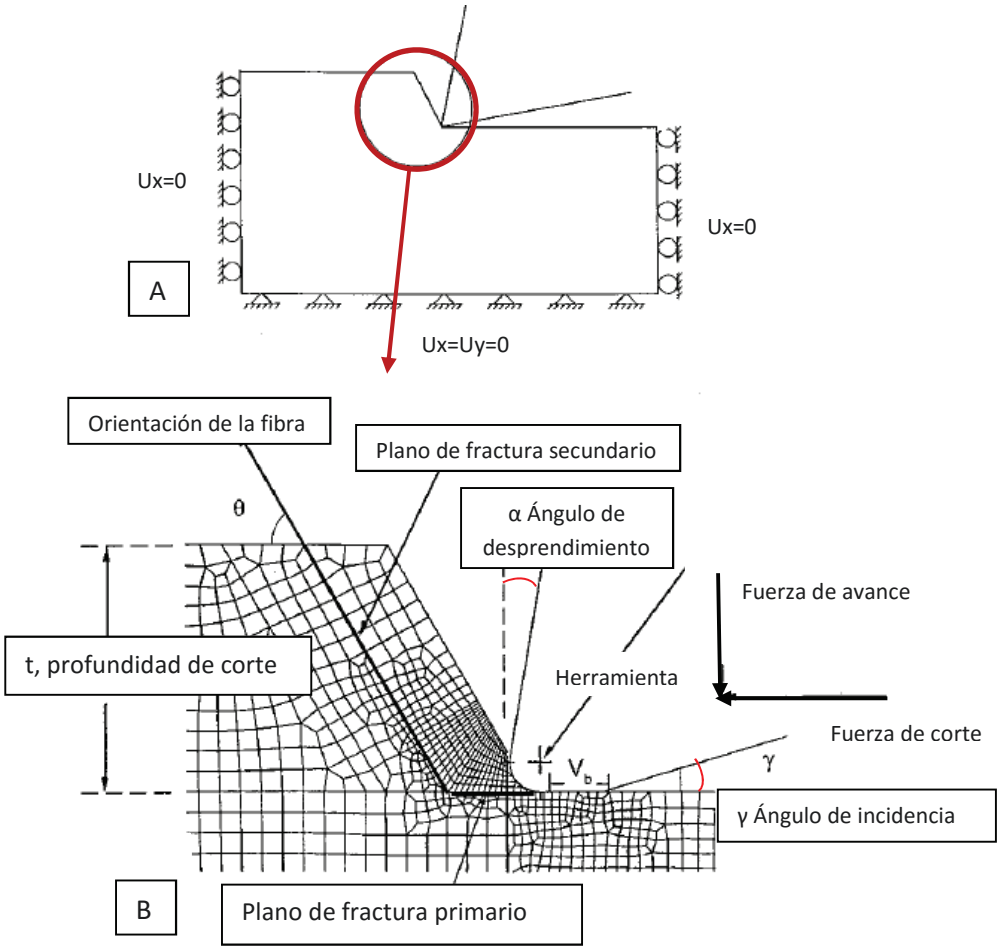

Figura 5.1: Diagramas esquemáticos de la discretización de la viruta (A) condiciones de contorno y pieza de trabajo y (B) planos de fractura primario y secundario Arola *et al*. [23].

Un modelo con un nuevo enfoque micro-mecánico fue propuesto por Nayak *et al*. [25]. La principal diferencia con los estudios anteriores es que el material no se considera homogéneo, si no que se definen diferentes propiedades para la matriz y la fibra. Este enfoque obtuvo una mejor predicción de las fuerzas de corte y del fallo por separación de la matriz y la fibra. La predicción de la desunión se limita sin embargo a la cara frontal de la fibra.

Un punto interesante es poder separar el daño sufrido en la matriz, del daño sufrido en las fibras durante el mecanizado. Los modelos anteriores no son capaces de realizar dichas predicciones debido a la asunción de homogeneidad del material. Ante este problema, Rao *et al*. [26] consiguió un modelo capaz de predecir la extensión de la fibra dañada considerando la fibra como elástica y midiendo las tensiones principales. Sin embargo, la separación de la interfaz fibra-matriz fue solo predicha en la cara frontal de la fibra. En la misma línea, Mkaddem *et al* [27] llevó a cabo simulaciones de mecanizado usando un alcance micro-macro en material unidireccional GFRP, comparando los resultados con la literatura existente. Tanto las fuerzas de corte como las de avance fueron predichas con un error menor que en las del modelo desarrollado por Nayak y Bhatnagar [1,2] como se observa en la Figura 5.2 (errores del 6% y 26 % respectivamente frente al 17% y 44%). Se comprobó que la fuerza de avance aumenta con el ángulo de orientación de la fibra hasta una orientación de 45° y disminuye cuando asciende hasta 90°.

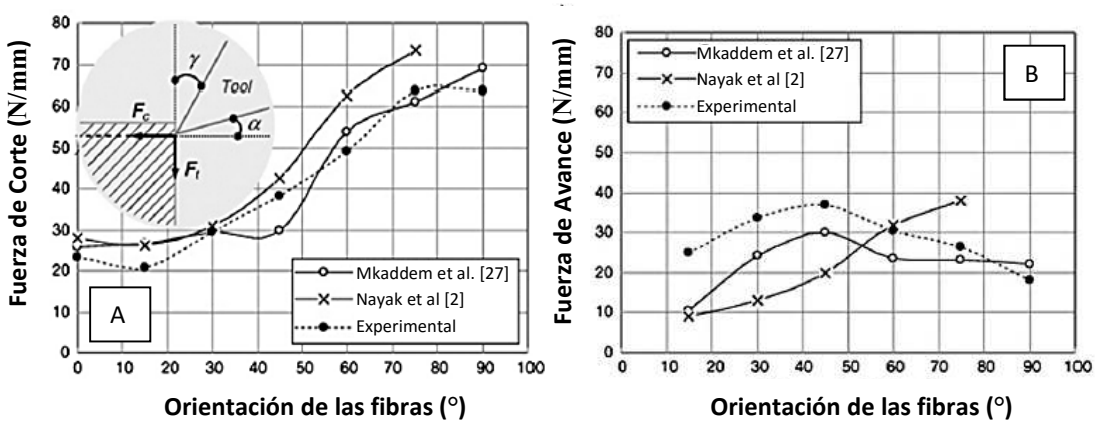

Figura 5.2: Valores experimentales y predichos con los modelos de Nyak y Bhatnagar [2] y Mkaddem *et al* [27] de las fuerzas de corte (A) y de avance (B) para el mecanizado de GFRP.

Dandekar y Shin [28] modelaron el mecanizado ortogonal de una lámina usando un modelo multi-fase capaz de predecir el fiber-pullout (extracción de la fibra de la matriz) y el despegue de la interfase entre matriz y fibra tanto en la parte frontal como en la cara posterior de la fibra. El modelo fue implementado para materiales CFRP y GFRP. Ambas simulaciones se compararon con datos experimentales en términos de fuerza de corte y predicción de daño. El fallo de Marigo [29] para materiales frágiles se utilizó para modelizar el daño en la fibra, mientras que el despegue matriz/fibra fue simulado utilizando interacciones cohesivas. Los resultados mostraron que la profundidad del despegue y el daño de la fibra decrecen cuando se incrementa la orientación de la fibra. En cuanto a las fuerzas del proceso, en el caso de materiales compuestos de epoxi reforzado con fibra de vidrio, la fuerza de corte aumenta con el aumento de orientación de la fibra y el ángulo de desprendimiento de la herramienta. En contraste, la fuerza de avance aumenta con la orientación de las fibras, pero se mantiene casi constante cuando se incrementaba el ángulo de desprendimiento. Ésta última variación no da lugar a ninguna pérdida de adherencia de la fibra de vidrio con la matriz. Para el material con fibras de carbono la fuerza de corte

promedio aumentó con el aumento de la orientación de las fibras hasta 90°, mientras que para ángulos mayores se observó una caída en el valor de la fuerza. Ésta disminución puede ser explicada por el efecto rebote que tiene lugar como consecuencia de la flexión desarrollada, en particular cuando las fibras se alinean quasi-paralelas a la dirección de la herramienta. La mayor fuerza de avance se obtuvo para una orientación de 45°, mientras que para ángulos mayores la fuerza se redujo drásticamente. Este comportamiento es consistente con las observaciones experimentales.

Un nuevo avance se dio en los modelos de corte ortogonal con la implementación del agrietamiento de la matriz independiente del daño causado en la fibra. Lasri *et al*. [31] dirigió uno de los primeros estudios en introducir este modo de fallo. El proceso de formación de la viruta y los modos de daño, tales como el agrietamiento de la matriz, la separación de las fibras de la matriz y la rotura de la fibra se modelaron usando varios criterios de daño para láminas unidireccionales reforzadas con fibra de vidrio. Se compararon tres criterios de daño diferentes: criterio de Hashin, criterio de tensión máxima y criterio de Hoffman. Los resultaron indicaron que, en el caso de los criterios de Hashin y de tensión máxima, el despegue de la interfaz fibra-matriz fue el primer daño desarrollado en la estructura durante el proceso de formación de la viruta, y se inició delante del filo de corte de la herramienta. Con el avance de la herramienta, el daño progresa en la dirección paralela a la fibra separando la matriz y la fibra. El fallo de la matriz se inició y progresó antes de completar la rotura de la viruta, propagándose en el interior del material y provocando la formación de la misma. En el caso del criterio de máxima tensión, el fallo de la matriz se inició más tarde y progresó gradualmente en la zona próxima al borde de la herramienta de corte. El fallo de la fibra es el último fenómeno que se observó en ambos criterios. Los autores concluyeron que la tendencia de las principales fuerzas de corte, independientemente del criterio utilizado, concuerdan bien con los datos experimentales siendo los valores predichos con el criterio de Hashin más cercanos a los experimentales. Contrario a esto, ninguno de los tres criterios predijo correctamente los valores de la fuerza de avance. Por otro lado, para todas las orientaciones de la fibra, tanto el daño sub-superficial, como la rotura de la matriz o el despegue de la fibra y la matriz, comenzaron cerca del filo de corte y se propagaron en dirección paralela y perpendicular a la fibra dentro de la pieza de trabajo. La extensión del daño, por tanto, depende fuertemente de la orientación de la fibra, como se ha comentado anteriormente y muestra la Figura 5.3.

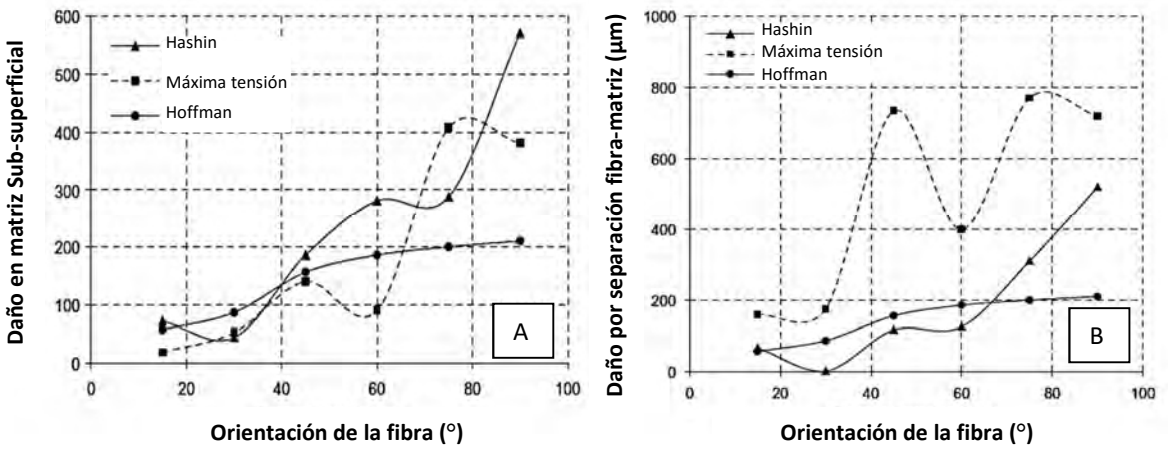

Figura 5.3: Variación del daño sub-superficial (debajo de la cara de incidencia) con la orientación de las fibras: Daño de la matriz (A) o despegue de la interfase fibra-matriz (B). El cálculo del daño se ha realizado con diferentes criterios [31].

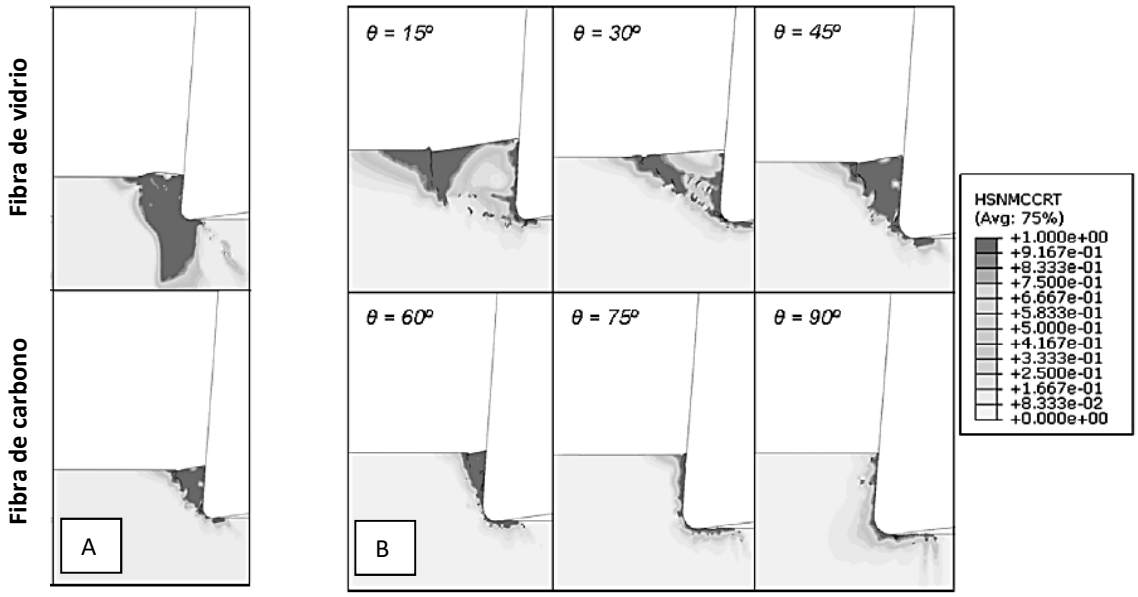

Figura 5.4: Comparación del daño en la matriz entre CFRP y GFRP para una orientación de las fibras de 45° (A), y evolución del daño en la matriz en función de la orientación de las fibras para el material CFRP (B).

Santiuste *et al*. [12] estudiaron las diferencias entre el mecanizado de GFRPs y CFRPs a través de las simulaciones FEM. El criterio de iniciación de daño para el material se basa en la teoría Hashin [31,32] que incluye cuatro modelos de fallo (tracción/compresión de la fibra y rotura/aplastamiento de la matriz). Los autores analizaron las diferencias entre ambos materiales midiendo el nivel de energía necesaria para alcanzar la ruptura completa del material. Basándose en las simulaciones FEM, se clasificó a los materiales GFRPs como materiales compuestos que exhiben un fallo progresivo de comportamiento dúctil bajo condiciones de mecanizado. En contraste, los materiales CFRPs mostraron un fallo catastrófico con poca o ninguna progresión en el daño y se clasificaron como quebradizos cuando se someten a procesos de corte. Los resultados de la Figura 5.4 muestra que el daño sub-superficial debido al mecanizado en los compuestos de fibra de carbono es menor que en los materiales compuestos de fibra de vidrio. Éstos últimos mostraron grandes deformaciones antes de la rotura, provocando una extensión del daño por debajo y por delante de la punta de la herramienta. Por otro lado, en el material compuesto de fibra de carbono el daño se localiza a lo largo de la viruta sin cortar, por delante de la herramienta, y un daño mínimo por debajo del filo de corte. El mecanismo de formación de la de viruta y el daño inducido dependen en gran medida de la orientación de la fibra. En las fibras con una orientación cercana a la dirección de la velocidad de corte en materiales CFRP se observó más fuertemente el efecto del momento de flexión, que implica tanto el daño por agrietamiento como por aplastamiento. El incremento del ángulo de orientación de la fibra conllevó un aumento del daño por aplastamiento por debajo de la superficie mecanizada como se observa en la Figura 5.4B.

A pesar de la importancia de seleccionar un adecuado tamaño y forma de malla en los modelos numéricos de elementos finitos, no es fácil encontrar trabajos que analicen el efecto de estos parámetros cuando se simula el corte de material compuesto. Uno de los trabajos más relevantes que estudian la influencia del tamaño de los elementos y la orientación de la malla

fue llevado a cabo por Soldani *et al*. [33] usando el enfoque 2D. Se encontró que las fuerzas de corte y de avance son variables de salida robustas que pueden considerarse independientes de los parámetros numéricos estudiados en el trabajo, mientras que el daño fue el factor más sensible. No sólo el tamaño de la malla influye en la predicción de los campos de daños, también la forma y la orientación de la misma. La distribución del daño también cambió significativamente con la variación del nivel de energía necesario para la rotura: cuanto menor era la energía, más frágil se comportaba el compuesto. En consecuencia, el daño tiende a ser reducido a un área pequeña que rodea la herramienta y por debajo de la superficie mecanizada. En cuanto al estudio de la geometría del filo de corte se comprobó que los valores más bajos del ángulo de desprendimiento de la herramienta conllevan valores de fuerza mayores. El incremento del radio de filo también produjo un incremento en las fuerzas ya que el filo de corte redondeado podría interpretarse como un ángulo de ataque efectivo disminuido. La morfología de la viruta estuvo fuertemente influenciada por el nivel de energía que se necesita para llegar a la rotura completa del elemento. El ángulo de desprendimiento también interactuó con la orientación de la fibra, provocando una modificación de la inclinación relativa con respecto a la superficie de incidencia, como muestra la gráfica de la Figura 5.5.

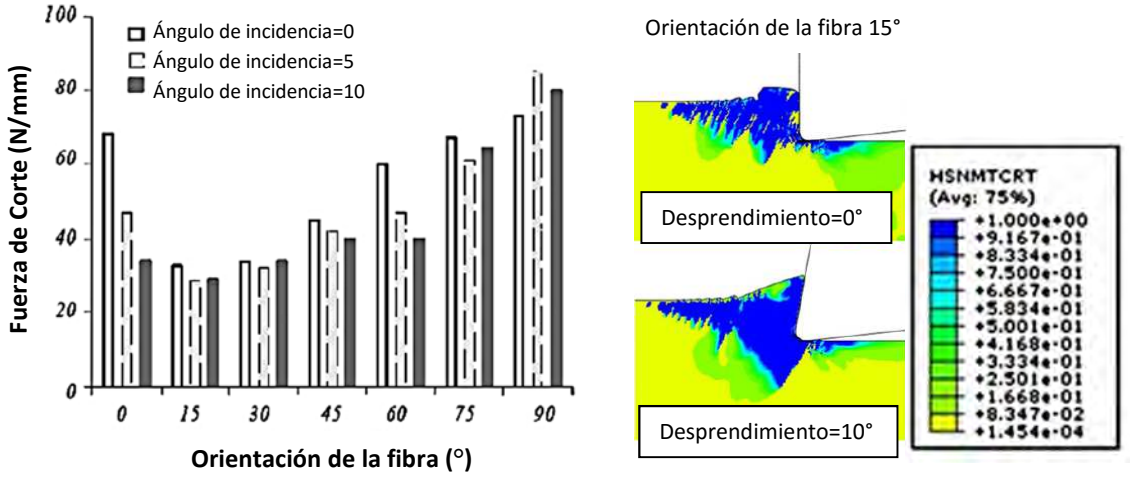

Figura 5.5: Fuerza de corte para diferentes ángulos de desprendimiento en función de la orientación de las fibras (A) y efecto del ángulo de desprendimiento en la rotura de la matriz (B) [33].

Iliescu *et al*. [34] También realizó un estudio de formación de la viruta mediante un modelo discreto FEM a nivel meso-escala. Se aplicó a materiales unidireccionales CFRP y a diferentes orientaciones de fibra, validando los resultados con observaciones experimentales. El modelo es capaz de predecir los valores de fuerza de corte, así como la forma de la viruta cuando la herramienta es nueva.

Una comparación entre dos modelos 2D fue llevado por Rentsch *et al*. [35]. El primer modelo presentaba un enfoque macroscópico basado en las propiedades anisotropícas del material con una orientación de las fibras definida implícitamente. El segundo modelo sin embargo, se implementó bajo un enfoque microscópico con la representación explicita de las fibras y la matriz con diferentes propiedades para cada componente de la lámina. El modelo de daño utilizado fue el de Hashin para ambos casos. Los resultados de ambas aproximaciones mostraron una buena estimación de la tendencia de las fuerzas de corte aunque subestimando ligeramente los

valores. El mecanismo de eliminación de material también fue bastante aproximado en ambos modelos (Figura 5.6).

Basándose en los experimentos de Iliescu *et al* [34], Zenia *et al* [36] desarrollaron uno de los modelos 2D más recientes de corte ortogonal para compuestos CFRP. Todos los modelos previos en la literatura se basan en criterios de fallo como Hashin, Hoffman o de máxima tensión. El uso de estos criterios limita la simulación en términos de formación de viruta, y de iniciación y la propagación del daño, ya que no tienen en cuenta la degradación progresiva del elemento. Lasri *et al*. [30] introdujo el concepto de la degradación de la rigidez para superar esta dificultad. En el modelo de Zenia *et al* [36], el material es considerado como homogéneo equivalente, cuyo comportamiento mecánico (comportamiento elasto-plástico) se basa en una ley constitutiva meso-mecánica. Esta ley combina el efecto de degradación de la rigidez del material, la plasticidad (utilizando el concepto de tensión efectiva y leyes de evolución para predecir el inicio de daño), y el crecimiento del daño durante el proceso de formación de la viruta. Teniendo en cuenta todos estos aspectos, este modelo permite una mejor comprensión de los fenómenos físicos observados durante la operación de corte y ofrece una herramienta numérica capaza de simular la formación de virutas sucesivas. También es capaz de predecir las fuerzas de corte, el daño sub-superficial inducido y la zona plastificada que se puede generar tanto en la matriz como en la interfaz fibra-matriz.

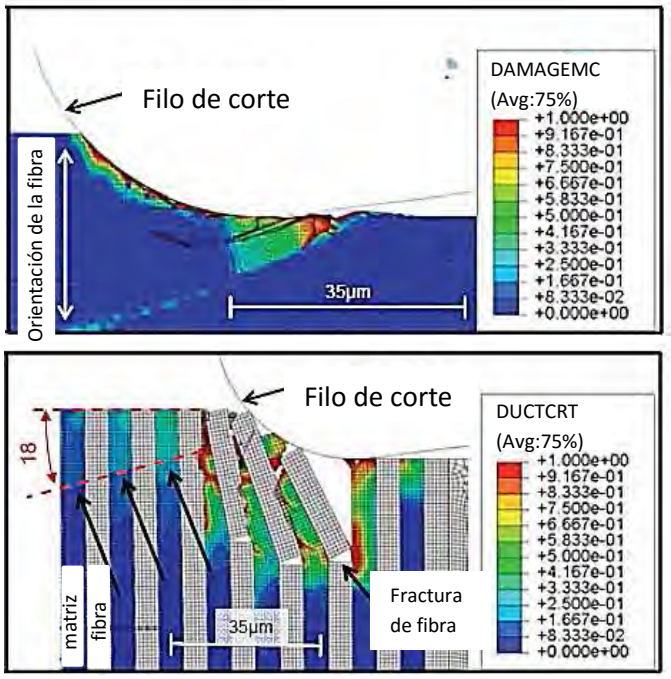

Figura 5.6: Daño de la matriz en el modelo macroscópico (A) y microscópico (B) para una orientación de la fibra de 90° [35].

5.2.2 MODELADO 3D

Uno de los problema que presenta el enfoque 2D es que sólo es válido para modelar laminados unidireccionales. Sin embargo, los laminados cuasi-isótropos son los más utilizados en aplicaciones industriales debido a su mejor comportamiento en servicio. Otro de los problemas del modelado 2D es que no predice el daño por delaminación, ya que está relacionado con las

tensiones fuera del plano. Como solución a ambos problemas se presenta el desarrollo de modelos 3D capaces de reproducir laminados multidireccionales. Sin embargo, a pesar de sus ventajas, el número de modelos tridimensionales que se puede encontrar en la literatura es muy limitado debido principalmente al alto coste computacional que llevan asociado.

Mahdi y Langchi [9] implementaron un modelo de celda unitaria (nivel meso), donde se diferencia entre fibra y matriz. Desarrollaron un algoritmo de mallado adaptativo (consistente en remallar en diferentes pasos) utilizando el criterio de máxima tensión a cortante. El método de remallado, aunque más costoso computacionalmente, mostraba mejores resultados de predicción para las fuerzas de corte que los modelos con malla fija.

Gopala *et al*. [37] implementaron un modelo de elementos finitos macro-mecánico a nivel lámina para material CFRP unidireccional. Se estudiaron la influencia de la orientación de las fibras, la profundidad de corte y el ángulo de desprendimiento. Las fuerzas de corte aumentaron con los dos primeros parámetros, pero resultaron menos influenciables con el ángulo de desprendimiento como se observa en la Figura 5.7. La formación de la viruta también se comparó con ensayos experimentales y el modelo predijo con bastante exactitud la geometría de la misma.

El modelo bidimensional comentado anteriormente de Santiuste *et al*. [12] fue modificado por los mismos autores para presentar un modelo 3D [13]. Este modelo tridimensional fue desarrollado con el fin de evaluar la validez de los supuestos que intervienen en la formulación del enfoque 2D a la hora de analizar una secuencia de apilamiento. El comportamiento mecánico del material LFRP se implementó mediante una subrutina VUMAT, utilizando la formulación de Hou [38] que incluía cuatro criterios de fallo: fallo de fibra, agrietamiento de la matriz, aplastamiento de la matriz y delaminación. La comparación de los resultados de ambos enfoques mostró que las simulaciones 2D, asumiendo una hipótesis de tensión plana, reproducen principalmente los fenómenos experimentados por las capas externas del laminado. Las simulaciones 3D, por otro lado, demostraron que cuanto más delgados son los laminados de capas unidireccionales más similares son los resultados entre ambos modelos (Figura 5.8). Estas observaciones indican la importancia de considerar los efectos fuera del plano durante el corte y deben de tenerse en cuenta al analizar los resultados obtenidos con en el caso 2D.

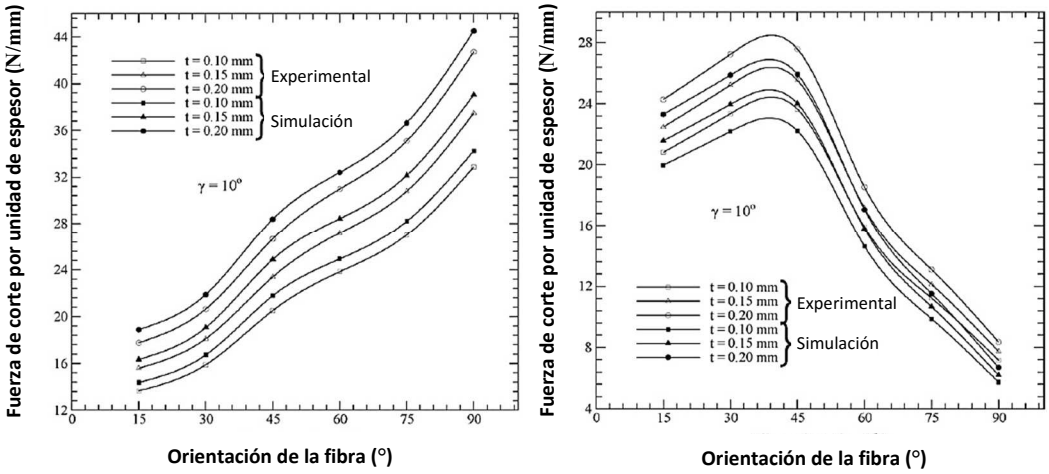

Figura 5.7: Variación de las fuerzas de corte con la variación de la orientación de las fibras en función de la profundidad de corte. Fuerza de corte (A) y fuerza de avance (B) [37].

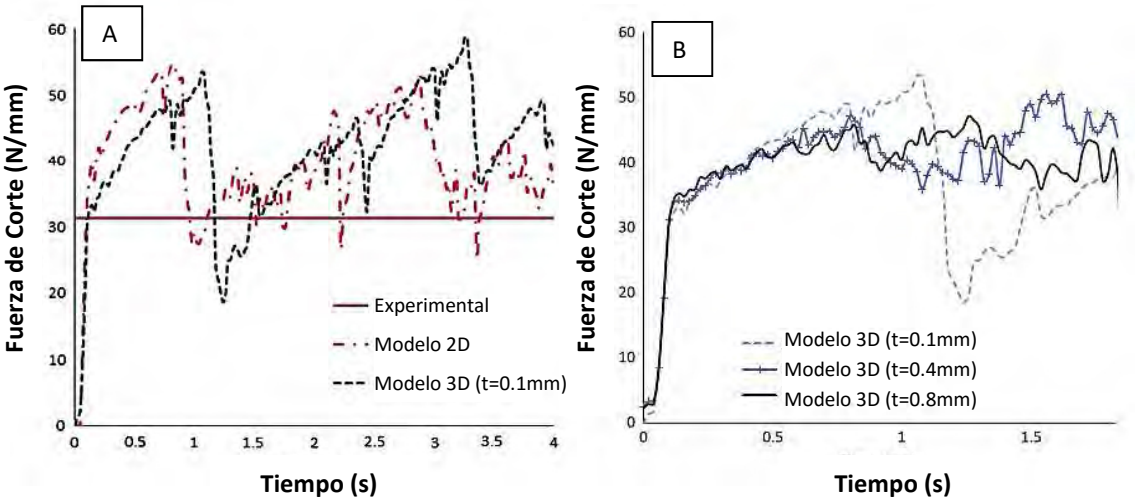

Figura 5.8: Comparación entre la fuerza de corte experimental [34] y de los modelos 2D y 3D (A) y fuerza de corte en función del espesor (B).

El enfoque 3D de Santiuste et al. [13] se empleó en la simulación de laminados cuasi-isótropos, y se demostró la influencia de la secuencia de apilamiento en el desarrollo del daño. Las capas se encuentran en la superficie libre, tienden a desarrollar zonas dañadas más grandes que las que se encuentran en la zona interior del laminado. Esta conclusión es importante para aplicaciones tales como las uniones atornilladas que establecen una secuencia de apilamiento preferente para el caso de carga dominante.

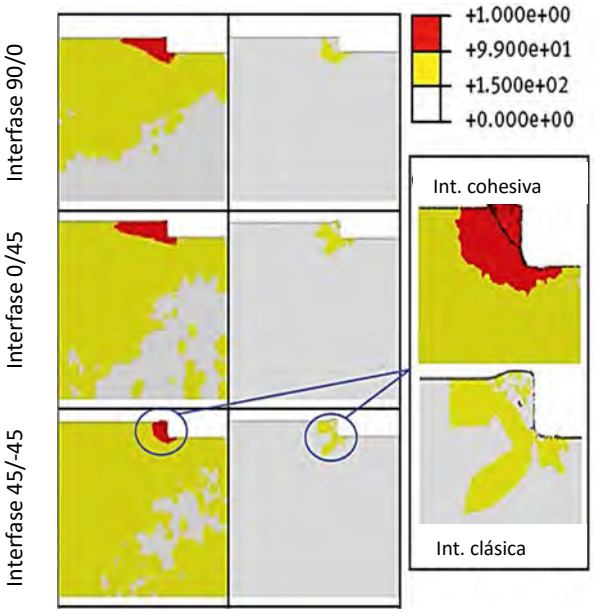

Figura 5.9: Predicción de la delaminación usando interacciones cohesivas (columna de la izquierda) y modelo de Hou (columna de la derecha) para la secuencia de apilamiento $[90/0/45/-45]_S$ [14].

Una nueva modificación de este modelo 3D, que consistió en introducir interacciones cohesivas entre las capas para reproducir la propagación de la delaminación, se presentó en un estudio más reciente [14]. Los valores implementados en el modelo fueron coherentes y equivalentes a los utilizados para el modelo de fallo fuera del plano de Hou [38]. El modelo 3D se aplicó para simular el corte ortogonal de laminados cuasi-isótropos considerando dos secuencias de

apilamiento $[45/-45/0/90]_S$ y $[90/0/45/-45]_S$. Las interacciones cohesivas implementadas en el modelo 3D mostraron diferencias importantes en la predicción de la zona dañada en comparación con la formulación clásica. Mientras que el enfoque de daño por delaminación de Hou infravalora los niveles y la extensión de este fenómeno, en el caso de la aplicación de las interacciones cohesivas se obtuvieron resultados más realistas. En ambos casos la comparación se llevó a cabo con resultados experimentales de la literatura con niveles significativos de daño. La fuerte influencia de la secuencia de apilamiento en el daño inducido por delaminación durante el mecanizado también quedó demostrada. Las áreas delaminadas más grandes se observaron en la interfaces de 0/90 ° y 0/-45 ° como refleja la Figura 5.9, por lo que los laminados con estas secuencias de apilamiento se deben evitar en la superficie libre, donde las capas tienden a desarrollar zonas dañadas más grandes.

Uno de los modelos 3D más recientes fue propuesto por Usui *et al*. [39]. El estudio presentó un esquema de elementos finitos que usa una formulación Lagrangiana no lineal para grandes deformaciones. La pieza de trabajo se modeló como una estructura mallada en dirección de las fibras en el plano de la lámina, permitiendo que la fisura se propague en estas direcciones. Los planos de fractura se definieron por los índices de Miller en la estructura mallada. Se consiguió modelar la propagación de fisuras transversales, la flexión de las fibras y la rotura de las fibras. Se simuló el corte ortogonal de láminas unidireccionales reforzadas con carbono con una orientación de 0°, 45°, -45° y 90°. La validación del modelo mostró una buena estimación de las fuerzas, y un razonable parecido físico de la extensión dañada y de la superficie mecanizada.

5.2.3 ELEMENTOS COHESIVOS Y DELAMINACIÓN

El daño por delaminación se produce, no sólo en el mecanizado de materiales compuestos, sino también en otros procesos dinámicos como por ejemplo la carga de impacto (ver [40]). Se acepta en la comunidad científica que la predicción de la delaminación requiere el uso, o bien de elementos cohesivos o bien de interacciones cohesivas en la interfaz inter-laminar [41]. Este tipo de interacciones se ha aplicado con éxito en el modelado de la carga dinámica de materiales compuestos (véase por ejemplo [42]), y en los modelos 3D de mecanizado que incluyen fallo por delaminación [14,20,21].

La Figura 5.10 muestra una típica respuesta de tracción-separación en modo mixto de esta interacción [44]; El elemento cohesivo funciona de la siguiente manera: Se considera un comportamiento elástico lineal hasta el inicio de la delaminación, lo que requiere un criterio de fallo para predecir el daño. Una vez que el daño se verifica, se define una ley de evolución del daño que degrada progresivamente la interacción cohesiva. En el trabajo anteriormente mencionado [14], el inicio de la delaminación fue definido por un criterio de tensión cuadrática considerando tensiones fuera del plano. Este criterio se describe en la ecuación 5.3 donde t_n es la tensión normal de tracción, t_s y t_t son las tensiones de cizallamiento y t^0_n, t^0_s y t^0_t son valores máximos admisibles de estas tensiones.

$$\left(\frac{t_n}{t_n^0}\right)^2 + \left(\frac{t_s}{t_s^0}\right)^2 + \left(\frac{t_t}{t_t^0}\right)^2 = 1 \qquad (5.3)$$

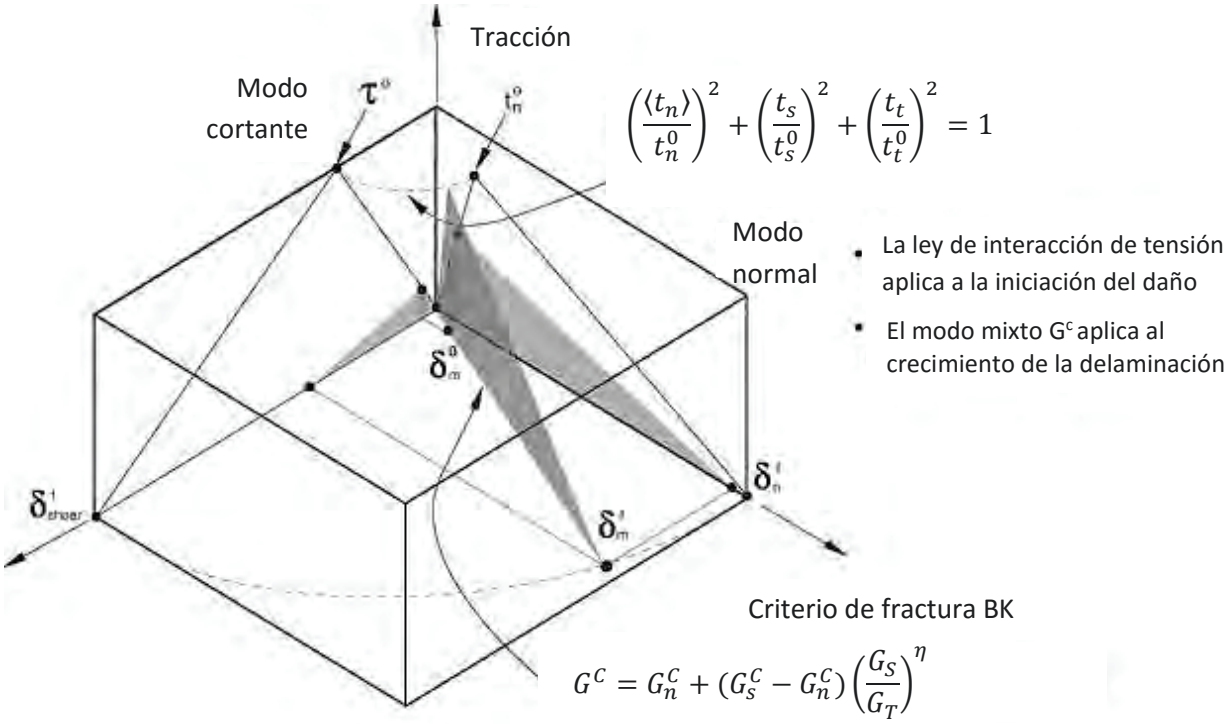

Figura 5.10: Respuesta tracción-separación para modo mixto en interacciones cohesivos [44].

Por otro lado, el comportamiento después del inicio del daño fue definido por el modelo de daño de Benzeggagh-Kenane (BK) [43]. Este modelo se basa en la energía disipada debido al fallo teniendo en cuenta una respuesta de tracción-separación de acuerdo con la ecuación 5.4, donde $G_S = G_s + G_t$ y $G_T = G_n + G_S$. Las variables G_n, G_s y G_t se refieren a la energía disipada por unidad de área mientras que las cantidades G^C_n, G^C_s and G^C_t se refieren a las energías de fractura críticas requeridas para causar el fallo en la dirección normal, y la primera y segunda direcciones de cizallamiento, respectivamente. η es un parámetro de la propiedad cohesiva. El modelo BK es especialmente útil cuando la energía crítica de fractura durante la deformación se da solamente a largo de la primera y la segunda dirección de cizallamiento y además coinciden; es decir $G_{cs} = G_{ct}$ [43].

$$G_n^C + \left(G_s^C + G_n^C\right)\left(\frac{G_S}{G_T}\right)^\eta = G^C \tag{5.4}$$

5.3 Taladrado

Como se ha comentado anteriormente, las operaciones de taladrado son necesarias antes de que los componentes estructurales se unan mecánicamente. Un porcentaje significativo de los componentes laminados de material compuesto rechazados en la fabricación de aeronaves se debe a la delaminación que se induce durante el taladrado. La delaminación es uno de los efectos no deseados del mecanizado cuando se utilizan parámetros de corte inadecuados o brocas desgastadas y ha recibido una gran atención en la literatura (ver secciones anteriores en las que se han comentado numerosos trabajos).

Los modelos tridimensionales de taladrado desarrollados hasta el momento se pueden clasificar en dos grupos claramente diferenciados:

- **Modelos simplificados**: tratan el problema como un proceso de perforación asemejando la broca a un punzón y reduciendo al mismo tiempo la compleja geometría de la broca. El movimiento de rotación no se reproduce y solo se considera el avance de la herramienta. Su principal ventaja es que conllevan un coste computacional bajo. Pese a la simplicidad de estos modelos, no existe en la literatura un gran número de estudios [15-17,44].

- **Modelos completos:** reproducen el proceso de taladrado rigurosamente incluyendo los movimientos de rotación y de avance de la herramienta. También se modela la penetración de la broca en la pieza de trabajo, el fallo del material y la erosión de los elementos del material compuesto, lo que conlleva un coste computacional mucho más elevado que el modelo simplificado. La modelización con elementos finitos del proceso de taladrado completo se logró recientemente en varios trabajos [20,21,48,50].

El interés en el modelado de procesos de taladrado es claro debido a la importancia de esta operación para la industria. Aun así, sigue siendo un desafío la inclusión de modelos numéricos de mecanizado en la industria, principalmente debido a la complejidad de los mismos y el tiempo de cálculo requerido. La disponibilidad de modelos sencillos que conduzcan a predicciones razonables podría ayudar en la amplia aplicación de herramientas de simulación en la industria.

5.3.1 MODELOS SIMPLIFICADOS

Como se ha mencionado anteriormente, el interés en los modelos de elementos finitos simplificados radica en su bajo coste computacional y su simplicidad en la representación de la geometría. Uno de los primeros modelos en taladrado de laminados compuestos unidireccionales fue llevado a cabo por Bhattacharya y Horrigan [46]. Se estudiaron dos condiciones de apoyo: pieza sin soporte y pieza con soporte elástico debajo del material. La aproximación de este modelo consistió en aplicar una presión distribuida de 600 N para representar la fuerza ejercida por la broca. Se concluyó que el factor de intensidad de tensiones es más grande para el caso sin apoyo, produciendo el fallo a un nivel de carga mucho menor. Las tensiones en el borde debidas a la flexión del material sin taladrar por debajo de la broca y las tensiones cortantes fueron excesivas para el caso sin soporte.

Durao *et al*. [15,16] presentaron varios estudios con modelos simplificados más avanzados sobre materiales reforzados con fibra de carbono. Un de las novedades respecto al modelo anterior, es que se representa la broca como parte del modelo, en vez de sustituirla por una fuerza equivalente. Los elementos cohesivos utilizados para simular la aparición y el crecimiento de la delaminación sólo se consideraron en las interfases en las que existe un cambio de orientación de la fibra entre las láminas. El modelo se basa en un proceso iterativo que consiste en aplicar un desplazamiento a la broca igual a la mitad del espesor de la lámina (Figura 5.11A). Al final de cada paso la capa de elementos se elimina y otro paso comienza con el contacto entre la broca y la cara superior de la nueva lámina, manteniendo las deformaciones del paso anterior. Este modelo no tiene en cuenta el movimiento de rotación de la herramienta. Se estudiaron dos geome-

trías de broca, cuyos resultados mostraron que la fuerza de inicio de delaminación es generalmente inferior a los modelos analíticos de Hocheng-Dharan [18] y Lachaud *et al* [47] con los que se comparó. Sin embargo, los tres modelos coincidieron en la predicción del espesor sin taladrar necesario para que se diera el inicio del daño por delaminación. El modelo FEM también mostró una predicción cercana a los valores máximos de fuerza de avance (Figura 5.11B), pero no es capaz de evaluar las consecuencias de variar los parámetros de corte en las fuerzas.

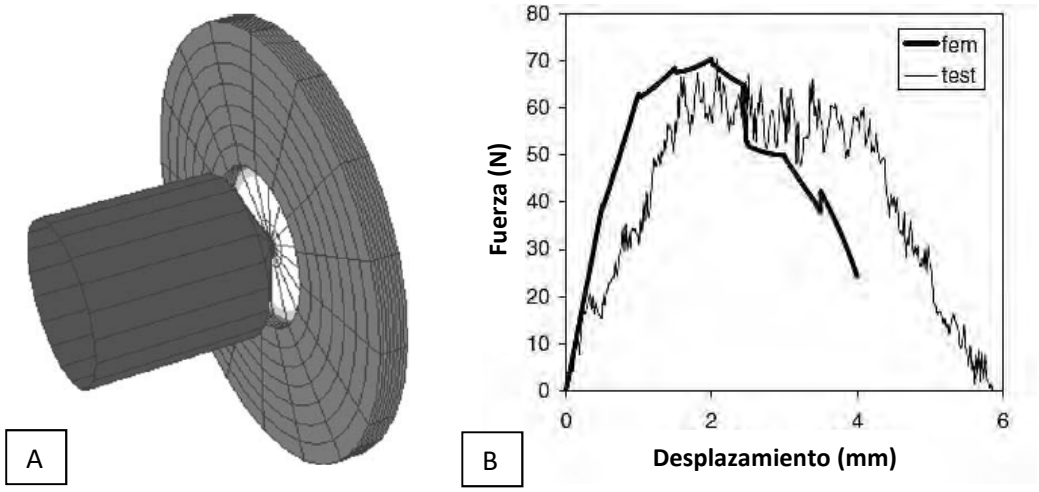

Figura 5.11: (A) Inicio de la simulación y (B) desplazamiento final de la broca del modelo de elementos finitos para broca helicoidal.

La utilización de brocas más realistas se introdujo en los modelos simplificados desarrollados por Singh *et al*. [17]. Para este estudio se seleccionaron láminas unidireccionales GFRP con agujeros pre-taladrado de 2 mm de diámetro. El fallo intra-laminar se modelizó con el criterio de fallo de Tsai Wu. No se utilizaron elementos cohesivos para el daño inter-laminar puesto que el estudio se centró en láminas y no en laminados. Los resultados demostraron que el ángulo de punta es relevante en la generación del daño siendo el ángulo de 90° el que menos daño provocó frente a los ángulos de 104° y 118°.

5.3.2 MODELOS COMPLETOS

Hasta el momento de publicar el modelo 3D presentado en el capítulo 6 de esta tesis, solo existía un modelo 3D de taladrado completo en material unidireccional CFRP en la literatura, desarrollado por Phadnis *et al.* [20]. Posteriormente, se han publicado varios trabajos más de modelos completos de taladrado [21,37,48-50,52]

En la Figura 5.12 se presenta el primer modelo 3D de taladrado desarrollado por Phadnis *et al*. [20]. La secuencia de apilamiento escogida fue $[0_4/90_8/0_4]$. La superficie inferior del laminado CFRP se fijó a un plato de apoyo para representar la condición de contorno experimental. El criterio de Hashin [31] fue utilizado para estimar el daño en la fibra mientras que el criterio de fallo de Puck [51] se utilizó para modelar el fallo en la matriz. Ambos criterios se implementaron a través de un modelo de material definido por el usuario (VUMAT) en el software de elementos finitos Abaqus/Explicit.

El modelo FE de este estudio fue capaz de predecir la fuerza de avance y el par de la broca durante el taladrado con una precisión razonable en comparación con los resultados experimentales. El uso de elementos cohesivos permitió estimar la forma y el tamaño de la delaminación a la entrada de taladro con una buena exactitud, mientras que a la salida del agujero, tanto la forma como el tamaño de la delaminación fueron sobrestimados como se observa en Figura 5.13. El modelo de taladrado validado se utilizó para determinar los parámetros de trabajo óptimos para el material compuesto CFRP estudiado, indicando que las velocidades bajas de alimentación (<150 mm/min) y las altas velocidades de corte (>600 rpm) son convenientes para la perforación de materiales carbono/epoxi.

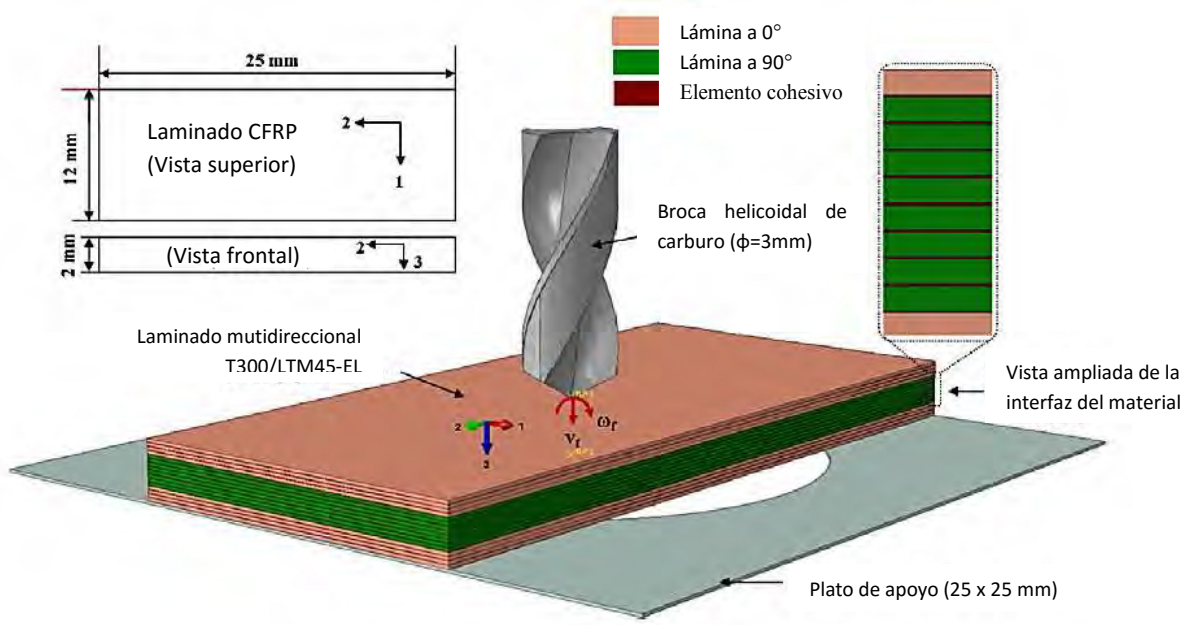

Figura 5.12: Modelo en elementos finitos del taladrado del laminado CFRP T300/LTM45-EL [20].

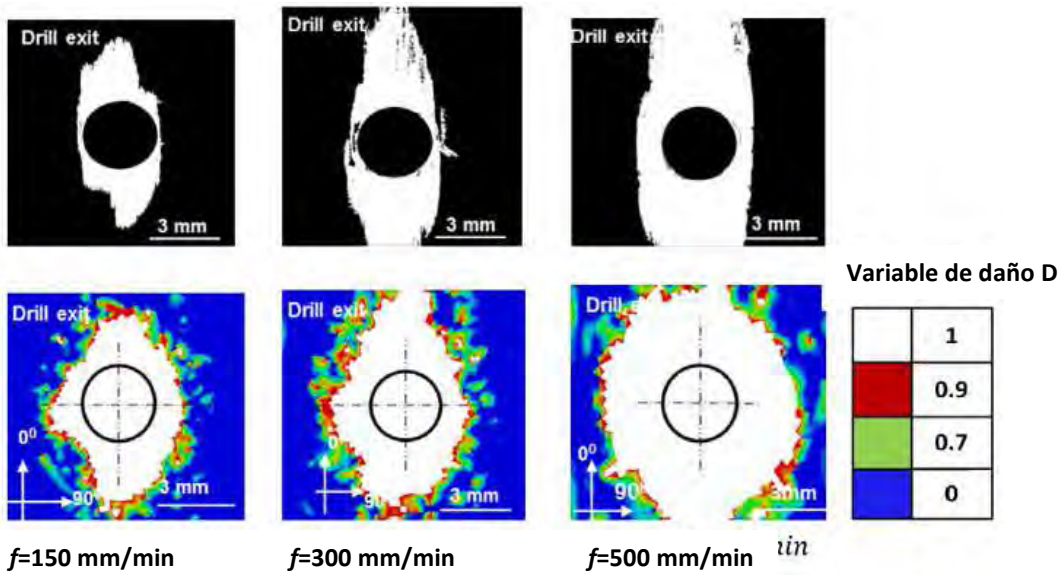

Figura 5.13: Análisis de delaminación a la salida de los agujeros mediante procesamiento de imagen (fila superior) y mediante el modelo de elementos finitos (fila inferior) [20]

Una variación del modelo descrito, fue presentada por Makhdum *et al*. [50] para reproducir el taladrado con vibración asistida de materiales CFRP. El comportamiento mecánico del laminado fue definido por la teoría potencial de Hill [52] para materiales anisótropos. Al modelo se le implementó también un criterio de plastificación que incluye el efecto de reblandecimiento por ultrasonidos. La formulación del modelo constitutivo que incorpora el efecto de reblandecimiento acústico en el material CFRP debido a la influencia de la vibración ultrasónica se puede encontrar en Phadnis *et al.* [53,54]. Los resultados obtenidos a partir de las simulaciones predijeron el nivel de la fuerza de empuje y su evolución durante el proceso de VAD (Vibration Assisted Drilling) de forma bastante aproximada. El par, sin embargo, mostró desviaciones con respecto a los datos experimentales. Esto se puede atribuir a la dinámica de la broca debido a las ondas ultrasónicas que se propagan en el taladro excitado y que no se incorporó en el modelo de elementos finitos; como resultado, el modelo capturó una respuesta positiva del par en contraste con un par de torsión alrededor de un promedio de cero medido en los experimentos. Aun así, fue significativamente más bajo que el nivel medido en el taladrado convencional.

Uno de los último modelos completos en taladrado fue desarrollado por Isilbir *et al* [21,48], quienes llevaron a cabo varios estudios en laminados ortotrópicos unidireccionales con una secuencia de apilamiento $[90/-45/0/45]_{2s}$. El modelo 3D desarrollado (Fig. 5.14A) predice la aparición y el crecimiento del daño intra-laminar e inter-laminar en laminados compuestos CFRP. Los modos de fallo, tales como la rotura de las fibras y el agrietamiento de la matriz se calcularon mediante un análisis de fallo progresivo utilizando el criterios de Hashin desarrollado para elementos sólidos 3D. Entre las láminas se incluyeron superficies cohesivas. Las simulaciones indicaron las ventajas de utilizar una broca escalonada en comparación con una broca helicoidal en el taladrado de materiales CFRP, mostrando un par y fuerza de avance reducidos bajo los mismos parámetros de corte (avance y revoluciones). Los resultados también indicaron que cuanto mayor ratio de escalón, menores son la fuerza de avance, el par y la delaminación, como muestra la Fig. 5.14B.

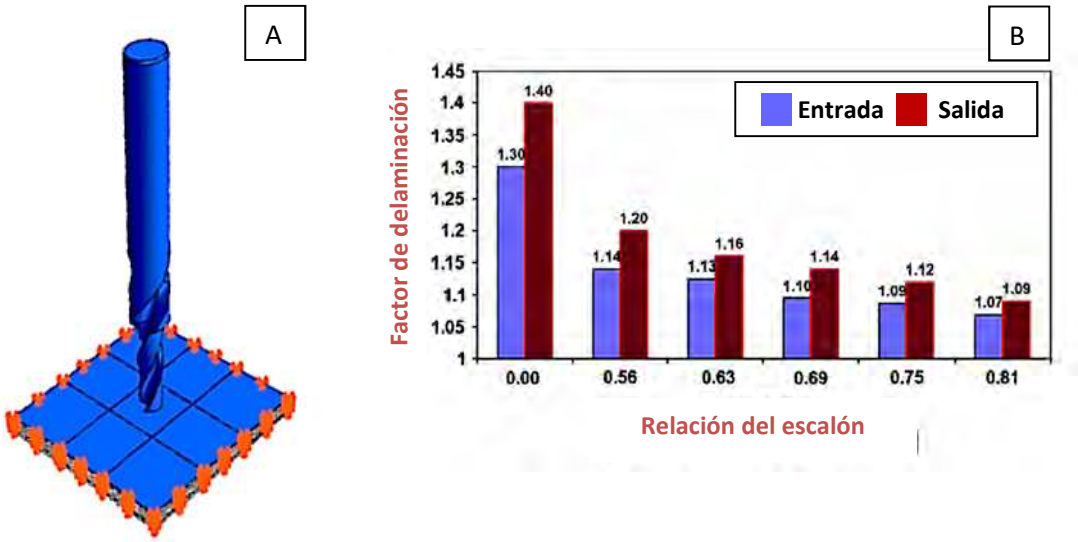

Figura 5.14: Modelo de taladrado con geometría de broca escalonada (A) y evaluación mediante el modelo numérico de la influencia del escalón en el factor de delaminación (B) [48].

5.4 Referencias

[1] Nayak D, Bhatnagar N, Mahajan P. Machining studies of uni-directional glass fiber reinforced plastic (UD-GFRP) composites part 1: effect of geometrical and process parameters. Mach Sci Technol 2005; 9:481–501.

[2] Nayak D, Bhatnagar N, Mahajan P. Machining studies of UD-FRP composites part 2: finite element analysis Mac Sci Technol 2005; 9;503–28.

[3] Bhatnagar N, Nayak D, Singh I, Chouhan H, Mahajan P. Determination of machining-induced damage characteristics of fiber reinforced plastic composite laminates. Mater Manuf Process 2004; 19(6):1009–23.

[4] Wang XM, Zhang LC. An experimental investigation into the orthogonal cutting of unidirectional fiber reinforced plastics. Int J Mach Tools Manuf 2003; 43:1015–22.

[5] Chinmaya R. Dandekar,Yung C. Shin, Modeling of machining of composite materials: A review. Int J Mach Tools Manuf 2012; 57:102–21.

[6] Miguélez MH, Soldani X, Molinari A. Analysis of adiabatic shear banding in orthogonal cutting of Ti alloy. Int J Mech Sci 2013; 75:212–22.

[7] Molinari A, Soldani X, Miguélez MH. Adiabatic shear banding and scaling laws in chip formation with application to cutting of Ti–6Al–4V. J Mechan Ph Solid, 2013; 61:2331–59.

[8] Arola D, Ramulu M. Orthogonal cutting of fiber-reinforced composites: a finite element analysis. Int J Mech Sci 1997; 39:597–613.

[9] Mahdi M, Zhang L. An adaptive three-dimensional finite element algorithm for the orthogonal cutting of composite materials. J Mater Process Technol 2001; 113:368–72.

[10] Mahdi M, Zhang L. A finite element model for the orthogonal cutting of fiber reinforced composite materials. J Mater Process Technol 2001; 113:373–7.

[11] Mkaddem A, El Mansori M. Finite element analysis when machining UGF reinforced PMCs plates: chip formation, crack propagation and induced damage. Mater Des 2009; 30(8):3295–302.

[12] Santiuste C, Soldani X, Miguélez MH. Machining FEM model of long fiber composites for aeronautical components. Compos Struct 2010; 92:691–8.

[13] Santiuste C, Miguélez MH, Soldani X. Out-of-plane failure mechanisms in LFRP composite cutting. Compos Struct 2011; 93:2706–13.

[14] Santiuste C, Olmedo A, Soldani X, Miguélez MH. Delamination prediction in orthogonal machining of carbon LFRP composites. J Reinf Plastic Comp 2012; 31(13):875–85.

[15] Durao LMP, de Moura MFSF, Marques AT. Numerical simulation of the drilling process on carbon/epoxy composite laminates. Composites: Part A 2006; 37:1325–33.

[16] Durao LMP, De Moura MFSF, Marques AT. Numerical prediction of delamination onset in carbon/epoxy composite drilling. Eng Fract Mech 2008; 75:2767–78.

[17] Singh I, Bhatnagar N, Viswanath P. Drilling of unidirectional glass fiber reinforced plastics: experimental and finite element study. Mater Des 2008; 29:546–53.

[18] Hocheng H, Dharan CKH. Delamination during drilling in composite laminates. J Eng Ind 1990; 112:236–9.

[19] Upadhyay PC, Lyons JS. On the evaluation of critical thrust for delamination free drilling of composite laminates. J Reinf Plast and Comp 1999; 18:1287–303.

[20] Phadnis VA, Makhdum F, Roy A, Silberschmidt VV. Drilling in carbon/epoxy composites: experimental inves-tigations and finite element implementation. Compos A 2013; 47:41–51.

[21] Isbilir O, Ghassemieh E. Numerical investigation of the effects of drill geometry on drilling in-duced delamination of carbon fiber reinforced composites. Compos Struct 2013; 105:126–33.

[22] Ramesh MV, Seetharamu KN, Ganesan N, Shivkumar MS. Analysis of machining of FRPs using FEM. Int J Mach Tools Manuf 1998; 38:1531–49.

[23] Arola D, Sultan MB, Ramulu M. Finite element modeling of edge trimming fiber reinforced plastics, Transactions of the ASME J Manuf Sci Eng 2002; 124(1):32–41.

[24] Díaz-Álvarez J, Cantero JL, Miguélez MH, Soldani X. Numerical analysis of thermomechanical phenomena influencing tool wear in finishing turning of Inconel 718. Int J Mech Sci 2014; 82:161-9.

[25] Nayak D, Singh I, Bhatnagar N, Mahajan P. Analysis of machining Induced damages in FRP composites — a micromechanics finite element approach. AIP Conference Proceedings 2004; 712:327–31.

[26] Rao GVG, Mahajan P, Bhatnagar N. Machining of UD-GFRP composites chip formation mechanism. Compos Sci Technol 2007; 67:2271–81.

[27] Mkaddem I, Demirci E, Mansori. A micro–macro combined approach using FEM for modeling of machining of FRP composites: cutting force analysis. Composites Sci Technol 2008; 68:3123–27.

[28] Dandekar C, Shin YC. Multiphase finite element modeling of machining unidirectional composites: prediction of de bonding and fiber damage. Transactions of the ASME J Manuf Sci Eng 2008; 130:510–6.

[29] Marigo JJ. Modelling of brittle and fatigue damage for elastic material by growth of microvoids. Eng Fract Mech 1985; 21(4):861-74.

[30] Lasri L, Nouari M, Mansor ME. Modelling of chip separation in machining unidirectional FRP composites by stiffness degradation concept. Compos Sci Technol 2009; 69:684–92.

[31] Hashin Z, Rotem A. A fatigue criterion for fiber-reinforced materials. J Compos Mater 1973; 7:448–64.

[32] Hashin Z. Failure criteria for unidirectional fiber composites. J Appl Mech 1980; 47:329–34.

[33] Soldani X, Santiuste C, Muñoz-Sánchez A, Miguélez MH. Influence of tool geometry and numerical parame-ters when modeling orthogonal cutting of LFRP composites. Composites Part A 2011; 42:1205–16.

[34] Iliescu D, GehinD, IordanoffI, GirotF, GutiérrezME. A discrete element method for the simulation of CFRP cutting. Compos Sci Technol 2010; 70:73–80.

[35] Rentxch R, Pecat O, Brinksmeier E. Macro and micro process modeling of the cutting of carbon fiber reinforced plastics using FEM. Proc Eng 2011; 10:1823-8.

[36] Zenia S, Ben Ayed L, Nouari M, Delamézière A. Numerical prediction of the chip formation process and induced damage during machining of carbón/epoxy composites. Int J Mech Sci 2015; 90:89–101.

[37] Gopala Rao GV, Mahajan P, Bhatnagar N. Three-dimensional macro-mechanical finite element model for machining of unidirectional-fiber reinforced polymer composites. Mat Sci Eng A 2008; 498:142–9.

[38] Hou JP, Petrinic N, Ruiz C, Hallett SR. Prediction of impact damage in composite plates. Compos Sci Technol 2000; 60(2):228–73.

[39] Usui S, Wadell J, Marusich T. Finite Element Modeling of Carbon Fiber Composite Orthogonal Cutting and Drilling. Procedia CIRP 2014; 14:211–6.

[40] Zaera R. Ballistic impacts on polymer matrix composites, composite armor, personal armor in impact engineeringof composite structures. In: Abrate S (ed.) Impact engineering of composite structures. New York, NY: Springer Vienna; 2011

[41] Wisnom MR. Modelling discrete failures in composites with interface elements. Compos Part A 2010; 41:795–805.

[42] Aymerich F, Dore F, Priolo P. Prediction of impact induced delamination in cross ply composite laminates using cohesive interface elements. Compos Sci Technol 2008; 68:2383–90.

[43] Benzeggagh ML, Kenane M. Measurement of mixed mode delamination fracture toughness of unidirectional glass/epoxy composites with mixed mode bending apparatus. Compos Sci Technol 1996; 56:439–49.

[44] Hibbit K. Sorensen Inc. ABAQUS user's manual 6.4-1; 2003.

[45] Camanho PP, Davila CG. Mixed-Mode Decohesion Finite Elements for the Simulation of Delamination in Composite Materials. NASA/TM-2002–211737 2002; 1–37.

[46] Bhattacharya D, Horrigan DPW. A Study of hole drilling in Kevlar composites. Compos Sci Technol 1998; 58:267–83.

[47] Lachaud F, Piquet R, Collombet F, Surcin L. Drilling of composite structures. Compos Struct 2001; 52:511–6.

[48] Isbilir O, Ghassemieh E.Three-dimensional numerical modelling of drilling of carbon fiber-reinforced plastic composites. J Compos Mater 2013; 48(10):1209-19.

[49] Zenia S, Ben Ayed L, Nouari M, Delamézière A. An elastoplastic constitutive damage model to simulate the chip formation process and workpiece subsurface defects when machining CFRP composites. Procedia CIRP 2015; 31:100–5.

[50] Makhdum F, Phadnis VA, Roy A, Silberschmidt VV. Effect of ultrasonically-assisted drilling on carbon-fibre-reinforced plastics. J Sound Vib 2014; 333:5939–52.

[51] Puck A, Schürmann H. Failure analysis of FRP laminates by means of physically based phenomenological models. Compos Sci Technol 1998; 7:1045–67.

[52] Hill R. Constitutive modelling of orthotropic plasticity in sheet metals. J Mech Phys Solids 1990; 38(3):405–17.

[53] Phadnis VA, Makhdum F, Roy A, Silberschmidt VV. Experimental and numerical investigations in conventional and ultrasonically assisted drilling of CFRP laminate. Procedia CIRP 2012; 1:455–9.

[54] Phadnis VA, Roy A, Silberschmidt VV. A finite element model of ultrasonically assisted drilling in carbon/epoxy composites. Procedia CIRP 2013; 8:141–6.

Capítulo 6

Numerical Prediction of Delamination in CFRP Drilling

El modelado mediante elementos finitos del proceso de taladrado de Polímeros Reforzados con Fibra de Carbono (CFRP) es una interesante herramienta para la predicción del daño por delaminación. En los últimos años se han desarrollado modelos en 3D, para laminados multidireccionales CFRPs, que incluyen el movimiento de rotación de la broca, la penetración en la placa y la erosión de los elementos. Sin embargo, el coste computacional de estos modelos complejos es una gran desventaja al compararlos con modelos simplificados que consideran la broca como un punzón que perfora el laminado. En este capítulo se desarrollan y se comparan ambos modelos, en términos de predicción de la delaminación. El modelo simplificado, presentó un reducido coste computacional, pero sobrestimando ligeramente el factor de delaminación en comparación con el modelo complejo. La influencia sobre la delaminación de la fuerza de avance, el uso de una placa de soporte inferior del laminado y la secuencia de apilamiento se estudiaron utilizando el modelo simplificado.

Este estudio se encuentra publicado bajo la siguiente referencia: **N. Feito**, J. López-Puente, C. Santiuste, M.H. Miguélez. “Numerical prediction of delamination in CFRP drilling”, Composite Structures (2014) Vol. 108, p. 677-683.

Numerical Prediction of Delamination in CFRP Drilling

Abstract

Delamination is one of the undesired effects of machining using non appropriate cutting parameters or worn drill. Finite element modeling of drilling of Carbon Fiber Reinforced Polymer (CFRP) composites is an interesting tool for damage prediction. Recently, complete modeling of the process including the rotatory movement of the drill, penetration in the composite plate and element erosion has been developed in the scientific literature. Computational cost of these complex models is a great disadvantage when comparing them with simplified models that consider the drill acting like a punch that pierces the laminate. In this paper both complete and simplified models were developed and compared in terms of delamination prediction. The simplified model, presenting reduced computational cost, slightly overestimates the delamination factor when compared with the complex model. The influence on delamination of thrust force, clamping area at the bottom surface of the laminate and the stacking sequence is studied using the simplified model.

Keywords: CFRPs, Drilling, Delamination, Modeling

6.1 Introduction

Carbon Fiber Reinforced Polymer (CFRP) composites combine fatigue and corrosion resistance, light weight and high specific stiffness and strength. These properties make CFRPs suitable for a wide range of high responsibility applications. Manufacturing and final assembly of the components commonly requires machining processes needed to achieve dimensional tolerances and assembly specifications. CFRP composites are difficult to cut materials due to the presence of hard fibers. On the other hand, they are vulnerable to the generation of damage during processing: delamination, fiber pull-out and matrix thermal degradation are usually observed when cutting parameters are not properly defined. Conventional machining operations of CFRPs, mainly milling and drilling, should be designed to be productive processes ensuring the quality of the resultant component. The surface quality plays an important role in the improvement of fatigue life of composite components [1].

Drilling operations are required before mechanical joining of the CFRP components [2]. A significant percentage of the component rejection in aircraft manufacturing is due to delamination induced during drilling. Delamination is one of the undesired effects of machining using non appropriate cutting parameters or worn drill and has received extensive attention in the literature. A brief summary of significant contributions is provided below.

Davim *et al*. [3] analyzed the influence of cutting parameters and the matrix on the specific cutting force, delamination factor and surface roughness. The feed rate was found to be the most influencing parameter on delamination factor.

Abrao *et al*. [4] checked the influence of tool geometry and cutting parameters on delamination during drilling of glass FRP. It was shown the strong influence of the drill geometry in competition with the thrust force, commonly assumed to be the most influencing factor. The authors demonstrated that the drill corresponding to the highest thrust force caused the second smallest delaminated area because of its favorable geometry.

Delamination factor after drilling FRP laminates was evaluated in [5] using a digital analysis. The digital analysis showed its suitability for control of drilling induced damage in CFRPs. This technique has been also applied to damage control in high speed drilling of glass FRP [6]. Delamination decreased as the cutting speed was increased within the cutting range tested, probably due to the enhanced cutting temperature with spindle speed, leading to increased softening of the matrix and less delamination.

The most important contributions in the field of composite drilling are summarized in a recent review [7] including techniques, tools and operations developed to minimize the occurrence of delamination.

The measurement of damage is expensive and sometimes requires destructive techniques, thus it is desirable to develop simulation tools able to predict damage mechanisms induced during machining. However, only few works in scientific literature deal with modeling of cutting processes in composite. These works are mostly focused on two dimensional (2D) approaches to orthogonal cutting although recently, some attempts in three dimensional (3D) modeling have been published. Of course, 3D analysis is required for drilling analysis. Main advantage of 2D modeling relies on the reduced computational cost, however it is not possible to reproduce neither out-of-plane failure mechanisms nor simulating quasi-isotropic laminates. 2D modeling has been developed by different authors, examples can be found in [8–12] analyzing, between other factors, the influence of fiber orientation, cutting parameters and material properties in orthogonal machining of LFRP composites.

The validity of the hypothesis assumed in 2D approaches to LFRP composite cutting has been analyzed in [13,14]. Out-of-plane failure in orthogonal cutting of composites was studied using a three dimensional model based on finite elements. The influence of stacking sequence on the generation of damage was demonstrated and delamination was predicted using cohesive interactions.

Finite element modeling of the complex drilling process has recently achieved in [15,16]. In these works drilling of CFRP was successfully reproduced including drill penetration in the workpiece, material failure and elements erosion. Good agreement between measured and predicted torque, thrust force and delamination extension was shown.

Previously, simplified models of CFRP drilling were developed, having the advantage of most reduced computational cost. Modeling of drilling processes involves elevated difficulty, because of the need of simulating drill rotation and feed movement. Common assumption in simplified models considers the drill acting like a punch that pierces the laminate, see for instance [17,18]. This was the approach used by Durao *et al*. [19] and Singn *et al*. [20] when studying GFRP drilling; they showed the influence of the drill point angle in the induced damage.

Main contributions in the field of composite machining modeling have been summarized in a recent work [21].

The interest of modeling drilling processes is clear due to the importance of this operation for industry. The available simulation tools assumes on one hand; simplifying hypothesis (treating the problem as a punching process, with efficient computational cost and reduced geometrical complexity); or model the drilling process rigorously simulating rotation and feed movement of the tool (including penetration of the drill in the workpiece and element erosion, leading to elevated computational cost). The implementation of machining models in industry is still a challenge, probably because of the complexity of the simulation tools and the computational time required. The availability of simple models leading to reasonably predictions could help in the wide implementation of simulation tools in industry.

In this paper a comparison between the predictions provided by a simplified and a complete drill model based on finite element is provided. The aim is giving an overview of the main advantages of both types of modeling, analyzing their accuracy when predicting delamination and study the influence of some parameters involved in delamination. The paper is structured in the present introduction, followed by models description and validation, results and discussion and main conclusions derived from the study.

6.2 Numerical Models and Validation

Two numerical models simulating respectively complete drilling and simplified punching of tape laminate, were developed using the commercial finite element code ABAQUS.

A scheme of the models, showing boundary conditions, is presented in Figure 6.1. In the simplified model the drill acts like a punch pushing the laminate (two stages of the drill penetration are simulated), see Figure 6.1A. The complete model reproduces the complex 3D process with rotary and feed movement (Figure 6.1B). The drill and the laminate characteristics were the same for both models and were obtained from Ref. [15] for model validation. Both models include restriction to displacement in Z di-

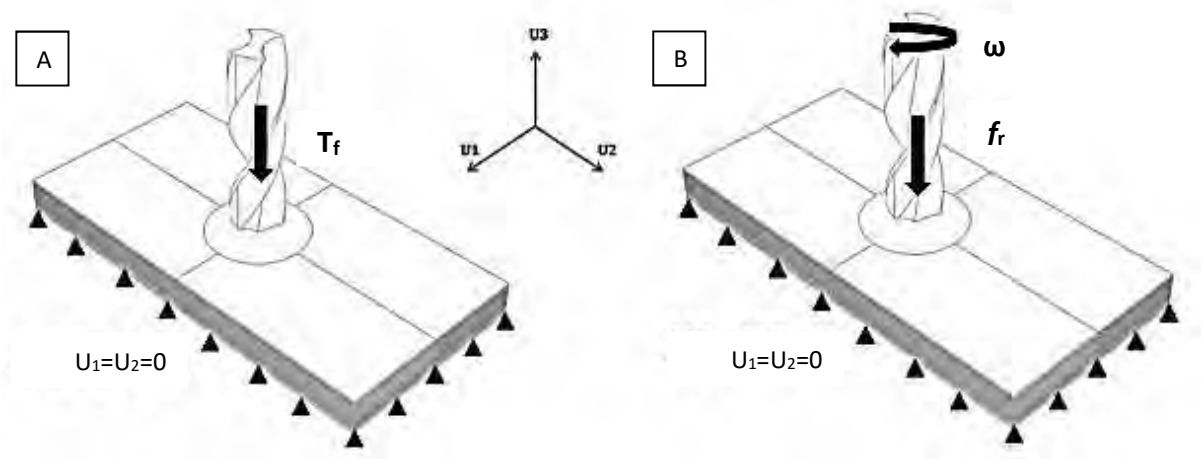

Figure 6.1: (A) Scheme of simplified model (T_f thrust force). (B) Scheme of the complete model (ω rotation speed, f_r feed rate).

rection in the base of the workpiece except inside a circumference with diameter 16 mm where the Z displacement is free. On the other hand, displacements were not allowed in the contour of the workpiece [15].

6.2.1 DRILL AND WORKPIECE DESCRIPTION

The main characteristics of the drill and the workpiece, common for both complete and simplified models, are presented below.

The drill was assumed to be rigid, with diameter equal to 3 mm and the tip angle equal to 120°.

The workpiece was similar to that used for experimental validation (see [15]): CFRP composite (UD T300/LTM45-EL) composed of tape plies with thickness 2 mm consisting of 16 plies with stacking sequence $[0_4/90_4]_s$ (being each ply 0.125 mm thick). Each ply was modeled at the zone close to the drill entrance using solid elements C3D6R with six nodes (1 element along the thickness). The use of wedge elements (prismatic element with triangular section) minimizes the dependence of the results with mesh orientation in the laminate plane. Minimum element size was 0.25 mm. Far from to the drill entrance zone hexagonal elements C3D8R with 8 nodes and reduced integration were used, with minimum element size around 1 mm [22].

The anisotropic composite was modeled using an elastic behavior up to failure. Elastic properties of the composite are presented in Table 6.1, where E_1 and E_2 are respectively longitudinal and transverse modulus, G_{12} and G_{23} are respectively in-plane and out-of-plane shear modulus and ν_{12} is major Poisson's ratio.

Table 6.1: Material ply properties [15] and critical values of the strain for element deletion.

Property	Value
ρ (kg/m3)	1600
E_1 (GPa)	127
E_2 (GPa)	9.1
G_{12} (GPa)	5.6
G_{23} (GPa)	4
ν_{12}	0.31
X_t (MPa)	2720
X_c (MPa)	1690
Y_c (MPa)	214
S_{12} (MPa)	115
ε_{1c}	0.0525
ε_{2c}	0.0525
ε_{3c}	0.07

The intra-laminar failure model was based on Hou criteria [23] and was introduced through a user subroutine VUMAT for the carbon/epoxy laminate. This model has been used widely in the literature (see for instance [24,25]).

This model considers three different types of damage (fiber failure and matrix cracking and crushing; Eqs. (6.1)–(6.3) defining different damage variables *d* (stress dependent) ranging from 0 (no damage) to 1 (fully broken).

$$d_f^t = \left(\frac{\sigma_{11}}{X_t}\right)^2 + \left(\frac{\tau_{12}}{S_{12}}\right)^2 \leq 1 \qquad (6.1)$$

$$d_m^t = \left(\frac{\sigma_{22}}{Y_t}\right)^2 + \left(\frac{\tau_{12}}{S_{12}}\right)^2 \leq 1 \qquad (6.2)$$

$$d_m^c = \frac{1}{4}\left(\frac{-\sigma_{22}}{S_{12}}\right)^2 + \left(\frac{Y_c^2\sigma_{22}}{4S_{12}^2 Y_c}\right)^2 - \left(\frac{\sigma_{22}}{Y_c}\right) + \left(\frac{\tau_{12}}{S_{12}}\right) \leq 1 \qquad (6.3)$$

where σ_{11} and σ_{22} are the stress in fiber and transverse direction respectively, and σ_{12} the in-plane shear stress. Constants X_t and Y_t are tensile strengths in longitudinal and transverse directions respectively; Y_c is the transverse compressive strength; and S_{12} is the in-plane shear strength. The values of these constants are summarized in Table 1. When one of the damage variables reaches the value 1, all the stress components that appear in the equation are set to zero. The stresses on a damaged element drop to values close to zero and hence large deformations appear. These elements do not contribute to the strength or the stiffness of the composite, but they can cause lack of convergence during simulation and instability problems. Erosion criterion based on maximum strain criteria was implemented in the VUMAT subroutine to remove the distorted elements. After each time increment the longitudinal strains (ε_{11}, ε_{22} and ε_{33}) were evaluated, and the element was removed if one of the strains reached a critical value (ε_{1c}, ε_{2c} and ε_{3c}) provided in Table 6.1.

The inter-laminar failure was modeled using cohesive elements. Small thickness was assigned to the interface (5 μm) in order to improve numerical behavior when elevated deformations are reached during calculation. Meshing strategy in the plane 1–2 was the same as that used in the ply, with one element along the thickness (direction 3).

The delamination modeling requires the establishment of a damage initiation criteria and a damage evolution law. The onset of delamination is commonly defined using criteria based on normal and shear stresses (Eq. 6.4) [23,26], where t_n, t_s and t_t are the strengths of the cohesive interface in the normal and in the two shear directions respectively.

$$\left(\frac{\sigma_{33}}{t_n}\right)^2+\left(\frac{\sigma_{13}}{t_s}\right)^2+\left(\frac{\sigma_{23}}{t_t}\right)^2\geq 1 \qquad (6.4)$$

This criterion is applied if one of the following conditions is reached:

$$\sigma_{33}\geq Z_t \quad \text{or} \quad \sqrt{\sigma_{12}^2+\sigma_{13}^2}\geq S_{23} \qquad (6.5)$$

where Z_t is the laminate strength under tension in the through thickness direction and S_{23} is the laminate shear strength.

Concerning the damage evolution, the most used laws are based on the energy dissipation because of the damage process (fracture energy). Examples of these laws are Benzeggagh–Kenane (BK) [27] and potential laws [21] expressed respectively with the following equations:

$$G_n^C+\left(G_s^C+G_n^C\right)\left(\frac{G_S}{G_T}\right)^{\eta}=G^C \qquad (6.6)$$

$$\left(\frac{G_n}{G_n^C}\right)^{\alpha}+\left(\frac{G_S}{G_s^C}\right)^{\alpha}+\left(\frac{G_t}{G_t^C}\right)^{\alpha}=1 \qquad (6.7)$$

where G_n, G_s and G_t are the released rate energy in the normal and in the two shear directions respectively; G^C_n; G^C_s and G^C_t are the critical values of the released rate energy, being α and η parameters of the model. The models of initiation and evolution of damage have been implemented in ABAQUS using cohesive elements provided in the FE code and widely used in different applications [28–30].

In the present work, a quadratic nominal stress criterion given in Eq. 6.4 has been used. The damage evolution is simulated through a potential law based on energy, see Eq. 6.7 with α = 1. Element erosion was produced as the failure criterion was reached. The response of the cohesive elements is governed by a traction-separation

law illustrated in Figure 6.2 for failure mode type I. The definition of this law requires the specification of the linear elastic behavior by means of the stiffness in the normal and in the two shear directions (K_{nn}, K_{ss} and K_{tt}), the interface resistance in each direction (t_n, t_s and t_t) and the damage evolution through the critical released rate energy (G^C_n, G^C_s and G^C_t). The properties related with the cohesive elements are summarized in the Table 6.2.

Table 6.2: Properties of the cohesive elements.

Parameter	Value
k_{nn}	2 GPa
$K_{ss} = K_{tt}$	1.5 GPa
t_n	60 MPa
$t_s = t_t$	90 MPa
G^c_n	0.287 N/mm
$G^c_s = G^c_t$	1.833 N/mm

The interaction between workpiece and tool was modeled using the algorithm surface–node surface contact available in ABAQUS/Explicit. The contact was defined between the drill surface and the composite plate nodes in the region adjacent to the contact area. In addition, a self-contact condition was used to avoid penetration between eroded composite elements. A constant coefficient of friction equal to 0.3 at the tool/workpiece interface was assumed.

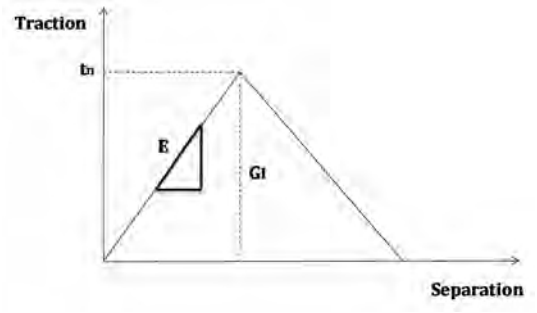

Figure 6.2: Behaviour of cohesive elements (E, elastic modulus; t_n, peak value of nominal stress when deformation is purely normal to interface; GI, instantaneous fracture energy in normal direction).

6.2.2 CHARACTERISTICS OF THE COMPLETE MODEL

This model involved a dynamic analysis including geometric non-linearity and large deformations options. The problem was solved using an explicit integration scheme (ABAQUS/Explicit). A compromise between accuracy and computational cost was achieved when selecting the element size (previously commented) directly involved in time step.

The rotatory movement of the drill

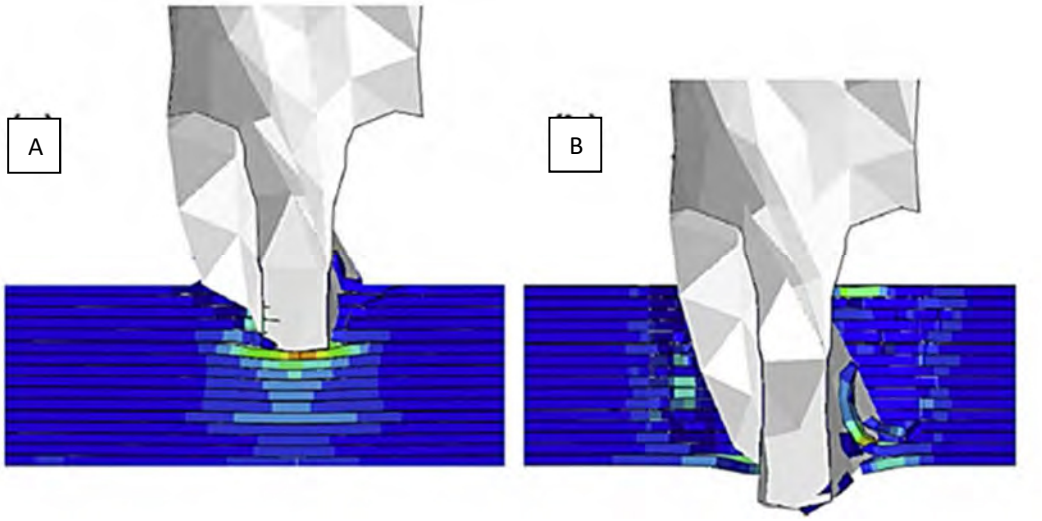

Figure 6.3: Section of the hole during penetration of the drill simulated with complete model: (A) entrance and (B) exit of the drill.

around the Y axis at constant spindle speed and the feed rate in direction Y were imposed. A section of the drilled hole simulated with the complete model is presented in Figure 6.3, showing the entrance and the exit of the drill.

The cutting parameters were stated equal to those provided in Ref. [15] used for validation. The rotary velocity was equal to 2500 rpm and feed rate was equal to 2.5, 5 and 8.3 mm/s.

The calculation time for simulation ranged from 4 days to 3 weeks in a workstation with 16 CPU.

6.2.3 CHARACTERISTICS OF THE SIMPLIFIED MODEL

This model involved a dynamic analysis carried out using also an explicit integration scheme (ABAQUS/Explicit). No rotation was imposed to the drill. A constant thrust force (obtained from the complete model previously validated) was applied at the top of the drill, corresponding to the level of penetration of the drill at the stage simulated.

The elements corresponding to the pre-drilled volume were removed from the model and the drill contacted the workpiece at a depth equal to H (see Figure 6.4). Two stages of the drill penetration across the workpiece were simulated: H equal to 1 mm and 1.625 mm (corresponding respectively to 8 and 13 plies drilled respectively). First stage corresponds to the maximum level of thrust force observed experimentally and also in simulations with the complete model. The second stage was selected because only few plies are not drilled and the origin of delamination is commonly observed close to the drill exit.

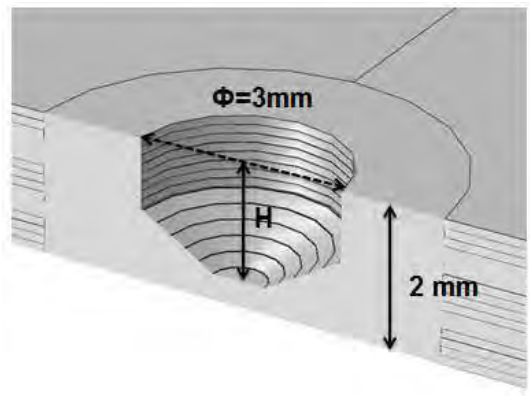

Figure 6.4: Scheme of the pre-drilled hole in the simplified model.

Efficient computation was achieved for simulation in the order of several min of calculation time in a workstation with 16 CPU.

6.3 Model Validation and Results

6.3.1 VALIDATION

The complete model was validated through the comparison with experimental results provided in a recent work [15] dealing with drilling of tape carbon–epoxy LFRP composite.

The model was validated in terms of delamination factor at the entrance of the drill, torque and thrust force. Delamination factor was calculated as the ratio between maximum diameter of delaminated area and the nominal diameter of the drill. Figures 6.5A–C shows reasonable accuracy when predicting these parameters.

6.3.2 COMPARISON BETWEEN SIMPLIFIED AND COMPLETE MODEL

The simplified model needs as an input the value of thrust force (obtained at the drill penetration simulated) and main

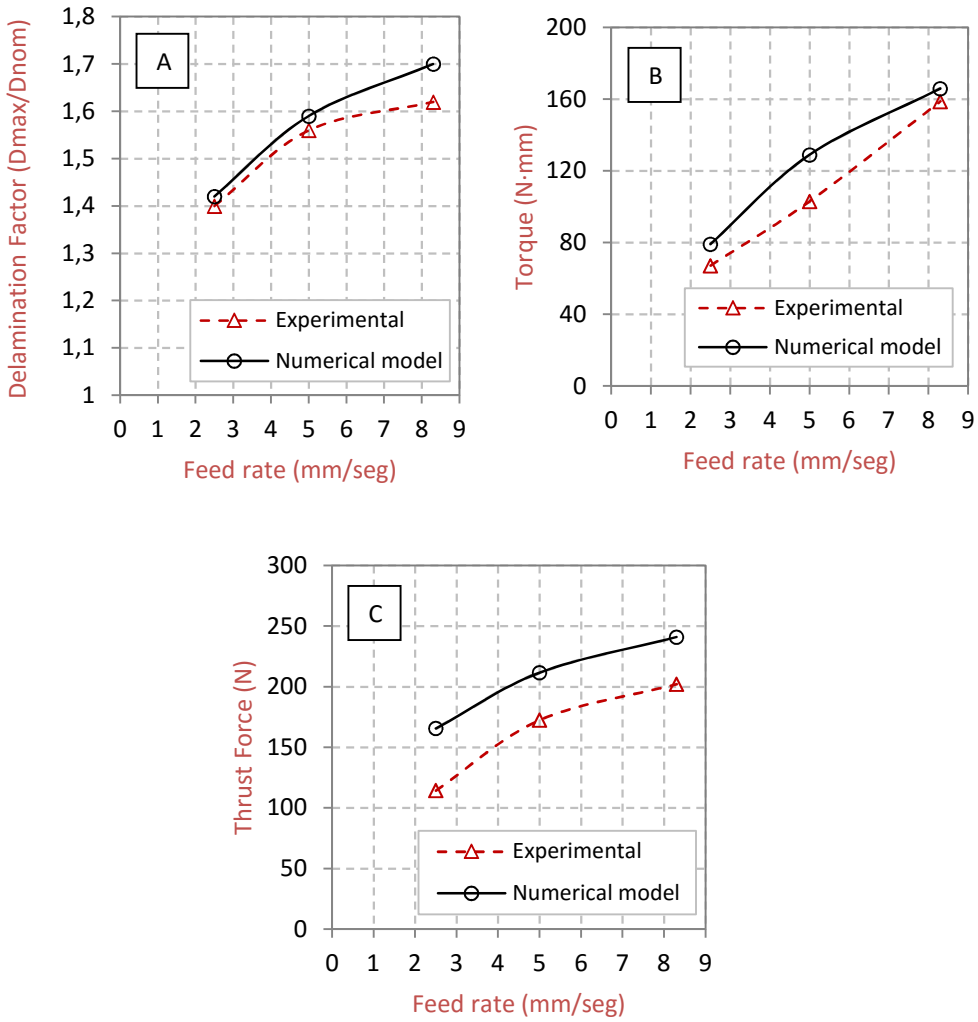

Figure 6.5: Validation of complete model though the comparison with experimental data in [15] (A) delamination factor at the entrance of the drill; (B) predicted and experimental torque; and (C) predicted and experimental thrust force.

output is the prediction of the delaminated area. The complete model also provides delamination but the input data are rotary velocity and feed rate. Figures 6.6A and 6.6B shows delamination factor predicted with both models for both stages of penetration considered (clamping was applied in direction Z at the bottom of the plate, except of a free circular surface with diameter 16 mm).

It is possible to observe the overestimation of delamination factor predicted with the simplified model; in particular it is slightly larger than that obtained with the complete model. It is important to highlight this result: the simplified model is conservative when predicting delamination.

During drill penetration it is also interesting to analyze intra-laminar damage. Matrix and fiber failure result in element erosion as the drill penetrates though the workpiece. The intra-laminar damage was observed beneath the drill tip as it advances though the composite or pushes it, depending on the model considered. The intra-laminar damage is observed in zones with lower diameter than the drill. Thus the damaged zone is eroded as the drill pene-

trates the composite plate. In consequence only the inter-laminar da mage, i.e. delamination is analyzed.

6.3.3 INFLUENCE OF THRUST FORCE

The simplified model was applied to the analysis of the influence of thrust force; results are presented in Figure 6.7. The force was varied from 50 to 500 N showing strong influence of the force on delamination factor in the range 120–250 N being the factor increased from 1.15 to 1.55.

At low values of the thrust force the value of delamination factor is close to 1 in agreement with other authors showing a minimum value for delamination onset: below this threshold no delamination is produced [7].

It is possible to observe a plateau for values of the thrust force higher than 250 N. The maximum value of delamination factor was compared with that obtained in a complete perforation of the plate. Simulation of complete perforation was achieved with a simple modification of the complete model: rotation of the drill was not considered and the drill pierces the plate at constant feed rate (perforation velocity was stated equal to 150 mm/s). The delamination factor obtained in the complete perforation at constant velocity (D around 1.57) was similar to that obtained at elevated thrust forces being an upper limit of delamination during drilling.

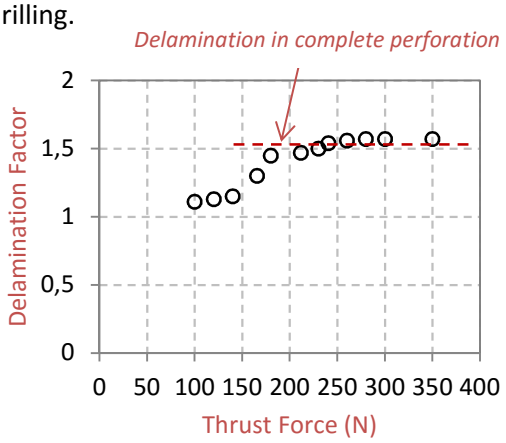

Figure 6.7: Influence of thrust force on delamination factor, maximum values tending to delamination observed in complete perforation of the plate.

This is an interesting result since simulations of drilling has an elevated computational cost, while the simulation of perforation at high velocity is more efficient.

6.3.4 INFLUENCE OF CLAMPING

The influence of clamping diameter was analyzed using the simplified model. The use of clamping is commonly desired in industry when drilling plates of composite in order to diminish delamination. Sometimes the configuration of the components does

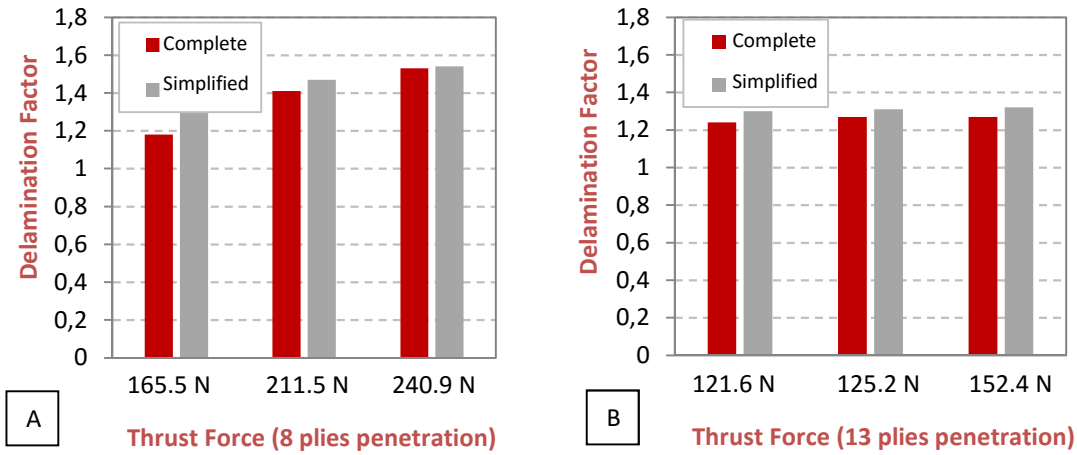

Figure 6.6: Predicted and experimental delamination factor, (A) penetration of the drill trough 8 plies and (B) penetration of the drill trough 13 plies.

not allow drilling with clamping consisting of a posterior metal plate or similar. To study the effect of the clamping the displacement in direction Z was restricted in the base of the workpiece except of a circle of diameter equal to 3 mm (drill diameter), 6 mm and 16 mm (16 mm is the nominal value used for validation and for the analysis described in previous sections). Also the case without clamping was analyzed.

Input forces corresponds with the maximum level of thrust force (small value of penetration H = 1 mm) obtained for each case of feed velocity analyzed (F_1 = 165.5 N, F_2 = 211.5 N and F_3 = 240.9 N respectively).

All cases analyzed (see Figure 6.8) showed variations of delamination factor around 20% when comparing the most restrictive clamping with the highest free area. The effect of clamping can be considered negligible for values of the free area higher than 15 mm and equivalent to free surface.

6.3.5 INFLUENCE OF STACKING SEQUENCE

The laminate studied in the paper is based on the stacking sequence $[0_4/90_4]_s$. It is interesting to test the influence of stacking sequence on delamination; in fact most used laminates are based on a quasi-isotropic configuration. Industrial applications commonly involve multi-axial load states and the superior behavior of quasi-isotropic laminates recommends the use of these stacking sequences. Two different configurations of quasi-isotropic laminates ($[45/-45/0/90]_4$ and $[90/0/45/-45]_4$) were simulated and compared for the different levels of thrust force considered (F_1=165 N, F_2=211N and F_3=241 N respectively). Quasi-isotropic laminates showed better behavior concerning delamination factor. Differences around 20% (see Figure 6.9) are observed when comparing delamination factor in quasi-isotropic laminate and the reference laminate.

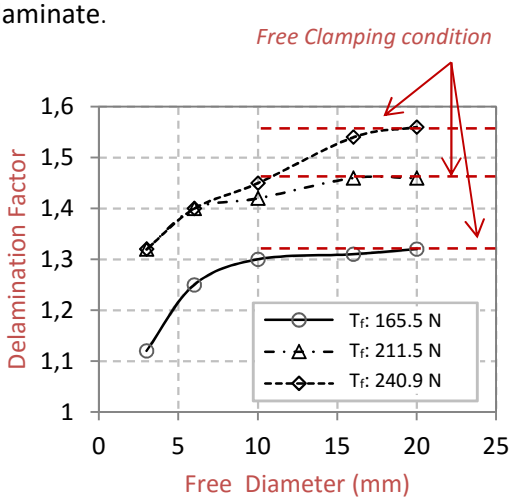

Figure 6.8: Delamination factor vs. diameter of the free surface at the bottom of the plate in the simplified model.

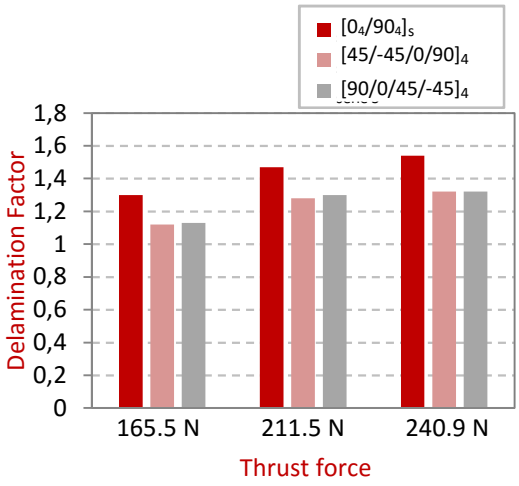

Figure 6.9: Influence of stacking sequence on delamination factor.

6.4 Conclusions

A numerical analysis of CFRP composite drilling is presented in this paper. Modeling was developed using two approaches. Firstly a complete model of drilling, including feed and rotation movements of the drill was developed. Secondly a simplified model, assuming that the drill acts like a punch

was done. Both models were compared in terms of factor of delamination prediction. Simplified model slightly overestimates the value of delamination factor, giving a conservative prediction of damage. This result is especially significant when the complexity and the calculation cost of both models are compared. Simplified simulations can be solved in several minutes while the complete model needs several days; this methodology could be considered when designing drilling processes with different drill geometries and cutting parameters. The implementation of numerical models in industry in order to help designing process requires simple and fast simulation tools.

Simplified model was used to study the influence of several factors involved in the drilling process. First of all, the influence of thrust force has been analyzed. It is well known the increasing trend in delamination factor as the force is increased. In this paper it is found a plateau limiting this increment of delamination factor at high enough thrust forces. The maximum level of delamination is coincident with that induced by complete piercing perforating the composite plate with a punch with similar geometry as the drill. Although perforation is not commonly used in hole manufacturing in composites, the delamination factor in this process can be used as an upper limit for the conventional drilling, giving valuable information for the designer.

The influence of clamping has been studied founding significant increment in delamination factor when the diameter of the free surface ranged from the value equal to the drill diameter to higher values up to five times the drill diameter. For higher values negligible influence of the clamping is observed.

Finally the simplified model was used to simulate other stacking sequences corresponding to laminates $[45/-45/0/90]_4$ and $[90/0/45/-45]_4$. The quasi-isotropic laminates presented similar delamination factor, in both cases lower than that exhibited by the laminate $[0_4/90_4]_s$.

6.5 Acknowledgement

The authors acknowledge the financial support for the work to the Ministry of Economy and Competitiveness of Spain under the Project DPI2011-25999.

6.6 References

[1] Pecata O, Rentscha R, Brinksmeier E. Influence of milling process parameters on the surface integrity of CFRP. Proc CIRP 2012; 1:466–70.

[2] Santiuste C, Barbero E, Miguélez MH. Computational analysis of temperature effect in composite bolted joints for aeronautical applications. J Reinf Plast Compos 2011; 30(1):3–11.

[3] Davim JP, Reis P, Conceição C. Drilling fiber reinforced plastics (FRP) manufactured by hand-layup influence of matrix (VIAPAL VUP 9731 and ATLAC 382-05). J Mater Process Technol 2004; 155–156:1828–33.

[4] Abrao AM, Campus Rubio J, Faria PE, Davim JP. The effect of cutting tool geometry on thrust force and delamination when drilling glass fiber reinforced plastic composite. Mater Des 2008; 29(2):508–13.

[5] Davim P, Campos Rubio J, Abrao AM. A novel approach based on digital analysis to evaluate the delamination factor after drilling composite laminates. Compos Sci Technol 2007; 67(9):1939–45.

[6] Rubio JC, Abrao A, Faria P, Esteves Correia A, Davim JP. Effects of high speed in the drilling of glass fiber reinforced plastic: evolution of the delamination factor. Int J Mach Tools Manuf 2008; 48:715–20.

[7] DeFu L, Yong Jun T, Cong WL. A review of mechanical drilling for composite laminates. Compos Struct 2012; 94:1265–79.

[8] Ramesh MV, Seetharamu KN, Ganesan N. Analysis of machining of FRPs using FEM. Int J Mach Tools Manuf 1998; 38:1531–49.

[9] Mahdi M, Zhang L. A finite element model for the orthogonal cutting of fiber reinforced composite materials. J Mater Process Technol 2001; 113:373–7.

[10] Iliescu D, Gehin D, Iordanoff I, et al. A discrete element method for the simulation of CFRP cutting. Compos Sci Technol 2010; 70:73–80.

[11] Santiuste C, Soldani X, Miguélez H. Machining FEM model of long fiber composites for aeronautical components. Compos Struct 2010; 92:691–8.

[12] Soldani X, Santiuste C, Muñoz-Sánchez A, Miguélez H. Influence of tool geometry and numerical parameters when modelling orthogonal cutting of LFRP composites. Compos A Appl Sci Manuf 2011; 42:1205–16.

[13] Santiuste C, Miguélez H, Soldani X. Out-of-plane failure mechanisms in LFRP composite cutting. Compos Struct 2011; 93:2706–13.

[14] Santiuste C, Olmedo A, Soldani X, Miguélez H. Delamination prediction in orthogonal machining of carbon long fiber-reinforced polymer composites. J Reinf Plast Compos 2012; 31(13):875–85.

[15] Phadnis VA, Makhdum F, Roy A, Silberschmidt VV. Drilling in carbon/epoxy composites: experimental investigations and finite element implementation. Compos A 2013; 47:41–51.

[16] Isbilir O, Ghassemieh E. Numerical investigation of the effects of drill geometry on drilling induced delamination of carbon fiber reinforced composites. Compos Struct 2013; 105:126–33.

[17] Durão LMP, Gonçalves DJS, Tavares JMRS, Albuquerque VH, Aguiar Vieira A, Torres Marques A. Drilling tool geometry evaluation for reinforced composite laminates. Compos Struct 2010; 92:1545–50.

[18] Durão LMP, de Moura MFSF, Marques AT. Numerical prediction of delamination onset in carbon/epoxy composites drilling. Eng Fract Mech 2008; 75:2767–78.

[19] Durão LMP, de Moura MFSF, Marques AT. Numerical simulation of the drilling process on carbon/epoxy composite laminates. Compos A 2006; 37:1325–33.

[20] Singh N, Bhatnagar N, Viswanath P. Drilling of uni-directional glass fiber reinforced plastics: experimental and finite element study. Mater Des 2008; 29:546–53.

[21] Chinmaya M, Dandekar R, Shin YC. Modeling of machining of composite materials: a review. Int J Mach Tools Manuf 2012; 57:102–21.

[22] Hibbit, Karlson, Sorensen Inc. ABAQUS user's manual 6.4-1; 2003.

[23] Hou JP, Petrinic N, Ruiz C, Hallett SR. Prediction of impact damage in composite plates. Compos Sci Technol 2000; 60(2):273–81.

[24] Santiuste C, Sánchez-Sáez S, Barbero E. A comparison of progressive-failure criteria in the prediction of the dynamic bending failure of composite laminated beams. Compos Struct 2010; 92(10):2406–14.

[25] López-Puente J, Zaera R, Navarro C. Experimental and numerical analysis of normal and oblique ballistic impacts on thin carbon/epoxy woven laminates. Compos A Appl Sci Manuf 2008; 39(2):374–87.

[26] Fish JC, Lee SW. Delamination of tapered composite structures. Eng Fract Mech 1989; 34(1):43–54.

[27] Benzeggagh ML, Kenane M. Measurement of mixed-mode delamination fracture toughness of unidirectional glass/epoxy composites with mixed mode bending apparatus. Compos Sci Technol 1996; 56:439–49.

[28] Camanho PP, Davila CG. Mixed-mode decohesion finite elements for the simulation of delamination in composite materials. NASA/TM-2002-211737; 2002. p. 1–37.

[29] Olmedo A, Santiuste C. On the prediction of bolted single-lap composite joints. Compos Struct 2012; 94:2110–7.

[30] Varas D, Artero-Guerrero JA, Pernas-Sánchez J, López-Puente J. Analysis of high velocity impacts of steel cylinders on thin

carbon/epoxy woven laminates. Compos Struct 2013; 95:623–9.

Capítulo 7

Numerical Analysis of Tool Wear Effect and Special Geometry When Drilling Woven CFRPs

La simulación del proceso de taladrado es un método eficaz que puede ser utilizado para optimizar la geometría de la broca y los parámetros de corte del proceso con el fin de mejorar la calidad del agujero y controlar la evolución del desgaste de la herramienta. En este capítulo se presenta un modelo en tres dimensiones (3D) de taladrado de tejido CFRP que reproduce herramientas nuevas y desgastadas. Dos ángulos de punta diferentes se han estudiado para el caso de herramienta nueva. El modelo considera el modo de fallo progresivo intra-laminar basado en el modelo de Chang y Chang, e inter-laminar (delaminación) mediante la utilización de elementos cohesivos. También ha demostrado su capacidad para predecir la fuerza de avance y la delaminación para un rango diferente de parámetros de corte. Las predicciones del modelo muestran la influencia de la geometría de la herramienta (incluyendo la influencia debida al desgaste) en la delaminación y otros defectos en la pieza de trabajo.

Este estudio se encuentra publicado bajo la siguiente referencia: **N. Feito**, J. Diaz-Álvarez, J. López-Puente, H. Miguelez. “Numerical analysis of the influence of tool wear and special cutting geometry when drilling woven CFRPs”, Composite Structures, (2016) Vol. 138, p. 285-294.

Numerical Analysis of Tool Wear Effect and Special Geometry When Drilling Woven CFRPs

Abstract

Drilling CFRP materials is a common process in the aerospace industry carried out prior to components assembly. Machining induced damage leads to elevated percentage of component rejection. Damage extension strongly depends on drilling geometry and cutting parameters. Drilling geometry changes with cutting time due to the wear progression and the risk for hole quality is enhanced. The influence of wear on hole quality has been analyzed mainly using an experimental approach. Simulation of drilling process is an effective method that can be used to optimize drill geometry and process parameters in order to improve hole quality and control the drill wear evolution. In this paper a three-dimensional (3D) model for drilling woven CFRP reproducing fresh and worn tools is presented. Two different point angles considering fresh and honed edge were modeled. A progressive intra-laminar failure model based on the Chang and Chang model is considered. Cohesive elements allowed the analysis of inter-laminar damage (delamination). The model demonstrated its ability to predict force, torque and delamination for different levels of feed rate and cutting speed. Model predictions show the influence of tool geometry (including variations induced due to wear) on delamination and other workpiece defects.

Keywords: Tool wear, CFRP, Modeling, Drilling.

7.1 Introduction

Carbon fiber reinforced polymer composites (CFRPs) are increasingly used in industry, not only in aircraft structures but also in other sectors. The excellent mechanical properties and low weight of CFRPs together with fatigue and corrosion resistance make them a suitable option for high responsibility applications [1].

Woven CFRPs present enhanced strength to weight ratio, fracture toughness and corrosion resistance when compared to tape composite. The improved mechanical properties contrast with the poor machinability of woven composites due to the architecture of the abrasive fibers.

Drilling operations do not allow direct observation since they are difficult to study in process. On the other hand, the efficiency of the process involves important economic consequences for companies since increasing exigent cutting conditions are required to optimize productivity [2].

Drilling is one of the most common operations in the composite component, required for further mechanical joining, for example in the airframe of commercial airplanes [3]. CFRPs are susceptible to suffer drilling induced damage causing a significant percentage of workpiece rejection. The enhancement of drilling process ensuring hole quality is still a challenge [4].

The influence of the cutting parameters [5, 6], the point angle [7-9] and the drill

diameter [10] for high speed steel and uncoated cemented carbide drills in drilling CFRPs have been analyzed in the literature.

Feed rate seems to be the most influencing factor in delamination (increasing with this parameter) while cutting speed shows lower influence. Moreover the effect of cutting speed is not clear and seems to have a cross effect with thickness and spindle speed. Davim *et al*. [5] showed that delamination increased with cutting speed during conventional drilling. However Gaitonde *et al*. [6] showed an opposite effect when drilling at high spindle speed in thin woven-ply CFRP composite laminates.

The effect of drill geometry was demonstrated in Karnik *et al*. [7] and Feito *et al*. [8]. It was observed that increasing the point angle of twist drill bit during conventional and high speed drilling of woven-ply CFRP composite laminates, delamination was increased. However Heisel *et al*. [9] reported that the delamination at the entry was decreased with the point angle. The increment of drill diameter also showed a large contribution on delamination as it was proved by Tsao *et al*. [10].

Geometrical modifications due to wear progression also influence resultant surface quality and delamination damage. Main wear mechanism in conventional drilling was identified to be abrasion (see for instance Mayuet *et al*. [11]) mainly due to the abrasive character of the fibers. Although abrasion is dominant, also adhesion was identified during the study. In this case exit delamination always increased with wear progression.

For high speed drilling, chipping was observed at the first stages of drilling process (Rawat *et al*. [12]), following by abrasion and adhesion as cutting time progresses. This study also proved that abrasive wear on the flank face of the primary cutting edge was stronger than the wear at the rake face.

Tool wear also affects the cutting forces. It has been reported in [13] that high feed rate increases the tool wear and consequently the thrust force. This fact is independent of the tool coating. Torque has demonstrated less sensibility to wear evolution than thrust force [13].The authors have also studied the influence of worn tools in cutting forces and delamination in [8]. Similar conclusions were derived: experimental results showed that crossed effect of feed rate and worn tool increases appreciably the thrust force. Concerning delamination, while entry damage diminished with wear progression, exit damage was enhanced.

The change of the geometry due to abrasion leading to cutting edge rounding (CER) was studied for different geometries by Faraz *et al*. [14]. Positive correlation was found between both delamination and cutting forces and the cutting edge roundness.

Despite the interest of experimental approaches, finite element analysis is a powerful tool that can be used to support testing, avoiding technical problems and elevated cost. With this method, it is possible to control all the variables that take part during the machining process and uncouple the influencing parameters. A recent review gives an overview of machining models of different types of composites [15].

Even if there is a strong interest in developing numerical models for the study of composite drilling, there are few works in the literature focusing on this topic. Most papers presenting numerical modeling of composite cutting focus on orthogonal due to its simplicity. Some examples of the

modelling strategies and material modeling used in scientific literature for a 2D approach to simulation of orthogonal cutting of composites can be found in [16-19]. 2D approaches only allow the simulation of unidirectional composite; moreover delamination cannot be study. To solve the problem of delamination in orthogonal cutting 3D modelling was developed to allow reproducing different stacking sequences [20, 21]. This model also was used to evaluate the validity of the assumptions involved in the formulation of 2D approaches. Focusing on current drilling operations, 3D modeling is required. Different approaches can be found in the literature. First models developed were based on a simplified quasi-static three-dimensional (3D) simulation of drilling, which considers the drill as a punch. Some examples of this approach were used by Durao *et al*. in [22, 23] for CFRPs materials and Singh *et al*. [24] in order to study drilling of glass fiber reinforced polymer composites (GFRPs). Main objective was obtaining a relation between delamination and the applied thrust force that seems to be one of the governing factors in the generation of out-of-plane failure during drilling as reported also in Upadhyay *et al*. [23]. These models were also used to study the influence of the drill point angle on delamination damage [22]. It was observed that 90° drill point angle gives better results than those obtained with 104° and 118°.

Further improvements of drilling simulation have led to the development of 3D complex drilling models for CFRPs. Drilling was successfully reproduced including drill penetration in the workpiece, material failure and elements erosion [26, 27]. Modelling of drilling processes involves elevated difficulty because of the need to simulate drill rotation and feed using both damage and erosion criteria involving high computational cost. The authors presented a recent work focusing on the comparison of simplified and complex models of composite drilling [28]. It was proved that simplified model can save computational time due to its simplicity while overestimates the prediction of damage.

This work presents a new 3D FEM analysis accounting for the effect of worn geometry when drilling woven materials. Also the effect of drill point angle and cutting parameters with new and worn tool was analyzed. The model has been validated in comparison with experimental work in terms of thrust force and delamination extension, showing good accuracy.

7.2 Experimental Work

7.2.1 WORKPIECE MATERIAL

The specimens were made using plain woven prepreg with AS4 fibre and 8552 epoxy matrix, denominated commercially AGP193-PW by its manufacturer Hexcel Composites.

Table 7.1: Mechanical properties of carbon-epoxy woven laminate [29].

Property	Value
ρ	1570 Kg/m^3
$E_1 = E_2$	68 Gpa
E_3	10 Gpa
υ_{12}	0.22
$X_t = Y_t$	880 Mpa
$X_c = Y_c$	880 Mpa
S_t	96 Mpa
$\varepsilon_1 = \varepsilon_2$	0.025
ε_3	0.05

This composite laminate, commonly used in aerospace industry, was cut in pieces of 120 mm × 29 mm in order to introduce

them in a confining device specially designed to avoid dispersion of the fiber chip (see previous work of the authors [8] with detailed description of confining device). The laminate was composed of 10 plies with bidirectional orientation of the fibers, with thickness equal to 2.2 mm. The characteristics and mechanical properties of this material are presented in Table 7.1 where ρ is density; E_i is the elastic modulus in the direction i, ν_{ij} is the Poisson coefficient, G_{ij} is the elastic modulus in shear directions, X_t, Y_t and S_t are the maximum tensile stress in longitudinal and shear directions respectively, X_c and Y_c are the maximum compressive stress in longitudinal directions and finally ε is the critical strain

7.2.2 TOOLS

Three different drill bits were selected. The first one was a conventional twist drill with different point angles (90° and 118°). Fresh drill corresponds to the geometry given by the tool manufacturer (Figures 7.1 case A). The second drill bit was a worn tool with honed edge wear with length equal to 0.05 mm. Honed edge is a consequence of wear mechanisms observed when drilling CFRP, as it was stated in a previous work of the authors [8]). In order to have a complete control of the worn geometry, it was artificially generated with a controlled grinding process by the manufacturer GUHRING [30] (Figures 7.1 case B). Finally the third case was a step twist drill with an initial diameter equal 4 mm, was also included on the study. The step had a length equal to 6.6 mm (Figures 7.1 case C). In all cases the nominal diameter was 6 mm.

7.2.3 MACHINING TESTS

Both thrust force and torque were measured during dry drilling tests using a rotating dynamometer (Kistler 9123C). A machining center (B500 KONDIA) was equipped with a confining system with a supporting back plate previously drilled with hole diameter equal to 10 mm (see Figure 7.2). The aim was avoiding chips spreading combining the confining box with a vacuum to remove them. Cutting parameters are summarized in Table 7.2.

The delamination factor (F_d), defined as the ratio between the maximum diameter of delaminated area and the nominal hole diameter, was calculated through the measurement of diameters from images taken with a stereo microscope (Optika SZR).

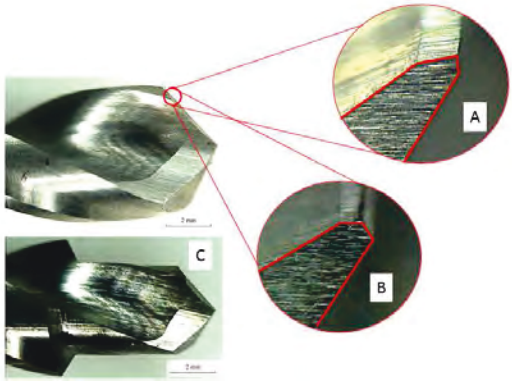

Figure 7.1: Drill bit geometries for fresh drill (A), honed edge drill (B) and step drill (C).

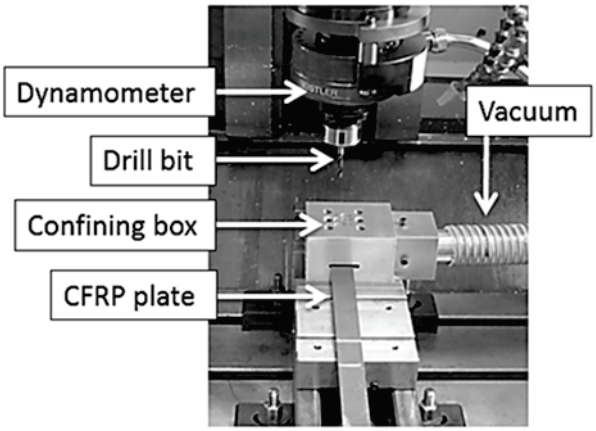

Figure 7.2: Set-up device for drilling tests showing confining box.

Table 7.2: Cutting parameters used in drilling tests: feed rate (*f*) and cutting speed (*V*).

Parameter	Range		
***f* [mm/rev]**	0.05	0.1	0.15
***V* [m/min]**	25	50	100

7.3 Numerical modelling

The model presented in this work, is able to reproduce drilling of woven composite including chip removal. The FEM code ABAQUS/Explicit, which was specially developed for dynamic non-linear problems, [31] was used to perform the numerical simulations. The complete movement of the drill including spindle speed and feed rate was simulated. Previous work of the authors [28] presented main advantages and drawbacks of this complex model when compared with simplified models assuming drilling as a punching process. Since the aim of this paper is simulating the effect of tool geometry changes induced by wear, the development of complete model including both rotary and feed movement and chip removal is required.

The scheme of the model developed is presented in the Figure 7.3. The displacement of the workpiece in Z direction was restricted at the base except at the zone inside a circumference with 10 mm diameter where it is free. This boundary condition reproduces the effect of the back plate used in the experiments.

7.3.1 DRILL AND WORKPIECE BEHAVIOR

The drill was assumed to be rigid with diameter equal to 6 mm. The woven laminate was modeled as an orthotropic elastic material until failure. This approach has been successfully implemented by López-Puente *et al* [32] to simulate dynamic loading (impact) in the same material. Both intra-laminar and inter-laminar damage mechanisms were defined. The first one was implemented by means of a user subroutine (VUMAT). The second one was achieved using cohesive elements. This implementation of different failure mechanisms has been used in previous work of the

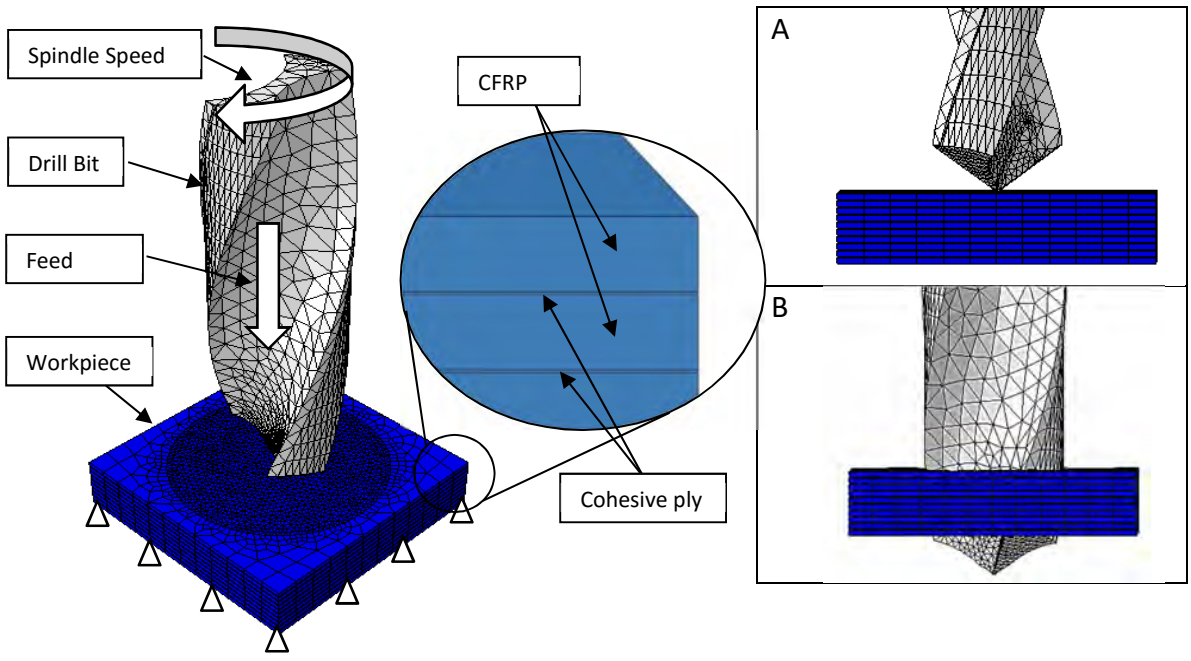

Figure 7.3: Scheme of the complete model. Drill entrance simulation; (A) Initial and (B) final location.

authors [29] in impact processes and drilling [28].

The fiber and matrix damages were defined in the equations 7.1-7.4 where the damage variables d_{ij} (stress dependent) range from 0 (undamaged) to 1 (fully broken). When the failure criterion is reached the stress components involved in the failure definition (fiber or matrix failure) are set to zero. To control the element erosion, strain tensor is calculated after each time increment. When one of the components reaches a critical value, the element is removed.

In woven laminates, fibers are located in orthogonal in-plane directions (1 and 2). Equations 7.1, 7.2) describe the fibre failure (d_{ij} equal to 1) in both directions:

$$d_{f1} = \begin{cases} \sigma_{11}/X_t \;\; if \;\; \sigma_{11} > 0 \\ |\sigma_{11}|/X_c \;\; if \;\; \sigma_{11} < 0 \end{cases} \quad (7.1)$$

$$d_{f2} = \begin{cases} \sigma_{22}/Y_t \;\; if \;\; \sigma_{22} > 0 \\ |\sigma_{22}|/Y_c \; if \;\; \sigma_{22} < 0 \end{cases} \quad (7.2)$$

Where σ_{11} and σ_{22} are the stresses in the warp and fill direction respectively, X_t and X_c are the strengths of the composite laminate in tension and compression for the warp direction, and Y_t and Y_c are the strengths in tension and compression for the fill direction.

On the other hand two different parameters are proposed corresponding to crushing matrix failure mode (d_{ij} equal to 1), the first one in the ply plane Equation 7.3 and the other one in the through-thickness direction equation 7.4.

$$d_{m12} = |\sigma_{12}/S_{12}| \quad (7.3)$$

$$d_{m3} = \frac{1}{4}\left(\frac{\sigma_{33}}{Z_c}\right)^2 + \frac{Z_c \times \sigma_{33}}{4 S_{13} S_{23}} + \left|\frac{\sigma_{33}}{Z_c}\right| + \max\left[\left(\frac{\sigma_{13}}{S_{13}}\right)^2, \left(\frac{\sigma_{23}}{S_{23}}\right)^2\right] \quad (7.4)$$

Where σ_{ij} are the components of the stress tensor, S_{12}, S_{13} and S_{23} are the shear strengths in the three different planes and Z_c is the strength in the through-thickness direction under compression. The equation 7.4 is applied only when $\sigma_{33} < 0$.

The cohesive elements used to estimate delamination are based on a traction-separation law. The linear elastic behavior is required by means of the respective stiffness (K_{nn}, K_{ss} and K_{tt}). In this work, a quadratic nominal stress criterion for the damage initiation, similar to equation 7.5, was selected where t_n, t_s and t_t are the strengths of the cohesive interface in the normal and in shear directions respectively. Equation 7.5 is applied if one of conditions on equation 7.6 is reached, where Z_t is the laminate strength under tension in the through thickness direction.

$$\left(\frac{\sigma_{33}}{t_n}\right)^2 + \left(\frac{\sigma_{13}}{t_s}\right)^2 + \left(\frac{\sigma_{23}}{t_t}\right)^2 \geq 1 \quad (7.5)$$

$$\sigma_{33} \geq Z_t \;\; or \;\; \sqrt{\sigma_{12}^2 + \sigma_{13}^2} \geq S_{23} \quad (7.6)$$

The damage evolution follows a potential law type based on energies, see Equation 7.7 where the parameter $\alpha = 1$; G_n, G_s and G_t are the released rate energy in the three aforementioned directions; and G^C_n; G^C_s and G^C_t are the critical values of the released rate energy. The values of these properties are shown in Table 7.3 [29].

$$\left(\frac{G_n}{G_n^C}\right)^{\alpha}+\left(\frac{G_s}{G_s^C}\right)^{\alpha}+\left(\frac{G_t}{G_t^C}\right)^{\alpha}\geq 1 \qquad (7.7)$$

Table 7.3: Parameters for the cohesive interface. [29]

K_{nn}	$K_{ss}=K_{tt}$	t_n	$t_s=t_t$	G_n	$G_s=G_t$
2	1.5 G	11	45	0.6	1.8
GPa/mm	Pa/mm	MPa	MPa	J/m^2	J/m^2

7.3.2 DRILL GEOMETRY AND WORK-PIECE MESHING

Each ply was modelled at the zone around the diameter of the drill using solid elements C3D6R (wedge elements) with six nodes in order to minimize the dependence of the results with mesh orientation in the laminate plane. Just one element is located along the ply thickness. Minimum element size was 0.2 mm around the penetration zone. Far from to the drill entrance zone hexagonal elements C3D8R with 8 nodes and reduced integration were used, with minimum element size around 1 mm. Delamination is modeled by means of cohesive elements. Small thickness was assigned to the interface (5 microns) in order to improve numerical behavior when high deformations occur during calculation. Meshing strategy in the interface plane 1-2 was the same as that used in the ply, with one element along the thickness (direction 3).

The geometry of the base model (corresponding to fresh tool, see Figure 7.4A) was modified simulating the honed edge (see Figure 7.4B). In addition, stepped drill geometry was simulated (Figure 7.4C). Geometrical changes strongly affect thrust force and delamination, as it is demonstrated in next section.

7.4 Results

7.4.1 MODEL VALIDATION

Model validation was carried out comparing experimental and numerical results, in terms of thrust force and maximum delamination. Maximum thrust force (being the peak value of the thrust force evolution with cutting time) was obtained from the experimental record and the numerical simulations. Figure 7.5 shows the trust force evolution with cutting time, showing good agreement between measured and predicted curves, both in terms of magnitude and shape. For these cases the cutting speed was equal to 100 m/min and the feed rate was equal to 0.010 mm/rev.

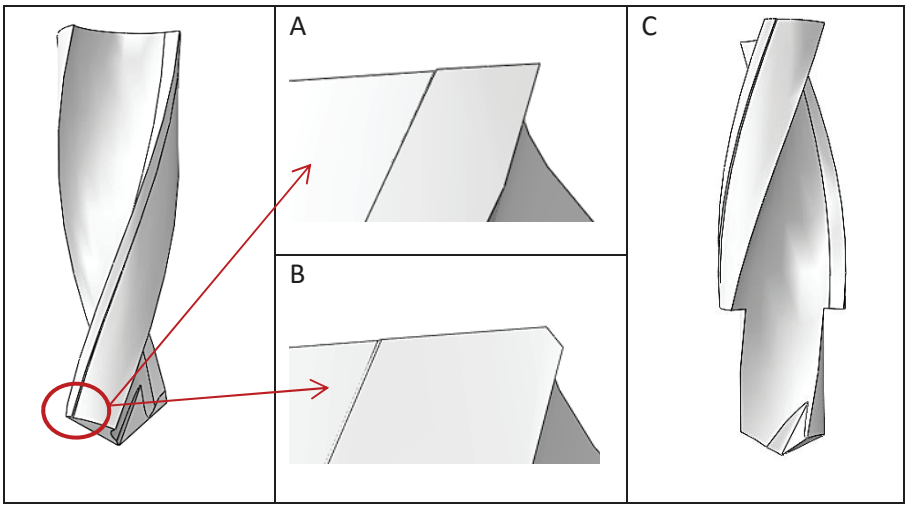

Figure 7.4: Model of the geometries: Helicoidal new (A), helicoidal honed (B) and step (C).

Figure 7.6 shows predicted and measured exit delamination in the case of point angle equal 90°, cutting speed equal 100 m/min and feed rate equal 0.10 mm/rev. The measurement of the maximum diameter of delaminated area allows the calculation of delamination factor defined as $F_d = D_{damaged} / D_{nominal}$.

Figure 7.7 summarizes the numerical and experimental results (in terms of maximum thrust forces and exit delamination factor) for different geometries of the drill bit.

For the case of fresh drill (Figure 7.7A), the maximum deviation in maximum thrust force and delamination factor were 7.7% and 2.6% respectively.

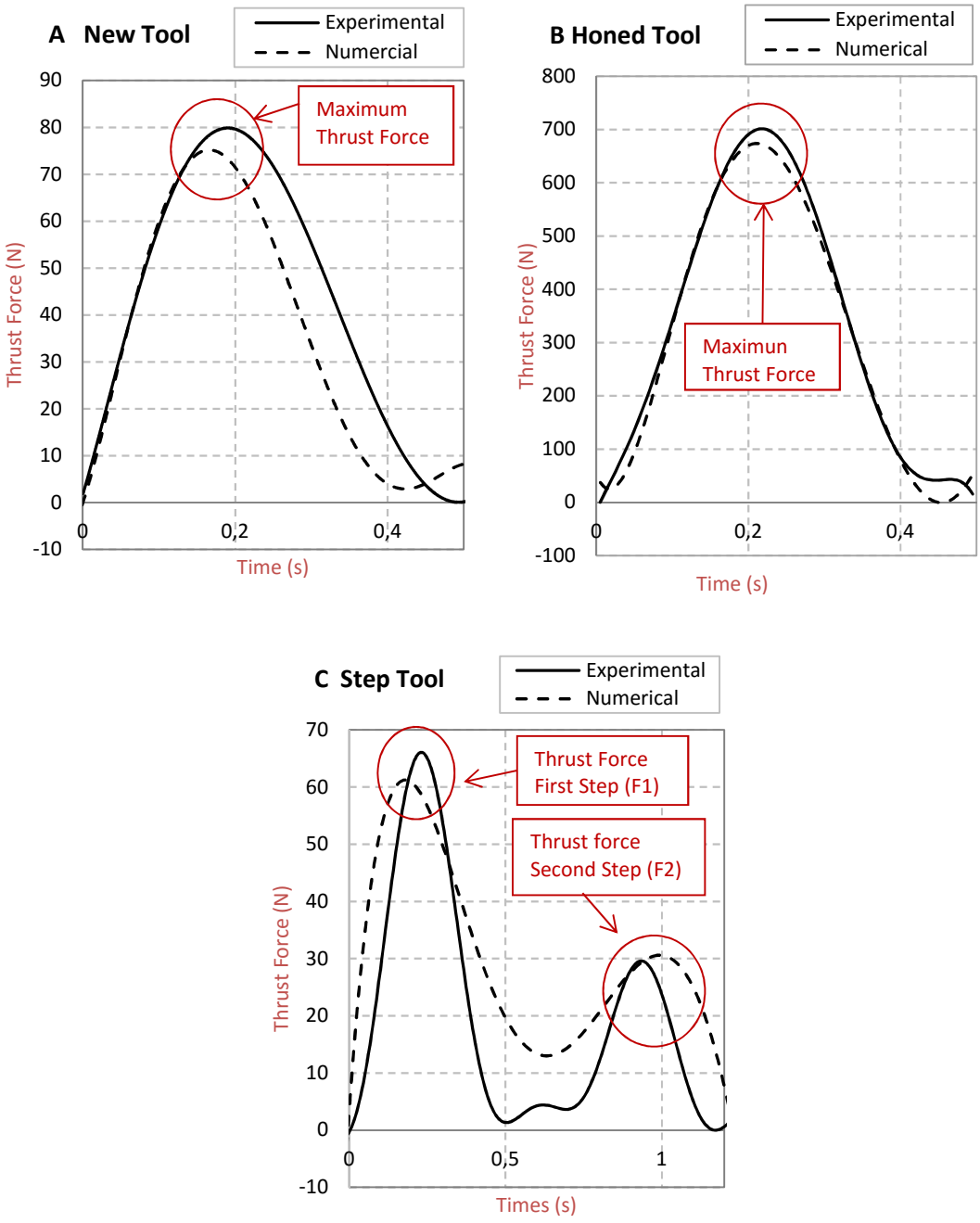

Figure 7.5: Numerical and experimental thrust force evolution (A, B, C, different geometries considered in this study).

The model was modified to simulate worn geometry (Figure 7.7B). In this case the drill point angle was 118° and the cutting speed was equal to 100 m/min. The difference between experimental and estimated values of thrust force was lower than 17%. Delamination factor presented maximum error around 3%.

Finally, the model was applied to the simulation of special stepped drill bit geometry. Figure 7.7C presents the results for this case. It can be observed very good predicted results in both thrust force and delamination factor with errors around 11.3% and 3.5% respectively.

In all cases analyzed, the model overestimates the delamination. This fact could be related to the characterization of the interface properties and the properties given to the cohesive elements (Equations. 7.5-7.7, Table 7.3). These properties are obtained from other study [29] which focuses on dynamic impact on the same woven CFRP. The properties required for cohesive elements do not account for strain rate dependence, but actually the response of the interface between plies could be influenced by the rate of the deformation.

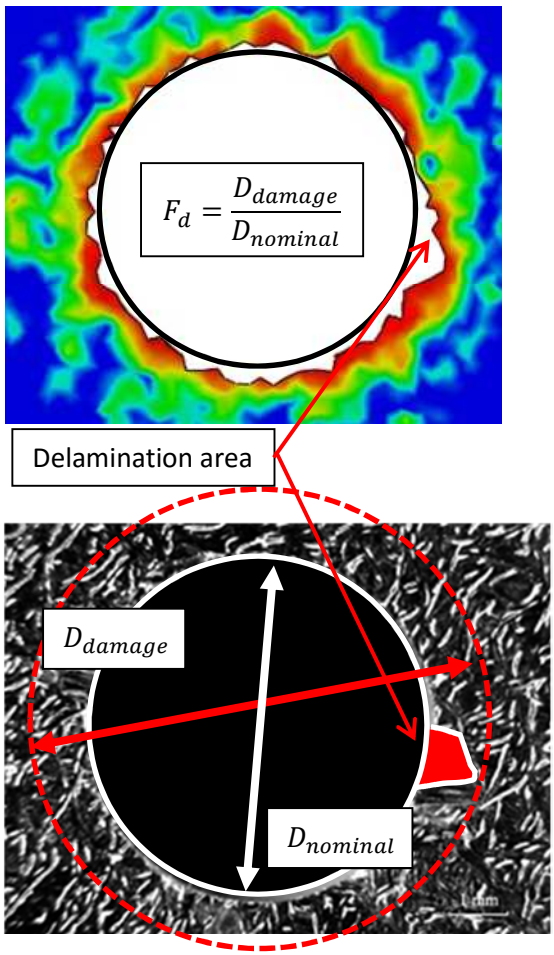

Figure 7.6: measured and predicted delamination (point angle: 90°; cutting speed: 100 m/min; feed rate: 0.10 mm/rev).

7.4.2 PARAMETRIC ANALYSIS

Once the model was validated in different conditions, a parametric analysis was carried out in order to study the influence of other cutting parameters in the predicted thrust force and delamination factor.

Figures 7.8 and 7.9 show the surface prediction for thrust force and delamination damage in the case of point angle equal 90° and 118° for new tool.

The feed is the most influencing factor in both thrust force and delamination. Although cutting speed has slight influence, the best combination in order to minimize damage is high cutting speed and low feed rate, since both force and delamination factor are decreased. These trends are in agreement with the experimental data found in the literature [6,8]. The use of the numerical model to obtain similar conclusions is interesting because of the possibility to apply the simulation to other materials, configurations and tools, avoiding expensive experimental work.

The numerical results obtained from the simulations allowed the adjustment of a mechanistic expression relating both thrust force and delamination factor to feed rate and cutting speed (see Table 7.4). With these equations, it is possible to determine

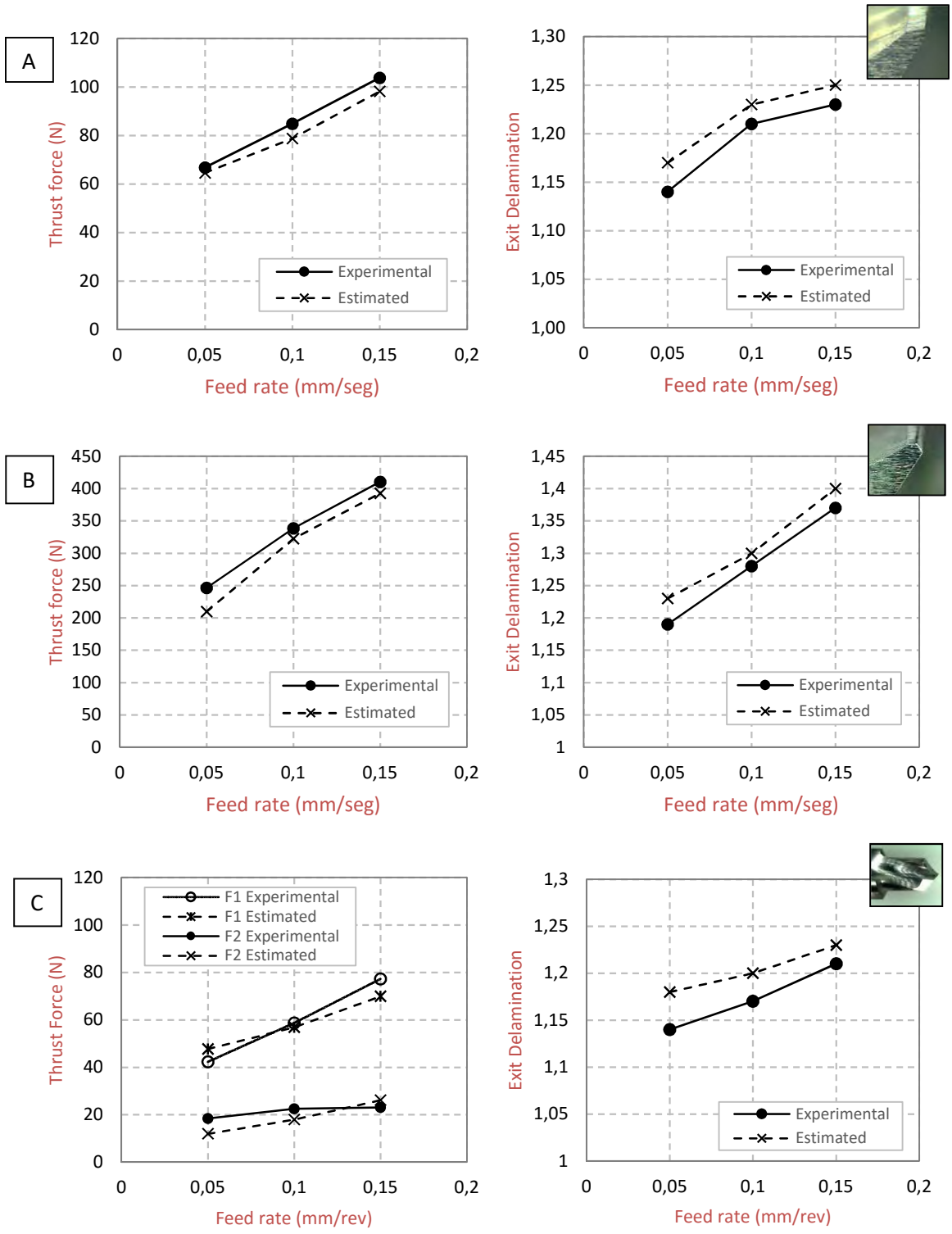

Figure 7.7: Model validation for new drill bit with point angle equal 90° and cutting speed equal 25 m/min (A), for honned drill bit with point angle equal 118° and cutting speed equal 100 m/min (B) and for stepped geometry with cutting speed equal to 100 m/min (C).

a diagram of evolution with both variables and estimate the values for a couple of cutting parameters (Figure 7.10).

The simulations for the case of worn drill bit have been carried for the point angle equal to 118°. The model has been used to predict force and damage in the material

changing the cutting speed. Numerical results are showed in Figure 7.11. The influence of feed rate is lower than the observed with fresh tool, also the influence of cutting speed is almost negligible. The effect of worn geometry is dominant and thus the selection of proper parameters for damage minimization is difficult with worn tool. It is worth noting the elevated value of delamination factor even for low values of feed rate.

It can be observed how the predicted values for thrust force and delamination for the case of honed edge drill bit are higher than the estimated for new drill bit. This is in concordance with the experimental re-

Table 7.4: Prediction equations (thrust force and delamination) for worn tool at different cutting speeds.

Point angle	Prediction equation	R^2
90	$T_f(N) = -16.2629 + 1.8649 \cdot V + 962.9183 \cdot f - 14.9973 \cdot V \cdot f - 0.0143 \cdot V^2 - 948.675 \cdot f^2 + 0.1011 \cdot V^2 \cdot f$	0.94
	$D_f = 1.1837 + 0.0001 \cdot V - 0.195 \cdot f - 0.0166 \cdot V \cdot f - 0.00001 \cdot V^2 + 10.5 \cdot f^2 + 0.0003 \cdot V^2 \cdot f - 0.128 \cdot V \cdot f^2$	0.93
118	$T_f(N) = 71.92 - 0.9585 \cdot V - 271.63 \cdot f + 14.6184 \cdot V \cdot f + 0.0056 \cdot V^2 + 2592 \cdot f^2 - 0.0653 \cdot V^2 \cdot f - 37.736 \cdot V \cdot f^2$	0.96
	$D_f = 1.0981 - 0.001 \cdot V - 0.2075 \cdot f + 0.0146 \cdot V \cdot f + 8E\text{-}6 \cdot V^2 + 2.25 \cdot f^2 - 0.0001 \cdot V^2 \cdot f$	0.92

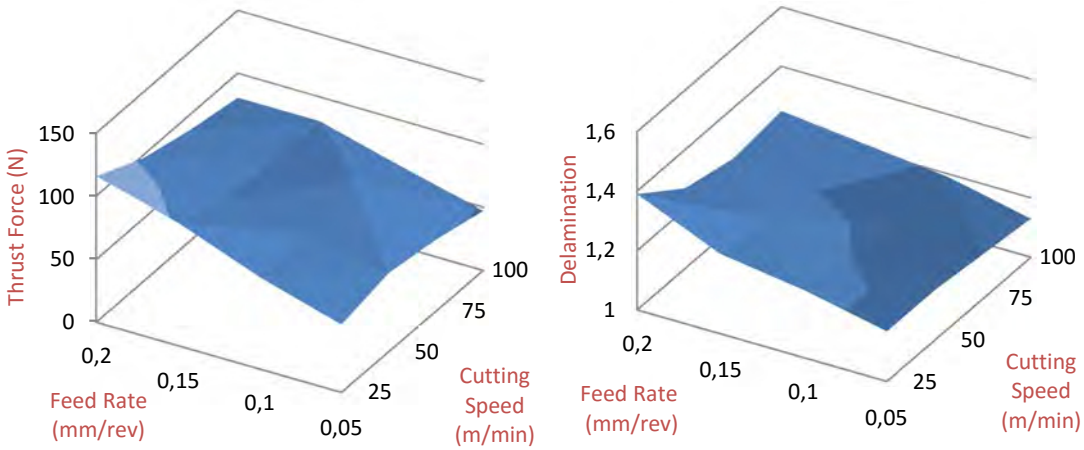

Figure 7.8: Surface diagram for thrust force and delamination for a helicoidal drill bit (point angle =90°).

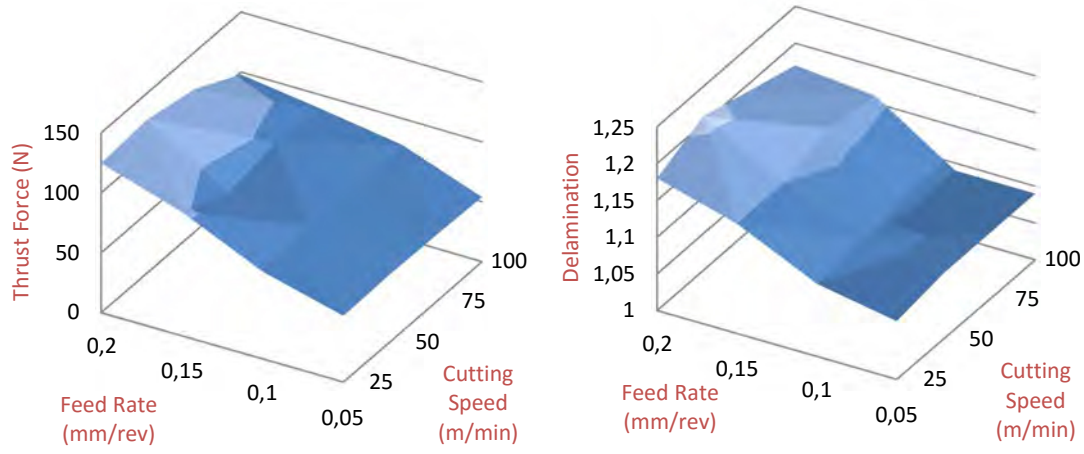

Figure 7.9: Surface diagram for thrust force and delamination for a helicoidal drill bit (point angle =118°).

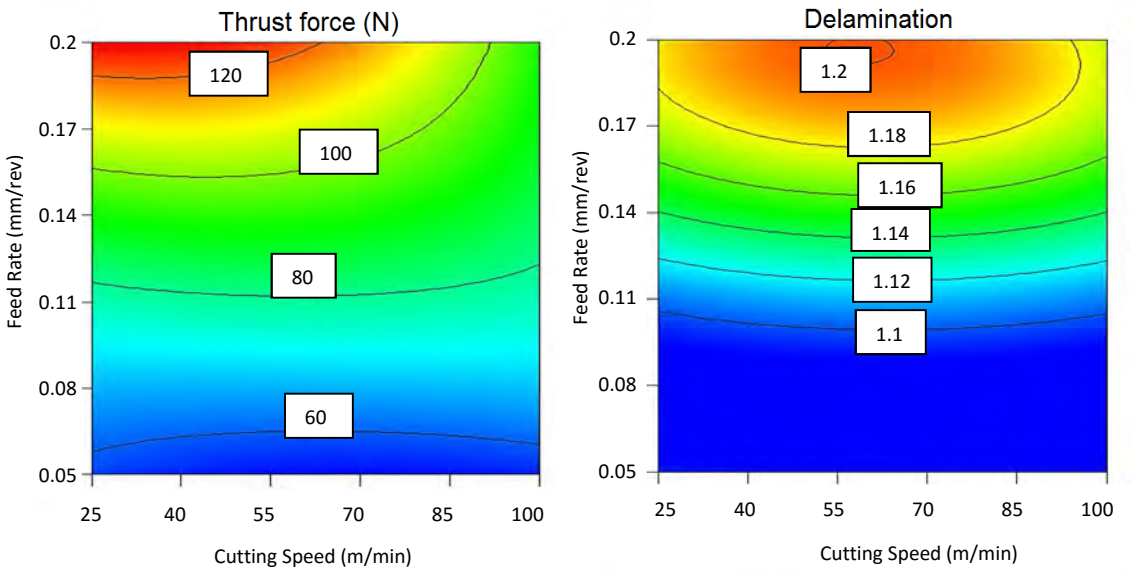

Figure 7.10: Diagrams to estimate thrust force and delamination for helicoidal drill bit with point angle equal 118°.

sults published in a previous work by the authors [6].

The numerical results obtained from the simulations allowed the adjustment of a mechanistic expression relating both thrust force and delamination factor to feed rate and cutting speed for the honed tool (see Table 7.5). Similar to the previous case, it is possible to develop graphics to predict the values of thrust force and delamination for a couple of cutting parameters selected (Figure 7.12).

Table 7.6 shows the results of a set of validation experiments (cutting speed equal 50 m/min) that were performed to assess the predictability of identified regression

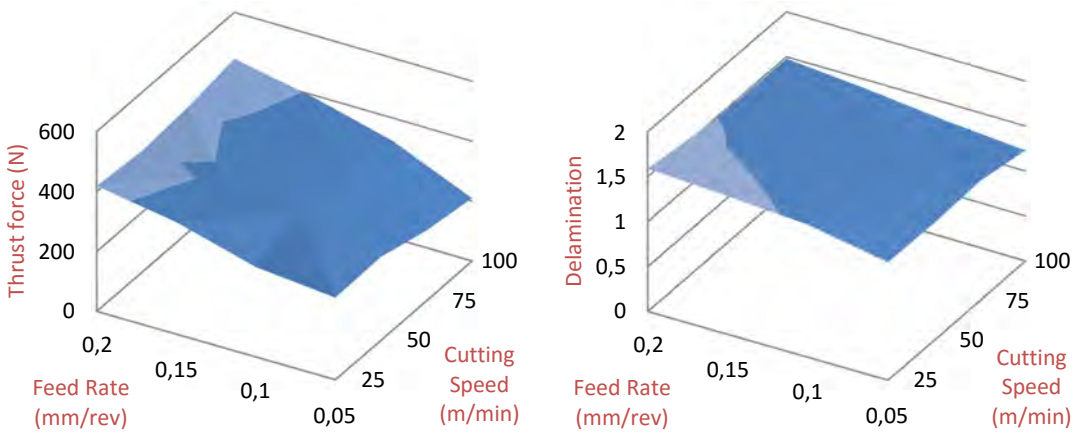

Figure 7.11: Surface diagram for thrust force and delamination for honed edge drill bit.

Table 7.5: Prediction equations (thrust force and delamination) for worn tool at different cutting speeds.

Point angle	Prediction equation	R^2
118	$T_f(N) = 272.0205 - 1.1143 \cdot V + 634.463 \cdot f + 8.1877 \cdot V \cdot f$	0.93
	$D_f = 0.9725 + 0.0075 \cdot V + 6.43 \cdot f - 0.0941 \cdot V \cdot f - 5.6E\text{-}5 \cdot V^2 - 14 \cdot f^2 + 0.00043 \cdot V^2 \cdot f + 0.152 \cdot V \cdot f^2$	0.96

presented before. The maximum relative difference between the experimental value and the predicted value was 13.8% for the thrust force and 2.92% for the delamination, providing a good confidence level regarding the applicability of the prediction equations.

7.5 Conclusions

In this work, a numerical model able to predict the response of carbon/epoxy woven laminates under drilling processes has been developed. The numerical simulations predict quite faithfully the delamination damage and the thrust force; this tool has a potential use in the understanding of the inter-laminar damage due to drilling in composites, allowing the reduction of experimental tests. In addition, the model is also able to estimate the damage for worn tools and complex geometries. This shows the possibility to extend the modeling to new geometries.

Validation was carried out comparing numerical results and experiments in terms of thrust force and induced delamination and good accuracy was found. The validated model was used to study the influence of different cutting parameters both in the case of new and worn tool. Clear influence of the feed rate and point angle has been observed and explained.

Finally a mechanistic model developed for rapid estimation of delamination

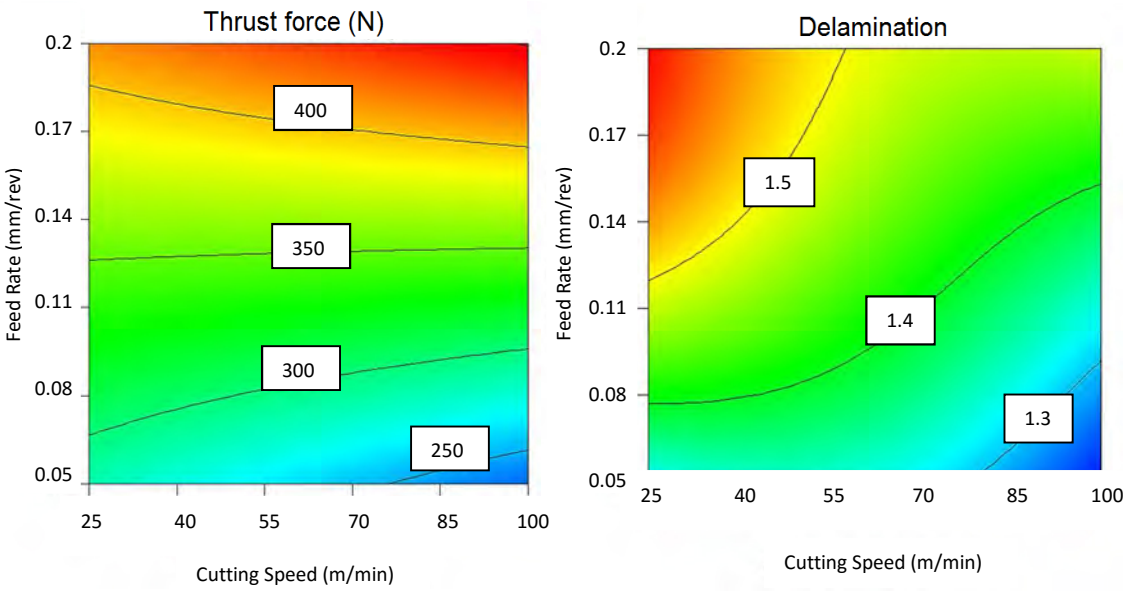

Figure 7.12: Example of diagrams to estimate thrust force and delamination for honned drill bit.

Table 7.6: Comparison between experiments and estimated values by regression equations.

		Thrust force			Delamination		
	Feed Rate (mm/rev)	**Estimated**	**Experimental**	**Error**	**Estimated**	**Experimental**	**Error**
Fresh Drill	0.1	74.76	68.24	9.6%	1.09	1.08	0.93%
	0.15	84.64	74.38	13.8%	1.16	1.14	1.75%
Honned Edge Drill	0.1	313.306	358.19	12.5%	1.37	1.41	2.92%
	0.15	375.73	395.035	5.1%	1.43	1.47	2.80%

and thrust force has been presented and validated with a very good confidence level. The expressions and surface diagrams deduced allowed prediction of thrust force and delamination once the feed rate and cutting speed are defined.

7.6 Acknowledgements

This study has been developed under the financial support of the Ministry of Economy and Competitiveness of Spain under the projects DPI2011-25999 and DPI2013-41094-R, and the FPI subprogram associated to the project DPI2011-25999 with the reference BES-2012-055162.

7.7 References

[1] Huang X. Fabrication and Properties of Carbon Fibers. Mater 2009; 2:2369-403.

[2] López de Lacalle LN, Fernández A, Olvera D, Lamikiz A, Olvera D, Rodríguez C, Elias A. Monitoring deep twist drilling for a rapid manufacturing of light high-strength parts. Mech Syst Sig Process 2011; 25:2745-52.

[3] López de la calle LN, Lamikiz A, F. J. Campa FJ, Fdz-Valdivielso A. Design and Test of a Multitooth Tool for CFRP Milling. J Compos Mater 2009; 43(26):3275-90.

[4] Liu D, Tang Y, Cong WL. A review of mechanical drilling for composite laminates. Compos Struct 2012; 94:1265-79.

[5] Davim JP, Reis P. Study of delamination in drilling carbon fiber reinforced plastic (CFRP) using design experiments. Compos Struct 2003; 59:481-7.

[6] Gaitonde VN, Karnik SR, Campos Rubio J, Esteves Correia A, Abrao AM, Paulo Davim J. Analysis of parametric influence on delamination in high-speed drilling of carbon fiber reinforced plastic composites. J Mater Process Technol 2008; 203:431-8.

[7] Karnik SR, Gaitonde VN, Campos Rubio J, Esteves Correia A, Abrao AM, Davim JP. Delamination analysis in high speed drilling of carbon fiber reinforced plastics (CFRP) using artificial neural network model. Mater Des 2008; 29:1768-76.

[8] Feito N, Díaz-Álvarez J, Díaz-Álvarez A, Cantero JL, Miguélez MH. Experimental Analysis of the Influence of Drill Point Angle and Wear on the Drilling of Woven CFRPs. Materials 2014; 7:4258-71.

[9] Heisel U, Pfeifroth T. Influence of Point Angle on Drill Hole Quality and Machining Forces when Drilling CFRP. Procedia CIRP 2012; 1:471-66.

[10] Tsao CC, Hocheng H. Taguchi analysis of delamination associated with various drill bits in drilling of composite material. Int J Mach Tools Manuf 2004; 44:1085-90.

[11] Mayuet P, Gallo A, Portal A, Arroyo P, Alvarez M, Marcos M. Damaged Area based Study of the Break-IN and Break-OUT defects in the Dry Drilling of Carbon fiber Reinforced Plastics (CFRP). Proc Eng 2013; 63:743-51.

[12] Rawat S, Attia H. Wear mechanisms and tool life management of WC–Co drills during dry high speed drilling of woven carbon fibre composites. Wear 2009; 267:1022-30.

[13] Iliescu D, Gehin D, Gutierrez ME, Girot F. Modeling and tool wear in drilling of CFRP. Int J Mach Tools Manuf 2010; 50:204-13.

[14] Faraz A, Biermann D, Weinert K. Cutting edge rounding: An innovative tool wear criterion in drilling CFRP composite laminates. Int J Mach Tools Manuf 2009; 49:1185-96.

[15] Chinmaya RD, Shin YC, Modeling of machining of composite materials: A review. Int J Mach Tools Manuf 2012; 57:102-21.

[16] Arola D, Ramulu M. Orthogonal cutting of fiber-reinforced composites: a finite element analysis. Int J Mech Sci 1997; 39:597-613.

[17] Mahdi M, Zhang L. A finite element model for the orthogonal cutting of fiber reinforced composite materials. J Mater Process Technol 2001; 113:368-72.

[18] Santiuste C, Soldani X, Miguélez MH. Machining FEM model of long fiber composites for aeronautical components. Compos Struct 2010; 92:691-98.

[19] Soldani X, Santiuste C, Muñoz-Sánchez A, Miguélez MH. Influence of tool geometry

and numerical parameters when modeling orthogonal cutting of LFRP composites. Composites: Part A 2011; 42:1205-16.

[20] Santiuste C, Miguélez MH, Soldani X. Out-of-plane failure mechanisms in LFRP composite cutting, Compos Struct 2011; 93:2706-13

[21] Santiuste C, Olmedo A, Soldani X, Miguélez MH. Delamination prediction in orthogonal machining of carbon LFRP composites. J Reinf Plastic Comp 2012; 31(13):875-85.

[22] Durao LMP, de Moura MFSF, Marques AT. Numerical simulation of the drilling process on carbon/epoxy composite laminates. Composites Part A, 2006; 37:1325-33.

[23] Durao LMP, de Moura MFSF, Marques AT. Numerical prediction of delamination onset in carbon/epoxy composite laminates. Eng Fract Mech 2008;75: 2767-78.

[24] Singh I, Bhatnagar N, Viswanath P. Drilling of uni directional glass fiber reinforced plastics: experimental and finite element study. Mater Des 2008; 29:546-53.

[25] Upadhyay PC, Lyons JS. On the evaluation of critical thrust for delamination free drilling of composite laminates. J Reinf Plast and Comp 1999; 18:1287-303.

[26] Isbilir O, Ghassemieh E. Numerical investigation of the effects of drill geometry on drilling induced delamination of carbon fiber reinforced composites. Compos Struct 2013; 105:126-33.

[27] Phadnis VA, Makhdum F, Roy A, Silberschmidt VV. Drilling in carbon/epoxy composites: experimental investigations and finite element implementation. Composites Part A 2013; 47:41-51.

[28] Feito N, López-Puente J, Santiuste C, Miguélez MH. Numerical prediction of delamination in CFRP drilling. Compos Struct 2014; 108:677-83.

[29] Varas D, Artero-Guerrero JA, Pernas-Sánchez J, López-Puente J. Analysis of high velocity impacts of steel cylinders on thin carbon/epoxy woven laminates. Compos Struct 2013; 95:623-29.

[30] http://www.guhring.com/

[31] Hibbit, Karlson, Sorensen Inc. ABAQUS user's manual; 2003.

[32] López-Puente J, Zaera R, Navarro C. Experimental and numerical analysis of normal and oblique ballistic impacts on thin carbon/epoxy woven laminates. Composites Part A 2008; 39:374-87.

Parte III

Conclusiones / Conclusions

1. Conclusiones

Las principales conclusiones derivadas de esta tesis doctoral se mencionan a continuación. Los párrafos siguientes resumen las aportaciones extraídas de los estudios experimentales:

- Se ha comprobado que la geometría de la broca es un parámetro con gran influencia en el daño generado durante el taladrado de materiales CFRP. La selección de una geometría adecuada es esencial para minimizar el daño. Las brocas escogidas presentaron diseños novedosos frente a otras geometrías previamente estudiadas. Entre las brocas ensayadas en este estudio, la geometría con filos rectos mostró los mejores resultados para ambas configuraciones de laminado: multidireccional y tejido.

- El efecto cruzado entre el ángulo de punta de la broca helicoidal y el desgaste sufrido en la herramienta también ha sido analizado. La fuerza de avance crece con ambos parámetros, siendo el daño más severo cuando el ángulo de punta es mayor. De este hecho deriva la recomendación de elegir ángulos de punta pequeños cuando se va a realizar un gran número de agujeros sin cambiar la broca. El estudio de diferentes tipos de desgastes inducidos artificialmente en las brocas presenta una novedad en el campo del taladrado de materiales LFRPs, aportando nueva información sobre la influencia del desgaste, tema poco tratado en la literatura.

- Los resultados del estudio de la influencia de los parámetros de corte en la fuerza de avance, y consecuentemente en la delaminación, han sido consistentes con los análisis previos de la literatura. Los datos obtenidos con las nuevas geometrías ensayadas amplían la información existente. Se reafirmó la teoría de que la velocidad de avance es la variable con mayor influencia independientemente de la geometría. Es conveniente, por tanto, el uso de avances pequeños y altas velocidades de corte cuando se taladra materiales compuestos.

- El laminado CFRP con láminas unidireccionales ha mostrado mucha más susceptibilidad al daño debido al taladrado que el material con capas tejidas. Sin embargo, esta segunda configuración alcanzó valores de fuerza mayores y un mejor acabado superficial bajo las mismas condiciones de corte. Esto implica que el material tejido ofrece una mejor resistencia al daño frente al material multidireccional, en condiciones iguales de fuerza de avance. La comparación entre los dos materiales también arroja nuevos datos de interés en el área de los materiales compuestos.

- Varias herramientas estadísticas se han utilizado como apoyo a los estudios experimentales, consiguiendo cuantificar la influencia de los parámetros de corte en el daño por delaminación y en las fuerzas de corte. El análisis ANOVA ha demostrado que el peso del avance y de la velocidad de corte dependen en gran medida de la geometría empleada y del desgaste. Por otro lado, se demostró que el ángulo de punta adquiere más importancia en la delaminación cuanto más crece el desgaste. El estudio ANOVA realizado es el más completo hasta el momento en el campo de taladrado de materiales compuestos, ya que ofrece una visión muy completa sobre la influencia de los parámetros de entrada en las fuer-

zas de corte y la delaminación. Esto se debe a que tiene en cuenta muchos más factores e interacciones entre las variables que los existentes en la literatura.

- Por último, se han desarrollado ecuaciones de predicción de daño y de fuerzas de corte para las herramientas desgastadas mediante la metodología de análisis por regresión. Las ecuaciones validadas se utilizaron para optimizar tanto los parámetros de corte como los geométricos, y obtener la mínima delaminación posible en el taladrado de material tejido CFRP con herramientas helicoidales. Este tipo de análisis no es muy común en la bibliografía por lo que el uso de ecuaciones cuadráticas que incluyan el ángulo de punta supone un avance en los estudios experimentales.

Las conclusiones relacionadas con los modelos números implementados durante la investigación se resaltan en los siguientes puntos:

- Se ha realizado un estudio comparativo de un modelo simplificado y un modelo completo de taladrado, ambos desarrollados en 3D, para laminados multidireccionales de fibra de carbono. Los modelos simplificados han presentado una ventaja considerable en su menor tiempo computacional, aunque sobreestimando ligeramente los resultados. El modelo completo, sin embargo, presenta una estimación más precisa de la fuerza de avance y de la delaminación. La evolución del daño inter-laminar se predice mejor en el caso del modelo completo ya que la operación de corte es continua.

- Con el modelo simplificado se realizó un estudio de diversos factores que condicionan el daño por delaminación como son la fuerza de avance, las condiciones de soporte o la secuencia de apilamiento. La selección de este modelo es debida a la ventaja del tiempo computacional que presenta frente al modelo completo. Se ha comprobado que la hipótesis de reducción del daño utilizando un plato de apoyo es válida para diámetros del agujero del soporte de hasta 5 veces el diámetro del taladro en agujeros pequeños. Por otro lado, los laminados cuasi-isótropos han presentado mejor resistencia al daño que otro tipo de apilamientos [0°/90°], lo que los hace mucho más recomendables para aplicaciones aeronáuticas.

- Se ha llevado a cabo la implementación de un modelo completo 3D para material tejido CFRP cuyos resultados comparados con ensayos experimentales dieron una buena predicción. El modelo se ha aplicado a diversas geometrías de broca (helicoidal, escalonada y desgastada) mostrando una tendencia crecientes tanto en la delaminación como en la fuerza de avance al incrementar el avance y el ángulo de punta. El modelo desarrollado es el primero que se presenta en la literatura para laminados CFRP con estructura tejida, y el primero también en el que se implementa una geometría desgastada.

- Finalmente, se han desarrollado modelos mecanísticos basados en los parámetros de corte, capaces de predecir la delaminación y la fuerza de avance con un buen nivel de confianza. Se aplicaron para desarrollar superficies de respuesta, basadas tanto en datos experimentales como obtenidos mediante simulación. Esta metodología, poco frecuente en los estudios de taladrado, ofrece una forma rápida para estimar ciertos parámetros de interés.

2. Trabajos Futuros

Algunas de las líneas de investigación futuras, continuación de la Tesis Doctoral presentada se muestran a continuación:

- La tendencia actual de la industria es apostar por materiales compuestos CFRP que incluyen láminas de titanio. Estos materiales continúan utilizando la metodología de remachado y por lo tanto requieren de operaciones de taladrado. Nuevas líneas de investigación se han abierto en este campo relacionadas con el desgaste excesivo producido por la introducción de láminas metálicas, la formación de la viruta y los problemas térmicos.

- Avanzar en los estudios referentes a los métodos de reducción de fuerza de avance, como son los agujeros pre-taladrados o las placas de apoyo. El estudio de diferentes dimensiones del agujero pre-taladro o del hueco de salida de la placa de apoyo bajo diferentes geometrías de broca, puede aportar nueva información en el campo. Reproducir estos experimentos en un modelo 3D también ayudaría a la optimización del diseño de las brocas empleadas.

- Desarrollar una metodología para estudiar la temperatura durante los procesos de taladrado en materiales LFRP. Un número muy limitado de estudios relacionados con este tema se han encontrado en la bibliografía debido a la complicación de medir temperaturas en el interior del agujero taladrado. Por esta razón la temperatura se mide solamente en los alrededores del taladro. La introducción de este parámetro en modelos numéricos en un trabajo complejo y difícil que, sin embargo, ayudaría a tener una mejor compresión sobre lo que realmente ocurre en la interfaz herramienta-pieza.

- Debido al alto coste de llevar a cabo ensayos según el proceso de taladrado a alta velocidad (HSD), el desarrollo de un modelo 3D se plantea interesante como apoyo a los escasos estudios experimentales existentes en la literatura. Los resultados de la influencia de las condiciones de corte en este proceso podrían utilizarse para desarrollar ecuaciones de predicción de daño y superficies de respuesta.

- Un paso más en la investigación de procesos de mecanizado en el ámbito de los materiales compuestos, consiste en incluir el proceso de fresado de materiales LFRP. Las escasas publicaciones referentes en este campo dejan abiertas amplias opciones tanto de experimentación como de simulación. Los modelos de fallo utilizados en esta tesis pueden ser implementados en procesos de fresado de materiales compuestos CFRP.

3. Conclusions

The main conclusions arising from this doctoral thesis are showed in the next paragraphs. The following points summarize the contributions drawn from experimental studies:

- It has been found that the geometry of the drill bit is a parameter with high influence on the damage generated during CFRP drilling. The selection of a suitable geometry is essential to minimize the damage. The drills presented innovative designs compared to

other geometries studied previously. Among the drill bits tested in this study, Reamer geometry has showed the best results for both configurations of laminate: multidirectional and woven.

- The cross effect between the point angle of the twist drill bit and the tool wear has been also analyzed. Feed force increases with both parameters, and the most severe damage is founded when the point angle is high. From this fact, derives the recommendation to choose small point angles when going to perform a large number of holes without changing the tool. The study of different types of artificially induced wear in drill bits presents a novelty in the field of drilling LFRPs materials, showing new information about the wear influence.

- Results of the influence of cutting parameters study on feed force, and consequently on delamination, have been in concordance with previous studies founded in the literature. The results increase the existing information in the literature for these new geometries. The theory that the feed rate is the most influential variable regardless of geometry was reaffirmed. Cutting variables recommended after the analysis were low feed rate and high cutting speed for composited drilling operations.

- The CFRP laminate with multidirectional configuration showed greater damage susceptibility by drilling than woven laminate. However, this second configuration reached higher values of force and better surface finish under the same cutting conditions. This involves that woven materials offers better damage resistance versus multidirectional material, under the same thrust force conditions. The comparison between both configurations also generates new interesting information in the area of the composites.

- Several statistical tools have been used to support experimental studies, reaching to quantify the influence of cutting parameters in delamination damage and cutting forces. ANOVA analysis shows that the influence of feed rate and cutting speed are highly dependent of geometry and tool wear. It is also concluded that point angle becomes relevant in delamination when wear increases in the tool. The ANOVA study is the most complete until now in the field of drilling of composite materials, because it offers a complete overview about the influence of the input parameters on cutting forces and delamination. This is because it considers more factors and interactions between the variables than others ANOVA founded in the literature.

- Finally, prediction equations of damage and cutting forces for worn tools have been developed, using regression analysis methodology. These equations are validated and used to optimize both cutting and geometric parameters, and get the least possible delamination in drilling CFRP woven with helicoidal tools. This type of analysis is not very abundant in the bibliography so the use of quadratic equations including point angle is a breakthrough in experimental studies.

The findings related to the models implemented during the investigation numbers are highlighted in the following points:

- A comparative study between a simplified model and a complete model of drilling, both developed in 3D, for multidirectional carbon fiber laminates has been carried out. The simplified model shows a considerable advantage in its lower computational time, but overestimates slightly the results. The complete model, however, presents a better estimation of thrust force and delamination. The evolution of inter-laminar damage is better predicted in the case of the complete model due to the cutting operation is continuous.

- The simplified model has been chosen to do a study with several factors which affecting delamination such as feed force, support conditions or stacking sequence. This model has been selected due to its minor computational time versus complete model. It has been found that the damage reduction hypothesis using a support plate is valid for diameters up to 5 times the diameter of the drill hole. It was also found that the quasi-isotropic laminates showed better resistance to damage than other laminates with [0°/90°] stacking sequences, which it makes them more desirable for aeronautical applications.

- It has been carried out the implementation of a complete three-dimensional model for woven CFRP whose results compared to experimental tests provided a good prediction. The model has been applied to different tool geometries (helicoidal, stepped and worn) showing a rising trend both delamination and thrust force when increasing feed rate and point angle. The developed model is a novelty in the literature for CFRP laminates with woven structure, and also the first in which a worn geometry is implemented.

- Finally, mechanistic models have been developed based on cutting parameters, able to predict delamination and thrust force with a good level of confidence. They have been applied to develop response surfaces based on both experimental and simulations data. This methodology, not very common in drilling studies, offers a quick way to estimate certain parameters of interest.

4. Future Works

Some of the future researching lines are outlined below:

- The current industry trend is to bet on CFRP composite materials with layers of titanium. These materials continue using rivets to join the structures and therefore require drilling operations. New lines have been open in this field related to excessive wear caused by the introduction of metal layers, chip formation and thermal problems.

- Advance in studies on methods to reduce the thrust force, using pre-drilled holes or backing plates. The study of different pre-drill hole dimensions or the exit hole in the supporting plate may provide new information in the field. Reproduce these experiments in a 3D model can help to optimize the design of the tools used.

- Developing a methodology to study the temperature during drilling processes in LFRP materials. Very limited studies related to this topic can be found in the literature, due to

difficulty of measure temperature inside the drilled hole. For this reason the temperature is measured only around the drill. The introduction of this parameter in numerical models is a complex and difficult work. However, it would be useful to have a better understanding about what really happens in the tool-workpiece interface.

- Due to the high cost of carrying out tests according to high speed drilling (HSD), the development of a 3D model could be an interesting tool as support of limited experimental studies in the literature. The results of the influence of cutting conditions in this process could be used to develop damage prediction equations and response surfaces.

- A further step in the investigation of machining processes in the field of composite materials is to include the milling of materials LFRPs. The few publications on this field leave open several lines in both experimental and simulation. The damage models used in this thesis can be implemented in CFRP composite materials milling processes.

Publicaciones

Publicaciones

Durante el desarrollo de la presente tesis se han llevado a cabo las siguientes publicaciones, ponencias y estancias:

ARTICULOS INDEXADOS

- **N. Feito**, J. Diaz-Álvarez, J. López-Puente, H. Miguelez, "Numerical analysis of tool wear and special geometry when drilling woven CFRPs", Composite Structures, 2016, 138, 285-294.

- **N. Feito**, A. Diaz-Álvarez, J.L. Cantero, M. Rodríguez-Millán, M. H. Miguélez, "Experimental analysis of special tool geometries when drilling woven and multidirectional CFRPs", Journal of Reinforced Plastics and Composite, 2016, 35, 33-55.

- **N. Feito**, A. S. Milani, A. Muñoz-Sánchez, "Drilling optimization of woven CFRP laminates under different tool wear conditions: a multi-objective design of experiments approach", structural and multidisciplinary optimization, 2015, 53, 239-251.

- **N. Feito**, J. Díaz-Álvarez, A. Díaz-Álvarez, J.L. Cantero, M. H. Miguélez, "Experimental analysis of the Influence of drill point angle and wear on the drilling of woven CFRPs", Materials, 2014, 7, 4258-4271.

- **N. Feito**, J. López-Puente, C. Santiuste, M.H. Miguélez, "Numerical prediction of delamination in CFRP drilling", Composite Structures, 2014, 108, 677-683

ARTÍCULOS NO INDEXADOS

- **N. Feito**, J. Díaz-Álvarez, A. Díaz-Álvarez, J. L. Cantero, H. Miguelez "Influencia de la Geometría de Herramienta en el Taladrado de CFRP", Interempresas, 2016, 74-82.

- **N. Feito**, J. Díaz-Álvarez, J.L. Cantero, M.H. Miguélez, "Influence of Special Tool Geometry in Drilling Woven CFRPs Materials", Procedia Engineering, 2015, 132, 636-638

- **N. Feito**, J. Díaz-Álvarez, A. Díaz-Álvarez, J. L. Cantero, J. López-Puente, M.H. Miguelez "Influence of tool geometry in drilling CFRP", 16TH ECCM, Seville, Spain, 22-26 June 2014

PONENCIAS EN CONGRESOS

- **N. Feito**, A. Sánchez-Muñoz, J. López-Puente, H. Miguelez, "Statistical and Numerical Analysis of wear Tool Geometry in Drilling CFRP", 20th International Conference on Composite Materials, Copenhagen, Denmark, 19 - 24 July 2015.

- **N. Feito**, J. Díaz-Álvarez, J.L. Cantero, M.H. Miguélez, "Influence of Special Tool Geometry in Drilling Woven CFRPs Materials", 6th Manufacturing Engineering Society International Conference, Barcelona, Spain, 22-24 July 2015.

- **N. Feito**, A. Díaz-Álvarez, J. López-Puente, M.H. Miguélez, "Modelling Special drill bit geometry for CFRP composite", 18th International Conference on Composite Structures, Lisbon, Portugal, 15-18 June 2015.

- **N. Feito**, J. Díaz-Álvarez, A. Díaz-Álvarez, J. L. Cantero, H. Miguelez "Influencia de la Geometría de Herramienta en el Taladrado de CFRP", XX Congreso Nacional de Ingeniería Mecánica, Málaga, Spain, 24-26 September 2014.

- **N. Feito**, J. Díaz-Álvarez, A. Díaz-Álvarez, J. L. Cantero, J. López-Puente, M.H. Miguelez "Influence of tool geometry in drilling CFRP", 16TH European Conference on Composite Materials, Seville, Spain, 22-26 June 2014.

- **N. Feito**, J. López-Puente, C. Santiuste, X. Soldani, M.H. Miguélez, "Numerical modelling of composite drilling", IV ECCOMAS Thematic Conference on the Mechanical Response of Composites, Açores, Portugal, 25-27 Sept 2013.

- **N. Feito**, J. López-Puente, C. Santiuste, M.H. Miguélez, "Modelling drilling of CFRP composite", 7th International Workshop 2013 on Dynamic Behaviour Of Materials and its Applications in Industrial Processes, Madrid, 8-10 May, 2013.

CAPÍTULOS DE LIBROS

- H. Miguélez, **N. Feito**, C. Santiuste, J. Díaz-Álvarez, M. Rodríguez-Millán, X. Soldani, "Numerical modeling of machining of LFRPs" in Machinability of Fibre-Reinforced Plastics, J. Paulo Davim ed., de Gruyter, June 2015 (ISBN: 978-3-11-029225-1).

ESTANCIAS

- Departamento de Ingeniería Mecánica de la Universidade do Porto, Portugal. Bajo la supervisión del profesor Pedro P. Camanho (4 meses).

- Grupo de investigación Composites Research Network (CRN) en la University of British Columbia, Canada. Bajo la supervisión del profesor Abbas S. Milani (4 meses)